

The University of Maine

DigitalCommons@UMaine

Electronic Theses and Dissertations

Fogler Library

Summer 8-17-2018

Feasibility of Hybrid Thermoplastic Composite-Concrete Load Bearing System

Camerin M. Seigars

University of Maine, linuslarrabee88@gmail.com

Follow this and additional works at: <https://digitalcommons.library.umaine.edu/etd>



Part of the [Manufacturing Commons](#), and the [Other Mechanical Engineering Commons](#)

Recommended Citation

Seigars, Camerin M., "Feasibility of Hybrid Thermoplastic Composite-Concrete Load Bearing System" (2018). *Electronic Theses and Dissertations*. 3144.

<https://digitalcommons.library.umaine.edu/etd/3144>

This Open-Access Thesis is brought to you for free and open access by DigitalCommons@UMaine. It has been accepted for inclusion in Electronic Theses and Dissertations by an authorized administrator of DigitalCommons@UMaine. For more information, please contact um.library.technical.services@maine.edu.

**FEASIBILITY OF HYBRID THERMOPLASTIC COMPOSITE-CONCRETE
LOAD BEARING SYSTEM**

By

Camerin Michael Seigars

B.S. University of Maine, 2016

A THESIS

Submitted in Partial Fulfillment of the

Requirements for the Degree of

Master of Science

In Mechanical Engineering

The Graduate School

The University of Maine

August 2018

Advisory Committee:

Dr. William Davids, Professor of Civil Engineering, Co-Advisor

Dr. Roberto Lopez-Anido, Professor of Civil Engineering, Co-Advisor

Dr. Senthil Vel, Professor of Mechanical Engineering

Copyright 2018 Camerin Michael Seigars

FEASIBILITY OF HYBRID THERMOPLASTIC COMPOSITE-CONCRETE LOAD BEARING SYSTEM

By Camerin Michael Seigars

Thesis Advisors: Dr. William Davids & Dr. Roberto Lopez-Anido

An Abstract of the Thesis Presented
in Partial Fulfillment of the Requirements for the
Degree of Master of Science
in Mechanical Engineering
August 2018

Thermoplastic composites have many advantages over thermoset composites such as being recyclable, rapidly manufacturable, and more impact resistant. The goal of this thesis is to assess the feasibility of using thermoplastic composites in structural applications through literature review, mechanical testing, design of a load-bearing hybrid composite-concrete structures, and the implementation of thermoplastic composites for tensile reinforcement of concrete. The study had four objectives covering the stated goal.

1. Conduct a literature review to direct thermoplastic material selection
2. Characterize thermoplastic material mechanical properties using standardized mechanical testing
3. Design a hybrid composite-reinforced concrete beam, and
4. Develop thermoplastic shear connectors to develop composite action between thermoplastic reinforcement and concrete

Initially, thermoplastics that can be reinforced with E-glass fibers to be used as a structural part were investigated. Materials were selected for experimental characterization after extensive literature review based on performance, cost and manufacturing methods. Two

industry accepted processes were selected for use in fabrication: vacuum infusion, a longstanding and highly accepted process traditionally used for the manufacturing of thermoset composites; and thermoforming, a fast production process that takes advantage of many properties of thermoplastic materials.

Next, properties of these materials required for structural applications were quantified through mechanical testing. These properties include the modulus of elasticity, Poisson's ratio and the ultimate strength in tension, compression and shear in principal material directions. Having a complete list of material properties is necessary in composite design.

A design for a load-bearing composite-concrete beam was developed. In conventional construction, steel reinforcing bars are used to carry the tension in a concrete beam, but steel is susceptible to corrosion. These hybrid composite-concrete structures rely on the transfer of forces (composite action) between the thermoplastic composite, which acts as reinforcement, and the concrete section of the beam. The composite action is necessary for the composite reinforcement to develop tension through shear flow at the interface. The initial design to demonstrate the use of thermoplastic composites in this manner is the fabrication of a simple prismatic beam with the bottom-face reinforced with the composite. This provides a simple structure to demonstrate the feasibility of this technology for use in structural applications.

Finally, the ability of the shear connectors developed to produce composite action in the proposed beam was experimentally assessed. Hybrid composite-concrete specimens were tested in compression to assess the feasibility of shear connectors (studs) to carry the shear flow at the interface between the thermoplastic reinforcement and concrete.

Conclusions and recommendations are presented in Chapter 5. Recommendations for future work include the implementation of small-scale short-beam tests in four-point bending to further assess the degree of composite action being generated in the structure. Recommendations for future research on more effectively achieving composite action in hybrid thermoplastic composite-concrete members is also addressed.

DEDICATION

Primarily I would like to dedicate this thesis to God, who has provided me with life and all those who help me through it. This amazing world and everything in it is thanks to him.

I would like to dedicate this thesis to Frasier and its amazing cast. Through the long, arduous, and more often than not stressful process of writing this thesis the show Frasier provided me with more than background noise, but good laughs, distraction, relaxation, support, and simple smiles.

I am not afraid to say I could not have done it without you. Thank you to Frasier, Niles, Martin, Daphne, and all the supporting cast for all being there for me!

ACKNOWLEDGEMENTS

There are more people than possible to acknowledge when someone completes a feat as daunting as a Master's degree. I would like to take the time to thank those who stand out the most as those who have helped me achieve this milestone in my life.

First, I would like to extend my thanks to my loving and supportive parents. Dad and Mom, I simply would not be the person I am without you. I love you deeply and am blessed to have you!

Dani Colson, my beautiful girlfriend and love of my life. Thank you for always being there for me, looking at my thesis when I needed you too, and being supportive through the entire writing process. I love you deeply.

My advisors Bill Davids and Roberto Lopez-Anido, I thank you both.

Bill, your support, feedback, and diligence in our weekly meetings not only helped me become a more proficient young engineer but your willingness to give me critical feedback will forever be appreciated. You have not only provided me with important knowledge as an engineer and young professional, but I feel like I have grown as a person under guidance.

Roberto, not only have we spent time at work discussing the project and engineering topics, but we have spent many hours out road biking or mountain biking in the snow. You provided me with support in my graduate career and valuable feedback while writing my thesis. You have taught me many things in graduate school and I hope to have many more trips together on our bikes.

Now the staff at the Advanced Structures and Composites Center (ASCC) who I owe a special thanks to as I draw this thesis to a close.

Joshua Clapp, over the last two years you have been more than a project manager to me, you have become a close and valued friend. I hope that we will have many more years of professional experience together, as well as maybe a fishing trip. You are beyond dedicated at the ASCC and always there when I need you. You have provided irreplaceable support and encouragement.

James Anderson, you have been an essential guide to me as a young professional and engineer. Your door is always open to provide guidance and wisdom; more times, than I can count I have leaned on you to check my ideas, discuss topics or simply to get advice. You are a valuable mentor and I look forward to the prospect of many more years of mutually rewarding work together.

Nicholas Fitzpatrick, after our time working together I confidently call you my friend and “buddy” as I often use in text messages. You simply are an awesome coworker and supportive friend. You work hard and are always there when someone needs you; the thermoplastics lab simply could not survive without your dedication and constant hard work. Thank you for your eternal dedication and assistance with stamp forming in my research.

Cody Sheltra, we have known each other a long time my friend. I appreciate your hard work at the ASCC and our bond as friends. Thank you for your dedication and ability to assist me in fabricating and achieving essential goals at the ASCC. I hope that my Master’s does not mark the end of our friendship, but just the beginning.

David Erb, thank you for having an open door to discuss various topics, the support with getting project materials, and most of all the after-hours advice on life. You have taught me many things and I hope we have many more years to work together.

I would also like to thank all the other staff at the ASCC who have assisted me along the way, Scott Tomlinson, Tom Snape, Shawn Sewall, Chris Urquhart, Sam Heathcote, Curtis Libby, Nate Faessler, Alex Cole, Maddy Wehrle, and Shawn Eary. You all have been awesome!

Students also make an essential part of the team at the ASCC, fellow graduate students and undergraduates are essential to making the ASCC the amazing and productive place that it is. I would like to not only thank the few specific students below, but all the students that make the ASCC what it is and have helped me along the way.

Sam McDonald, I hope your time at the ASCC has not only served to help pay the bills but has also taught you many things that will help you in life. I know you have been an amazing friend to me and eternally dedicated to the work we do at the ASCC. You have been the single most valuable undergraduate and trusted help that I have had during this phase of my life. You will do amazing things, no matter what you choose as your future. May you future fly high and bright!

Ben Smith, though our friendship is relatively new I count you among the best friends I have. You are more than just a valuable colleague and coworker, you are a supportive friend and I value the time we spend playing EDH, Catan, and I look forward to not only working together but many adventures playing Pathfinder.

Phil Bean, I don't think I say it often enough but thank you for being a supportive coworker and constant resource when I need a sounding board, a valuable friend, and fellow Christian. You are always willing to listen and offer an opinion. I hope we have many more years of friendship ahead of us.

Now to thank all the other people in my life who have been there for me, not only in graduate school for academic reasons, but also in life as a whole.

Ryan Cullen, you were the best friend I made in undergrad and I have a lot of awesome memories from our time together. I appreciate our friendship and look forward to many more years together. You simply are one of the best people God has put in my life.

Jordan Brown, you have left a mark on my life as a friend which I could not replace. We have had many irreplaceable years to bond as friends and many, but not nearly enough bike rides together. I look forward to many more years as close friends in life.

Erin Eldridge, you are a great friend and much-appreciated editor of my thesis. Your friendship means a lot to me and I will always be thankful for your writing advice.

Emily Anderson, simply said you are an amazing friend and an eternal wealth of support. I adore you and always will, thank you for being my friend through it all.

Nick Bucci, Comrade, close friends will we always be. Though life has put distance between us in these recent years you will always be my best friend. Thank you for that. There is no protocol for life, but people like you make it worth living.

Now, a special thank you to all the other people who have helped me in life! Sylvia Seigars my loving Nana, Burton Holt my amazing Grandfather, Tim Seigars who I will always

affectionately refer to as Uncle, Lindsey Lewis an amazing friend, Jim Rose a supportive friend and fellow cyclist, Brian Eggert my supportive Pastor, Lydia Morrison who I adore texting, Jade Hobart who I have had the pleasure of reconnecting with, David Fitzpatrick, Brent Martin, Ashley Dyer, John Herlahee, Jesse Rochester, Tamera Thompson, Wendy Jean, Brianna Smith, Anthony Diba, Dante Guzzi, and so many others, thank you!

TABLE OF CONTENTS

DEDICATION	iii
ACKNOWLEDGEMENTS	iv
LIST OF TABLES	xiv
LIST OF FIGURES	xvii
LIST OF EQUATIONS	xxii
CHAPTER 1 INTRODUCTION	1
1.1 Project Background.....	1
1.2 Significance of Research & Objectives	3
1.3 Organization of this Thesis	6
CHAPTER 2 MATERIAL SELECTION AND MANUFACTURING	7
2.1 Thermoplastic Composite Material Selection.....	7
2.1.1 Elium Acrylic Liquid Resin System	10
2.1.2 E-glass/PETg Pre-Impregnated Tapes	13
2.2 Manufacturing Methods.....	19
2.2.1 Vacuum Infusion Consolidation	20
2.2.2 Manual Stamp Thermoforming.....	27
2.2.3 Automated Stamp Thermoforming	31
2.3 Summary of Constitutive Material Properties	49
2.4 Conclusions.....	51

CHAPTER 3 MATERIAL CHARACTERIZATION	52
3.1 Characterization of Thermoplastic Composites for Structural Applications	52
3.1.1 Mechanical Properties of Composite Laminas and Laminates	52
3.1.2 Experimental Methodology and Equipment	54
3.2 Material Testing Results	58
3.2.1 Thermoplastic Material Feasibility Testing	58
3.2.2 Thermoplastic Composite Material Characterization	71
3.2.2.1 Comparison of Experimental Mechanical Properties	71
3.2.2.2 Composite Predictions of Elastic and Strength Properties	77
3.2.2.3 Unidirectional E-glass/Elium Test Results	91
3.2.2.4 Unidirectional E-glass/Derakane Test Results.....	95
3.2.2.5 Unidirectional E-glass/PETg Test Results.....	99
3.2.2.6 Beam Layup E-glass/PETg Test Results	101
3.3 Conclusions and Recommendations	107
CHAPTER 4 SHEAR CONNECTORS.....	110
4.1 Purpose.....	110
4.2 Hybrid Reinforced-Concrete Structures	110
4.2.1 Hybrid Steel-Concrete Structures	111

4.2.2 Hybrid Thermoset FRP-Concrete Structures	113
4.2.2.1 Externally Bonded Thermoset FRP	114
4.2.2.2 Mechanically Fastened Thermoset FRP	115
4.2.3 Hybrid Thermoplastic FRP-Concrete Structures	115
4.2.3.1 Unreinforced Shear Stud attached by Friction Welding	121
4.2.3.2 Reinforced Shear Stud attached by Friction Welding.....	123
4.2.3.3 Friction Welded Shear Stud Selection	124
4.2.3.4 Fiber-Reinforced Shear Stud by Resin Infusion	124
4.2.4 AASHTO Shear Stud Design & Spacing.....	126
4.3 Manufacturing.....	127
4.3.1 Friction Welding Methods	127
4.3.1.1 Feasibility Welding Trial	128
4.3.1.2 Instron Testing Frame Welding	128
4.3.1.3 Mobile Device Welding.....	131
4.3.2 Vacuum Infusion of Reinforced Shear Studs.....	133
4.4 Strength and Stiffness Testing	137
4.4.1 TP Stud Shear Custom Test Fixture.....	137
4.4.2 Testing of Instron Welded Studs in Double TP Stud Shear Loading	138
4.4.3 Testing of Instron Welded Studs in Single TP Stud Shear Loading.....	143
4.4.4 Testing of Mobile Welded Studs Single TP Stud Shear Loading.....	147

4.4.5 Testing in Concrete-TP Stud and Concrete-CFRTP Stud Configurations....	150
4.4.5.1 Specimen Design	150
4.4.5.2 Specimen Manufacturing	152
4.4.5.3 Test Setup & Instrumentation	154
4.4.5.4 Predicted Fiber-Reinforced Thermoplastic Shear Stud Results.....	157
4.4.5.5 Tabulated Numerical Results	159
4.4.5.6 Concrete-TP and Concrete-CFRTP Stud Graphical Results	162
4.5 Discussion of Experimental Results	171
4.6 Redesigned E-glass/Elium Concrete-CFRTP Stud Specimen	177
4.7 Conclusions and Recommendations	180
CHAPTER 5 CONCLUSIONS AND RECOMMENDATIONS	184
5.1 Conclusions.....	184
5.1.1 CFRTP Manufacturing Feasibility & Mechanical Properties.....	184
5.1.2 Thermoplastic Shear Stud Feasibility	187
5.2 Recommendations for Future Work.....	190
5.2.1 Thermoplastic Composite Materials	190
5.2.2 Thermoplastic Composite Shear Connectors.....	191
5.2.3 Small-Scale Beam Testing.....	192
5.2.4 Develop Optimal Cross-Sections.....	193
5.2.5 Explore Other Structural Applications of Thermoplastics.....	194

REFERENCES	195
APPENDIX A: CALIBRATION INFORMATION.....	202
APPENDIX B: TECHNICAL DATA SHEETS	203
APPENDIX C: CLASSICAL LAMINATION THEORY (CLT) MATLAB CODE	215
BIOGRAPHY OF THE AUTHOR.....	233

LIST OF TABLES

Table 1: Elium Resin Properties of a 4-mm Unfilled Casting [20]	12
Table 2: Technical Properties of IE 5842 Thermoplastic Prepreg [30]	18
Table 3: Common Properties of Two Infusible Resin Systems	22
Table 4: Processing Times & Parameters for Two Polymer Systems [20] [33]	26
Table 5: Composite Laminate Results from Two Polymer Systems	26
Table 6: Manual Stamp Forming Parameters for IE 5842 PETg Prepreg Tapes	30
Table 7: Manual Stamp Forming Results for Trial 1-6.....	31
Table 8: Automated Thermoforming Trial 2 Processing Parameters	36
Table 9: Automated Stamp Forming Results for Trial 2-2.....	36
Table 10: IE 5842 Automated Thermoforming Trial 3 Processing Parameters	39
Table 11: Trial 3 IR Oven Settings	39
Table 12: Automated Stamp Forming Results for Trial 3-1	39
Table 13: IE 5842 Automated Thermoforming Trial 4 Processing Parameters	42
Table 14: Trial 4 IR Oven Settings	42
Table 15: TailorGen Welding Parameters for Trial 5 Processing.....	44
Table 16: IE 5842b Trial 5 Concrete-CFRTP stud Panel Processing Parameters	45
Table 17: Trial 5 IR Oven Settings	45
Table 18: Automated Stamp Forming Results for Trial 5-1	46
Table 19: IE 5842b Automated Thermoforming Trial 6 Processing Parameters	48
Table 20: Trial 6 IR Oven Settings	48
Table 21: Automated Stamp Forming Results for Trial 6-1	49
Table 22: Summary of Matrix Material Properties.....	50

Table 23: Summary of Fiber Material Properties	50
Table 24: Specimen Dimensions and Tolerances Summary.....	56
Table 25: Feasibility E-glass/Elium Composite Mechanical Property Results	60
Table 26: Feasibility E-glass/Elium Failure Types.....	62
Table 27: Feasibility E-glass/PETg Composite Mechanical Property Results.....	64
Table 28: Feasibility E-glass/PETg (IE 5842) Sample Failure Types	67
Table 29: Comparison of Longitudinal Thermoplastic Properties to a Thermoset	72
Table 30: Comparison of Transverse Thermoplastic Properties to a Thermoset.....	73
Table 31: Predicted vs Experimental Elastic Properties (E-glass/Elium $V_f = 43.2\%$)	85
Table 32: Predicted vs Experimental Elastic Properties (E-glass/Derakane $V_f = 40.0\%$) 86	
Table 33: Predicted vs Experimental Elastic Properties (E-glass/PETg $V_f = 36.4\%$)	87
Table 34: Predicted vs Experimental Strength Properties	88
Table 35: Detailed E-glass/Elium UD Sample Failure Types	93
Table 36: E-glass/Derakane UD Failure Types	97
Table 37: IE 5842b E-glass/PETg UD Failure Types.....	101
Table 38: E-glass/PETg [+/- 45 90 0]s Composite Mechanical Property Results.....	103
Table 39: IE 5842b E-glass/PETg [+/- 45 90 0]s Failure Types.....	106
Table 40: Friction Welding TP Stud Shear Test Matrix	120
Table 41: Double TP Stud Shear Specimen Results.....	140
Table 42: Single TP Stud Shear Specimen Results	144
Table 43: Single TP Stud Shear Mobile Welder Specimen Type 5 Sample Results	148
Table 44: Concrete-TP/CFRTP Stud Test Matrix	151
Table 45: IE 5842b Friction Welded Concrete-TP Stud Test Results	160

Table 46: E-glass/Elium 150 Infused Concrete-CFRTP Stud Test Results.....	161
Table 47: Concrete-TP and Concrete-CFRTP Stud Comparison	172
Table 48: Major Testing Equipment Calibration Information	202

LIST OF FIGURES

Figure 1: Elevation View of Composite-Concrete Hybrid Beam Concept.....	4
Figure 2: Reduced Table Adapted from Tangram Periodic Table of Thermoplastics.....	15
Figure 3: Vacuum Infusion Fabrication Setup.....	20
Figure 4: Typical Vacuum Infusion Setup at the ASCC.....	24
Figure 5: Infused UD Elium 150 Panel.....	25
Figure 6: Infused UD Derakane 610-C Panel.....	25
Figure 7: Manual Stamp Forming Press.....	28
Figure 8: Trial 1-6 Consolidated Laminate (IE 5842).....	29
Figure 9: Dieffenbacher Fiber Forge Relay 2000 Tape Layup Machine.....	32
Figure 10: Techni-Modul Infrared (IR) Oven.....	33
Figure 11: 650 Metric Ton Utah Hydraulic Press.....	34
Figure 12: Trial 2-1 IE 5842 Thermoformed Part.....	35
Figure 13: Improved UD PETg Thermoformed Panel.....	38
Figure 14: Pre-Consolidated PETg Prepreg in Aluminum Consolidation Frame.....	40
Figure 15: IE 5842b Consolidated Concrete-CFRTP stud Tailored Blank.....	47
Figure 16: Coordinate Systems for a Composite Lamina and Laminate.....	53
Figure 17: ASTM Standard Test Fixture Setups.....	57
Figure 18: Feasibility E-glass/Elium Long. Tension Stress-Strain Response.....	61
Figure 19: Feasibility E-glass/Elium Long. Compression Stress-Strain Response.....	61
Figure 20: Feasibility E-glass/Elium In-Plane Shear Stress-Strain Response.....	61
Figure 21: Feasibility E-glass/Elium XGM Failure Long. Tension Sample.....	62
Figure 22: Feasibility E-glass/Elium BGM Failure Long. Compression Sample.....	62

Figure 23: Feasibility E-glass/Elium HGN Failure In-Plane Shear Sample.....	63
Figure 24: Feasibility E-glass/PETg Long. Tension Stress-Strain Response	65
Figure 25: Feasibility E-glass/PETg Trans. Tension Stress-Strain Response	65
Figure 26: Feasibility E-glass/PETg Bias Tension Stress-Strain Response	66
Figure 27: Feasibility E-glass/PETg Long. Compression Stress-Strain Response.....	66
Figure 28: Feasibility E-glass/PETg Trans. Compression Stress-Strain Response	66
Figure 29: Feasibility E-glass/PETg Bias Compression Stress-Strain Response	66
Figure 30: Feasibility E-glass/PETg In-Plane Shear Stress-Strain Response.....	67
Figure 31: E-glass/PETg UD Multiple Failures Long. Tension Samples.....	69
Figure 32: E-glass/PETg UD Failed Trans. Tension Sample	69
Figure 33: E-glass/PETg Bias Modified N2 Tension Sample	70
Figure 34: E-glass/Elium UD HAT Failure Trans. Compression Sample.....	70
Figure 35: E-glass/PETg UD VGN Failure In-Plane Shear Sample.....	70
Figure 36: Tensile Stress-Strain Response of Representative Samples.....	76
Figure 37: Compressive Stress-Strain Response of Representative Samples.....	76
Figure 38: In-Plane Shear Stress-Strain Response of Representative Samples	77
Figure 39: Comparison of Long. Elastic Modulus for Various Fiber-Orientations.....	90
Figure 40: E-glass/Elium UD Longitudinal Tension Stress-Strain Response	92
Figure 41: E-glass/Elium UD Transverse Tension Stress-Strain Response	92
Figure 42: E-glass/Elium UD Longitudinal Tension Stress-Strain Response	92
Figure 43: E-glass/Elium UD Transverse Compression Stress-Strain Response	92
Figure 44: E-glass/Elium UD In-Plane Shear (G_{xy}) Stress-Strain Response.....	93
Figure 45: E-glass/Elium UD In-Plane Shear (G_{yx}) Stress-Strain Response.....	93

Figure 46: E-glass/Elium UD DGM Failure Long. Tension Sample.....	94
Figure 47: E-glass/Elium UD VSA Failure (G_{xy}) In-Plane Shear Sample	95
Figure 48: E-glass/Derakane UD Long. Tension Stress-Strain Response	96
Figure 49: E-glass/Derakane UD Trans. Tension Stress-Strain Response	96
Figure 50: E-glass/Derakane UD Long. Compression Stress-Strain Response.....	96
Figure 51: E-glass/Derakane UD Trans. Compression Stress-Strain Response	96
Figure 52: E-glass/Derakane UD In-Plane Shear (G_{xy}) Stress-Strain Response	97
Figure 53: E-glass/Derakane UD In-Plane Shear (G_{yx}) Stress-Strain Response	97
Figure 54: E-glass/Derakane UD Multiple Failures Long. Tension Samples	98
Figure 55: E-glass/PETg UD Long. Tension Stress-Strain Response	99
Figure 56: E-glass/PETg UD Trans. Tension Stress-Strain Response	99
Figure 57: E-glass/PETg UD Long. Compression Stress-Strain Response.....	100
Figure 58: E-glass/PETg UD Trans. Compression Stress-Strain Response	100
Figure 59: E-glass/PETg UD In-Plane Shear (G_{xy}) Stress-Strain Response.....	100
Figure 60: E-glass/PETg UD In-Plane Shear (G_{yx}) Stress-Strain Response.....	100
Figure 61: E-glass/PETg [+/- 45 90 0]s Long. Tension Response	105
Figure 62: E-glass/PETg [+/- 45 90 0]s Long. Compression Response	105
Figure 63: E-glass/PETg [+/- 45 90 0]s In-Plane Shear Response	105
Figure 64: E-glass/PETg [+/- 45 90 0]s Failed Tension Sample	106
Figure 65: E-glass/PETg [+/- 45 90 0]s Failed Compression Sample	107
Figure 66: E-glass/PETg [+/- 45 90 0]s Failed In-Plane Shear Sample	107
Figure 67: Drawn Arc Stud Welding [54]	112
Figure 68: T-Hat Cross-Section SOLIDWORKS Model	113

Figure 69: Friction Welding (Spin Welding) Phases	117
Figure 70: 2D Friction Welded Stud Concept Design (mm)	122
Figure 71: 2D Infused Shear Stud Concept Design (mm)	125
Figure 72: Cross-Section of Feasibility Weld.....	128
Figure 73: Instron Welding Setup.....	129
Figure 74: Initial Instron Welding Trial Specimen with neat-resin PETg.....	130
Figure 75: Failed Initial Instron Welding Trial Specimen.....	130
Figure 76: Instron Welded Specimen with CFRTP Plate	131
Figure 77: Mobile Device Welding Setup	132
Figure 78: Mobile Welded Stud to IE 5842.....	133
Figure 79: Mobile Welded Stud to IE 5842b.....	133
Figure 80: Vacuum Infused Shear Stud Mold (Half) Concept Design.....	134
Figure 81: Rolled E-BX 2400 Double Bias E-glass [78] for Infused Stud.....	135
Figure 82: E-glass/Elium Shear Stud Infusion Result	136
Figure 83: Untested Vacuum Infused Elium Shear Studs	136
Figure 84: TP Stud Shear Testing Custom Fixture.....	138
Figure 85: Double TP Stud Shear Specimen (front).....	138
Figure 86: Double TP Stud Shear Specimen (side)	138
Figure 87: Load-Deformation of Studs in Double TP Stud Shear Loading	141
Figure 88: Failed Instron Welded Double TP Stud Shear Specimen (side 1)	142
Figure 89: Failed Instron Welded Double TP Stud Shear Specimen (side 2)	142
Figure 90: Failed Instron Welded Single TP Stud Shear Specimen	145
Figure 91: Single TP Stud Shear Ductility Comparison.....	146

Figure 92: Load-Deformation of Studs in Single TP Stud Shear	147
Figure 93: Type 5 Mobile Welder Single TP Stud Shear Results	149
Figure 94: Failed Mobile Welded Single TP Stud Shear Specimen.....	149
Figure 95: Concrete-CFRTP Stud 76.2-mm Concept Design	151
Figure 96: Concrete-TP Specimen Plate & Formwork.....	153
Figure 97: Neat-Resin Shear Stud.....	154
Figure 98: Concrete-TP Stud Testing Setup	155
Figure 99: Elium Concrete-CFRTP Stud Configuration 1 (left) & 2 (right)	156
Figure 100: Concrete-TP Stud 76.2-mm Specimen 3-1 Results.....	162
Figure 101: Concrete-TP Stud 152.4-mm Specimen 6-3 Results.....	163
Figure 102: Failed PETg Concrete-TP Stud Specimen (CFRTP side).....	164
Figure 103: Failed PETg Concrete-TP Stud Specimen (Concrete side).....	164
Figure 104: E-glass/Elium Concrete-CFRTP Stud Specimen 4 (8-Studs)	166
Figure 105: Elium Concrete-CFRTP Stud Specimen 5 (8-Studs)	167
Figure 106: Elium Concrete-CFRTP Stud Specimen 5 Failure Mode	167
Figure 107: Untested Configuration 2 Specimen.....	168
Figure 108: Elium Concrete-CFRTP Stud Specimen 3 (4-Studs)	169
Figure 109: Elium Concrete-CFRTP Stud Specimen 2 (4-Studs)	170
Figure 110: PETg Neat-resin PETg Shear Studs Embedded in Concrete	176
Figure 111: E-glass/Elium Shear Studs Embedded in Concrete.....	176
Figure 112: Tested E-glass/Elium Shear Studs (Broken out of Concrete)	177
Figure 113: Stud Single Shear Test Setup (Adapted from Brena et al. [80])	179
Figure 114: Proposed Beam Specimen Concept Design	193

LIST OF EQUATIONS

Equation 1: Fiber Weight Fraction (W_f).....	27
Equation 2: Fiber Volume Fraction (V_f).....	27
Equation 3: Lamina Longitudinal Elastic Modulus (E_1).....	78
Equation 4: Poisson’s ratio in the 1-2 plane (ν_{12}).....	78
Equation 5: Halpin-Tsai Elastic Modulus Parameter (η_E).....	79
Equation 6: Halpin-Tsai Equation for Transverse Elastic Modulus (E_2).....	79
Equation 7: Halpin-Tsai Shear Modulus Parameter (η_G).....	79
Equation 8: Halpin-Tsai Equation for In-Plane Shear Modulus (G_{12}).....	79
Equation 9: Halpin-Tsai Shear Modulus Parameter 4 (η_4).....	80
Equation 10: Halpin-Tsai Equation for Intralaminar Shear Modulus (G_{23}).....	80
Equation 11: Isotropic Relation for Transverse Poisson’s ratio (ν_{23}).....	80
Equation 12: Hill’s Elastic Moduli k for Fibers (k_f).....	80
Equation 13: Hill’s Elastic Moduli l for Fibers (l_f).....	80
Equation 14: Hill’s Elastic Moduli m for Fibers (m_f).....	80
Equation 15: Hill’s Elastic Moduli n for Fibers (n_f).....	81
Equation 16: Hill’s Elastic Moduli p for Fibers (p_f).....	81
Equation 17: Hill’s Elastic Moduli k for Matrix (k_m).....	81
Equation 18: Hill’s Elastic Moduli l for Matrix (l_m).....	81
Equation 19: Hill’s Elastic Moduli m for Matrix (m_m).....	81

Equation 20: Hill’s Elastic Moduli n for Matrix (n_m).....	81
Equation 21: Hill’s Elastic Moduli p for Matrix (p_m).....	81
Equation 22: Hill’s Effective Elastic Moduli k (k).....	81
Equation 23: Hill’s Effective Elastic Moduli l (l).....	81
Equation 24: Hill’s Effective Elastic Moduli m (m).....	81
Equation 25: Hill’s Effective Elastic Moduli n (n).....	81
Equation 26: Hill’s Effective Elastic Moduli p (p).....	82
Equation 27: Hill’s Effective Engineering Longitudinal Elastic Modulus (E_1).....	82
Equation 28: Hill’s Effective Engineering Transverse Elastic Modulus (E_2).....	82
Equation 29: Hill’s Effective Engineering Poisson’s ratio (ν_{12}).....	82
Equation 30: Hill’s Effective Engineering In-Plane Shear Elastic Modulus (G_{12}).....	82
Equation 31: Hill’s Effective Engineering Intralaminar Shear Elastic Modulus (G_{23})....	82
Equation 32: Lamina Longitudinal Tensile Strength (fiber-dominated) (F_{1t}).....	82
Equation 33: Lamina Longitudinal Tensile Strength (matrix-dominated) (F_{1t}).....	83
Equation 34: Lamina Compressive Strength Factor (χ).....	83
Equation 35: Lamina Longitudinal Compressive Strength (F_{1c}).....	83
Equation 36: Lamina Tensile Strength Factor (Λ_{22}^0).....	83
Equation 37: Lamina Transverse Tensile Strength (F_{2t}).....	83
Equation 38: Lamina Transverse Compressive Strength (F_{2c}).....	83
Equation 39: Lamina Shear Strength Factor (Λ_{44}^0).....	83
Equation 40: Lamina In-Plane Shear Strength (F_6).....	84

Equation 41: Reduced Compliance Matrix [$S_{reduced}$]	89
Equation 42: Transformation Matrix [T]	89
Equation 43: Transformed Compliance Matrix	89
Equation 44: Effective Elastic Modulus (E_x)	90
Equation 45: Stud Strength (Double TP Stud Shear)	139
Equation 46: Ductility (Double and Single TP Stud Shear)	139
Equation 47: Stud Strength (Single TP Stud Shear)	147
Equation 48: Critical Buckling Load ($P_{critical}$)	178

CHAPTER 1

INTRODUCTION

1.1 Project Background

The U.S. Army Engineer Research and Development Center (ERDC) has an interest in investigating methods for low-logistic, rapidly deployable, versatile, load-bearing thermoplastic composite-concrete structures. The Advanced Structures and Composites Center (ASCC) is working with ERDC to research the feasibility of this technology and methods for implementing it. These systems being considered for the future of this technology may include beams, decking, columns, and retaining walls. This thesis details the research done in exploring the feasibility of using thermoplastic composites as an alternative to traditional structural methods of constructing hybrid composite-concrete beams as a first step in assessing this technology.

Additionally, infrastructure is a critical industry in the United States and abroad. In the U.S., nearly all money spent on transportation infrastructure comes from federal, state, and local governments. The need for investment in American infrastructure was made apparent by the 2017 *Infrastructure Report Card* by the American Society of Civil Engineers (ASCE) which gave America's cumulative infrastructure a D+ score overall [1]. This recent and insightful report puts America's current infrastructure in perspective. The report begins with "Our nation is at a crossroads. Deteriorating infrastructure is impeding our ability to compete in a thriving global economy, and improvements are necessary to ensure our country is built for the future. While we have made some progress, reversing the trajectory after decades of underinvestment in our infrastructure requires transformative action from Congress, states, infrastructure owners, and the American people." [1]. The

research done in this study explores new technologies that could be used in making the necessary infrastructure improvements America needs by adding potential new options for bridges and other structures.

What generates an interest in thermoplastic materials for use in composites over traditional thermosetting plastic materials (thermosets)? Before exploring this question, it is necessary to define the difference between the two materials. Thermoplastic polymers can be defined as materials that reach their melting temperature before their decomposition temperature. Thermosetting materials however, reach their decomposition temperature before their melting temperature [2]. Further, thermosets can be described as, “materials that are liquid or malleable in their initial state but are converted into a solid form. The conversion process involves a chemical reaction typically triggered by heat, oxygen, UV light, a reagent material or catalyst. Regardless of their initial state, the important thing to remember about thermosets is that the conversion process is irreversible.” [3]. Thermoplastics on the other hand can be described as, “materials which melt upon heating, and solidify upon cooling. During the molten phase (which usually involves heat and pressure), the materials are malleable and can be easily formed into another shape. Upon cooling they become a solid, and retain that shape. The melting/solidifying process is fully reversible, and most thermoplastic materials can be molded again and again and again.” [3]. More detail on the differences between these materials will be explored in this thesis. In addition, the properties of thermoplastics make them more amenable to rapid and automated manufacturing methods, which are addressed in this study.

This study was born from a desire to conduct exploratory research into utilizing these emerging thermoplastic materials in hybrid structural applications. It was proposed that the

thermoplastic materials could be used in similar ways to industry use of thermoset composites and even steel construction. The question is, are thermoplastics capable of meeting these structural needs? This study ventures to answer that question by exploring thermoplastic composite material characteristics, methods for reinforcing concrete in a hybrid structure, and developing a novel way to achieve the necessary composite action.

1.2 Significance of Research & Objectives

The study of thermoplastic composites as an alternative to traditional thermosets and steel construction is important. In conjunction with ERDC the ASCC is working to develop feasible methods for the implementation of thermoplastic composite-concrete structures.

The study is divided into four objectives, which encompass the started goal.

Study Objectives:

1. Literature review, material investigation, and selection
2. Material characterization through standardized mechanical testing
3. Hybrid composite-concrete load-bearing structural concept design
4. Assessment of thermoplastic shear connectors to develop composite action

In the early stages of the conceptual designs, it was decided to focus on the development of a small-scale hybrid composite-concrete beam for this feasibility study. Further decisions were made in order to focus the objectives of this study. The fiber reinforcement chosen for this study was continuous unidirectional E-glass due to its cost-effectiveness and good mechanical properties, which can support the reinforcement needs of beams and decking in most cases. In addition, two thermoplastic materials were chosen to combine

with the E-glass to fabricate the composites for this study. Choosing two thermoplastics for the matrix in the composite allows for a multi-point comparison with existing thermoset materials such as an epoxy vinyl-ester. The composite constructed from continuous E-glass reinforcement and thermoplastic matrix will be referred to as CFRTP for continuous fiber-reinforced thermoplastic composite. The basic two-dimensional concept design for the beam in this study for demonstrating the feasibility of a hybrid thermoplastic composite-concrete load bearing system is shown in Figure 1.

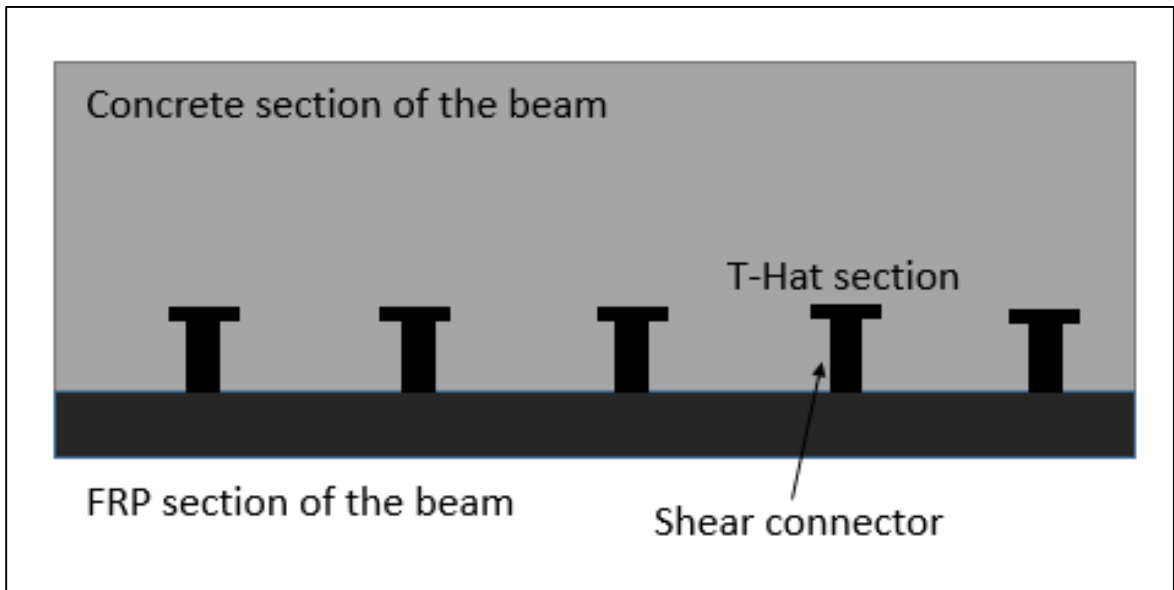


Figure 1: Elevation View of Composite-Concrete Hybrid Beam Concept

The beam shown would be constructed with flat composite reinforcement on the bottom face of the beam to reinforce the structure in tension, replacing normal steel tension reinforcing. The composite tension reinforcement is mechanically attached to the concrete with thermoplastic shear connectors that mimic shear studs used in steel-concrete composite beams. Replacing steel as the tension-reinforcement with composites has the advantage of eliminating corrosion concerns, and using a mechanical connection

eliminates the need for adhesives, which often require rigorous surface preparation, have long cure times, and require a secondary process to be performed in the construction. These adhesives, which are often used with thermosets, may not be compatible with the thermoplastic polymers being explored and increase the construction difficulty significantly. The normal weight concrete used in this study had a specified compressive-strength of at least 41.4-MPa (approx. 6000-psi).

Significant effort was devoted to the investigation of the connection interface for the composite-concrete beam. The major considerations that were taken into account when assessing shear connector types were the following.

- Manufacturability
- Ease of construction
- Shear Strength at the Interface
- Resistance to Pullout

When taking these four major points into account, it was decided that a purely mechanical connection is the best method for optimizing the design since it can be achieved as part of the concrete pouring process. This is also consistent with assumptions made when designing with traditional steel connectors. Traditional methods for using thermoset composites to reinforce concrete rely on adhesive bonds or mechanical fasteners. Adhesive bonding requires extensive surface preparation and is difficult to achieve with thermoplastics.

This thesis presents material characterization, concept designs for load-bearing hybrid structures, and the development of novel, purely mechanical methods for developing

composite action by utilizing the advantages of thermoplastic materials. The exploration of thermoplastic materials as potentially feasible options in structural applications advances the state-of-the-art by contributing valuable groundwork for their further research and potential application.

1.3 Organization of this Thesis

This thesis is divided into five chapters, which cover the work done to achieve the study objectives.

- Chapter 1: Introduction, covers the project background and the significance of this research and its detailed objectives.
- Chapter 2: Material Selection & Manufacturing Methods, covers the criteria for selection of two thermoplastic materials and the methods for fabricating composites with them.
- Chapter 3: Material Characterization, covers the analysis of physical and mechanical properties, generated through standardized test methods to characterize the fabricated thermoplastic composites.
- Chapter 4: Shear Connectors, covers the shear connectors developed, designed, and tested in order to develop composite action in the proposed hybrid load-bearing structure.
- Chapter 5: Conclusions & Recommendations, explains how the four thesis objectives have been accomplished by presenting the main findings and contributions of the thesis with a bullet list of conclusions and the recommendations for the future research.

CHAPTER 2

MATERIAL SELECTION AND MANUFACTURING

The first objective in this thesis was to conduct literature review, material investigation, and selection to assess possible options for using thermoplastics reinforced with continuous fibers as tension reinforcement in concrete beams. These materials are called continuous fiber-reinforced thermoplastic composite materials (CFRTP) to differentiate them from common thermoplastic composites with discontinuous and short-fiber reinforcement. The type of fiber reinforcement adopted for this thesis is E-glass fibers due to their lower cost compared to other types of fibers (e.g., carbon fibers).

After the literature review based on performance, cost, and manufacturing methods, two CFRTP materials were selected for experimental characterization. These materials were fabricated using vacuum infusion, a longstanding and highly accepted process traditionally used for manufacturing thermoset composites; and stamp thermoforming, a fast production process that takes advantage of the ability of thermoplastic materials to be heated and reformed with little to no loss of strength and stiffness.

2.1 Thermoplastic Composite Material Selection

A literature review of thermoplastics and an assessment of their properties relevant to structural applications including corrosion resistance, amenability to rapid manufacturing, impact resistance, high strength-to-weight ratio, and recyclability was undertaken at the start of this study. Two thermoplastic materials were chosen based on this review: Elium, an acrylic two-part liquid thermoplastic resin, and polyethylene terephthalate glycol (PETg) pre-impregnated (prepreg) tapes.

A brief overview of some publications reviewed at the beginning of this study pertaining to composites is given here. Composites are suitable for both chemical and outdoor exposure because they do not rust or corrode. The resin used in composite applications not only serves to bind the fiber-reinforcement together but also protects it from the environment the material is subjected to [4]. Many thermoplastic composites have good to excellent chemical and environmental resistance, the performance of particular polymers can be found in literature [5] [6].

The high strength-to-weight ratio of composites is a well-known advantage over other materials such as steel. This comes from their uniquely high strength and stiffness and low density [7]. Examining the stiffness-to-weight ratio of composites it is possible to achieve lighter weight structures with the same properties, due to the very low densities of thermoplastics, approximately 1/8 to 1/10 that of steel [3]. The impact resistance of materials is often linked to its toughness [3]. Thermoplastics in general exhibit high toughness due to having high fracture energy values and the ability to absorb energy without brittle failure. Thermosetting polymers tend to show more brittleness due to the high level of cross-linking in the polymers not is not present with thermoplastics [8] [9].

Thermoplastic materials are especially suitable for rapid manufacturing based on their ability to be processed from raw material to end use product in fewer steps than would be necessary with other options. In addition, thermoplastic materials are often suitable for the fabrication of near-net shape manufacturing. Processing technologies used with thermoplastics such as stamp forming (pressure molding) and injection molding allow for a part to be fabricated into its final or net shape in a single operation. Often times processing technologies with other materials require multiple steps or several discrete parts to achieve

the same thing a single thermoplastic part does [3] [10]. This study has not investigated all forms of thermoplastic manufacturing but it is of note that thermoplastic composites are not limited to the size of stamp forming presses or other size limiting technologies, continuous processing methods such as roll forming or pultrusion. Thermoplastic pultrusion is capable of manufacturing long constant cross-section fiber-reinforced composites by pulling fibers impregnated with matrix through a die [10].

Investigating the cost of thermoplastic composites does not only include the cost of material itself, but also the cost to take the raw materials and make them into an end use product. Many resources in literature allow for the comparison of different thermoplastic resin systems in regard to cost [9] [11] [12] [6], in many cases, the costs of thermoplastic materials are lower than other choices [3]. A useful tool for assessing the relative costs of thermoplastic polymers is the Tangram Periodic Table [13]. As was previously discussed thermoplastic materials can often achieve the same end use product in fewer steps than other material options. The ability to reduce the amount of work than needs to go into producing a product reduces the cost of making that product, contributing to the potential cost savings of using thermoplastic materials [3].

A unique feature of thermoplastic composites over thermoset composite technologies is the ability to recycle them. Thermoplastics are easily recycled because the polymer chains do not degrade when melted down, thermoplastics polymers are held together by van der waal forces, which attract molecules to each other. These are broken at lower temperatures than ones which damage the chemical bonds between monomers allowing the thermoplastic polymer to be melted and reformed repeatedly [14] [15]. A common method of recycling

a thermoplastic composite after use is to grind up the composite and reuse the compounds through injection molding [16].

The particular E-glass fiber materials chosen depend on the fabrication system being used, but were selected to be continuous fibers for their relatively high strength and stiffness properties. The Elium resin system uses dry E-glass fiber reinforcement suitable for vacuum infusion, and PETg prepreg is reinforced with E-glass fiber provided by the manufacturer.

2.1.1 Elium Acrylic Liquid Resin System

One product, Elium by Arkema, was identified early in the study. Elium is an in-situ polymerized infusible thermoplastic resin system, which was chosen due to favorable mechanical properties reported by the manufacturer Arkema, its unique recycling abilities, and the following manufacturing advantages for vacuum infusing Elium [17]:

- Viscosity of 100 mPa.s at ambient temperature, which is suitable for infusing structural parts
- Uses the vacuum resin infusion process
- Manufacturing process compatible with thermoset resin tooling
- Can be post-thermoformed (heated consolidation, welding, gluing)

During the literature review, it was found that Elium is the first liquid thermoplastic commercialized to be used in similar ways to thermosetting composites. Elium works by combining two liquid constituents: the first is a combination of a methyl methacrylate and acrylic copolymers, [18] and the second, an organic peroxide activator [19]. When mixed, the resin undergoes radical polymerization to produce a thermoplastic which can be

combined with a fiber understructure to form a composite [20]. This process can be done at room temperature using equipment designed for use with thermosetting resins in vacuum infusion, resin transfer molding (RTM), and is a styrene free process [17]. Styrene is a common chemical in the composites industry for many reasons; particularly, it is a primary ingredient in unsaturated polyester resin. Styrene is a key crosslinking agent in these resin systems, however it has a particularly strong odor and is a potentially hazardous material [21].

The reported viscosity and mechanical properties of the Elium resin system were a major contributing factor in the choice to include it as one of the two thermoplastic materials in this study. Viscosity is a critical property when infusing composite materials because it controls how well the resin flows through the dry fabric part during infusion. This can affect the complexity and size of parts that are possible for fabrication. The reported Brookfield LVF #2 viscosity at 25 degrees Celsius is 100 mPa.s for Elium 150 [20]. The viscosity of Elium is comparable to other liquid resin systems used for vacuum infusion and RTM, which are typical in the composites industry. Table 1 gives the reported values for a 4 mm neat-resin casting of Elium provided by Arkema [20].

Table 1: Elium Resin Properties of a 4-mm Unfilled Casting [20]

Technical Property	Value	ISO Method Used
Tensile Strength	76 MPa	527
Tensile Modulus	3.300 MPa	527
Tensile Deformation	6 %	527
Compressive Strength	130 MPa	684
Flexural Strength	130 MPa	178
Flexural Modulus	3.250 MPa	178
Specific Gravity	1.19	1183
Heat Deflection Temperature	109 C	75/A
Maximum Continuous Service Temperature	85 C	-
Coefficient of Linear Expansion	65×10^{-6} mm/mm/C	2155-1
Water Uptake (8 days)	0.5 %	62
Rockwell Hardness (M)	100	2039
Shore D Hardness	85-90	868
Fracture Toughness Stress Intensity, K_{1C}	$1.2 \text{ MPa}\cdot\text{m}^{0.5}$	13586

One other feature of this resin system that resulted in its selection is its ability to be recycled in two ways. One method is through mechanical recycling, which involves grinding up the composite at the end of its life and heating the resulting granules to reform them into new parts. This is similar to methods of recycling used with other thermoplastic composites. The second is reactive recycling, which also begins with the process of grinding the composite parts, followed by heating the fragments in order to recover the constituent materials through de-polymerization. Once the initial raw materials have been recovered, the monomer can be reused in a variety of ways to make new composites [22]. This method of reactive recycling is a unique trait of Elixir, which gives composites made with it more versatility at the end of their service life.

The E-glass fiber chosen for the vacuum infusion of Elixir panels for mechanical testing in this study was E-LR 1208 [23] by VectorPly Performance Composite Reinforcements. This stitched E-glass unidirectional (UD) fabric has a weight of 405 g/sq.m (11.95 oz/sq.yd) with a 31 g/sq.m (0.90 oz/sq.yd) polyester veil. This fabric is ideal for resin infusion due to the veil, which aids in resin travel through the composite during the fabrication process. The choice of a UD fabric was ideal for coupon testing because the results are easily compared with predictions from classical lamination theory (CLT), which is widely used in composite design.

2.1.2 E-glass/PETg Pre-Impregnated Tapes

The second material in this study, a pre-impregnated (prepreg) unidirectional (UD) tape was chosen to utilize available rapid manufacturing of thermoplastic composites using heated consolidation. This was done at the ASCC using two common processes: manual stamp forming and automated stamp forming. Stamp forming uses heated consolidation to

generate laminates from tailored blanks. More details on this process are given in the manufacturing sub-section.

The literature review conducted showed that there are eight major companies which produce thermoplastic prepreg tapes in various types. These eight companies are Polystrand (PolyOne), TenCate, Barrday, Tohotenax, SGL Group, Porcher, Celanese and Vector Systems. Of these eight companies only Polystrand, TenCate, SGL, Celanese and Vectorams list the capability to make glass-fiber reinforced tapes. Each of these companies offers different polymer capabilities, which are:

- Polystrand: PETg, PP Homopolymer, PP Copolymer [24]
- TenCate: PEKK, PAEK, PEEK, PPS, PET, PA6, PP, HDPE [25]
- SGL Group: Polyamide 6 (Nylon), ** [26]
- Celanese: ABS, TPU, HDPE, POM, PP, PVDF, PA12, PA6, PES, PBT, PET, PA66, PPS, PPA, PEEK [27]
- Vector Systems: PEEK, PEI, PPS, PP, PE, PC, PET, PES, PBT, (Nylon) PA12, PA11, PA6, PA6.10, PA4.1, PEKK) [28]

*** Reports that thermoplastic of choice can be used but does not give specifics.*

When comparing these options as potential choices many factors were taken into consideration: formability, balance between amorphous and crystalline structure, processing temperature, mechanical properties, and cost-effectiveness. A useful tool that was used in the first phase of the selection process is the Tangram Periodic Table of Thermoplastics [29], which was used to generate a reduced table for the materials considered in this study, shown as Figure 2.

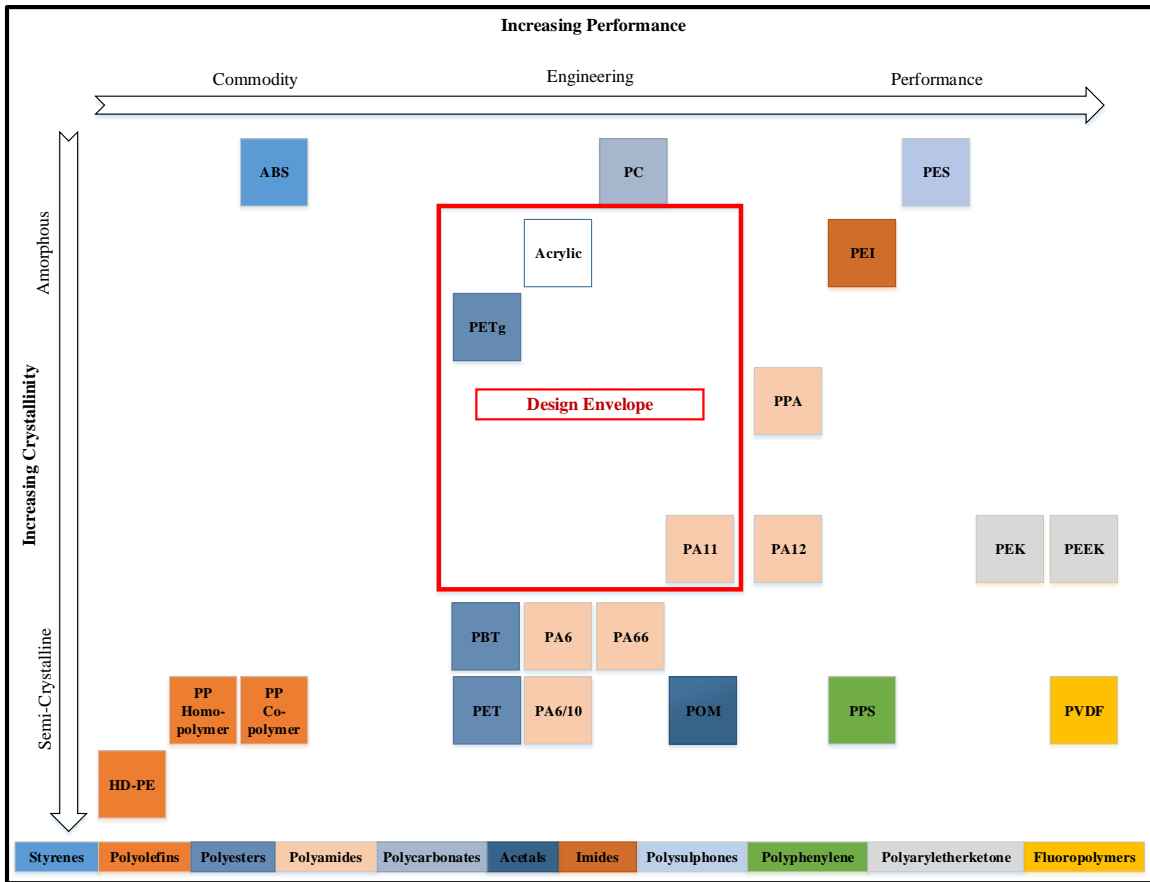


Figure 2: Reduced Table Adapted from Tangram Periodic Table of Thermoplastics

Figure 2 visually represents the level of crystallinity and performance of a variety of thermoplastics. One polymer was added to the chart which was not on the Tangram table, acrylic, to represent the Elium polymer in reference to other available options. The position of Acrylic was based on the available properties provided by Arkema and represents this study's best estimate of its relative performance and crystallinity position. For the purposes of this study, a desirable polymer choice would meet the following remaining criteria:

- Good mechanical properties
- Readily available and cost-effective
- Balance of amorphous and crystalline structure

- Relatively amenable to processing

Polymers from the Engineering region of the performance scale and near the middle of the crystallinity range on Figure 2 meet the first and third criteria in the bulleted list. Polymers in the performance range may have higher mechanical properties but are less cost effective. Comparing the available UD tapes from Polystrand, TenCate, SGL Group, and Vector Systems to the described area shown as the design envelope on Figure 2, PETg and PA 11 are desirable options.

These two options best meet the balance of crystallinity and are considered engineering grade thermoplastics. PETg was chosen because it met the criteria for the second material choice in this study and is a polymer identified as of interest to ERDC, our collaborator on this project. PETg was viewed as more desirable than PA 11 for this study due to being more amorphous and therefore more formable for these initial manufacturing trials.

The PETg sourced for this study came from Polystrand (PolyOne) and came in two different forms; IE 5842 an E-glass/PETg prepreg tape and IE 5842b an E-glass/PETg prepreg tape which were used for different phases of the study.

The first, IE 5842, came on a roll 635-mm (25-inch) wide with the E-glass fiber reinforcement running in the length direction. The PETg resin in this prepreg comes in its natural form, a green color. This material was used for the initial feasibility trials for fabricating PETg/E-glass laminates through stamp forming.

Once feasibility was shown the second version of the material was acquired, IE 5842b. This is the same base material as IE 5842, however the resin is dyed black, as indicated by the “b” in the technical designation, rather than being left un-dyed in its natural color. The

IE 5842b material originally came on a roll like IE 5842, but was slit to various widths between 50-mm and 150-mm for use with the Dieffenbacher tape layup machine at the ASCC. The IE 5842b variation of the material was advantageous for many reasons, which are elaborated in the manufacturing sub-section of this chapter.

The technical properties of both PETg variations procured from Polystrand are taken from the provided technical data sheet that is shared for both materials and are given in Table 2.

Table 2: Technical Properties of IE 5842 Thermoplastic Prepreg [30]

Technical Property	Value	Method
Glass Content	58 wt%	ASTM D3647
Areal Weight	405 g/m ²	-
Thickness	0.3 mm	-
Longitudinal Tensile Strength	571 MPa	ASTM D3039
Longitudinal Tensile Modulus	28.5 GPa	ASTM D3039
Transverse Tensile Strength	1.5 MPa	ASTM D3039
Transverse Tensile Modulus	0.52 GPa	ASTM D3039
Longitudinal Compressive Strength	29.5 MPa	ASTM D6641
Longitudinal Compressive Modulus	0.71 GPa	ASTM D6641
Transverse Compressive Strength	5.5 MPa	ASTM D6641
Transverse Compressive Modulus	0.26 GPa	ASTM D6641
In-Plane Shear Strength	21 MPa	ASTM D7078
In-Plane Shear Modulus	0.21 GPa	ASTM D7078
Transverse Shear Strength	6.7 MPa	ASTM D7078
Transverse Shear Modulus	0.17 GPa	ASTM D7078
Flexural Strength	602 MPa	ASTM D790
Flexural Modulus	4.18 GPa	ASTM D790
In-Plane Poisson's Ratio	0.27	ASTM D3039

During this study, an independent investigation was undertaken at the ASCC to further investigate the properties of commercially available thermoplastic materials [31], which was beneficial in supplementing the review done for this study during material selection.

Polyethylene terephthalate (PET) has homogenous monomers that are arranged in a semi-crystalline fashion, a highly ordered and closely packed solid-state molecular structure [31]. Glycolized polyethylene terephthalate (PETg) is a co-polyester created to be more amorphous and formable than the base polymer PET.

A summary of the advantages of PETg polymer as a matrix for composites is given below.

- Competitive engineering mechanical properties
- Availability and cost-effectiveness
- Balance between amorphous and crystalline structure
- Relatively low processing temperatures

In addition, PETg can be used in injection molding, extrusion blow molding, and 3D printing due to its amorphous nature. Due to its amorphous nature, PETg is a forgiving material for 3D printing, and is rated as equally easy to print as PLA, which is often considered the easiest material to print [32]. As 3D printing grows in interest and becomes more versatile, the ability to use this polymer in fiber-reinforced thermoplastics as well as print it in filament form could be of interest.

2.2 Manufacturing Methods

Both thermoplastic materials chosen were manufactured with E-glass reinforcing fibers. E-glass composites were fabricated in a vacuum infusion process similar to what is

traditionally done with thermosets. Whereas PETg composites were formed through stamp forming of prepreg tapes.

2.2.1 Vacuum Infusion Consolidation

The vacuum infusion process is widely accepted in the composites industry and has a straightforward setup, which requires minimal lab equipment. Figure 3 displays a setup showing the key components of the process. First, dry E-glass fibers are placed on an aluminum or glass surface treated with a mold release agent. Then a non-stick layer—referred to as ‘peel-ply’ – is applied to the top of the glass to prevent the part from sticking to the bag. Flow media is placed on top of the peel-ply to assist in resin travel as well. Then lines are put in place for the vacuum pump and resin inlet (as shown), and the part is enclosed in a bag and pulled under a vacuum.

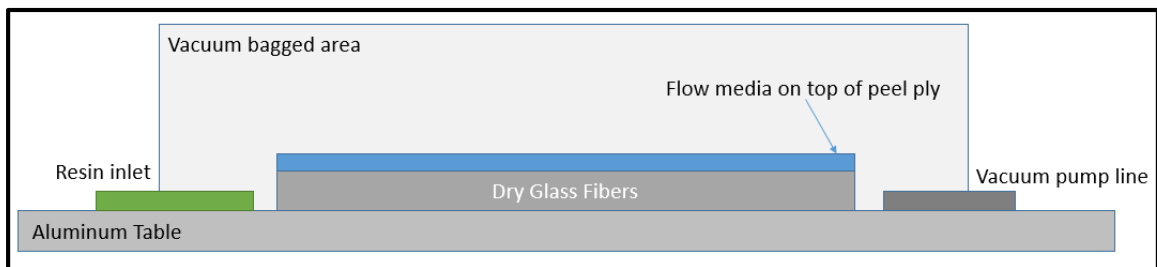


Figure 3: Vacuum Infusion Fabrication Setup

Although this process is labor-intensive, it has a variety of advantages, which are outlined in the following bulleted list.

- Infusion allows for the fabrication of large parts
- Infusion can be done over a mold or specified shape
- Parts can be made with various weights of dry fabrics

- External heating or consolidation under pressure is not required

Elium has the unique ability as an in-situ two-part thermoplastic to be used with existing thermosetting fabrication processes. Since Elium is fabricated using two parts, a monomer and a peroxide activator, it is uniquely suited to existing thermosetting fabrication processes, such as vacuum infusion. As part of testing the feasibility of Elium it was decided that the infusions for acquiring mechanical properties would be repeated with a common thermoset as the resin in order to show that Elium is suitable for similar applications. Derakane 610-C by Ashland was chosen as the thermosetting resin system because it is commonly used in structural applications and is familiar to the ASCC. The use of this system allowed for the knowledge and skill acquired through using thermosets to be used in the fabrication of Elium.

Many properties of a resin system affect how well it will perform in a variety of ways. For vacuum infusion, one of the most important properties is the viscosity of the resin since this controls how easily the resin will flow through the part during the infusion process. Important performance properties are the strength, modulus, and heat deflection temperature. Some of these common properties of the two discussed infusible resin systems are reported in Table 3. The properties chosen in this table are ones reported on both the technical data sheets for Elium 150 and a comparable engineering thermoset resin system Derakane 610-C.

Table 3: Common Properties of Two Infusible Resin Systems

Property	Elium 150 [20]	Derakane 610-C [33]	Elium Method Derakane Method
Viscosity (25 C)	100 mPa.s *	130 mPa.s **	Brookfield (LVF*, LVT**)
Specific Gravity	1.19	1.07	-
Tensile Strength	76 MPa	71 MPa	ISO 527 ASTM D638
Tensile Modulus	3300 MPa	3530 MPa	ISO 527 ASTM D638
Compressive Strength	130 MPa	-	ISO 684
Flexural Strength	130 MPa	129 MPa	ISO 178 ASTM D790
Flexural Modulus	3250 MPa	3920 MPa	ISO 178 ASTM D790
Heat Deflection (Distortion) Temperature	109 C	76 C	ISO 75/A*** ASTM D648

*** ISO 75 reported for both resin systems, A only specified for Elium.

It should be noted that the Elium 150 sheet specifies only ISO standards whereas the Derakane 610-C sheet specifies both ISO standards and analogous ASTM standards. Several iterations of Elium composite panels were vacuum infused at the ASCC as a part

of this study. This was necessary because of the lack of familiarity with the Elium 150 resin system at the start of this study.

The first panels made with Elium were unidirectional because that is the most suitable for mechanical testing to find base properties of a composite for use with classical lamination theory (CLT). These early UD panels experienced warping as the resin polymerized due to the shrinking which occurs during this process. The first round of material testing with Elium dealt with this shrinking by having a 90-degree layer on the surface of the composite and post curing the panels after infusion at 80 degrees Celsius for four hours [20]. As more experience was acquired with Elium and the vacuum infusion process, fully unidirectional panels could be fabricated without noticeable warping effects from shrinkage during polymerization. Mechanical testing was done with both the original $[90, 0, 0, 0]_s$ panels and the later iteration $[0]_{10}$ panels of E-glass/Elium composite. The results of this testing are discussed in chapter three of this thesis.

Fully UD vacuum infusions were also done using Derakane 610-C as a part of this study. This was done in order to facilitate a fair comparison between the thermoplastic Elium resin system and a thermosetting resin system. Infusions with both resin systems used for comparison were done in close proximity to each other using the same fabrication methods and glass fiber reinforcement.

Figure 4 show a typical UD infusion setup conducted at the ASCC. The second phase of vacuum infused coupon testing conducted was done in this manner to get the most comparable results from the two resin systems.

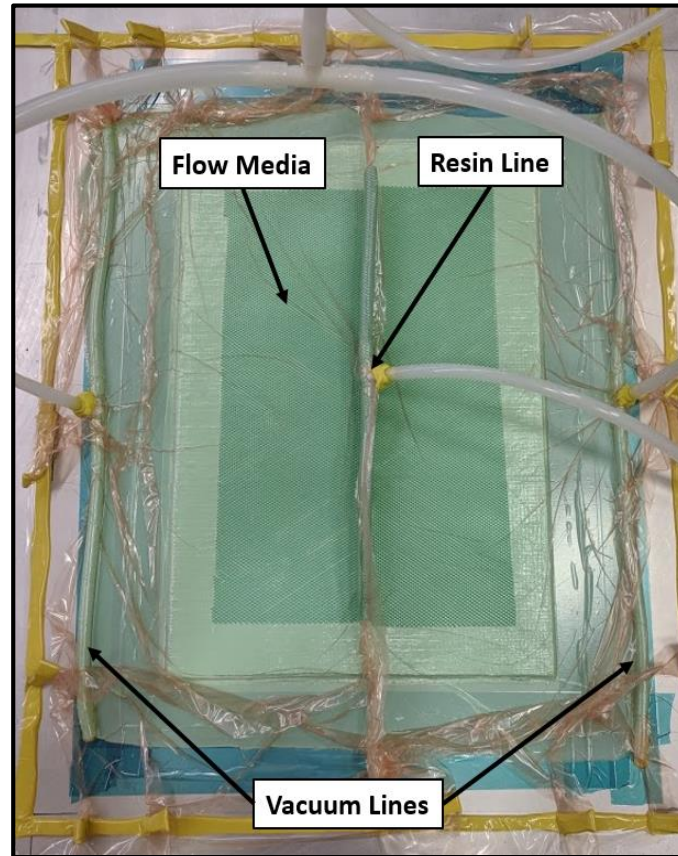


Figure 4: Typical Vacuum Infusion Setup at the ASCC

Note that in these infusions, the resin line is in the center of the part and the vacuum lines are on two sides. This is advantageous because if there is a leak in the setup it will be pulled to the side outside of the composite part. This is done because it provides a more complete wet out in the part during the infusion.

Figure 5 and Figure 6 show infused composite panels reinforced with 10-layers of E-LR 1208 UD E-glass fibers 38.1-cm (15-inches) by 53.34-cm (21-inches) in size using Elium 150 and Derakane 610-C resin-systems respectively.



Figure 5: Infused UD Elium 150 Panel

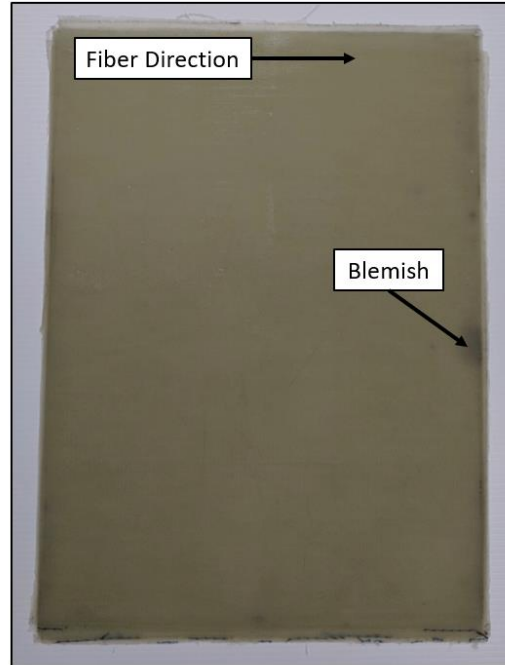


Figure 6: Infused UD Derakane 610-C Panel

The two infused panels are very similar in nature; cured Elium 150 has a light green color whereas Derakane 610-C has a darker, more yellow-green color when cured. The infused Elium panel in Figure 5 is seen to be free of internal blemishes though peel ply has stuck to the sides of the panel. The infused Derakane panel in Figure 6 has one blemish shown on the right side of the panel, which could be from a variety of things, such as permanent marker in the dry glass prior to the infusion. Otherwise this panel did not show any dry spots and both were found suitable for creating testing specimens. The area of the black blemish on the Derakane panel was not used. Average processing times and parameters for the vacuum infusion consolidation process of the two polymer matrix materials into composite laminates investigated are shown in Table 4.

Table 4: Processing Times & Parameters for Two Polymer Systems [20] [33]

Polymer Matrix System	Infusion open time (minutes)	Infusion peak time (minutes)	Post-Cure time (hours)	Post-Processing temperature (C)
Thermoset Vinyl ester	29*	56	24	60
Thermoplastic Acrylic	20	33	4	80

* *The infusion open time cited for the thermoset vinyl ester is the gel time given.*

In Table 4 the infusion open time is defined as the time in which the viscosity of the resin is low enough for it to be inserted into the part. Demolding of the parts can be done at various times after the infusion peak depending on the system. Elium 150 can be demolded 5-10 minutes after the infusion peak has been reached [20]. A safe time past peak is not given for the Derakane 610-C in the technical data sheet. The results of composite laminates made using the two polymer matrix systems used in this study and E-LR 1208 unidirectional E-glass as reinforcement are given in Table 5.

Table 5: Composite Laminate Results from Two Polymer Systems

Polymer Matrix System	Number of Layers	Density [34] (g/cm ³)	Average thickness (mm)	Fiber weight fraction	Fiber volume fraction
Derakane 610-C	10	1.75	4.23	55.62 %	38.27 %
Elium 150	10	1.80	4.37	53.48 %	37.87 %

The density was found by water displacement using ASTM D792-13. The fiber weight fraction (W_f) and fiber volume fraction (V_f) reported are calculated values found by using equations 1 and 2.

$$W_f = \frac{\text{Mass of Fibers}}{\text{Mass of Composite}} \quad \text{Equation 1}$$

$$V_f = \frac{\text{Volume of Fibers}}{\text{Volume of Composite}} \quad \text{Equation 2}$$

The mass of fibers used in equation 1 was measured in the lab prior to infusion as well as the mass of composite. The volume of fibers used in equation 2 was found using the known density of E-glass fibers which is 2.54 g/cm³ and the volume of composite which was measured. All calculated density, fiber weight fraction and fiber volume fraction values presented in Chapter 2 of this study were determined in this way.

2.2.2 Manual Stamp Thermoforming

The second manufacturing method selected for investigation is manual stamp forming. This method used a heated hydraulic consolidation press with a capacity of 650-tonnes (700-US tons), shown in -, that measures 0.914-meters (3-feet) by 0.914-meters (3-feet). This press was used for forming the selected E-glass/PETg prepreg UD tapes. This was the first work done with this method during this study and there were several challenges to this process, including migration of fibers from their original orientation in the material (fiber wash), uneven or incomplete consolidation, and entrapped air in the part.

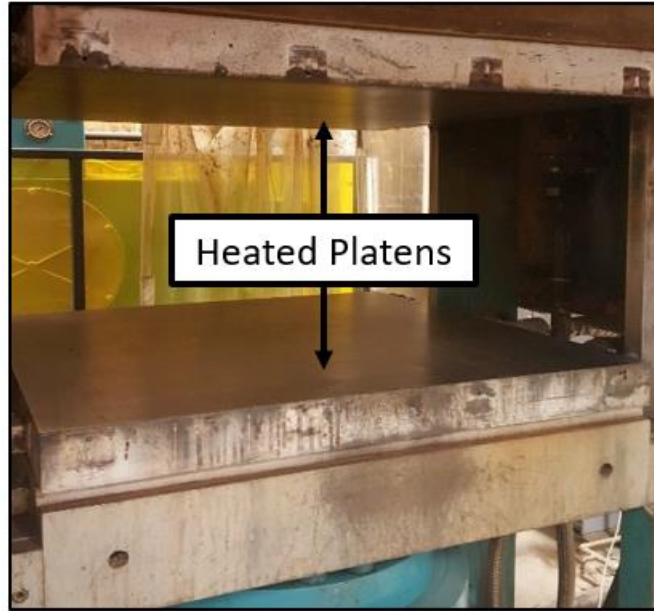


Figure 7: Manual Stamp Forming Press

Several iterations of this process were conducted, with Trial 1-3 introducing a frame around the tapes to reduce fiber wash, some variations in dwell time, and increased pre-consolidation pressure in Trials 1-5 and 1-6 to force out entrapped air between the layers of prepreg. The quality of parts was increased dramatically with these modifications.

The initial manual stamp forming efforts are referred to as Trail 1. – shows a consolidated E-glass/PETg laminate made with Trial 1-6 parameters, the most successful from these trials. Several problems still existed, however the quality of the parts was improved through the trial iterations. Some observations on this method are given.

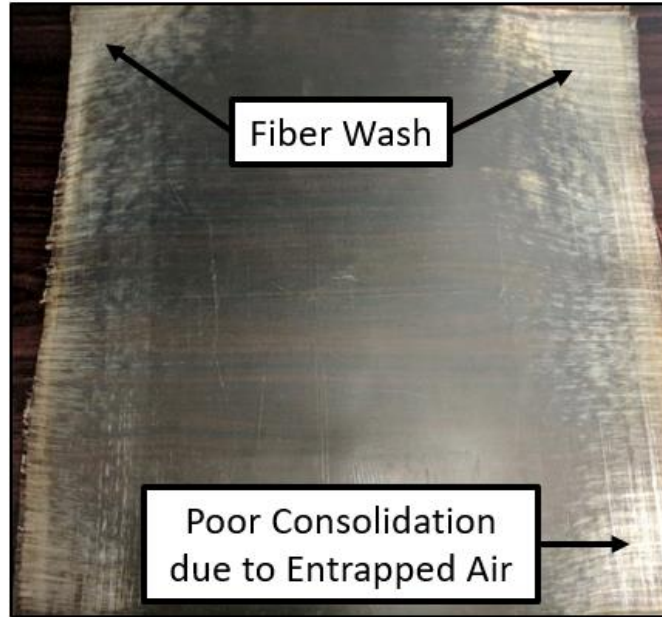


Figure 8: Trial 1-6 Consolidated Laminate (IE 5842)

Trial Observations:

- Prolonged heating under pressure causes the fibers to migrate out of alignment in the flowing thermoplastic. This is called fiber wash and occurs even when the composite is in a containment frame
- Since the prepreg tapes are naturally curled because they are stored on a roll, it is difficult to force air trapped between layers out of the composite.
- The total fabrication time per laminate is very long in comparison to other fabrication methods discussed later in this section.

Due to these trial observations and the slow nature of this method of heated consolidation, the study moved to a second method of composite fabrication, which resulted in substantially better results. The parameters used to fabricate PETg composite laminates from IE 5842 prepreg tapes are summarized in Table 6. For each manufacturing trial

multiple iterations of fabrication were conducted, and the trial iteration is indicated by the second number in the trial identifier.

Table 6: Manual Stamp Forming Parameters for IE 5842 PETg Prepreg Tapes

Trial Number	Press Temp (°C)	Pre-Consolidation Dwell Time (minutes)	Pre-Consolidation Pressure (kPa)	Heated Stamping Dwell Time (minutes)	Cooling Stamping Dwell Time (minutes)	Stamping Pressure (kPa)
Trial 1-1	213	-	-	45	100	758
Trial 1-2	213	15	137	5	100	757
Trial 1-3	216	20	137	5	100	757
Trial 1-4	216	45	137	5	100	757
Trial 1-5	216	*	*	30	100	759
Trial 1-6	216	15	2758	5	100	757

**The pre-consolidation phase for Trial 1-5 was a multi-step process as follows: 20 seconds at 173.06 kPa, 20 seconds at 344.05 kPa, 20 seconds at 517.11 kPa, 20 seconds at 690.17 kPa, 40 seconds at 1378.95 kPa, 40 seconds at 2069.12 kPa, 45 seconds at 2757.9 kPa, a final step of 40 seconds at 1378.95 kPa.*

Trial 1-6 the final iteration of manual stamp forming, incorporated a large change in pre-consolidation pressure as indicated. This large change in pre-consolidation pressure was done based on institutional knowledge on manual stamp forming at the ASCC. The increased pre-consolidation pressure was used to force entrapped air from between the layers of prepreg out of the part. Trial 1-5 and 1-6 introduced two variations of this and they both saw a significant decrease in the white haze, which can be seen in Figure 8 around the edges of the part from entrapped air.

Table 7 shows the calculated properties of the composite fabricated in Trial 1-6 of manual stamp forming.

Table 7: Manual Stamp Forming Results for Trial 1-6

Processing Trial Number	Number of Layers	Density (g/cm ³)	Average thickness (mm)	Fiber weight fraction	Fiber volume fraction
Trial 1-6	10	2.01	1.87	70.03 %	55.50 %

2.2.3 Automated Stamp Thermoforming

The third manufacturing process in this study is thermoforming through automated stamp forming. This process is favored for its unique thermoforming capabilities and represents an industry standard for thermoplastic material fabrication. It uses heat and pressure with a desired dwell time to form multiple pre-impregnated layers of thermoplastic material into a complete laminate.

The University of Maine (UMaine) has formed the Consortium for Manufacturing Innovation in Structural Thermoplastics (CMIST) to develop a thermoplastic composites technology roadmap [35]. This roadmap has identified key applications for structural thermoplastics by linking market drivers and value streams with projects. UMaine's ASCC has established the Alford Advanced Manufacturing Laboratory for Structural Thermoplastics, which is a state-of-the-art automated manufacturing cell for the stamp-thermoforming process.

The automated thermoforming line in this lab contains a Dieffenbacher Fiber Forge Relay 2000 automated tape layup machine, a Techni-Modul infrared (IR) oven, and a 650 tonne Utah Hydraulic press with automated transport capability between machines.

The first step in the automated thermoforming line is the Dieffenbacher Fiber Forge Relay 2000 automated tape layup machine shown in Figure 9. This machine uses a translating and rotating table as a construction surface to place slit thermoplastic tapes between 50 mm

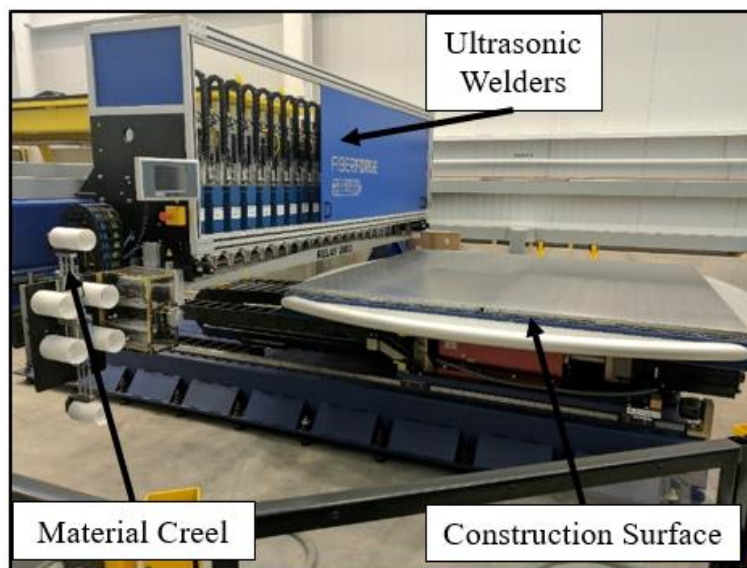


Figure 9: Dieffenbacher Fiber Forge Relay 2000 Tape Layup Machine

and 150 mm pulled off the material creel in desired orientations, and then uses a bank of ultrasonic welders to spot weld the tapes together to form what is called a tailored blank. Once the tailored blank is completed it can be transported via robotic arm from the tape layup machine to the next part of the automated thermoforming process.

The second step in the process is heating the tailored blank in the Techni-Modul infrared (IR) oven shown in Figure 10. The robot arm, which is also shown, moves the tailored blank from the tape layup machine onto the IR oven tray, which closes into the oven and heats the part under the desired conditions. Then the oven tray opens and the robotic arm moves the heated blank into the hydraulic press to be consolidated.

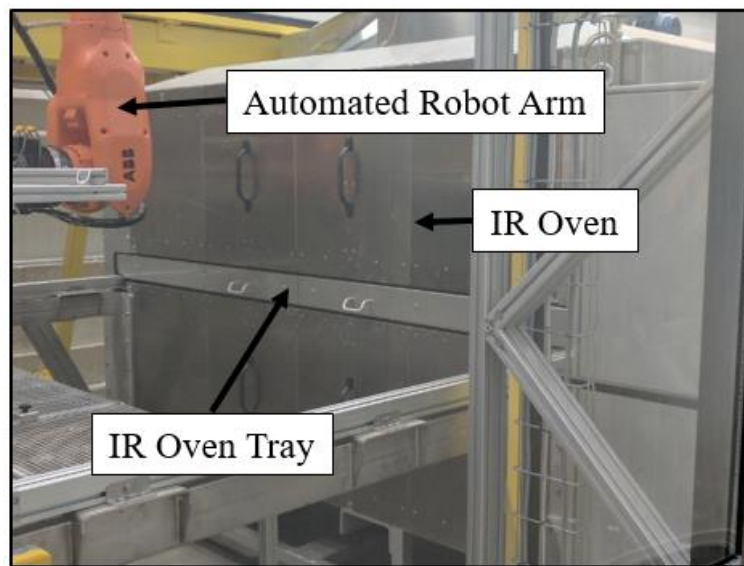


Figure 10: Techni-Modul Infrared (IR) Oven

The robot arm moves the heated tailored blank into the 650 metric ton Utah hydraulic press shown in Figure 11 and moves out of the way. The stamping press then rapidly moves down to apply pressure and cool the part. The pressure and temperature of the press can be controlled to provide the processing parameters desired for this step. Once the pressing portion of the process is completed and the part is cooled, the automated stamp forming

process is finished. For all processing trials of automated stamp forming conducted as a part of this study if a stamping temperature is not given in the processing parameters it was the ambient temperature of the lab, approximately 25 degrees Celsius.



Figure 11: 650 Metric Ton Utah Hydraulic Press

Several iterations of fabrication were conducted before mechanical testing was performed. The first trials and initial mechanical testing were done using Polystrand IE 5842 PETg prepreg tape which has the resin in its natural green color.

The first composite laminate fabricated by automated stamp forming process is shown as Figure 12. Many improvements were made after this original consolidation which will be outlined in this section. The original PETg material acquired was not slit for use on the automated tape layup machine because feasibility trials were desired before the study committed to this material choice.

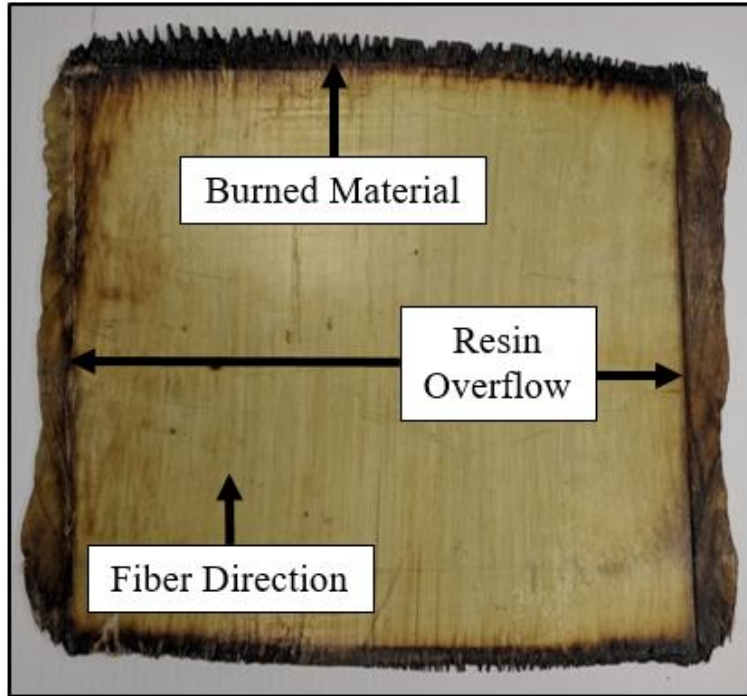


Figure 12: Trial 2-1 IE 5842 Thermoformed Part

Therefore, parts fabricated using natural PETg were laid up by hand then processed on aluminum caul sheets coated in non-stick Teflon and heated in the IR-oven. Then the automated robot arm transported the caul sheets with the material into the stamp forming press, which cools the part under the desired pressure in the IR-oven and stamp forming press. These first trials done using automated thermoforming are referred to as Trial 2. It can be seen in the Trial 2-1 part that significant burning of material occurred on the ends of the part where the glass-fiber was more exposed. In addition, resin flowed out of the sides of the aluminum caul sheets and gathered on the left and right edges. This would significantly affect the resin content in the usable part area, which is not desirable. Table 8 shows the progression of processing parameters used during Trial 2.

Table 8: Automated Thermoforming Trial 2 Processing Parameters

Processing Trial Number	Material System	Number of layers	IR-Oven Temperature (Celsius)	IR-Oven Dwell Time (seconds)	Stamping Pressure (kPa)	Stamping Time (seconds)
Trial 2-1	IE 5842	10	232	200	1380	30
Trial 2-2	IE 5842	10	216	175	1380	30

When processing material in the automated stamp forming line at the ASCC the operator needs to set the zones in the IR-oven in order to control the heat output in that area of the oven. For Trial 5 the IR-Oven zones were all set to 100%. Table 9 shows the calculated results of Trial 2-2 from the first trial of automated stamp forming done as a part of this study.

Table 9: Automated Stamp Forming Results for Trial 2-2

Processing Trial Number	Number of Layers	Density (g/cm ³)	Average thickness (mm)	Fiber weight fraction	Fiber volume fraction
Trial 2-2	10	1.86	2.34	53.85 %	39.47 %

The first change from Trial 2 to Trial 3 was developing a method for pre-consolidation of the PETg prepreg tapes in a convection oven to increase fiber alignment in the final

consolidated plates. This step was necessary in order to relax the tapes, which come off a roll of material and therefore curl easily before they are consolidated.

In order to create a successful pre-consolidation process several iterations with varying processing were attempted. It was found that the most effective processing steps were:

- Heat oven to 150 degrees Celsius
- Place plies (pre-preg sheets) in the oven one at a time
- Heat sheet for about 1 minute and remove

This version of the pre-consolidation process was used when preparing the trial 3 PETg for consolidation in the automated stamp forming process.

After pre-consolidation the automated thermoforming unit was used to rapidly heat the PETg tape in the IR-Oven and consolidate it in the hydraulic press to form the final laminate. Another change that was made is that the exposed face of the aluminum caul sheets used to transport the material were painted with a black paint. In order to reduce reflections off the metal surface that disrupted the pyrometers which is suspected to have caused issues with burning when fabricating the Trial 2 parts.

The first goal in investigating the feasibility of using E-glass/PETg composite as a structural reinforcement was preparing UD specimens for testing to ascertain mechanical properties.

Figure 13 shows the consolidated E-glass/PETg laminate fabricated through automated stamp forming with manual tailored blanks. Manual tailored blanks are generated by pre-consolidating the layers of IE 5842 enough to take the curl out of the layers from being stored on the roll and tack them to each other. After pre-consolidation in a convection oven, the blank was processed in the same fashion as the Trial 2 blanks with the modifications outlined previously. The blank was still unrestrained while in the oven and press which explains the small amount of fiber wash seen on the edges of the panel in Figure 13. Table 10 shows the processing parameters used to generate these UD laminates. The IR-Oven settings used for Trial 3 are shown in Table 11 and Table 12 shows the calculated results of Trial 3-1 from the automated stamp forming done as a part of this study. Panels fabricated in this way were tested using standardized methods, the results of which are presented in chapter 3 of this thesis.

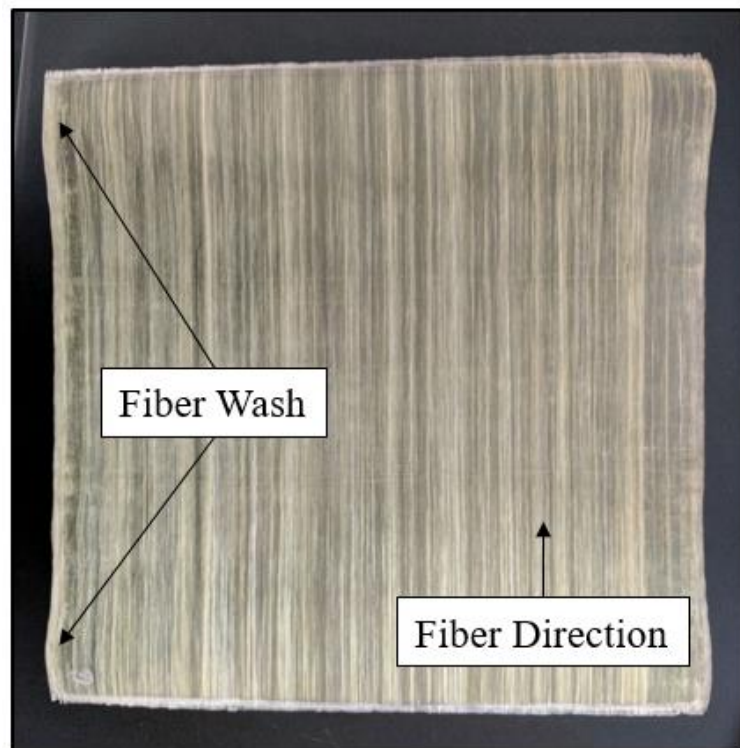


Figure 13: Improved UD PETg Thermoformed Panel

Table 10: IE 5842 Automated Thermoforming Trial 3 Processing Parameters

Processing Trial Number	Material System	Number of layers	IR-Oven Temperature (Celsius)	IR-Oven Dwell Time (seconds)	Stamping Pressure (kPa)	Stamping Time (seconds)
Trial 3-1	IE 5842	10	218.3	435	1380	60

Table 11: Trial 3 IR Oven Settings

IR Oven - Coefficient	Value (%)
Zone 1 Upper	50
Zone 2 Upper	50
Zone 3 Upper	30
Zone 4 Upper	5
Zone 5 Upper	30
Zone 1 Lower	65
Zone 2 Lower	55
Zone 3 Lower	30
Zone 4 Lower	5
Zone 5 Lower	65

Table 12: Automated Stamp Forming Results for Trial 3-1

Processing Trial Number	Number of Layers	Density (g/cm ³)	Average thickness (mm)	Fiber weight fraction	Fiber volume fraction
Trial 3-1	10	1.77	2.35	57.92 %	40.27 %

After creating panels for cutting coupons for mechanical testing the next phase of this study was to fabricate panels to be used for testing friction-welding parameters.

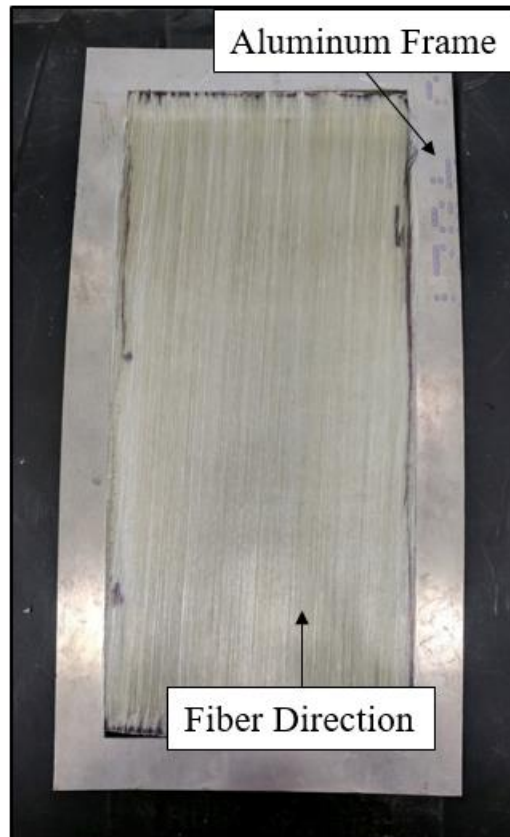


Figure 14: Pre-Consolidated PETg Prepreg in Aluminum Consolidation Frame

Figure 14 shows a 15.9-cm (6.25-inch) by 35.6-cm (14.0-inch) UD pre-consolidated panel of PETg prepreg tapes, which represents the fourth trial with this material. The desired thickness of the consolidated panel after processing was meant to be approximately 6.35-mm (0.25-inch), which was achieved with 35-layers of prepreg tape.

In order to solve the fiber wash seen in the UD panels for mechanical testing shown in Figure 13, an aluminum frame was used in order to restrain the edges of the material during

consolidation. The frame acts as a boundary to restrain resin flow and helps keep the fibers in alignment.

The pre-consolidation process for Trial 4 differs from that used for Trial 3 because of the increased thickness of the panel. The process used for trial 4 was as follows:

- Heat oven to between 150 & 175 Celsius
- Place plies in the oven up to five at a time
- Place parchment paper and a 50 lb weight on the material in the aluminum frame
- Heat sheet for about 25 minutes and remove

Table 13 shows the Trial 4 friction-welding unidirectional panel processing parameters used for this study. The IR-Oven settings used for Trial 4 are shown in Table 14. Fiber weight and volume fractions were not found for Trials 4-1 and 4-2 because they were not used for mechanical testing and were simply thicker laminates made from IE 5842 used in Trial 3-1.

Table 13: IE 5842 Automated Thermoforming Trial 4 Processing Parameters

Processing Trial Number	Material System	Number of layers	Design thickness (mm)	IR-Oven Temperature (°C)	IR-Oven Dwell Time (s)	Stamping Pressure (kPa)	Stamping Time (s)
Trial 4-1	IE 5842	35	6.35	218.3	690	2760	60
Trial 4-2	IE 5842	18	3.175	218.3	345	2760	60

Table 14: Trial 4 IR Oven Settings

IR Oven - Coefficient	Value (%)
Zone 1 Upper	50
Zone 2 Upper	30
Zone 3 Upper	30
Zone 4 Upper	0
Zone 5 Upper	0
Zone 1 Lower	95
Zone 2 Lower	95
Zone 3 Lower	85
Zone 4 Lower	0
Zone 5 Lower	0

With manufacturing feasibility proven on the automated stamp forming line with IE 5842 PETg the ASCC acquired IE 5842b, a dyed black version of IE 5842, in order to use the automated tape layup machine to generate the tailored blanks, fully utilizing the automated process. In addition, this material eliminates the need for pre-consolidating the material

prior to heating and consolidating it by using the tape layup machine to adhere the layers together, which further automated and shortened the fabrication process.

The IE 5842b material was slit into various widths between 50-mm and 150-mm for use on the tape layup machine. The most common width used was 50.8-mm (2-inch). The panels processed for this study in this way are considered Trial 5.

When operating the tape layup machine a critical component is the ultrasonic welding of the individual tapes to each other in order to form them into a tailored blank. This holds the layers together until they can be heated and consolidated. The ultrasonic welder settings used for trial 5 are shown in Table 15 as taken from TailorGen, the software used for operating the tape layup machine.

Table 15: TailorGen Welding Parameters for Trial 5 Processing

Weld Only	Time Increment (ms)	Energy Increment (%)	Actual Time (ms)	Actual Energy (%)
	1.5	1.5	65.0	65.0
	1.5	1.5	66.5	66.5
X	1.5	1.5	66.5	66.5
X	1.5	1.5	66.5	66.5
	1.5	1.5	68.0	68.0
	1.5	1.5	69.5	69.5
	1.5	1.5	71.0	71.0
	1.5	1.5	72.5	72.5
	1.5	1.5	74.0	74.0
	1.5	1.5	75.5	75.5
X	1.5	1.5	75.5	75.5
X	1.5	1.5	75.5	75.5
X	1.5	1.5	75.5	75.5
X	1.5	1.5	75.5	75.5
X	1.5	1.5	75.5	75.5

Once the tailored blanks have been created on the tape layup machine, the part was heated in the IR-Oven and then consolidated in the stamp forming press. Table 16 shows the Trial

5 concrete-CFRTP stud panel processing parameters used for this study. The IR-Oven settings used for Trial 5 are shown in Table 17. Table 18 shows the calculated results of Trial 5-1 from the automated stamp forming done as a part of this study.

Table 16: IE 5842b Trial 5 Concrete-CFRTP stud Panel Processing Parameters

Trial Number	Material System	Number of layers	IR-Oven Temperature (Celsius)	IR-Oven Dwell Time (seconds)	Stamping Pressure (kPa)	Stamping Time (seconds)
Trial 5-1	IE 5842b	8	218.3	30	2760	60

Table 17: Trial 5 IR Oven Settings

IR Oven - Coefficient	Value (%)
Zone 1 Upper	50
Zone 2 Upper	50
Zone 3 Upper	30
Zone 4 Upper	5
Zone 5 Upper	30
Zone 1 Lower	65
Zone 2 Lower	55
Zone 3 Lower	30
Zone 4 Lower	5
Zone 5 Lower	65

Table 18: Automated Stamp Forming Results for Trial 5-1

Trial Number	Number of Layers	Density (g/cm ³)	Average thickness (mm)	Fiber weight fraction	Fiber volume fraction
Trial 5-1	8	1.75	2.04	55.75 %	38.47 %

Once the panels are fully processed and consolidated into a composite laminate they need to be trimmed in order to be used as concrete-CFRTP stud panels. The concrete-CFRTP stud test will be described in detail during chapter 4 of this study. When processing the IE 5842b material several observations were made which were new to automated stamp forming of tailored blanks made on the tape layup machine. The observations from Trial 5 are as follows:

- Edges of parts must be trimmed off
- Welds were still visible after consolidation
- Gaps occurred between the tapes

Figure 15 shows a consolidated full concrete-CFRTP stud panel to illustrate the gaps that occurred between the tapes.

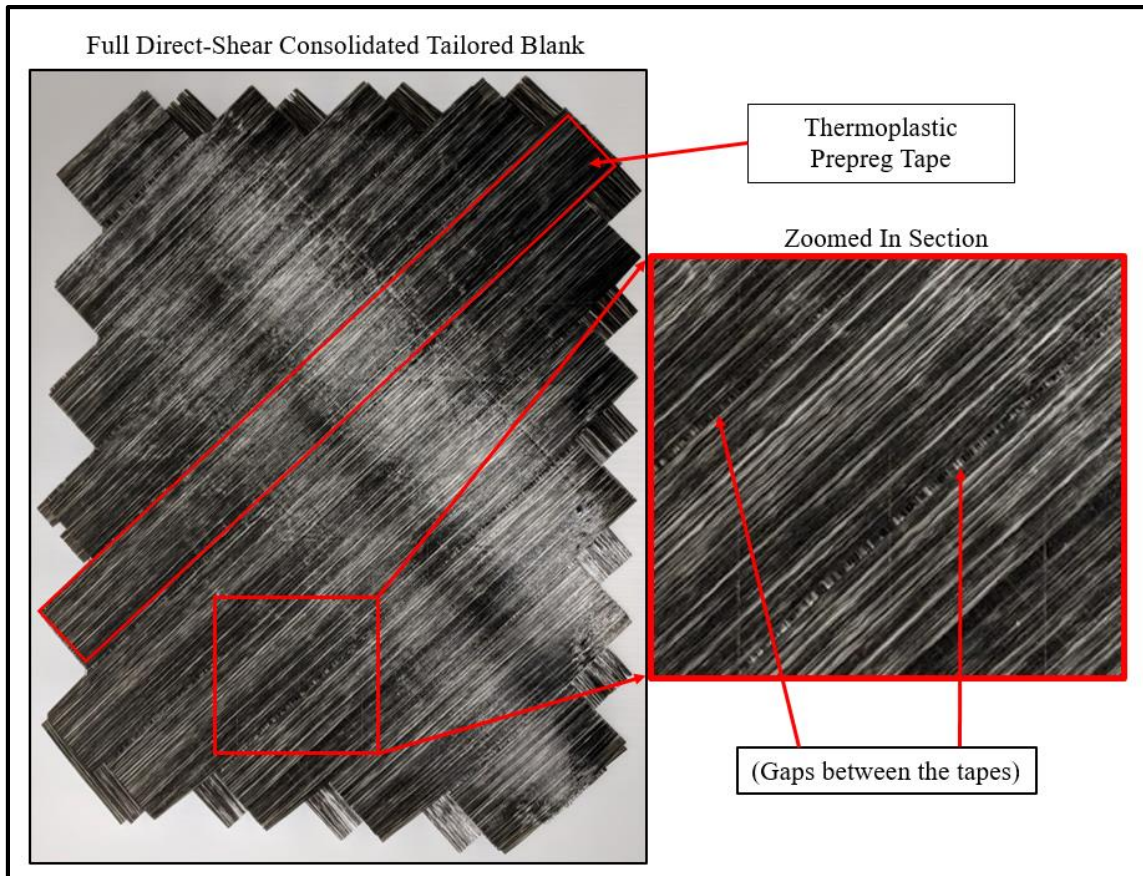


Figure 15: IE 5842b Consolidated Concrete-CFRTP stud Tailored Blank

The material selection and manufacturing trials done for this study advanced the knowledge and capabilities for processing thermoplastics at the ASCC by proving the feasibility of processing amorphous thermoplastic materials. From the manufacturing trials done in this study, it is apparent that automated stamp forming with tailored blanks made on the tape layup machine is the most time effective process for fabricating consolidated composite laminates. A unique phenomenon was also discovered in the processing of IE 5842b material, which is that the edges of the tapes shrink during heating. Future investigating was done on the causes of tape shrinking by Benjamin Smith, a Graduate Research Assistant at the ASCC.

With the tape shrinking solved on the automated stamp forming line by pre-heating the tailored blanks in the press in order to bond the surface layers together Trial 6 was conducted to fabricate unidirectional laminates from IE 5842b material to verify similar results were obtained to that of Trial 3. Table 19 shows the processing parameters used to generate these UD laminates. The IR-Oven settings used for Trial 6 are shown in Table 20 and Table 21 shows the calculated results of Trial 6-1 from the automated stamp forming done as a part of this study.

Table 19: IE 5842b Automated Thermoforming Trial 6 Processing Parameters

Trial Number	Material System	Number of layers	IR-Oven Temp. (°C)	IR-Oven Dwell Time (s)	Stamp Pressure (kPa)	Stamp Temp. (°C)	Stamp Time (s)
Trial 6-1	IE 5842b	10	223.9	30	1380	76.67	60

Table 20: Trial 6 IR Oven Settings

IR Oven - Coefficient	Value (%)
Zone 1 Upper	50
Zone 2 Upper	50
Zone 3 Upper	30
Zone 4 Upper	5
Zone 5 Upper	30
Zone 1 Lower	65
Zone 2 Lower	55
Zone 3 Lower	30
Zone 4 Lower	5
Zone 5 Lower	65

Table 21: Automated Stamp Forming Results for Trial 6-1

Processing Trial Number	Number of Layers	Density (g/cm ³)	Average thickness (mm)	Fiber weight fraction	Fiber volume fraction
Trial 6-1	10	1.75	2.41	56.38 %	38.83 %

The mechanical properties found from standardized testing done on these materials are discussed in chapter 3 along with comparison to predictions from CLT using constitutive properties if the thermoplastic materials presented in this chapter.

2.3 Summary of Constitutive Material Properties

For the materials selected in this study a summary of their constitutive elastic behavior and strength properties in Table 22 for matrix properties and Table 23 for fiber properties. These properties, necessary for use with micromechanics to predict the elastic and strength properties. A comparison of predicted composite properties using these material properties is compared to the experimental values collected for composites in chapter 3.

Table 22: Summary of Matrix Material Properties

Property (units)	PETg Resin	Elium Resin	Derakane Resin
Elastic Modulus E_m (GPa)	2.2 [36]	3.3 [20]	3.5 [33]
Longitudinal Tensile Strength, F_{mt} (MPa)	53 [36]	76 [20]	71 [33]
Longitudinal Compressive Strength F_{mc} (MPa)	55 [36]	130 [20]	127 [7]
Poisson's Ratio ν_m (-)	-	-	0.35 [7]

Table 23: Summary of Fiber Material Properties

Fiber Material	Longitudinal Elastic Modulus E_f (GPa)	Longitudinal Tensile Strength F_{ft} (MPa)	Poisson's Ratio ν_f (-)
E-glass	73 [7]	3450 [7]	0.23 [7]

The technical documentation used for the thermoplastic resin-systems chosen for this study did not provide Poisson's ratios. This is a necessary material property for micromechanics

analysis therefore a typical thermoplastic value for PEI of 0.37 from Barbero [37] was assumed for both PETg and Elium resin.

2.4 Conclusions

From the literature review, material selection, and manufacturing trials conducted in this study objective 1 of this study was completed. The following conclusions presented in a bullet list were made from the work conducted:

- Elium 150 presents a unique thermoplastic option for composites as it utilizes widely accepted fabrication techniques developed for use with industry accepted thermosetting polymer resin-systems.
- Limited options are available for amorphous engineering grade thermoplastic prepreg tapes reinforced with glass fibers.
- PETg prepreg tapes are a potentially suitable option for structural applications based on competitive mechanical properties, availability, cost effectiveness, and relatively low processing temperatures for an engineering grade thermoplastic.
- Manufacturing of fiber-reinforced thermoplastic composites is feasible through both vacuum infusion using the Elium 150 resin-system and stamp forming of PETg prepreg tapes.
- Automated stamp forming of PETg prepreg tapes achieved higher quality results with reduced manufacturing time compared to manual stamp forming.

CHAPTER 3

MATERIAL CHARACTERIZATION

The standardized material level testing for this study was conducted at the ASCC to characterize the two selected thermoplastic materials and an infusible thermosetting composite for comparison. These composites were characterized using ASTM standardized test methods, which are outlined in this report.

3.1 Characterization of Thermoplastic Composites for Structural Applications

The most important design properties are often in the longitudinal direction of a unidirectional laminate, also referred to as the fiber-direction. This is the direction along which all the fiber tows are oriented in a unidirectional specimen, and is the direction of the greatest stiffness and greatest tensile and compressive strength. In some cases, the properties transverse or perpendicular to the fiber direction are of interest as well.

3.1.1 Mechanical Properties of Composite Laminas and Laminates

The longitudinal and transverse properties make up the base properties of a composite lamina and can be used in design in conjunction with micromechanics and macromechanics theories for composites analysis [7] [37]. Micromechanics uses the properties of constituent materials to provide an analytical estimate of lamina strengths and stiffnesses. Classical lamination theory (CLT), which implements macromechanics, uses the strength and stiffness of individual lamina to predict the properties of a multidirectional laminate. Figure 16 shows the commonly used coordinate axes for composite laminas and laminates where longitudinal (0-degree) corresponds to the fiber-direction and transverse (90-degree)

is perpendicular to the fiber-direction for a lamina and correspond to the x-direction and y-direction respectively for a laminate. For a composite laminate, the bias-direction is defined as the direction 45-degrees from the longitudinal direction. It should also be noted that sometimes testing multi-directional laminates, especially off-axis laminates, could be of interest to characterize these laminates for specific scenarios [7].

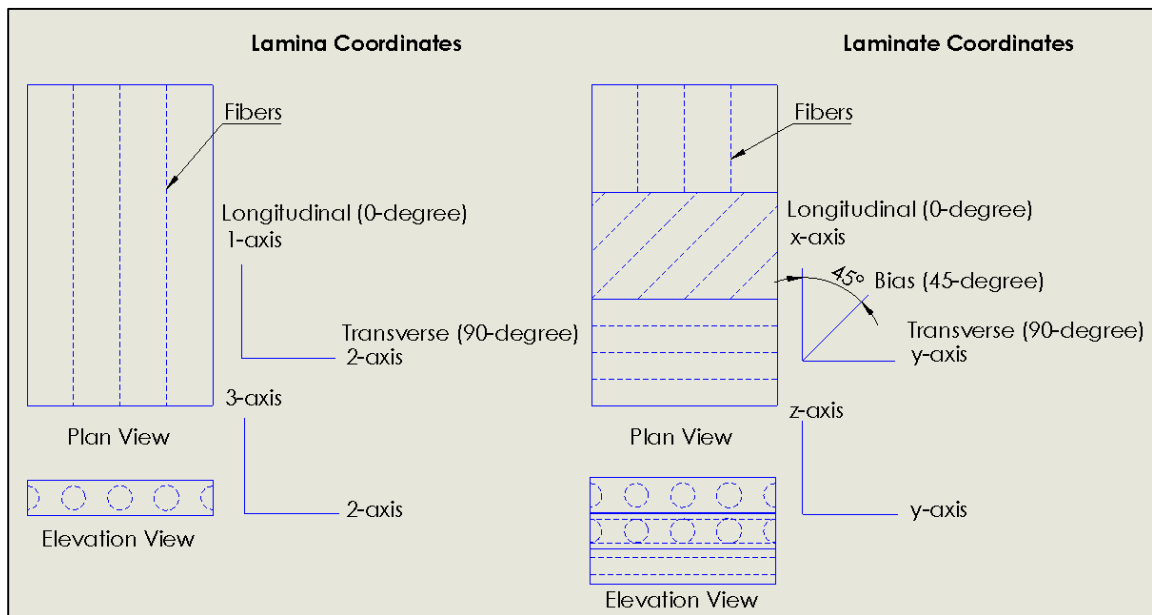


Figure 16: Coordinate Systems for a Composite Lamina and Laminate

The common nomenclature used for describing the mechanical properties in the longitudinal and transverse directions for a thin composite lamina subjected to in-plane stresses are given in the following bulleted lists.

The in-plane elastic properties are:

- Elastic modulus in the longitudinal direction in tension (E_{1t})
- Elastic modulus in the longitudinal direction in compression (E_{1c})
- Elastic modulus in the transverse direction in tension (E_{2t})

- Elastic modulus in the transverse direction in compression (E_{2c})
- Elastic modulus in shear in the x-y plane (G_{12})
- Poisson's ratio in the x-y plane (ν_{12})

The in-plane strength parameters are:

- Longitudinal tensile strength (F_{1t})
- Longitudinal compressive strength (F_{1c})
- Transverse tensile strength (F_{2t})
- Transverse compressive strength (F_{2c})
- In-plane shear strength (F_6)

Theoretically E_{1t} equals E_{1c} and E_{2t} equals E_{2c} , however experimentally these values can vary. In addition, the fiber volume fraction (V_f) is an important property, and is found through theoretical calculations or experimentally using burn-off tests for E-glass reinforced composites.

3.1.2 Experimental Methodology and Equipment

The objective of the material testing conducted for this thesis was to characterize the principal properties of the laminates through the testing of unidirectional specimens to get lamina properties for design use with classical lamination theory. Additionally, selected specialized testing was conducted to support the use of thermoplastic composites in beam or panel webs and other specific structural areas in future applications. This testing was done in accordance with the principles described in the desired mechanical properties section of the introduction.

Repeatable testing is important in material characterization. Coupon level testing was conducted on pristine specimens using the following standards.

- ASTM D3039-14 Standard Test Method for Tensile Properties of Polymer Matrix Composite Materials [38] with standard-sized specimens
- ASTM D3039-14 Standard Test Method for Tensile Properties of Polymer Matrix Composite Materials [38] with notched specimens (denoted as the modified N2 specimen) [39]
- ASTM D6641-14 Standard Test Method for Compressive Properties of Polymer Matrix Composite Materials Using a Combined Loading Compression (CLC) Test Fixture [40]
- ASTM D7078-12 Standard Test Method for Shear Properties of Composite Materials by V-Notched Rail Shear Method [41]
- ASTM D792-13 Standard Test Method for Density and Specific Gravity (Relative Density) of Plastics by Displacement [42]
- ASTM D3171-15 Standard Test Methods for Constituent Content of Composite Materials [43]

The tension, compression, and shear tests outlined above were performed on a 100-kN (22.5kip) Instron load frame equipped with hydraulic wedge grips. Instron data including applied force and actuator position were recorded at 100-Hz. A summary of the specimen dimensions and tolerances used during testing at the ASCC is given in Table 24.

Table 24: Specimen Dimensions and Tolerances Summary

Standard Used	Property Type	Laminate Architecture Type	Dimension	Measurement (mm)	Tolerance (mm)
ASTM D3039 [38]	Tension	Unidirectional*	Length Width Thickness	250 25 Ply-Thickness Dependent	See Standard $\pm 1\%$ of Width $\pm 4\%$ of Thickness
Modified N2 [39]	Tension	Off-axis	Refer to [39]		See ASTM D3039
ASTM D6641 [40]	Compression	Unidirectional* (Or) Off-axis	Length Width Thickness	140 12 Ply-Thickness Dependent	± 0.01 12 nominal
ASTM D7078 [41]	Shear	Unidirectional* (Or) Off-axis	Length Notch Height Width Thickness	56 30.6 76 Ply-Thickness Dependent	± 2.5 ± 0.75 ± 2.5

Note *: These specimens may be completely unidirectional or mostly unidirectional in nature, some specimens will have almost all unidirectional fibers with a ninety-degree outer layer.

The Modified N2 notched specimens for tension testing use a specific geometry for a tension coupon [39]. The advantage of the Modified N2 coupon is that it increases the development length of the fibers in the composite coupon so the test will get the true strength of the composite in fiber dominated failure instead of a much lower strength if failure is driven by the matrix. Under-engaged fibers in tension testing is discussed in subsection 6.4 of ASTM D3039, which states that “Premature failure and lower stiffnesses are observed as a result of edge softening in laminates containing off-axis plies. Because of this, the strength and modulus for angle ply laminates can be drastically underestimated.” [38].

Examples of the setups used in the ASCC to perform the tests described above are shown in Figure 17, which displays ASTM 3039 [38], ASTM 6641 [40], and ASTM 7078 [41] from left to right respectively.

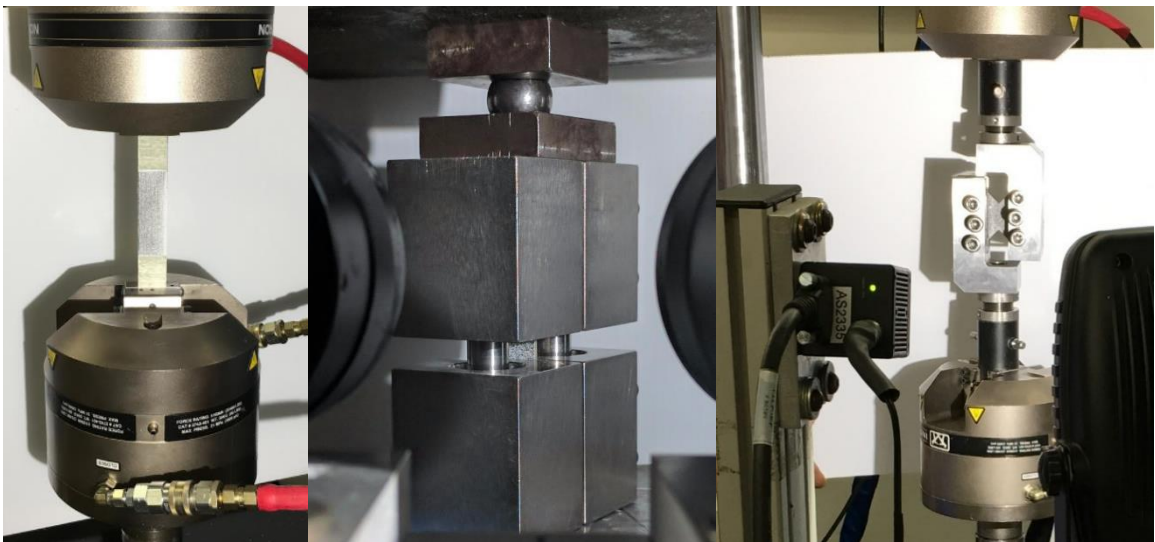


Figure 17: ASTM Standard Test Fixture Setups

Data for determining the modulus (strain measurements) were recorded using three-dimensional (3D) digital image correlation (DIC) techniques that rely on photogrammetry. Photogrammetry was developed to create maps from aerial photographs [44]. Cameras measure digitized light intensity values in a rectangular array of pixels. The correlation process for this is well documented for 3D DIC [45] [46] [47]. The DIC system uses cameras with either 8-mm, 12-mm or 50-mm focal lengths depending on the desired volume to capture and ARAMIS [48] software to process the images of test specimens painted with a random speckle pattern over a background of white paint to calculate strain measurements. Calibration of the cameras for testing was done using a series of photos of a specified calibration object for the chosen volume at precisely measured distances. As part of post-processing, the data after testing all samples were classified by failure type using the designations stated in the respective standard for each test.

Appendix A provides equipment calibration information for the ASCC facilities used, Appendix B provides technical data sheets for materials used in this study, and Appendix C provides the laminate analysis code used for calculations in this thesis.

3.2 Material Testing Results

Two thermoplastic materials were selected for characterization: Elium acrylic, and PETg prepreg tapes. Two types of PETg prepreg tapes were tested; IE 5842 natural colored tapes, and IE 5842b black colored tapes.

3.2.1 Thermoplastic Material Feasibility Testing

The first coupon-level testing assessed the feasibility of using the selected continuous fiber reinforced thermoplastic (CFRTP) composites in structural applications. The E-

glass/Elium composite laminates tested for this initial data had a fiber architecture of $[90\ 0\ 0\ 0]_S$ which is not ideal for material characterization. This multi-directional architecture was chosen to mitigate warping, which was observed during fabrication of laminates. The 90-degree layer was found to provide enough transverse stiffness to overcome this warping effect. The E-glass/PETg composite laminates tested for this initial data had a fiber architecture of $[0]_{10}$ which is ideal for material characterization.

Original testing done with Elium did not use a unidirectional laminate due to fabrication issues in the vacuum infusion process. During early fabrication trials warping was common in the panels fabricated due to the high rate of shrinking experience in the resin during curing. This was alleviated by introducing a 90-degree layer into the laminate by rotating one layer the Vector Ply E-LR 1208 [23] unidirectional E-glass on each outside face of the panel to provide transverse strength to reduce warping. The original results collected are shown in Table 25.

Table 25: Feasibility E-glass/Elium Composite Mechanical Property Results

Properties with coefficient of variation (COV)	E-glass/ Elium
Fiber Volume Fraction, V_f (%)	41.2 (1.9%)
Longitudinal Tensile Strength, F_{xt} (MPa)	687 (1.6%)
Longitudinal Compressive Strength, F_{xc} (MPa)	573 (8.6%)
In-Plane Shear Strength, F_{xy} (MPa)	57.58 (2.4%)
Longitudinal Tensile Elastic Modulus, E_{xt} (GPa)	24.1 (6.11%)
Longitudinal Compressive Elastic Modulus, E_{xc} (GPa)	25.6 (9.0%)
In-Plane Shear Elastic Modulus, G_{xy} (GPa)	3.48 (11.5%)
Poisson's Ratio, ν_{xy} (-)	0.116 (103%)
Longitudinal Ultimate Tensile Strain, ϵ_{xt}^u ($\mu\epsilon$)	30,500 (0.48%)
Longitudinal Ultimate Compressive Strain, ϵ_{xc}^u ($\mu\epsilon$)	24,400 (14.7%)
Longitudinal Ultimate In-Plane Shear Strain, ϵ_{xy}^u ($\mu\epsilon$)	210,000 (17.2%)
Average Composite Panel Thickness, t (mm)	3.3

Note: COV percentages reported with respective measured value in parenthesis.

Figure 18 through Figure 20 show the tension, compression and in-plane shear stress strain responses from the testing of the Elium feasibility coupons respectively. Figure 20 and all following in-plane shear stress-strain response figures show a dotted vertical line at 5% strain where the strength was calculated or no dotted line if 5% strain was not reached and the ultimate load was used per ASTM D7078 recommendation.

Table 26 shows the type of failure as classified using the respective ASTM standard and the number of failures per failure type.

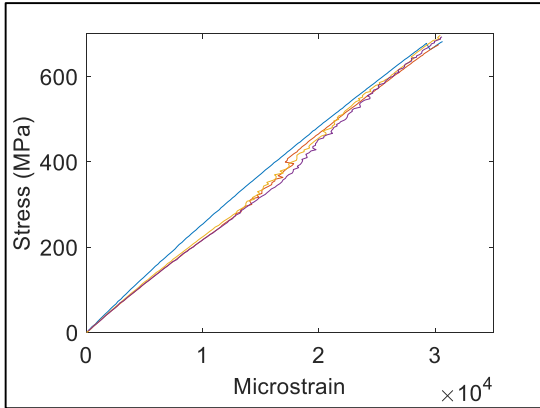


Figure 18: Feasibility E-glass/Elium Long. Tension
Stress-Strain Response

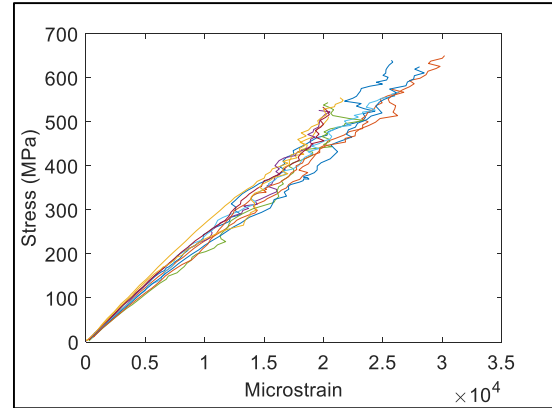


Figure 19: Feasibility E-glass/Elium Long. Compression
Stress-Strain Response

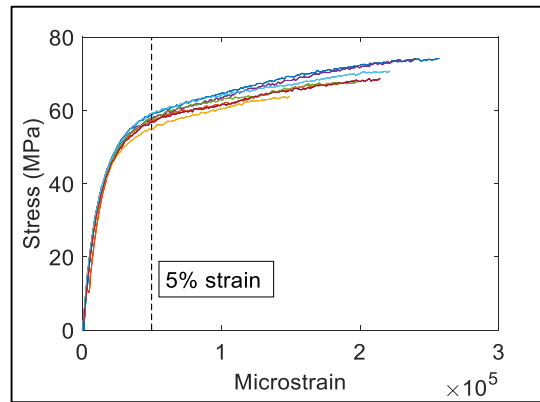


Figure 20: Feasibility E-glass/Elium In-Plane Shear Stress-Strain Response

Table 26: Feasibility E-glass/Elium Failure Types

Specimen Type	ASTM D3039 Tension [38]	ASTM D6641 Compression [40]	ASTM D7078 In-Plane Shear [41]
Failure Type	XGM, OAV	BGM	HGN
Number of Failures	4, 2	10	7

Figure 21 illustrates failure mode explosive-gage-middle (XGM) exhibited by all the valid feasibility Elium tension samples tested. Figure 22 shows failure mode brooming-gage-middle (BGM) exhibited by all the compression samples tested. Figure 23 shows failure mode horizontal cracking-gage-between notches (HGN) seen by all the in-plane shear samples tested. The other-at grip/tab-various (OAV) tension failures were not shown because it was a grip failure, not a valid failure in the composite specimen.



Figure 21: Feasibility E-glass/Elium XGM Failure Long. Tension Sample



Figure 22: Feasibility E-glass/Elium BGM Failure Long. Compression Sample



Figure 23: Feasibility E-glass/Elium HGN Failure In-Plane Shear Sample

The second material system chosen for this study, PETg in the form of prepreg unidirectional E-glass tapes was tested to assess feasibility as well. The tapes tested were IE 5842 sourced from Polystrand. Additional material testing of stamp formed PETg-composites fabricated with IE 5842 was done to support design concepts for specimens in this study. In addition to the unidirectional samples, a bias layup of +/-45-degree layers was tested to provide information on the performance of off-axis fibers typically used to carry shear. Table 27 shows the data collected from PETg-composite material characterization for all three sets of tests.

Table 27: Feasibility E-glass/PETg Composite Mechanical Property Results

Properties with COV	Longitudinal (x-direction)	Transverse (y-direction)	Bias (+/-45-degree)
Fiber Volume Fraction V_f (%)	38.91 (2.6 %)	-	-
Tensile Strength (MPa)	761 (6.4 %)	17.97 (8.71 %)	65.0 (6.42 %)
Compressive Strength (MPa)	333 (5.15 %)	49.3 (2.94 %)	55.6 (5.42 %)
In-Plane Shear Strength (MPa)	23.2 (12.4 %)	-	-
Tensile Elastic Modulus (GPa)	31.1 (4.18 %)	4.46 (8.35 %)	4.80 (5.02 %)
Compressive Elastic Modulus (GPa)	31.6 (9.17 %)	5.78 (4.54 %)	4.80 (21.2 %)
In-Plane Shear Elastic Modulus (GPa)	1.43 (9.99 %)	-	-
Poisson's Ratio (-)	0.344 (3.04 %)	0.063 (31.4 %)	0.168 (23.2%)
Ultimate Tensile Strain ($\mu\epsilon$)	27,000 (10.96 %)	4,140 (9.04 %)	80,600 (36.4 %)
Ultimate Compressive Strain ($\mu\epsilon$)	11,000 (2.79 %)	16,400 (14.5 %)	230,000 (19.7 %)
Ultimate In-Plane Shear Strain ($\mu\epsilon$)	55,500 (35.9 %)	-	-
Average Composite Panel Thickness (mm)	2.35	-	-

Note: COV percentages reported with respective measured value in parentheses.

The results from the feasibility trial are favorable based on comparison to thermoset composite properties in literature and indicate that both composite laminate types could be used in structural applications. From the results, it was seen that the Elium composite has 10 % less tensile strength than the E-glass/PETg material, but has 42 % more compressive strength and a 67 % greater shear strength.

Figure 24 through Figure 30 show the tension, compression and in-plane shear stress strain responses from the testing of the PETg feasibility coupons, respectively. Table 28 shows the type of failure as classified using the respective ASTM standard and the number of failures per failure type.

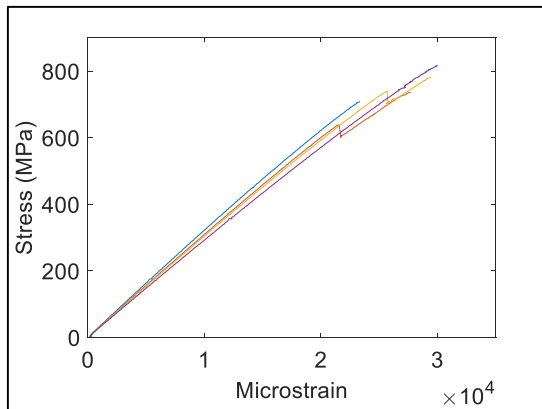


Figure 24: Feasibility E-glass/PETg Long. Tension Stress-Strain Response

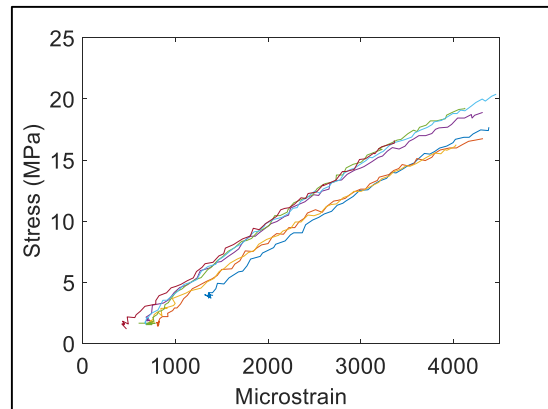


Figure 25: Feasibility E-glass/PETg Trans. Tension Stress-Strain Response

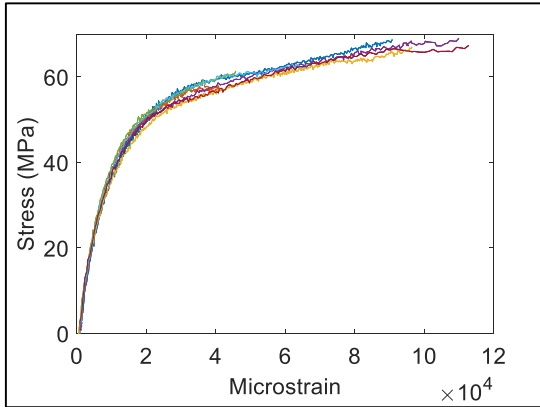


Figure 26: Feasibility E-glass/PETg Bias Tension
Stress-Strain Response

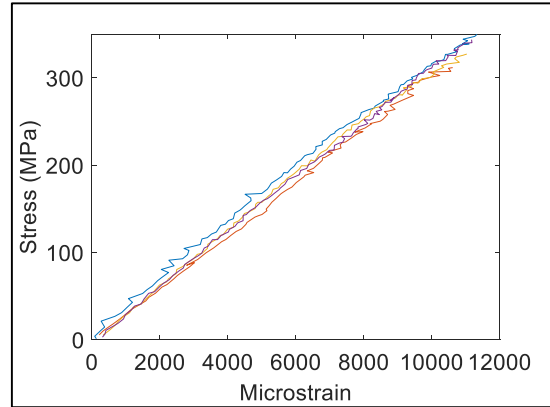


Figure 27: Feasibility E-glass/PETg Long. Compression
Stress-Strain Response

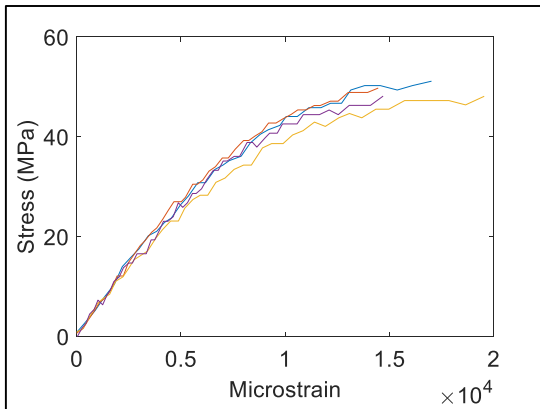


Figure 28: Feasibility E-glass/PETg Trans. Compression
Stress-Strain Response

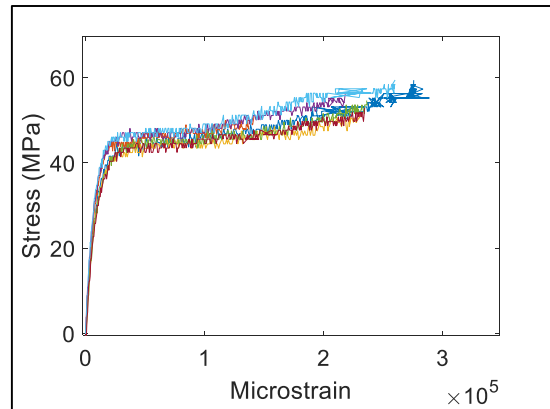


Figure 29: Feasibility E-glass/PETg Bias Compression
Stress-Strain Response

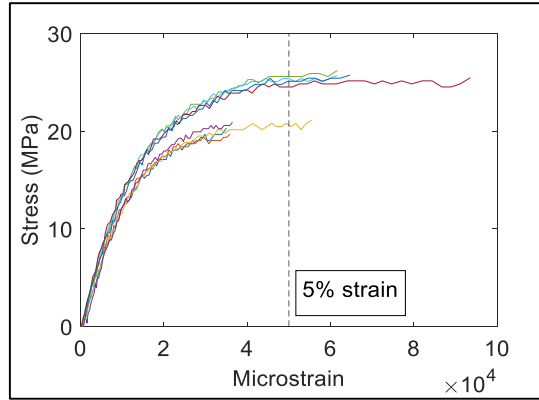


Figure 30: Feasibility E-glass/PETg In-Plane Shear Stress-Strain Response

Table 28: Feasibility E-glass/PETg (IE 5842) Sample Failure Types

Specimen Orientation	Specimen Type	ASTM D3039 Tension [38]	ASTM D6641 Compression [40]	ASTM D7078 In-Plane Shear [41]
Longitudinal	Failure Type	XGM, LGT, SGM	BGM, HIT	VGN
	Number of Failures	5, 1, 2	4, 1	8
Transverse	Failure Type	LGT	HAT, HIT	-
	Number of Failures	7	4, 1	-
Bias (45-degree)	Failure Type	*	TGM	-
	Number of Failures	7	7	-

**Note: The tension coupon used for the web-orientation was not an ASTM standard coupon, but was the modified N2 coupon introduced earlier in this chapter. Therefore, failure types could not be given.*

For the feasibility testing of stamp formed E-glass/PETg composites there were consistent failure modes for each type of coupon in each of the specimen-orientations except for longitudinal tension testing which saw three different failure types. The XGM sample example is on top, the lateral-gage-top (LGT) sample example is in the middle, and the long-splitting-gage-middle (SGM) sample is shown on the bottom. The transverse tension samples all failed in the same mode, LGT, as shown in Figure 32. The bias tension samples tested used the modified N2 type coupon, which is not an ASTM standard coupon type but is well documented in [39]. Therefore, these samples were not given a failure classification; however, they all shared the failure mode shown in Figure 33. The longitudinal compression samples had the same failure mode as the Elium feasibility samples tested (refer to Figure 22 to see this failure mode). The transverse compression samples failed in the through-thickness-at grip/tab-top (HAT) type failure shown in Figure 34 for a unidirectional Elium transverse compression sample that better displayed this failure type. The bias compression samples had transverse shear-gage-middle (TGM) type failure like the longitudinal samples but showed much higher strain to failure. The in-plane shear samples all failed in the same mode shown in Figure 35. The through-thickness-inside grip/tab-top (HIT) compression failures were not counted, as they are not characterized as acceptable failure modes.

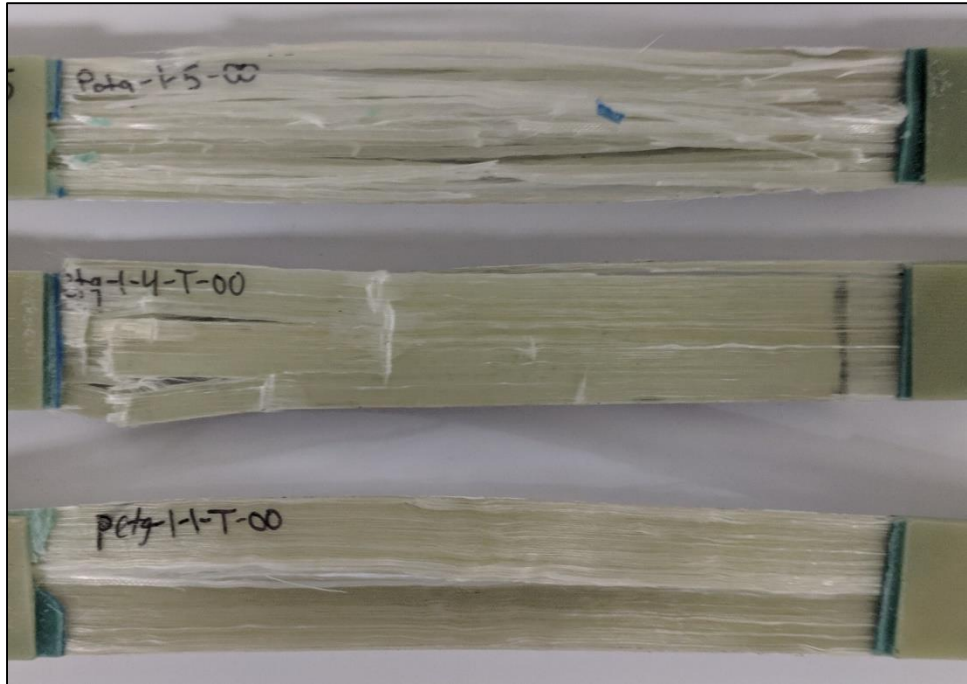


Figure 31: E-glass/PETg UD Multiple Failures Long. Tension Samples



Figure 32: E-glass/PETg UD Failed Trans. Tension Sample

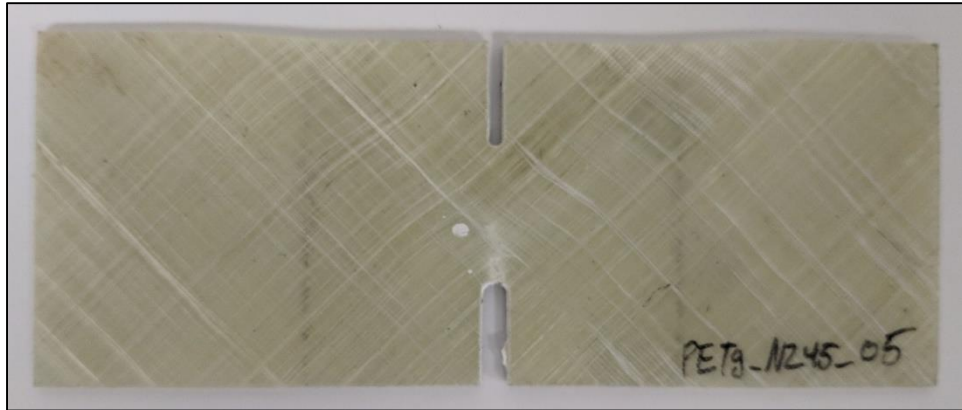


Figure 33: E-glass/PETg Bias Modified N2 Tension Sample



Figure 34: E-glass/Elium UD HAT Failure Trans. Compression Sample

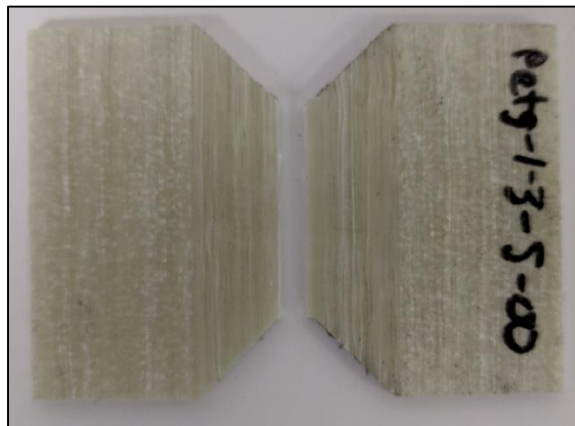


Figure 35: E-glass/PETg UD VGN Failure In-Plane Shear Sample

From these results based on comparing them to other glass reinforced composites in literature both material systems were shown to have comparable mechanical properties

showing them to be feasible as structural reinforcement in a hybrid composite-concrete structure. Therefore, more in depth and refined testing was done as detailed next.

3.2.2 Thermoplastic Composite Material Characterization

In the second phase of coupon tests, both the longitudinal and transverse properties of Elium were assessed in order to find the properties of a truly unidirectional Elium panel to be used with CLT for composite design. Original fabrication methods made this difficult due to warping effects, however lessons learned from experience with the Elium 150 resin made it possible for later iterations of panels to be made with $[0]_{10}$ fiber architecture. The infusion conducted for this testing used E-LR 1208 E-glass fabric.

3.2.2.1 Comparison of Experimental Mechanical Properties

Longitudinal and transverse properties derived from material testing of Elium, IE 5842 PETg, and Derakane E-glass are compared in Table 29 and Table 30 respectively, followed by a discussion of the experimental properties. Following the comparative discussion of experimental mechanical properties collected in this study comparison to micromechanics predictions calculated analytically from the constitutive material properties is given. Micromechanics predictions were done using both the Halpin-Tsai method and Mori-Tanaka method for comparison to experimental results.

Table 29: Comparison of Longitudinal Thermoplastic Properties to a Thermoset

Properties and COV	E-glass/ Elium	E-glass/ PETg	E-glass/ Vinyl ester
Fiber Volume Fraction V_f (%)	43.2 (1.4 %)	36.4 (3.0 %)	40.0 (4.3 %)
Tensile Strength F_{1t} (MPa)	741 (6.54 %)	623 (10.2 %)	835 (4.23 %)
Tensile Elastic Modulus E_{1t} (GPa)	33.15 (1.07 %)	28.2 (3.65 %)	33.37 (1.31 %)
Compressive Strength F_{1c} (MPa)	634 (2.16 %)	310 (17.7 %)	539 (15.8 %)
Compressive Elastic Modulus E_{1c} (GPa)	33.8 (6.40 %)	23.5 (14.68 %)	30.1 (9.93 %)
In-Plane Shear Strength F_6 (MPa)	42.0 (7.01 %)	28.8 (5.25 %)	42.2 (2.32 %)
In-Plane Shear Elastic Modulus G_{12} (GPa)	3.21 (6.75 %)	1.48 (18.9 %)	3.50 (4.65 %)
Poisson's Ratio ν_{12} (-)	0.313 (1.68 %)	0.353 (2.52 %)	0.31 (1.79 %)
Ultimate Tensile Strain ϵ_{1t}^u ($\mu\epsilon$)	23,600 (8.57 %)	23,300 (12.8 %)	27,000 (8.2 %)
Ultimate Compressive Strain ϵ_{1c}^u ($\mu\epsilon$)	18,100 (5.15 %)	12,300 (15.2 %)	18,100 (14.6 %)
Ultimate In-Plane Shear Strain ϵ_{1y}^u ($\mu\epsilon$)	22,700 (20.1 %)	49,800 (25.0 %)	18,700 (9.93 %)

Note: COV percentages reported with respective measured value in parenthesis.

Table 30: Comparison of Transverse Thermoplastic Properties to a Thermoset

Properties and COV	E-glass/ Elium	E-glass/ PETg	E-glass/ Vinyl ester
Tensile Strength F_{2t} (MPa)	29.2 (32.1 %)	14.5 (17.7 %)	41.7 (3.11 %)
Tensile Elastic Modulus E_{2t} (GPa)	8.38 (11.51 %)	4.43 (10.9 %)	9.23 (3.83 %)
Compressive Strength F_{2c} (MPa)	134 (3.14 %)	65.0 (6.92 %)	122 (2.58 %)
Compressive Elastic Modulus E_{2c} (GPa)	9.04 (9.48 %)	4.98 (13.9 %)	11.2 (6.19 %)
In-Plane Shear Strength F_6 (MPa)	58.9 (1.07 %)	31.1 (4.02 %)	58.6 (3.15 %)
In-Plane Shear Elastic Modulus G_{21} (GPa)	3.25 (5.30 %)	1.53 (6.67 %)	3.29 (3.07 %)
Poisson's Ratio ν_{21} (-)	0.069 (24.0 %)	0.823 (11.4 %)	0.084 (3.92 %)
Ultimate Tensile Strain ϵ_{2t}^u ($\mu\epsilon$)	3,900 (20.6 %)	3,400 (16.4 %)	5,000 (2.88 %)
Ultimate Compressive Strain ϵ_{2c}^u ($\mu\epsilon$)	31,500 (14.8 %)	24,700 (32.1 %)	12,900 (6.41 %)
Ultimate In-Plane Shear Strain ϵ_{2x}^u ($\mu\epsilon$)	245,000 (46.3 %)	251,000 (23.3 %)	143,000 (63.9 %)
Avg. Composite Panel Thickness t (mm)	4.4	2.4	4.3

Note: COV percentages reported with respective measured value in parenthesis.

The mechanical testing results presented in Table 29 show that of the two thermoplastic composites tested the E-glass/Elium composite was 16% stronger in longitudinal tension, 51% stronger in longitudinal compression, and 31% stronger in in-plane shear than the IE 5842b E-glass/PETg. In addition the Elium composite was 15% stiffer in tension, 30% stiffer in compression, and 54 % stiffer in shear. Overall, the Elium composite, which was fabricated through vacuum infusion performed better than the E-glass/PETg composite. This could be an artifact of the higher V_f achieved with the Elium composite, the type of glass used in the composites, Elium composites used E-LR 1208 from VectorPly and IE 5842b used an E-glass pre-combined with the matrix by the tape manufacturer.

Normalizing the longitudinal tensile strength and modulus to a V_f of 40% for comparison to the Derakane results by multiplying the experimental results by 40% over their respective experimental V_f value resulted in strength and modulus values of 686-MPa and 30.7-GPa respectively for Elium, and 685-MPa and 31.0-GPa for PETg. This normalization brought the two thermoplastic results much closer to each other. Both the Elium and PETg composites were approximately 18% weaker in strength and 7% less stiff than the Derakane composite when normalized in this way. Similar normalizations were done on thermoplastic composites tested in compression in Warren [2], the amorphous PETg compression results in that study showed a longitudinal compressive strength of 483.8-MPa with a V_f of 55%. Normalizing that result to a V_f of 40% for comparison to the PETg tested in this study the strength was 351-MPa, which is 3% higher than the normalized result of 341-MPa from this study.

Normalizing the longitudinal compressive strength and modulus to a V_f of 40% for comparison in the same way as was done for longitudinal tension. The

resulting strength and modulus values were 587-MPa and 31.3-GPa respectively for E-glass/Elium, and 341-MPa and 25.8-GPa respectively for E-glass/PETg. This normalization brought the E-glass/Elium results closer to the E-glass/Derakane results; however, the E-glass/PETg results are still significantly lower than the other two composites.

Comparing the longitudinal properties of the two thermoplastic composites to the thermoset vinyl ester Derakane, both thermoplastics were weaker in tension, though the Elium composite was closer in strength and had nearly the same stiffness. In compression, the Elium composite was stronger than Derakane, which was stronger than the PETg composite. It should be noted that compression samples might experience bending effects during testing, which could result in lower strength and modulus from the experiment. In addition, the volume used to capture ARAMIS data on the sample for a D6641 compression test is small in comparison to the other tests, which can lead to difficulties collecting accurate strain data. These factors may contribute to the low compressive strength seen by the E-glass/PETg samples as well as the differences in the longitudinal tensile and compressive elastic modulus, which should be the same theoretically. Another factor which is likely to have contributed to the low compressive strength of the E-glass/PETg samples is the low compressive strength of 55-MPa for PETg polymer compared to 130-MPa for Elium acrylic polymer, and 127-MPa for Derakane epoxy vinyl ester polymer. The in-plane shear strengths and elastic moduli of the Elium and Derakane CFRTP composites were very close; however, the PETg composite did not perform as well. The transverse properties in Table 30 followed the same comparative trend as the longitudinal properties. Figure 36 through Figure 38 show the stress-strain responses for tension, compression, and

in-plane shear for a representative sample from testing done on E-glass/Elium, E-glass/Derakane, and E-glass/PETg composites respectively.

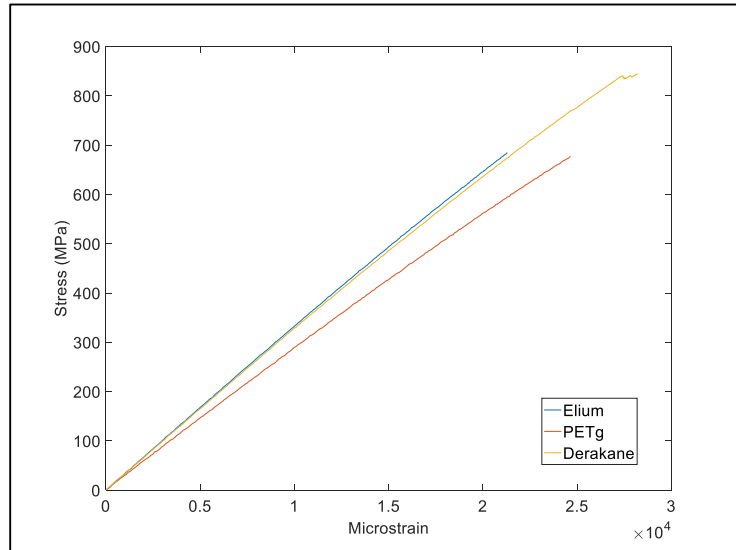


Figure 36: Tensile Stress-Strain Response of Representative Samples

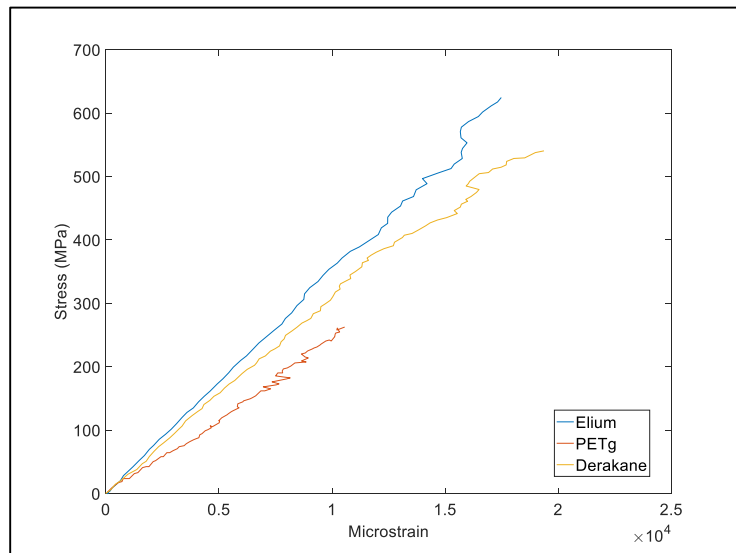


Figure 37: Compressive Stress-Strain Response of Representative Samples

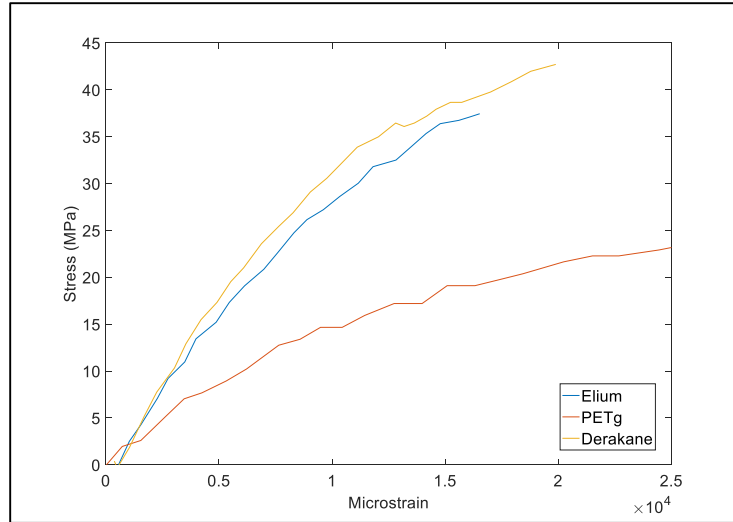


Figure 38: In-Plane Shear Stress-Strain Response of Representative Samples

The fact that the two vacuum infused composites, Elium and Derakane, used for this study performed in a similar nature is reasonable given that they both used the same E-glass reinforcement when infused and the majority of the failures seen in testing were fiber-dominated failures. This further reinforces that based on strength and stiffness, the Elium 150 resin-system is suitable option for circumstances where an infused thermoset composite would traditionally be of interest.

3.2.2.2 Composite Predictions of Elastic and Strength Properties

As a method to provide context for the experimental results, composite micromechanics theory was used to predict values for the unidirectional laminates tested by predicting the analytical properties of a single unidirectional lamina. The properties of the glass-fibers and polymer matrices used were summarized in Table 22 and Table 23 in chapter 2. The V_f used for this analysis were assumed to match the ones observed from experiments in order to make the predictions as comparable as possible. The fracture toughness mode I

and II values were assumed to be $G_{Ic} = 334 \frac{J}{m^2}$ [37] and $G_{IIc} = 456 \frac{J}{m^2}$ [37] respectively for an E-glass/Polyester because values were not known for the material used in this study.

Two types of micromechanics analysis were performed to calculate analytical results for comparison with the experimental results. The elastic behavior was predicted analytically in two ways: using the Rule of Mixtures and Halpin-Tsai method [7] [37] (shown in equations 3 through 4 and 5 through 10 respectively), the Poisson's ratio out of plane was found using an isotropic relationship [7], and the Mori-Tanaka method [49] [50] (shown in equations 12 through 31). Then micromechanics analysis was performed to analytically predict the strength of the composite laminas based on constitutive properties and calculated elastic behavior [7] [37] (shown in equations 32 through 40).

Longitudinal elastic properties for continuous fiber composites (loaded in the direction of fibers, i.e. 1-direction) are dominated by the fibers because they are typically stronger, stiffer, and have lower ultimate strain than the matrix. If a perfect bond between fibers and matrix is assumed then the longitudinal strains are uniform throughout the composite leading to the Rule of Mixtures equations for longitudinal elastic modulus (E_1) and in-plane Poisson's ratio (ν_{12}) shown in equations 3 and 4 respectively [7].

$$E_1 = E_f V_f + E_m (1 - V_f) \quad \text{Equation 3}$$

$$\nu_{12} = \nu_f V_f + \nu_m (1 - V_f) \quad \text{Equation 4}$$

Transverse elastic properties for continuous fiber composites (loaded perpendicular to the direction of fibers, i.e. 2-direction) are influenced by a nonuniform stress-state in the matrix surrounding the fibers in the composite. The transverse elastic modulus (E_2) is dominated

by the matrix and can be estimated using the Halpin-Tsai semiempirical relation, which uses an elastic modulus parameter (η_E) combined with an equation for the transverse elastic modulus (E_2) shown in equations 5 and 6 respectively [7]. The Halpin-Tsai method uses a curve fitting parameter (ξ), which was assumed to be 2 for circular fibers [37] for all analysis done in this study.

$$\eta_E = \frac{\frac{E_f}{E_m} - 1}{\frac{E_f}{E_m} + \xi} \quad \text{Equation 5}$$

$$E_2 = \frac{E_m(1 + \xi\eta_E V_f)}{1 - \eta_E V_f} \quad \text{Equation 6}$$

Similar to the transverse elastic properties the in-plane shear elastic properties are dominated by the matrix (loaded under in-plane shear, i.e. shear in the 1-2 plane) [7]. Halpin-Tsai semiempirical relationships are known for calculating both the in-plane and out-of-plane shear modulus. This method uses a shear modulus parameter (η_G) combined with an equation for the in-plane shear modulus (G_{12}) [7] [37], and a shear modulus parameter 4 (η_4) combined with an equation for out-of-plane (intralaminar) shear modulus (G_{23}) [37] shown in equations 7 through 10 respectively.

$$\eta_G = \frac{\frac{G_f}{G_m} - 1}{\frac{G_f}{G_m} + \xi} \quad \text{Equation 7}$$

$$G_{12} = \frac{G_m(1 + \xi\eta_G V_f)}{1 - \eta_G V_f} \quad \text{Equation 8}$$

$$\eta_4 = \frac{3 - (4\nu_m + \frac{G_m}{G_f})}{4(1 - \nu_m)} \quad \text{Equation 9}$$

$$G_{23} = \frac{G_m(V_f + \eta_4 V_m)}{\eta_4 V_m + \frac{V_f G_m}{G_f}} \quad \text{Equation 10}$$

In a transversely isotropic material i.e. a unidirectional composite lamina an isotropic relationship can be used to relate the Poisson's ratio and shear modulus in the plane of isotropy i.e. the 2-3 plane [7]. Equation 11 shows the application of this relationship to solve for the out-of-plane transverse Poisson's ratio (ν_{23}).

$$\nu_{23} = \frac{E_2}{2G_{23}} - 1 \quad \text{Equation 11}$$

An alternative to the previous methods discussed to get the elastic properties of a composite is the Mori-Tanaka method. The Mori-Tanaka method employs a mean field approach, which relates the microscale stresses and strains in the fiber and matrix to the average microscale stresses and strains through the phase concentration tensors [51].

The equations for the Mori-Tanaka method are commonly expressed in terms of the Hill's elastic moduli which use the elastic properties of the base materials shown in equations 12 through 16 for the fibers and equations 17 through 21 for the matrix [51] [49] [50].

$$k_f = \left(\frac{4}{E_f} - \frac{1}{G_f} - \frac{4\nu_f^2}{E_f} \right)^{-1} \quad \text{Equation 12}$$

$$l_f = 2\nu_f k_f \quad \text{Equation 13}$$

$$m_f = G_f \quad \text{Equation 14}$$

$$n_f = E_f + \frac{l_f^2}{k_f} \quad \text{Equation 15}$$

$$p_f = G_f \quad \text{Equation 16}$$

$$k_m = \frac{E_m}{(2 - 2\nu_m - 4\nu_m^2)} \quad \text{Equation 17}$$

$$l_m = 2\nu_m k_m \quad \text{Equation 18}$$

$$m_m = \frac{E_m}{2(1 + \nu_m)} \quad \text{Equation 19}$$

$$n_m = E_m + \frac{l_m^2}{k_m} \quad \text{Equation 20}$$

$$p_m = \frac{E_m}{2(1 + \nu_m)} \quad \text{Equation 21}$$

Next the effective Hill's elastic moduli are found for a unidirectional fiber reinforced composite using equations 22 through 26 [51] [49] [50].

$$k = \frac{V_f k_f (k_m + m_m) + V_m k_m (k_f + m_m)}{V_f (k_m + m_m) + V_m (k_f + m_m)} \quad \text{Equation 22}$$

$$l = \frac{V_f l_f (k_m + m_m) + V_m l_m (k_f + m_m)}{V_f (k_m + m_m) + V_m (k_f + m_m)} \quad \text{Equation 23}$$

$$m = \frac{m_m m_f (k_m + 2m_m) + k_m m_m (V_f m_f + V_m m_m)}{k_m m_m + (k_m + 2m_m)(V_m m_f + V_f m_m)} \quad \text{Equation 24}$$

$$n = V_m n_m + V_f n_f + \frac{(l - V_f l_f - V_m l_m)(l_f - l_m)}{k_f - k_m} \quad \text{Equation 25}$$

$$p = \frac{2V_f p_m p_f + V_m (p_m p_f + p_m^2)}{2V_f p_m + V_m (p_f + p_m)} \quad \text{Equation 26}$$

From the effective Hill's elastic moduli the effective engineering properties of a composite can be found using equations 27 through 31 [51] [49] [50].

$$E_1 = n - \frac{l^2}{k} \quad \text{Equation 27}$$

$$E_2 = \frac{4m(kn - l^2)}{(k + m)n - l^2} \quad \text{Equation 28}$$

$$\nu_{12} = \frac{l}{2k} \quad \text{Equation 29}$$

$$G_{12} = p \quad \text{Equation 30}$$

$$G_{23} = m \quad \text{Equation 31}$$

Analytically solving for the theoretical strength properties of composite materials is also important. The longitudinal tensile strength i.e. tensile strength in the 1-direction (F_{1t}) is found either by equation 32 for fiber-dominated failure or equation 33 for a matrix dominated failure [7]. The longitudinal compressive strength i.e. compressive strength in the 1-direction is found by equations 34 and 35, which are a lamina compressive strength factor (χ) and the equation for the longitudinal compressive strength (F_{1c}) respectively [37].

$$F_{1t} = F_{ft} \left[V_f + \frac{E_m}{E_f} V_m \right] \quad \text{Equation 32}$$

$$F_{1t} = F_{mt} \left[V_f \frac{E_m}{E_f} + V_m \right] \quad \text{Equation 33}$$

$$\chi = \frac{G_{12} \alpha_\sigma}{F_6} \quad \text{Equation 34}$$

$$F_{1c} = G_{12} (1 + 4.76\chi)^{-0.69} \quad \text{Equation 35}$$

The transverse tensile strength i.e. tensile strength in the 2-direction was found using equations 36 and 37, which are a lamina tensile strength factor (Λ_{22}^0) and the equation for transverse tensile strength (F_{2t}) respectively [37]. The transverse compressive strength i.e. the compressive strength in the 2-direction (F_{2c}) was found using equation 38 [37].

$$\Lambda_{22}^0 = 2 \left(\frac{1}{E_2} - \frac{\nu_{12}^2 E_2^2}{E_1^3} \right) \quad \text{Equation 36}$$

$$F_{2t} = \sqrt{\frac{G_{Ic}}{1.122^2 \pi \left(\frac{t_t}{4} \right) \Lambda_{22}^0}} \quad \text{Equation 37}$$

$$F_{2c} = F_{mc} C_v \left[1 + (V_f - \sqrt{V_f}) \left(1 - \frac{E_m}{E_f} \right) \right] \quad \text{Equation 38}$$

The in-plane shear strength i.e. the shear strength in the 1-2 plane was found using equations 39 and 40, which are a lamina shear strength factor (Λ_{44}^0) and the equation for in-plane shear strength (F_6) respectively [37].

$$\Lambda_{44}^0 = \frac{1}{G_{12}} \quad \text{Equation 39}$$

$$F_6 = \sqrt{\frac{G_{IIc}}{\pi \left(\frac{t_t}{4}\right) A_{44}^0}} \quad \text{Equation 40}$$

Table 31 through Table 33 give the analytical predictions from both the Halpin-Tsai [7] method and Mori-Tanaka method for the elastic behavior of E-glass/Elium, E-glass/Derakane, and E-glass/PETg respectively compared to the experimental results collected in this study. Table 34 gives the analytically predicted strength properties for the three composite materials compared to experimental results. Predicted composite strengths from micromechanics were condensed to one table because only some of the strength properties use the lamina elastic behavior when calculated. These properties (longitudinal compressive strength, transverse tensile strength, and in-plane shear strength) give both the results using Halpin-Tsai and Mori-Tanaka predicted lamina elastic properties respectively in the table.

Table 31: Predicted vs Experimental Elastic Properties (E-glass/Elium $V_f = 43.2\%$)

Elastic Property	Halpin-Tsai Analytical Prediction	Mori-Tanaka Analytical Prediction	Experimental Results
Longitudinal Elastic Modulus, E_1 (GPa)	33.4	33.4	33.2 (tension) 33.8 (compression)
Transverse Elastic Modulus, E_2 (GPa)	9.32	7.66	8.38 (tension) 9.04 (compression)
In-Plane Shear Elastic Modulus, $G_{12} = G_{13}$ (GPa)	3.45	2.8	3.21
Intralaminar Shear Elastic Modulus, G_{23} (GPa)	2.63	2.56	-
Poisson's Ratio, $\nu_{12} = \nu_{13}$ (-)	0.31	0.30	0.31
Poisson's Ratio ν_{23} (-)	0.78	0.50	-

Table 32: Predicted vs Experimental Elastic Properties (E-glass/Derakane $V_f = 40.0\%$)

Elastic Property	Halpin-Tsai Analytical Prediction	Mori-Tanaka Analytical Prediction	Experimental Results
Longitudinal Elastic Modulus, E_1 (GPa)	28	28	33.4 (tension) 30.1 (compression)
Transverse Elastic Modulus, E_2 (GPa)	5.51	4.6	9.23 (tension) 11.2 (compression)
In-Plane Shear Elastic Modulus, $G_{12} = G_{13}$ (GPa)	2.03	1.65	3.50
Intralaminar Shear Elastic Modulus, G_{23} (GPa)	1.54	1.52	
Poisson's Ratio, $\nu_{12} = \nu_{13}$ (-)	0.32	0.31	0.31
Poisson's Ratio ν_{23} (-)	0.79	0.52	

Table 33: Predicted vs Experimental Elastic Properties (E-glass/PETg $V_f = 36.4\%$)

Elastic Property	Halpin-Tsai Analytical Prediction	Mori-Tanaka Analytical Prediction	Experimental Results
Longitudinal Elastic Modulus, E_1 (GPa)	31.3	31.3	28.2 (tension) 23.5 (compression)
Transverse Elastic Modulus, E_2 (GPa)	9.09	7.44	4.43 (tension) 4.98 (compression)
In-Plane Shear Elastic Modulus, $G_{12} = G_{13}$ (GPa)	3.41	2.8	1.48
Intralaminar Shear Elastic Modulus, G_{23} (GPa)	2.61	2.55	-
Poisson's Ratio, $\nu_{12} = \nu_{13}$ (-)	0.30	0.30	0.35
Poisson's Ratio ν_{23} (-)	0.74	0.46	-

For all three materials analyzed and tested in this study the Halpin-Tsai and Mori-Tanaka methods showed similar behavior in how they predicted the elastic response compared to the experimental results. Halpin-Tsai and Mori-Tanaka predict the same value for longitudinal elastic modulus; Halpin-Tsai consistently predicts higher values than Mori-Tanaka for transverse elastic modulus, in-plane shear modulus, intralaminar shear

modulus, and Poisson's ratio in the 2-3 plane. Due to the higher predictions calculated for transverse and shear modulus using Halpin-Tsai method, which are used in the micromechanics methods for lamina strengths, slightly higher predictions for strength are found when used than when using Mori-Tanaka moduli predictions as inputs.

Table 34: Predicted vs Experimental Strength Properties

Property	Micromechanics Prediction or Experimental	E-glass/ Elium	E-glass/ PETg	E-glass/ Derakane
V_f (%)	Experimental	43.2	36.4	40.0
F_{1t} (MPa)	Mori-Tanaka	769	672	635
	Halpin-Tsai	769	672	635
	Experimental	741	623	835
F_{1c} (MPa)	Mori-Tanaka	447	312	447
	Halpin-Tsai	515	359	511
	Experimental	634	310	539
F_{2t} (MPa)	Mori-Tanaka	46.5	36.1	45.9
	Halpin-Tsai	51.4	39.5	50.7
	Experimental	29.2	14.5	41.7
F_{2c} (MPa)	Mori-Tanaka	102	42.2	98.9
	Halpin-Tsai	102	42.2	98.9
	Experimental	134	65	122
F_6 (MPa)	Mori-Tanaka	52	40	52
	Halpin-Tsai	57.8	44.3	57.4
	Experimental	42	28.8	42.2

During the feasibility testing conducted on the E-glass/PETg composites specimens were tested to get longitudinal, transverse, and bias properties. Figure 39 shows the experimental results for longitudinal tension elastic modulus for longitudinal, transverse and bias fiber-orientations and the corresponding macromechanics prediction for longitudinal elastic modulus as it varies with fiber-orientation. Macromechanics predictions were calculated twice for this comparison. First, the lamina properties from the properties of the E-glass and PETg matrix were used as input, and second the experimental lamina properties collected during the material feasibility testing for this study were used as input. Micromechanics calculations to predict the lamina properties were done using the rule of mixtures and Halpin-Tsai methods given in equations 3 through 10 [7] [37]. Macromechanics calculations to get the effective tensile modulus for different fiber orientations in a composite lamina was done using equations 41 through 44 [7] [37].

$$[S_{reduced}] = \begin{bmatrix} \frac{1}{E_1} & -\frac{\nu_{12}}{E_1} & 0 \\ -\frac{\nu_{12}}{E_1} & \frac{1}{E_2} & 0 \\ 0 & 0 & \frac{1}{G_{12}} \end{bmatrix} = \begin{bmatrix} S_{11} & S_{12} & 0 \\ S_{21} & S_{22} & 0 \\ 0 & 0 & S_{66} \end{bmatrix} \quad \text{Equation 41}$$

$$[T] = \begin{bmatrix} m^2 & n^2 & 2mn \\ n^2 & m^2 & -2mn \\ -mn & mn & m^2 - n^2 \end{bmatrix} \quad \text{Equation 42}$$

$$[S_{transformed}] = \begin{bmatrix} S_{xx} & S_{xy} & S_{xs} \\ S_{yx} & S_{yy} & S_{ys} \\ \frac{1}{2}S_{sx} & \frac{1}{2}S_{sy} & \frac{1}{2}S_{ss} \end{bmatrix} = [T^{-1}] \begin{bmatrix} S_{11} & S_{12} & 0 \\ S_{21} & S_{22} & 0 \\ 0 & 0 & \frac{1}{2}S_{66} \end{bmatrix} [T] \quad \text{Equation 43}$$

$$E_x = \frac{1}{S_{xx}} \quad \text{Equation 44}$$

Where:

- Equations 41 through 43 implement the stress-strain relations for a thin lamina [7] to get the reduced compliance matrix, transformation matrix, and transformed compliance matrix respectively
- Theta (θ) is the fiber orientation from the longitudinal-direction, and $m = \cos(\theta)$ and $n = \sin(\theta)$ [7]
- E_x is the effective elastic modulus calculated at the desired theta (θ) orientation of the reinforcement fibers, which is E_{xt} for effective tensile elastic modulus.

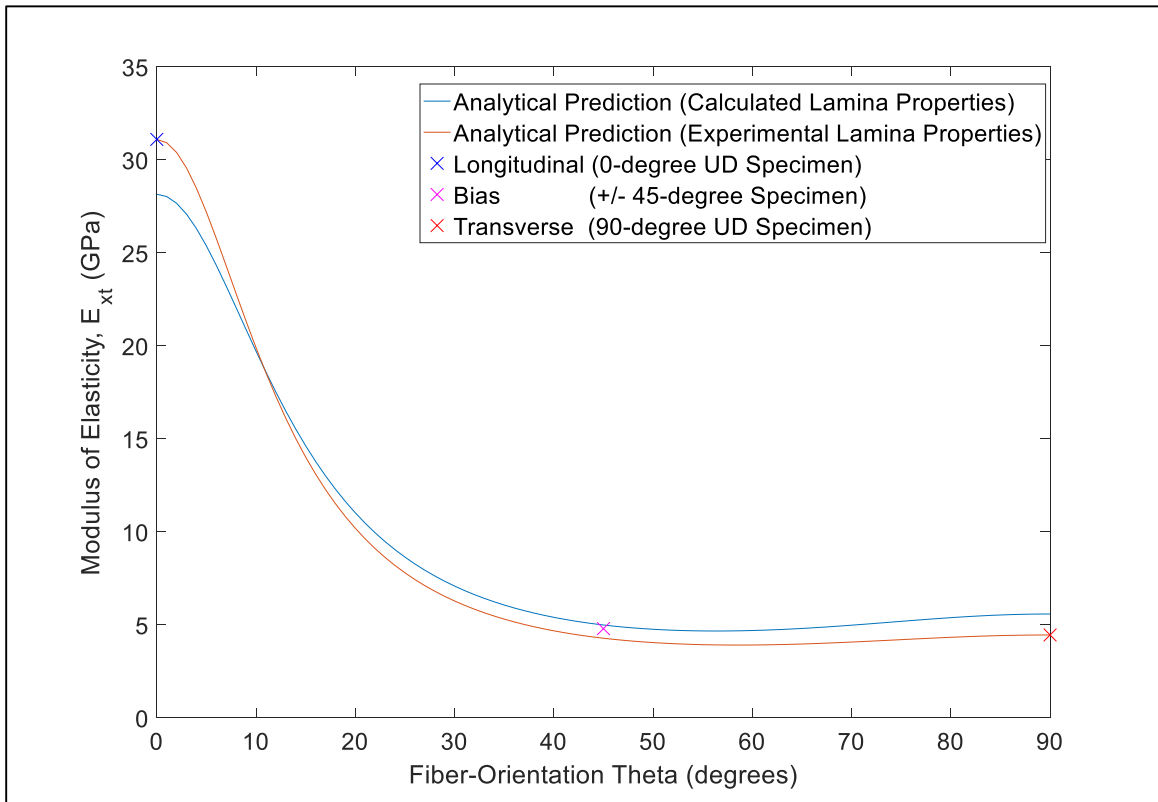


Figure 39: Comparison of Long. Elastic Modulus for Various Fiber-Orientations

Figure 39 shows a plot of the effective modulus of elasticity in the x-direction versus the fiber-orientation theta for two methods of analytical prediction and three points from experimental data taken in this study. Both methods of macromechanics predictions show the same type of behavior as the modulus varies with fiber-orientation. However, since the method using experimental lamina properties exactly matches the longitudinal and transverse specimen values the domain of the curve is slightly different, but has the same shape as the calculated lamina properties prediction. The calculated lamina property prediction shows a lower value for the longitudinal (0-degree) modulus of elasticity in tension by 9 % and a higher value for the transverse (90-degree) modulus of elasticity in tension by 14 %. For the bias modulus of elasticity in tension, macromechanics with calculated lamina properties overestimates its value by 4 % and macromechanics with experimental properties underestimates its value by 11 %.

3.2.2.3 Unidirectional E-glass/Elium Test Results

Table 29 and Table 30 in section 3.2.3.1 Comparison of Mechanical Properties shows the detailed E-glass/Elium composite material mechanical property numerical results. The composite panels used for this testing were observed to have an average thickness of 4.4-mm. Figure 40 through Figure 45 show the longitudinal and transverse tension, compression, and in-plane shear stress-strain responses for the unidirectional E-glass/Elium tested and Table 35 shows the failure classifications for the unidirectional E-glass/Elium specimens tested.

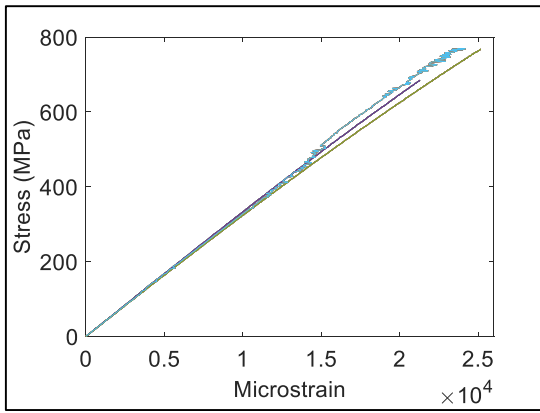


Figure 40: E-glass/Elium UD Longitudinal Tension
Stress-Strain Response

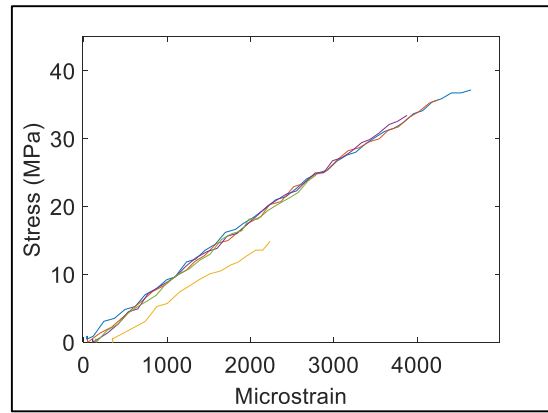


Figure 41: E-glass/Elium UD Transverse Tension
Stress-Strain Response

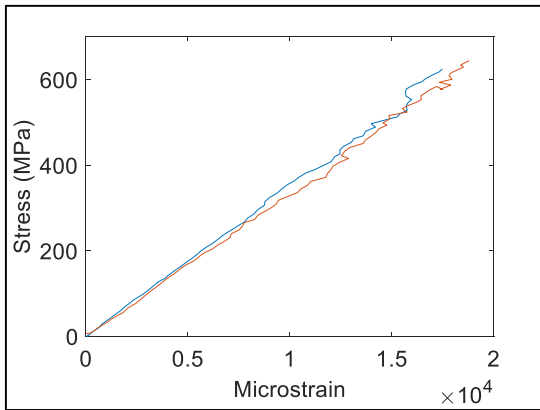


Figure 42: E-glass/Elium UD Longitudinal Tension
Stress-Strain Response

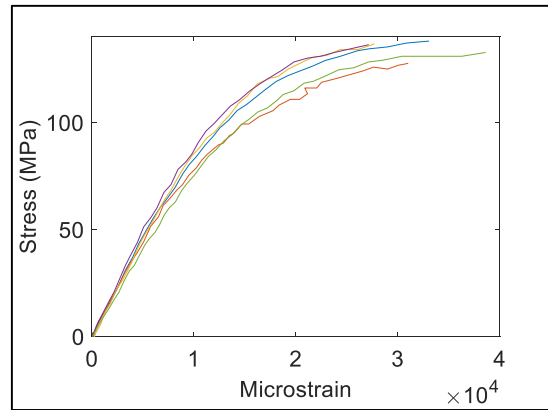


Figure 43: E-glass/Elium UD Transverse Compression
Stress-Strain Response

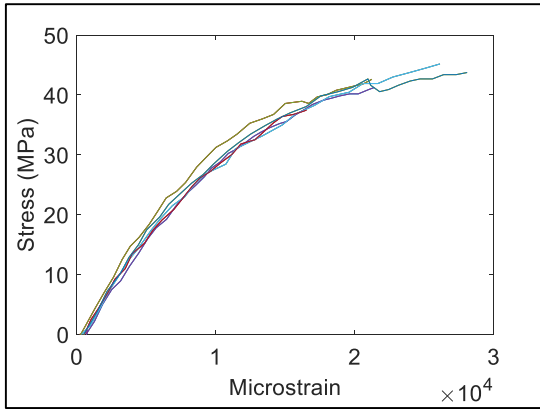


Figure 44: E-glass/Elium UD In-Plane Shear (G_{xy})

Stress-Strain Response

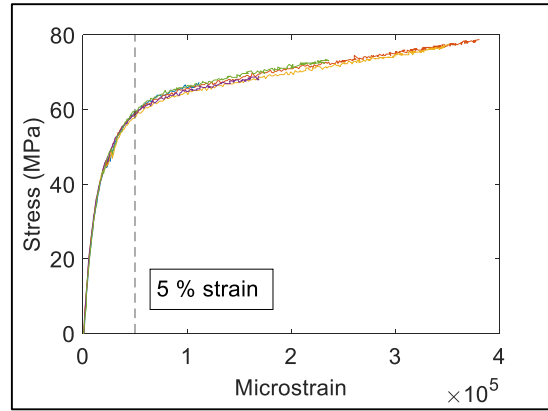


Figure 45: E-glass/Elium UD In-Plane Shear (G_{yx})

Stress-Strain Response

Table 35: Detailed E-glass/Elium UD Sample Failure Types

Specimen Orientation	Specimen Type	ASTM D3039 Tension [38]	ASTM D6641 Compression [40]	ASTM D7078 In-Plane Shear [41]
Longitudinal	Failure Type	DGM, OAV	BGM, CIT	VSA
	Number of Failures	3, 5	2, 3	5
Transverse	Failure Type	LGT, LAT	HAT	HGN
	Number of Failures	5, 3	5	5

The longitudinal tension samples tested all shared the same failure type, edge delamination-gage-middle (DGM) that is shown in Figure 46. Failure type LGT exhibited by the

transverse tension samples is shown previously in Figure 32. In addition failure type BGM exhibited by the longitudinal compression samples was shown in Figure 22. Figure 34 shows failure type HAT, which was exhibited by all the transverse compression samples tested for this material. Figure 47 shows the vertical cracking-side region-adjacent to notches (VSA) failure seen by all the G_{xy} orientation in-plane shear samples tested for the unidirectional E-glass/Elium. This not the typical failure mode seen in these samples at the ASCC, however due to the relative vertical weakness of the matrix between the fiber toes running from top to bottom it was viewed as acceptable. All of the G_{yx} in-plane shear samples tested of this material experienced failure type HGN previously shown in Figure 23. The OAV and lateral-at grip/tab (LAT) tension failures, and end-crushing-inside grip/tab-top (CIT) compression failures were not used when characterizing the material because they are not considered valid failures.



Figure 46: E-glass/Elium UD DGM Failure Long. Tension Sample

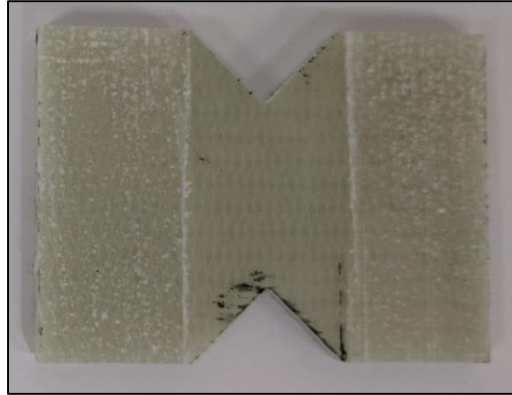


Figure 47: E-glass/Elium UD VSA Failure (G_{xy}) In-Plane Shear Sample

3.2.2.4 Unidirectional E-glass/Derakane Test Results

To assess the feasibility of the thermoplastic composites in this study for structural applications, a traditionally infused thermoset Derakane 610-C was used to create samples for testing in order to have a baseline to compare the thermoplastic composites against examples against. Derakane 610-C is an industry accepted resin-system by for use in structural composites and was familiar to the ASCC. The mechanical property testing results for the unidirectional 10-layer E-Glass/Derakane samples are shown in Table 29 and Table 30 in section 3.2.3.1 Comparison of Mechanical Properties.

Figure 48 through Figure 53 show the longitudinal and transverse tension, compression and in-plane shear stress-strain responses for the unidirectional E-glass/Derakane thermoset composite tested. Table 36 shows the failure types and number of coupons tested for the unidirectional E-glass/Derakane composites tested for this study.

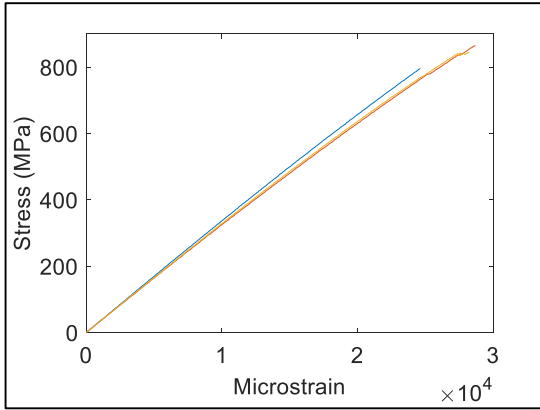


Figure 48: E-glass/Derakane UD Long. Tension Stress-Strain Response

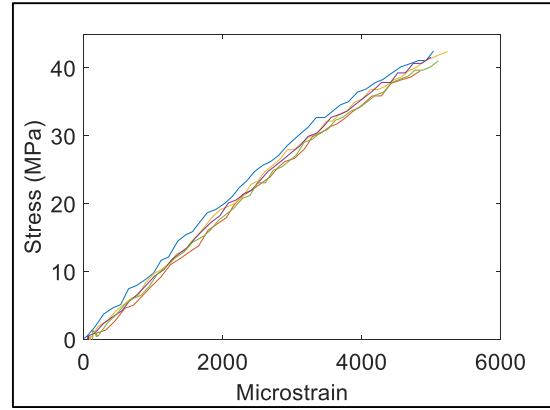


Figure 49: E-glass/Derakane UD Trans. Tension Stress-Strain Response

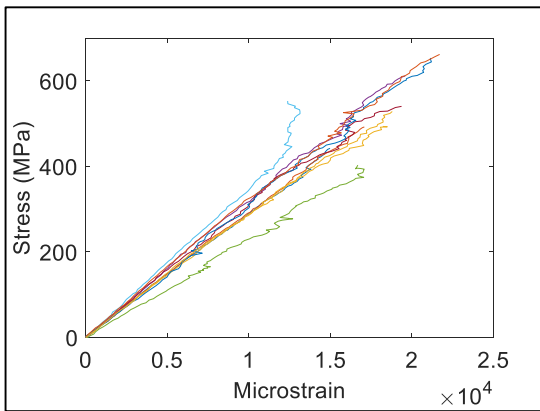


Figure 50: E-glass/Derakane UD Long. Compression Stress-Strain Response

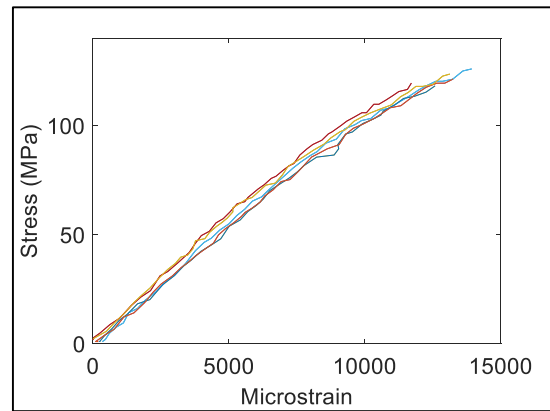


Figure 51: E-glass/Derakane UD Trans. Compression Stress-Strain Response

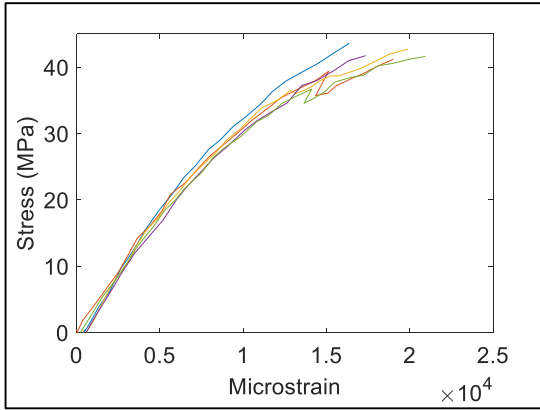


Figure 52: E-glass/Derakane UD In-Plane Shear (G_{xy})

Stress-Strain Response

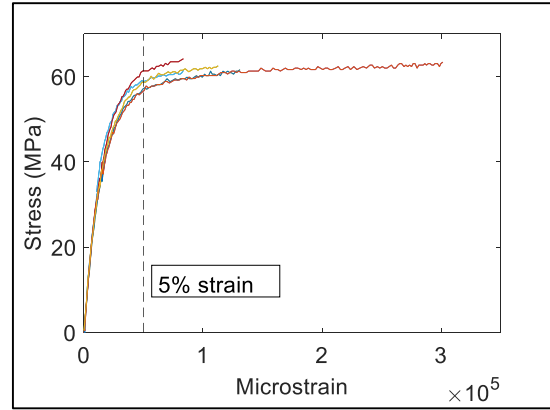


Figure 53: E-glass/Derakane UD In-Plane Shear (G_{yx})

Stress-Strain Response

Table 36: E-glass/Derakane UD Failure Types

Specimen Orientation	Specimen Type	ASTM D3039 Tension [38]	ASTM D6641 Compression [40]	ASTM D7078 In-Plane Shear [41]
Longitudinal	Failure Type	XGR, DGT, OAV	BGM	VGN, VSE
	Number of Failures	1, 2, 4	10	5, 1
Transverse	Failure Type	LGT	HAT	HGN
	Number of Failures	5	5	5

Figure 54 shows the two types of failures seen by E-glass/Derakane longitudinal tension composite samples that were tested. The top sample showed explosive-gage-right (XGR)

type failure similar to the XGM failure seen in other longitudinal tension samples in this study. The bottom samples showed edge delamination-gage-top (DGT) type failure, which is similar to DGM type failure seen in other samples. The four tension samples with the OAV failure mode indicating the grips failed and not the specimen were not used because they are not a valid failure mode.

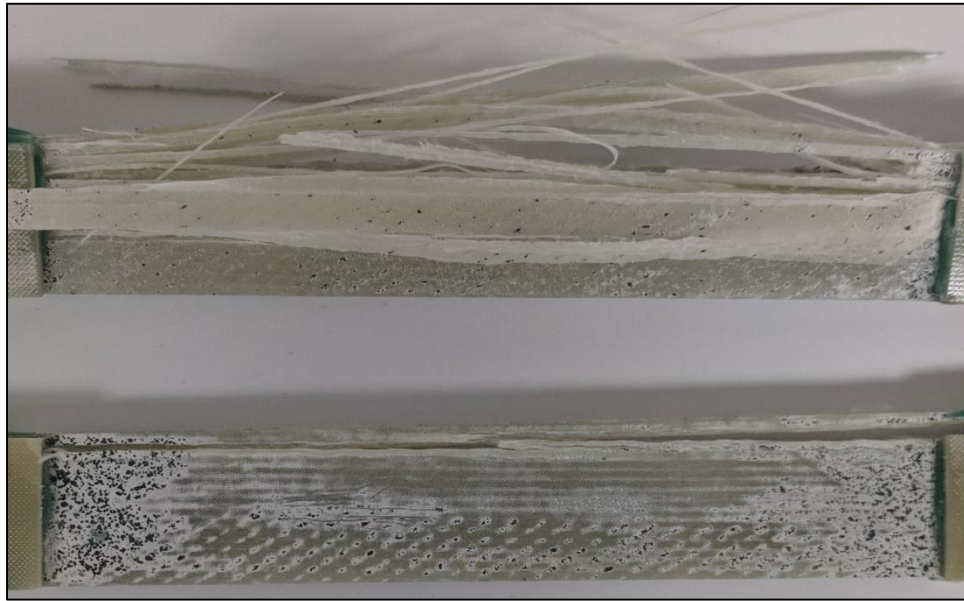


Figure 54: E-glass/Derakane UD Multiple Failures Long. Tension Samples

The transverse tension samples exhibited LGT type failure as was shown in Figure 32. The longitudinal and transverse compression samples showed failure types BGM shown in Figure 22 and HAT shown in Figure 34 respectively. The G_{xy} in-plane shear samples showed failure type VGN as previously seen in Figure 35. The vertical cracking-side region-top and/or bottom edge (VSE) samples were not shown because this is not a valid failure mode.

3.2.2.5 Unidirectional E-glass/PETg Test Results

The fully automated thermoforming process used for the final phases of manufacturing in this study uses IE 5842b instead of the original PETg material, IE 5842, that was used for the feasibility testing. The only difference in these two materials is that IE 5842b is dyed black. However to reflect improvements in manufacturing and verify the new material properties unidirectional coupons 10-layer unidirectional samples were made with IE 5842b and tested. The mechanical properties from these tests is shown in Table 29 and Table 30 in section 3.2.3.1 Comparison of Mechanical Properties.

Figure 55 through Figure 60 show the longitudinal and transverse tension, compression, and in-plane shear stress-strain response of the coupons tested. Table 37 shows the failure types and number of failures for the IE 5842b E-glass/PETg samples tested.

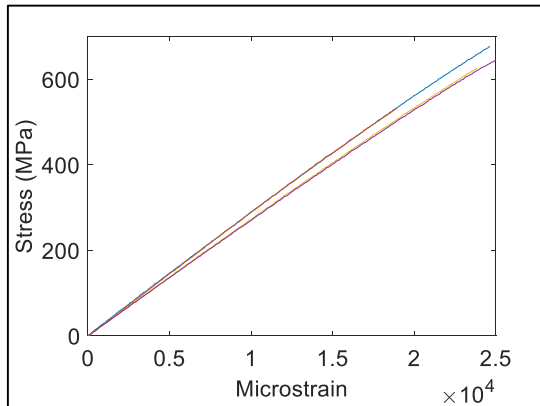


Figure 55: E-glass/PETg UD Long. Tension Stress-Strain Response

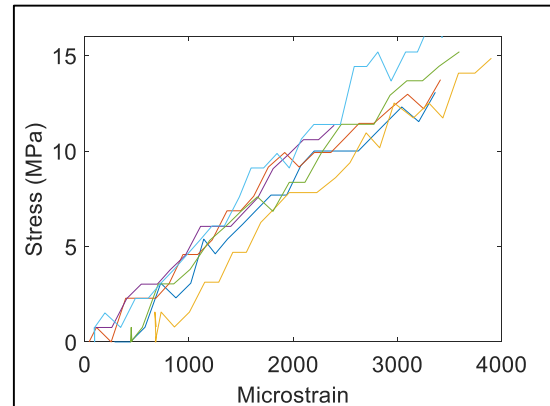


Figure 56: E-glass/PETg UD Trans. Tension Stress-Strain Response

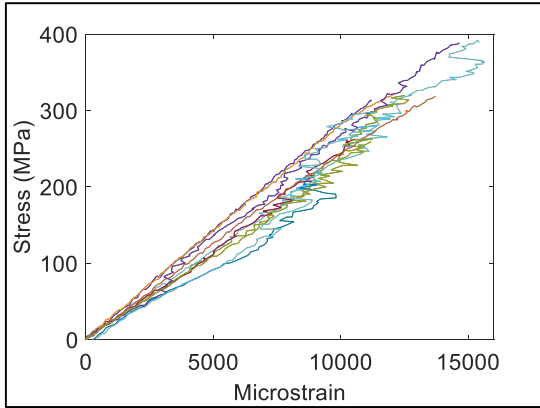


Figure 57: E-glass/PETg UD Long. Compression Stress-Strain Response

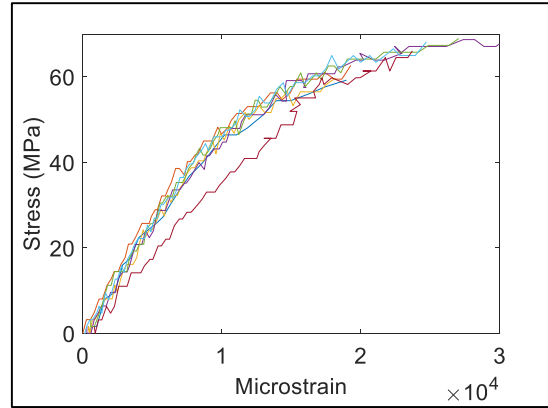


Figure 58: E-glass/PETg UD Trans. Compression Stress-Strain Response

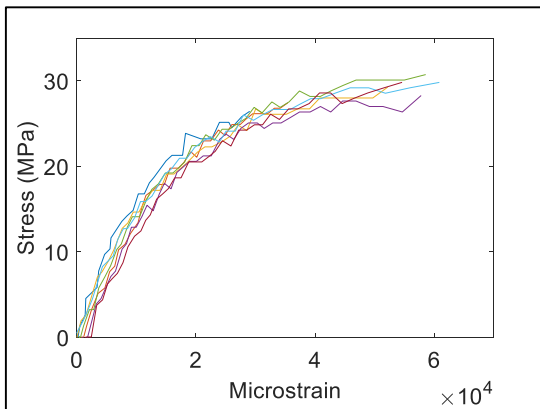


Figure 59: E-glass/PETg UD In-Plane Shear (G_{xy}) Stress-Strain Response

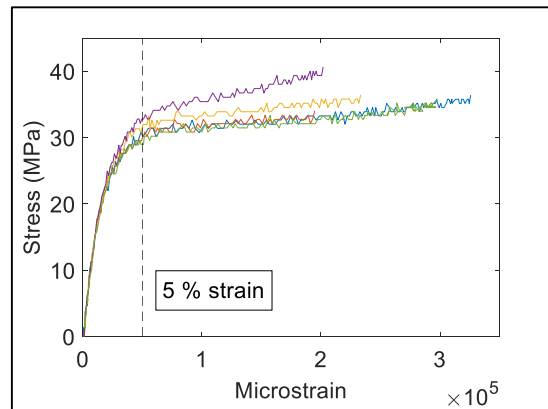


Figure 60: E-glass/PETg UD In-Plane Shear (G_{yx}) Stress-Strain Response

Table 37: IE 5842b E-glass/PETg UD Failure Types

Specimen Orientation	Specimen Type	ASTM D3039 Tension [38]	ASTM D6641 Compression [40]	ASTM D7078 In-Plane Shear [41]
Longitudinal	Failure Type	DGM, OAV	BGM, HAT	VGN
	Number of Failures	5, 3	7, 3	7
Transverse	Failure Type	LGT	HAT	HGN
	Number of Failures	6	8	5

The failure modes exhibited by the longitudinal and transverse tension samples were DGM shown in Figure 46 and LGT shown in Figure 32 respectively. The failure modes seen by the longitudinal and transverse compression samples were BGM shown in Figure 22 and HAT shown in Figure 34 respectively. The failure modes seen by the in-plane shear samples were previously shown in Figure 35 and Figure 23 respectively. The tension samples with failure type OAV were not used because this is not a valid failure mode.

3.2.2.6 Beam Layup E-glass/PETg Test Results

To support the design discussed in Chapter 4 of this thesis for a hybrid composite-concrete structure a fiber architecture was developed for a beam specimen. Consolidated laminates of the beam layup, [+/- 45 90 0]_s, using IE 5842b material, were stamp formed and tested to compare against results found by using the unidirectional IE 5842b E-glass/PETg material characterization and classical lamination theory [7] [37]. Composite

macromechanics techniques were used to implement the unidirectional testing results as lamina input parameters to develop effective engineering properties for the beam layup multidirectional laminate to estimate strengths and stiffnesses based on first and second-ply failure. The results are shown in Table 38.

Table 38: E-glass/PETg [+/- 45 90 0]s Composite Mechanical Property Results

Properties with COV	Experimental Results	CLT Results First-Ply Failure	CLT Results Second-Ply Failure
Fiber Volume Fraction, V_f (%)	41.1 (1.6 %)	-	-
Tensile Strength, F_{xt} (MPa)	223 (11.6 %)	39.5	152
Compressive Strength, F_{xc} (MPa)	106 (10.9 %)	133	143
In-Plane Shear Strength, F_{xy} (MPa)	90.8 (13.9 %)	29.5	36.1
Tensile Elastic Modulus, E_{xt} (GPa)	10.9 (8.67 %)	12.1	13.0
Compressive Elastic Modulus, E_{xc} (GPa)	10.7 (9.71 %)	12.1	13.0
In-Plane Shear Elastic Modulus, G_{xy} (GPa)	5.20 (2.79 %)	4.5	5.5
Poisson's Ratio, ν_{xy} (-)	0.32 (3.54 %)	0.338	0.655
Longitudinal Ultimate Tensile Strain, ε_{xt}^u ($\mu\varepsilon$)	24,200 (8.34 %)	-	-
Longitudinal Ultimate Compressive Strain, ε_{xc}^u ($\mu\varepsilon$)	11,300 (14.2 %)	-	-
Longitudinal Ultimate In-Plane Shear Strain, ε_{xy}^u ($\mu\varepsilon$)	20,800 (13.1 %)	-	-
Average Composite Thickness, t (mm)	2.0	-	-

Note: COV percentages reported with respective measured value in parenthesis.

The results from CLT have been presented twice, once for first-ply failure and again for second-ply failure. First-ply failure results predict that the 90-degree layer fails first with a tensile strength that is 18 %, a compressive strength of 125 %, and an in-plane shear strength of 87 % of what was seen experimentally. From this first-ply failure was more conservative in both the tension and in-plane shear modes, but less conservative in the compression mode. Second-ply failure results predict that the bias (45) layers would fail next predicting a tensile strength of 68 %, a compressive strength of 135 %, and an in-plane shear strength of 106 % of what was seen experimentally. The tensile strength prediction from second-ply failure is closer to the experimental result observed than first ply failure, which could be due to how the experiment was conducted. Comparing the CLT results to the experimental results higher experimental results could be because first and second ply failures do not imply laminate failure; the laminate may still have significant additional capacity beyond some plies failing.

Samples tested at the ASCC were tested until a large drop in the load the sample could carry was experienced during testing. This yielded results which showed visually the +/- 45-degree layers on the surface of the composite failing. However, these layers could have failed before the end of the test which could explain the higher experimental tensile strength results as this would mean the 0-degree layers continued to be loaded during testing past second-ply failure. This can be seen in Figure 64 that shows a failed tension sample for the mechanical testing that was conducted.

Figure 61 through Figure 63 show the longitudinal tension, compression, and in-plane shear stress-strain responses of the beam specimens tested respectively. From the beam

layup specimens tested. Table 39 shows the type of failure as classified using the respective ASTM standard and the number of failures per failure type.

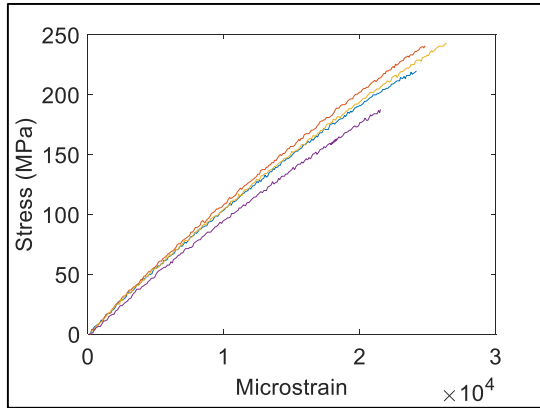


Figure 61: E-glass/PETg [+/- 45 90 0]s Long.
Tension Response

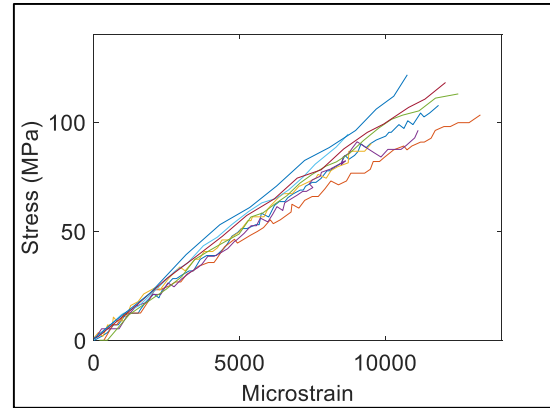


Figure 62: E-glass/PETg [+/- 45 90 0]s Long.
Compression Response

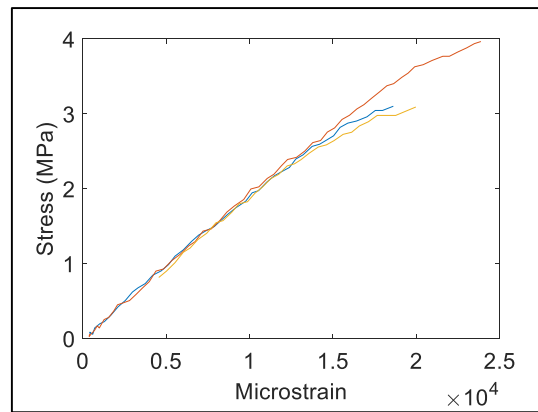


Figure 63: E-glass/PETg [+/- 45 90 0]s In-Plane Shear Response

Table 39: IE 5842b E-glass/PETg [+/- 45 90 0]s Failure Types

Specimen Type	ASTM D3039 Tension [38]	ASTM D6641 Compression [40]	ASTM D7078 In-Plane Shear [41]
Failure Type	AGM, GIT	BGM	HGN, AMV
Number of Failures	4, 6	8	3, 2

An example of each valid failure type for each of the three specimen types tested for the beam layup are shown in Figure 64 through Figure 66 these illustrate the most non-unidirectional samples tested as a part of this study. Figure 64 illustrates failure type angled-gage-middle (AGM) seen in all valid beam layup tension samples tested. Figure 65 shows failure type BGM seen by all beam layup compression samples tested. Figure 66 shows failure type HGN seen in all beam layup in-plane shear samples tested. The tensile samples and in-pane shear samples with the grip/tab-inside grip/tab-top (GIT) and angled-multiple areas-various (AMV) failure modes respectively were not used because this is not a valid failure mode.



Figure 64: E-glass/PETg [+/- 45 90 0]s Failed Tension Sample



Figure 65: E-glass/PETg [+/- 45 90 0]s Failed Compression Sample

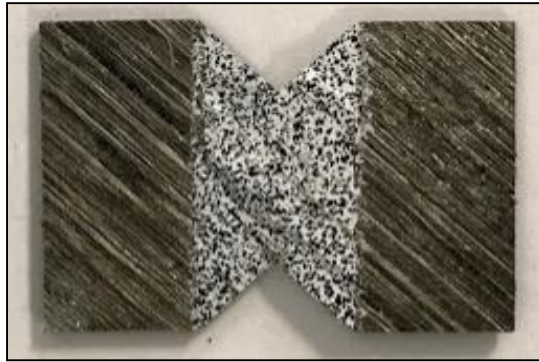


Figure 66: E-glass/PETg [+/- 45 90 0]s Failed In-Plane Shear Sample

3.3 Conclusions and Recommendations

From the standardized mechanical testing conducted to meet object two during this study, the following conclusions were made about the relative strengths and moduli of the Elium, PETg, and Derakane composites tested.

For strengths in the longitudinal direction:

- The average tensile strength was 835-MPa for Derakane, 741-MPa for Elium, and 623-MPa for PETg, which are 11 % and 25 % lower than Derakane respectively.
- The average compressive strength was 634-MPa for Elium, 539-MPa for Derakane, and 310-MPa for PETg, which are 15 % and 51 % lower than Elium respectively.

- The average in-plane shear strength was 42.2-MPa for Derakane, 42.0-MPa for Elium, and 28.8-MPa for PETg, which are less than 1 % and 32 % lower than Derakane respectively.

For moduli in the longitudinal direction:

- The average tensile elastic modulus was 33.37-GPa for Derakane, 33.15-GPa for Elium, and 28.2-GPa for PETg, which are 1 % and 15 % lower than Derakane respectively.
- The average compressive elastic modulus was 33.8-GPa for Elium, 30.1-GPa for Derakane, and 23.5-GPa for PETg, which are 11 % and 30 % lower than Elium respectively.
- The average in-plane shear elastic modulus was 3.50-GPa for Derakane, 3.21-GPa for Elium, and 1.48-GPa for PETg, which are 8 % and 58 % lower than Derakane respectively.

From these results, it is clear that the infused Elium and Derakane composites perform similarly in the longitudinal direction for strength and stiffness. The PETg composite performs close to these in tension, but worse in compression and in-plane shear. From these results, the thermoplastic composites perform well in comparison to the industry accepted structural thermoset, Derakane, especially when loaded in tension. This shows that the thermoplastic composites are feasible for hybrid composite-concrete applications where they would be used as tension reinforcing for the concrete.

From the testing conducted in this study, the following recommendations are given:

- Manufacturing methods be examined to find reasons for the low V_f fractions seen in the composite panels that were fabricated and tested.
- Examine more crystalline thermoplastics such as Nylon or PET for their mechanical properties to see if they are feasible for use in structural applications.
- Examine inter-laminar properties for further characterization of thermoplastic materials.

CHAPTER 4

SHEAR CONNECTORS

4.1 Purpose

Shear connectors mechanically connect the continuous fiber-reinforced thermoplastic (CFRTP) tension reinforcement plate to the concrete cross-section. This mechanical connection transfers shear between the concrete and the CFRTP reinforcement plate, effectively reducing or preventing slip at the interface between the two materials and developing tension in the CFRTP material through composite action. The following subsections address details of the mechanical shear connection as well as the investigation of friction welded shear studs and vacuum infused shear studs: design, manufacturing, and strength and stiffness testing.

4.2 Hybrid Reinforced-Concrete Structures

The shear connector designs chosen in this study take existing knowledge and concepts from steel-concrete construction methods and apply the same principles to the CFRTP-concrete load-bearing system. This section provides background information on routinely used steel shear studs to establish basic concepts. Following this, current methods of fiber-reinforced polymer (FRP) tension reinforcing for concrete beams are briefly reviewed. Building on this information, the remaining sections focus on the friction welded and infused thermoplastic shear studs developed in this study.

4.2.1 Hybrid Steel-Concrete Structures

The hybrid structure takes advantage of both material systems to achieve a stronger and/or stiffer structure than possible with either of the separate constituents. One of the most common structural systems for bridges, decking, columns, and retaining walls is steel-concrete hybrid construction.

The example of the composite action between a steel beam and concrete slab in bending is used to illustrate the function of shear studs because it closely resembles the application of the CFRTP-concrete hybrid system developed in this study. Headed mechanical shear studs, which can transfer shear and resist pullout from the concrete, are widely used in steel-concrete structures.

Drawn arc welding is used to attach the shear studs to the top flange in the beam [52] [53]. An example of this process on a bridge is shown in Figure 67 [54]. This process is partially automatable, but often labor intensive and done on site.



Figure 67: Drawn Arc Stud Welding [54]

This method is effective because it creates a strong bond between the steel flange and the shear stud due to the T-shaped cross-section of the welded stud. Figure 68 illustrates a typical T-shaped cross-section that could be used in this application. The stud not only generates composite action through the shaft of the stud but also resists the stud pulling out of the concrete deck through the hat section at the top of the T-shape.

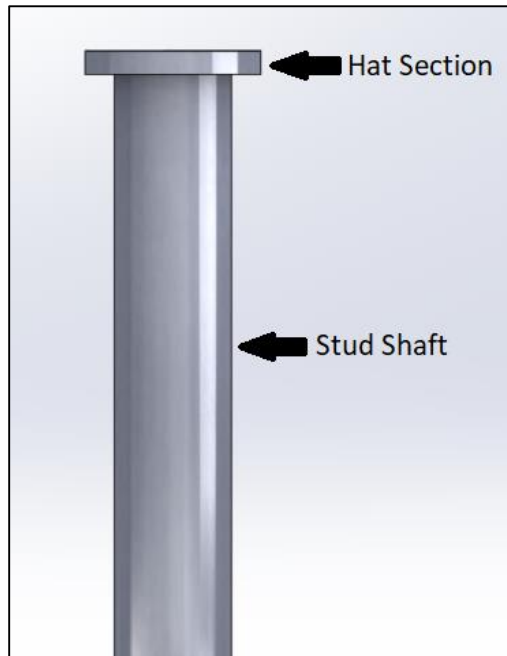


Figure 68: T-Hat Cross-Section SOLIDWORKS Model

4.2.2 Hybrid Thermoset FRP-Concrete Structures

Another important hybrid system is a composite-concrete system. The majority of existing implementations use thermoset composites and are a repair or strengthening method, not a form of new construction. In concrete-FRP hybrid structures, thermoset FRP is attached to the concrete to assist in carrying the tension. Two methods that exist for adhering the external FRP to concrete are externally bonded thermoset FRP (EB-FRP), which is an accepted technology, and mechanically fastened thermoset FRP (MF-FRP), which is less common. Both methods are an alternative to traditional external reinforcement techniques for reinforced-concrete (RC) structures, which include steel plate bonding and steel or concrete column jacketing. FRP has several advantages over these more traditional methods, including:

- Resistance to electrochemical corrosion

- Electromagnetic inertness
- Excellent durability in numerous harsh environmental conditions
- High strength to weight ratios (up to five times that of steel)
- Mechanical properties which can be tailored to specific applications

These advantages make thermoset FRP composites good candidates for retrofitting concrete structures [55] [56].

4.2.2.1 Externally Bonded Thermoset FRP

EB-FRP method of retrofitting RC structures involves using an adhesive to bond an external thermoset FRP plate to the structure in order to add flexural strength. Early studies were done to assess the static strength of RC beams retrofitted by gluing glass-fiber-reinforced-plastic (GFRP) to the tension-reinforcement. The results of this study showed that the flexural strength of RC beams can be noticeably increased by the addition of externally bonded glass-fiber-reinforced polymer (GFRP) to the tension face [57]. That experimental study was followed by an analysis and parametric study on RC beams strengthened with FRP plates [58]. Numerous additional studies have discussed how EB-FRP can be used in civil infrastructure applications and their effectiveness [59] [60] [61] [62].

EB-FRP is widely accepted for strengthening RC structures based on this foundational and continued research. The American Concrete Institute (ACI) and the American Association of Highway and Transportation Officials (AASHTO) have both published guidelines for the design and use of EB-FRP as flexural reinforcement [63] [64].

Some drawbacks of using EB-FRP for strengthening RC structures are the need for careful surface preparation in order to achieve good adhesion when bonding the FRP, lengthy adhesive cure times, and the additional attention required to reinforcement termination due to peeling stresses, which can develop at the bond line [65]. These drawbacks led to the exploration of MF-FRP.

4.2.2.2 Mechanically Fastened Thermoset FRP

The goal of using mechanically fastened thermoset FRP (MF-FRP) is the same as that of using EB-FRP, but MF-FRP achieves the bond between RC structure and FRP with a mechanical connection as opposed to an adhesive bond. This can serve to eliminate the drawbacks of surface preparation and long adhesive cure times. When considering the use of MF-FRP, it is important to consider the imperfect bond, or slip, between the FRP and concrete that can happen [65]. Several studies have investigated the use of MF-FRP in the strengthening of RC structures and have found it an effective method. Several methods of mechanical fastening have been used, such as powder-actuated fasteners and expansion anchors [66], large diameter concrete screws [67], commercially available SafStrip® [68] material attached with powder-actuated fasteners and threaded fasteners [69], and epoxy anchors [65].

4.2.3 Hybrid Thermoplastic FRP-Concrete Structures

The selection of a shear connection for this study was based on the desire to achieve a purely mechanical connection and utilize the advantages of thermoplastic materials. A literature review was conducted on joining methods that could be used with thermoplastic materials in order to assess which method could best achieve the mechanical connection.

The following methods were investigated as a part of the literature review:

- Friction welding
- Heated tool welding
- Ultrasonic welding
- Mechanical fastening
- Vacuum infusion

Based on its advantages, friction welding was chosen. Because shear studs are generally circular in cross-section, the method of friction welding chosen was spin welding. Spin welding has the following advantages [70] [71].

- Simple setup
- High energy efficiency
- Rapid heating and cooling times
- Suitable for automation
- No introduction of foreign materials (adhesives, solvents, etc.)
- Suitability to small and large parts
- High weld quality and reproducibility

With a manufacturing method selected, further literature review was conducted so the process could be more deeply understood and welding parameters could be selected. These phases are illustrated on the temperature versus time plot shown as Figure 69 [71].

The process of spin welding can be summarized by the following four phases.

- Phase I, heat is generated by solid friction through spinning the rod at a desired speed under a desired pressure
- Phase II, the plastic is melted and the heating mechanism changes from solid friction to shear dissipation
- Phase II, the steady-state phase where heat-loss and heat-generation are in equilibrium
- Phase IV, the rotation is brought to a stop and the forging pressure is applied as the polymer solidifies

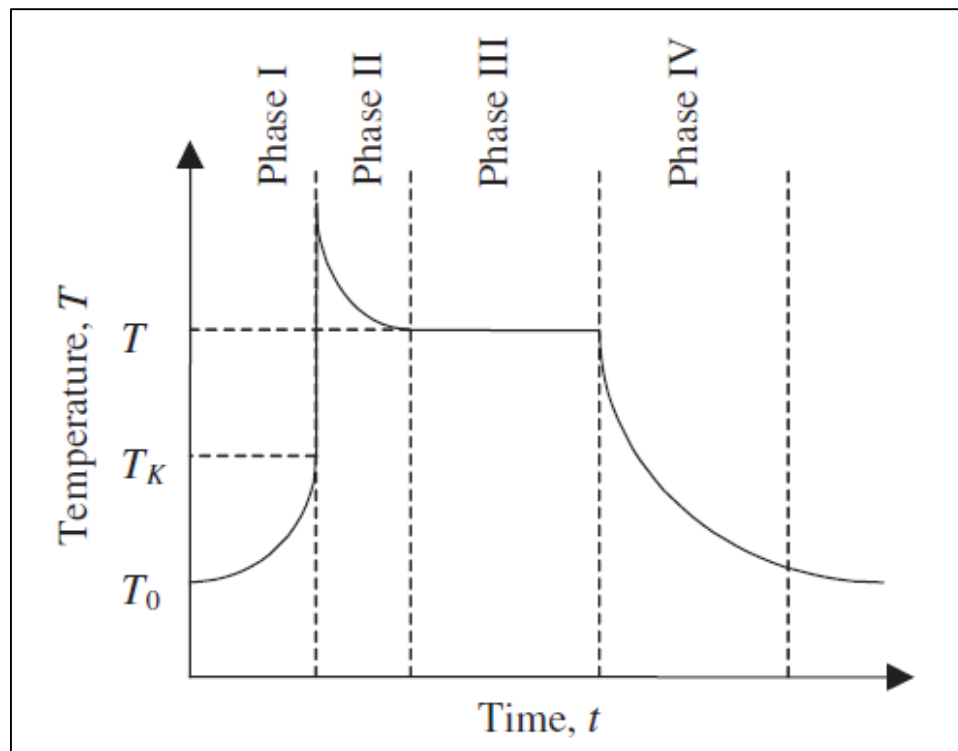


Figure 69: Friction Welding (Spin Welding) Phases

Four parameters drive the spin welding process: spinning velocity (rotational linear speed), welding pressure (the pressure applied during phases I through III), forging pressure (the pressure applied during phase IV), and welding time (time for phases I through III) [70].

Specific welding parameters were not found for use with PETg, the thermoplastic being used in this study. Therefore, a study was necessary in order to select suitable parameters inside the ranges give in the literature. Three sources were used to define the suitable ranges for parameter settings.

Fusion Bonding/Welding of thermoplastic composites [70]:

- Spinning velocity: 1 – 20 meters per second (m/s)
- Welding pressure: 80 – 150 kilopascals (kPa)
- Forging pressures: 100 – 300 kilopascals (kPa)
- Welding time: 1 – 20 seconds (s)

Handbook of Plastics Joining [71]:

- Spinning velocity: 200 – 14000 rotations per minute (rpm)
- Welding pressure: N/A
- Forging pressures: Ensure intimate contact between parts
- Welding time: 0.5 – 4 seconds (s)*

Advances in fusion bonding techniques for joining thermoplastic matrix composites [72].

- Spinning velocity: 1 – 20 meters per second (m/s)
- Welding pressure: 50 – 150 kilopascals (kPa)
- Forging pressures: 100 – 300 kilopascals (kPa)
- Welding time: 1 – 20 seconds (s)

**Handbook specifies that for materials with higher melting temperatures, longer welding times will be required due to the need for higher energy input. In addition, 1 – 2 seconds*

are described apart from the traditional four phases for the rotational speed to be achieved
[71].

Table 40 shows the testing matrix generated based on the recommendations in literature and the properties of the PETg thermoplastic being used. The test matrix uses a four-factor, two-level model to cover the entire parameter space chosen.

Table 40: Friction Welding TP Stud Shear Test Matrix

Sample #	Welding Pressure (kPa)	Forging Pressure (kPa)	Time (s)	Velocity (m/s)
1	50	100	15	10
2	50	100	15	15
3	50	100	20	10
4	50	100	20	15
5	50	300	15	10
6	50	300	15	15
7	50	300	20	10
8	50	300	20	15
9	150	100	15	10
10	150	100	15	15
11	150	100	20	10
12	150	100	20	15
13	150	300	15	10
14	150	300	15	15
15	150	300	20	10
16	150	300	20	15

Note: A tachometer was used to correlate velocity to router speed setting.

Weld times were selected at the upper end of the range of the suggested parameters for the following reasons.

- The relatively high melting temperature of PETg, 250 degrees Celsius [73], compared to commodity thermoplastics, which can a range from low melting temperatures of 110 degrees Celsius [74] for low-density polyethylene (LDPE), to 160 degrees Celsius [75] for polypropylene (PP), to higher ones of 212 degrees Celsius [76] for polyvinyl chloride (PVC), that are more commonly friction welded.
- The inability of our custom welder to reach velocities in the upper suggested range.
- To ensure complete heating of the solid part to avoid the generation of residual stresses from non-uniform heating [70].

4.2.3.1 Unreinforced Shear Stud attached by Friction Welding

The first type of shear stud explored in this study was the friction welded shear stud. Friction welding was chosen as the primary method to explore because it takes advantage of two aspects of thermoplastic materials: their ability to be melted and reformed with the same properties, and their amenability to automated manufacturing. The latter benefit was realized through friction (spin) welding that takes advantage of the traditionally cylindrical shape of a shear stud, which was maintained for this design.

The cross-section chosen for this design mimics that used for steel-concrete construction: a cylindrical cross-section with a larger diameter head on top to give a T-shaped cross-

section. Spacing limitations for shear studs from the edges of the concrete and from stud to stud were based on AASHTO specifications for steel-concrete construction [77].

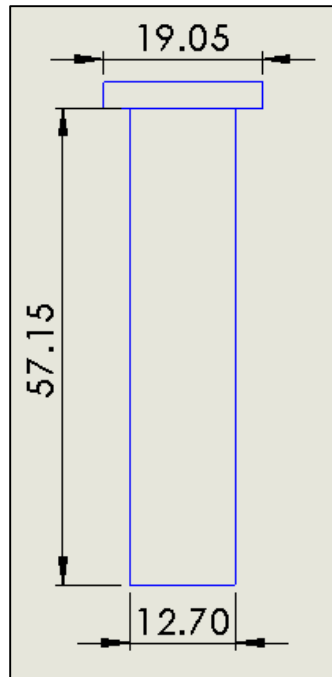


Figure 70: 2D Friction Welded Stud Concept Design (mm)

Figure 70 shows the concept design of the circular friction welded stud being investigated for this study with dimensions given in millimeters (mm). The shaft of the neat resin stud was chosen to be 57.15-mm (2.25-inches) to ensure the stud met the AASHTO [77] height requirement of 50.8-mm (2-inches) after welding, and the diameter of the circular stud was chosen to be 12.7-mm (0.5-inches). Pull out resistance for this initial design would be done by fastening a washer to the top of the stud using a self-tapping screw. This is shown as the 19.05-mm (0.75-inch) diameter cross-section on top of the stud shaft. This process could easily be automated for rapid installation of shear studs with pull out resistance. Using neat-resin studs, the mechanical connection has the following advantages and

disadvantages, which were considered when selecting the stud for friction welding in this study.

Advantages	Disadvantages
<ul style="list-style-type: none">• Resin rich welding interface• Easier to generate complete bond at the welding interface• Available from multiple suppliers in a variety of diameters• Process is fast and automatable	<ul style="list-style-type: none">• Shaft only as strong as neat-resin• Only available from suppliers in rods with a constant cross-section• Secondary process needed to facilitate pull out resistance

4.2.3.2 Reinforced Shear Stud attached by Friction Welding

Another type of shear stud considered for friction welding as a part of this study was reinforced shear studs. This still takes advantage of thermoplastic material properties like the neat-resin studs by utilizing the melting and reforming of the resin, and could easily be designed into an automated process to mimic steel connectors. These studs would be similar to the neat-resin studs with potential strength advantages from the introduction of fiber-reinforcement. A custom fabrication method would need to be developed to make these studs, which could integrate more complex geometries beyond the straight rod available off-the-shelf for neat-resin PETg.

Friction welding reinforced shear studs could have the advantage of fiber interaction at the interface between the shear stud and CFRTP reinforcement. If this interaction was developed enough the fibers could provide more strength and stiffness for increased composite action. A possible disadvantage of this is decreased strength of the welded bond. The introduction of fiber reinforcement or other fillers at the weld interface may have an effect on the weld strength by decreasing the amount of polymer available for welding [71].

One method of custom fabrication was considered as part of this study that was not included in the scope of work. This was the creation of reinforced Elium shear studs fabricated through vacuum infusion. The method discussed involved coating a PVC pipe in a mold release agent, then filling it with fiber-reinforcement and bagging it in a vacuum infusion setup as discussed in chapter 2. Then the resin could be infused into the mold with circular cross-section, and once the resin cured, reinforced shear studs could be cut to length for friction welding.

4.2.3.3 Friction Welded Shear Stud Selection

Based on the relative advantages and disadvantages and recognizing that successfully completing this initial study would require straightforward shear stud fabrication, neat-resin shear studs were chosen for this initial study. It is recommended that future studies investigate the use of fiber-reinforced shear studs to assess any strength benefits.

4.2.3.4 Fiber-Reinforced Shear Stud by Resin Infusion

The second type of shear stud chosen for this study was vacuum infused shear studs. This was chosen because it is similar to what is done in industry with thermosetting composites, and is possible because Elium is a thermoplastic liquid resin-system. Vacuum infused studs

also have the advantage of fiber-reinforcement in the shaft, which can be extended into the tension reinforcement, increasing shear strength at the stud-plate interface.

In order to fabricate the vacuum infused shear studs, it was decided to co-infuse the studs with the reinforcement plates in order to achieve a strong interaction between the fiber-reinforced shear stud and the reinforcement plate. The 2D concept design chosen for the circular stud has a fluted shape as shown in Figure 71. The smaller top radius of 9.525-mm (0.375-inches) will allow the concrete to flow around the stud but still allow for resistance to pull out. The bottom radius of 19.05-mm (0.75-inches) is larger in order to maximize the transfer of forces between the shear stud and the plate or minimize the shear stresses experienced. The shaft at the center of the stud was chosen to be 12.7-mm (0.5-inches), the same as the friction welded studs. The total height of the stud was designed to be 50.8-mm (2-inches) to meet AASHTO guidelines [77] for the height of steel shear studs, which were followed in this research.

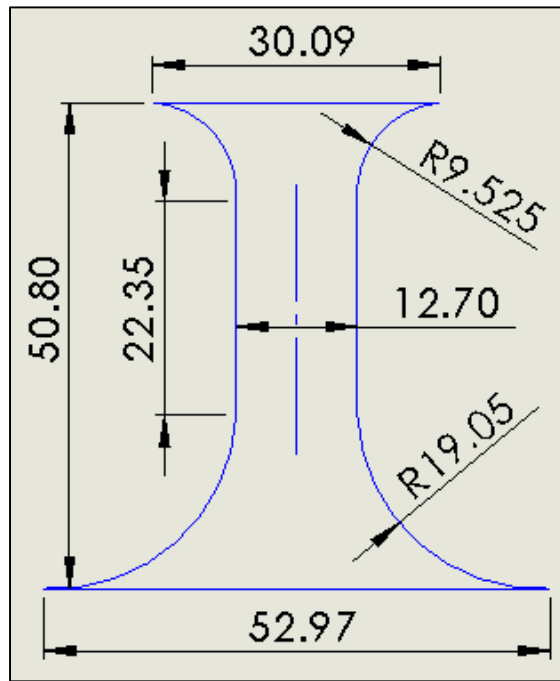


Figure 71: 2D Infused Shear Stud Concept Design (mm)

4.2.4 AASHTO Shear Stud Design & Spacing

For the purposes of this study in conjunction with Benjamin Smith, another Graduate Research Assistant at the ASCC, the AASHTO LRFD Bridge Design Specifications [77] for steel shear studs was used to select two stud spacings for a composite-concrete beam. The guidelines for steel shear studs were assumed to apply to the thermoplastic shear studs being explored in this study.

Since the stud size being used in this study was limited by the friction welder to 12.7-mm (0.5-inches) in diameter it was adopted for use with the guidelines for stud spacing choices. For these tests two rows of studs were chosen, which resulted in a suitable beam-width of 127-mm (5-inches). Assuming the beam to have a relatively short span to depth ratio of 12 in an effort to increase the concrete shear strength in the beam and adhering to the manufacturing limits of the ASCC automated stamp forming press the resulting beam length would be 1524-mm (60-inches) with a depth of 127-mm (5-inches). This small-scale proposed beam specimen would allow the CFRTP reinforcement plate to be manufactured in house on the automated stamp forming line used during this study.

The required center-to-center spacing along the span of the beam (longitudinal) was at least six stud diameters, but no more than 610-mm (24-inches). Two beam specimen designs for use with PETg friction welded shear studs were developed. The first had the minimum stud spacing (pitch) of 76.2-mm (3-inches) resulting in 40 studs per beam in order to observe the maximum strength achievable while following the guidelines. For the second beam, a pitch of 152.4-mm (6-inches) was chosen in order to observe the effects of varying this parameter on the specimen performance.

The transverse (perpendicular to the span) center-to-center stud spacing was required to be at least four stud diameters, using the chosen stud diameter this was 50.8-mm (2-inches). The shear studs were also required to penetrate the concrete by at least 50.8-mm (2-inches) and have 50.8-mm (2-inches) of concrete to cover them. All studs were also required to be at least 25.4-mm (1-inch) inside of the beam from each edge panel to the stud edge.

For the purposes of this study, the beams were not fabricated but the concrete-CFRTP stud specimens discussed in section 4.4.3 were designed to simulate the PETg friction welded studs in concrete-CFRTP stud with these two stud spacing designs. E-glass fiber/Elium shear studs were only tested using the larger stud spacing due to the time-consuming nature of their fabrication.

4.3 Manufacturing

4.3.1 Friction Welding Methods

Two welding methods were developed in support of this project. The first was welding on an Instron test frame to facilitate a highly controlled environment for parameter selection and the second mobile welding for welding to larger objects and mimics a possible method that could be implemented in the field.

4.3.1.1 Feasibility Welding Trial

Preliminary tests were conducted with a drill press to spin the pure resin PETg rods spun into a pure resin PETg plate in order to verify the feasibility of the friction welding process.

Figure 72 is a photo of a cross-section of PETg rods friction welded to a PETg plate.

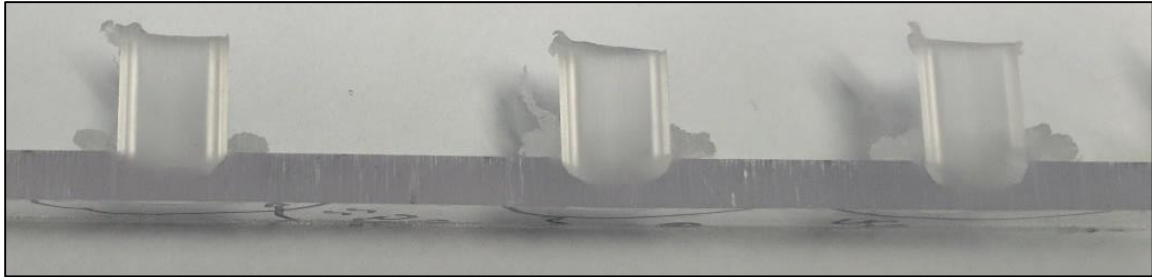


Figure 72: Cross-Section of Feasibility Weld

These preliminary tests indicated that it is feasible to manufacture thermoplastic shear studs using this method. Figure 72 shows that the rods embedded in the plate. Although the studs successfully bonded to the plate, the interface between the two components is still visible and the penetration tapers off as the cross-section moves from the center of the stud toward the outer edge. It is also clear that the material pushed from the penetrated portion of the stud collected on the surface around the stud as heat and pressure was applied.

The next step in evaluating this application of friction welding was to develop a more controlled method of installing shear studs using friction welding that would allow for a study on the effect of processing parameters. This study of welding parameters was done in an Instron testing frame in order to control the welding pressures.

4.3.1.2 Instron Testing Frame Welding

A spin welding apparatus was developed using a DeWalt router for spinning the thermoplastic shear stud and an Instron hydraulic test frame with a 9-kN load cell to control

the pressure applied during welding and forging. Figure 73 shows the Instron welding setup developed at the ASCC.



Figure 73: Instron Welding Setup

The CFRTP reinforcement plate was gripped in the top of the fixture and a thermoplastic stud inserted into the router collet pointing up. The router as shown was mounted upside down such that the Instron could control the pressure from the hydraulic actuator mounted in the top of the test frame.

Test samples made using this apparatus were done with neat-resin PETg plates, neat-resin PETg rod and a manual switch to turn the router on and off in order to prove feasibility. Once feasibility was proved a LabView program was written to control a relay that turned the router on and off in a more repeatable way. The Instron was then programmed using the WaveMatrix software environment to control welding pressure, forging pressure, and time without the need for the operator to control the transitions between phases in the process.

The first trials conducted using the Instron friction welder used neat-resin PETg rods and plates. Neat-resin was chosen for initial trials to avoid complications from interactions with fiber-reinforcement at the welding interface. Figure 74 shows a specimen welded using neat resin PETg for the rod and plate.



Figure 74: Initial Instron
Welding Trial Specimen with
neat-resin PETg

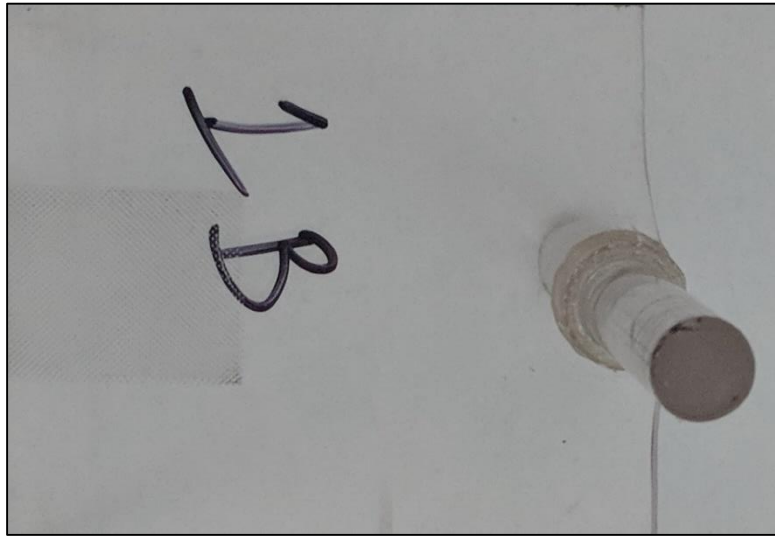


Figure 75: Failed Initial Instron Welding Trial Specimen

These initial samples were tested but did not fail the shear stud. The mode of failure was cracking across the neat-resin plate near the weld point as shown in Figure 75. On the right side of the failed specimen, the plate can be seen as failed as opposed to the stud. At this point testing moved to spin welding neat-resin studs to CFRTP plates, shown in Figure 76.



Figure 76: Instron
Welded Specimen with
CFRTP Plate

The CFRTP plates used, as described in chapter 2, were purely unidirectional IE 5842 material. Two plate thicknesses were used when friction welding to IE 5842 material: 6.35-mm (0.25-inch) and 3.175-mm (0.125-inch) plates. All test results reported in this thesis used 6.35-mm reinforcement plates for welding. 3.175-mm plates were used for trials and practice to save on material preparation and usage.

4.3.1.3 Mobile Device Welding

A mobile welding unit was constructed in order to mimic the process done on the Instron in a way that was more suitable for large parts and is closer to a device that could be used

in the field for friction welding in a similar application. The mobile welding setup is shown in Figure 77.



Figure 77: Mobile Device Welding Setup

The mobile welder uses the same DeWalt router as the Instron welder, but the mobile welder applies the stud to the CF RTP from the top instead of from the bottom. The mobile setup has the router mounted to a carriage, which is on linear rails, so that the router can move up and down freely. The carriage and router weigh more than the load necessary for the desired pressure, so a counter-weight system was built in order to control the pressure applied to the stud during welding. The spinning time for the router was controlled using an Arduino programmed with preset times. Welding a single stud with the mobile welding unit took approximately 1-minute when done by a trained operator.

Welding trials using the mobile device including using both unidirectional IE 5842 material as was used with the Instron welder and IE 5842b material in the beam layup discussed in chapter 3 of this thesis. Figure 78 and Figure 79 show the mobile welded studs to IE 5842 and IE 5842b respectively.



Figure 78: Mobile Welded Stud to IE 5842



Figure 79: Mobile Welded Stud to IE 5842b

4.3.2 Vacuum Infusion of Reinforced Shear Studs

A fiber-reinforced shear stud made with a liquid acrylic thermoplastic (Elium) that can be vacuum infused on the CFRTP plate was also explored. While labor intensive compared to friction welding, vacuum infusion allows for designed fiber reinforcement of the shear studs as described in the design sub-section. Figure 71 shows the concept of a vacuum infused shear stud that was implemented.

The first step in developing this fabrication method was to establish a feasible infusion method and reinforcement architecture. It was decided that the studs would be co-infused with the reinforcement plate in wooden molds. The wooden mold tool was fabricated in two halves so it could be split for removal from the finished studs. A model of one half of the mold is shown in Figure 80.

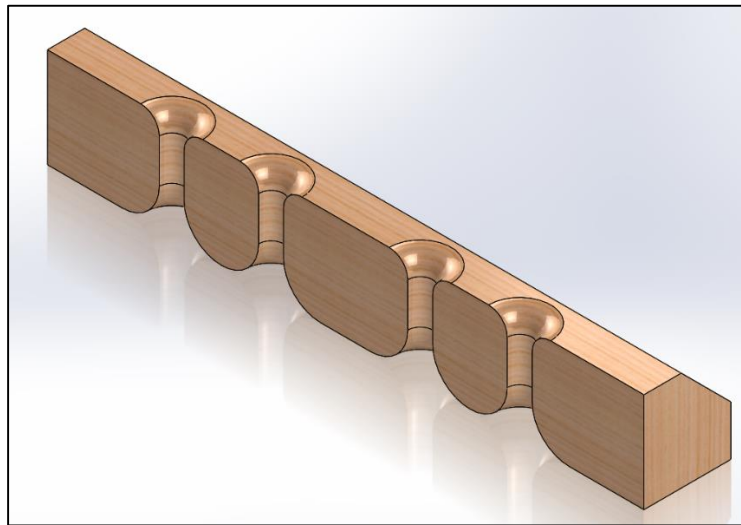


Figure 80: Vacuum Infused Shear Stud Mold (Half) Concept Design

The height of the infused shear stud was chosen to be 50.8-mm (2-inches) and the shaft diameter to be 12.7-mm (0.5-inches) to be consistent with the height design of the spin welded shear studs. The actual mold constructed was originally made of wood as a proof of concept but was replaced by one made of 60-lb high-density foam to add durability for repeated use.

The infusions were setup on a plate made of E-LR 1208 fabric with fiber architecture of $[\pm 45/90/0]_s$ to match the beam-layup designed for the end use of this feasibility study. The studs were then made of 19 grams of E-BX 2400 double bias E-glass fabric [78] that

was rolled until the shaft would fit in the 12.7-mm (0.5-inch) diameter shaft. Figure 81 shows the rolled fabric.



Figure 81: Rolled E-BX 2400 Double Bias E-glass [78] for Infused Stud

Once the fabric was rolled, the shaft portion for the mold was held together with heat-shrink tape and the ends were flared out to fill out the radii in the mold as shown in Figure 71. The top radius was chosen to be 9.525-mm (0.375-inches) in order to provide pull out resistance while still leaving room for the wet concrete to fully form around the shear stud. The bottom radius was 19.05-mm (0.75-inches) in order to provide increased shear strength beyond the capability of the stud shaft alone. An advantage of vacuum infusion is that these radii can be tailored to suite design needs.

Each infusion was done with two molds, which each help four studs. This allowed for each infusion to create an entire concrete-CFRTP stud sample that is discussed in section 4.4.3. The end product of an infusion is shown in Figure 82. This shows the results of half of an infusion.



Figure 82: E-glass/Elium Shear Stud Infusion Result

Figure 83 shows two different views of Elium shear studs that were fabricated and not used in testing. These shear studs were used when practicing fabrication techniques and have a smaller upper radius than the studs tested in the concrete-CFRTP stud configuration but still give an accurate example of the general appearance of the E-glass/Elium shear studs when untested.



Figure 83: Untested Vacuum Infused Elium Shear Studs

4.4 Strength and Stiffness Testing

Two types of strength and stiffness testing were conducted. TP stud shear testing was used to determine optimum parameters inside of the recommended parameter ranges from literature for friction spin welding of PETg studs to CFRTP. Concrete-TP stud and Concrete-CFRTP stud testing of both friction spin welded PETg and vacuum infused E-glass fiber/Elium shear studs embedded in concrete was conducted to find better design values for hybrid structural design. Vacuum infused E-glass fiber/Elium shear studs were only tested in the concrete-CFRTP stud configuration because there were no welding parameters to explore.

Strength and stiffness testing were conducted on samples using the test matrix shown in Table 40 in section 4.2.3 in order to select effective welding parameters. Three phases of TP stud shear testing were conducted in preparation for the concrete-CFRTP stud test of PETg samples.

4.4.1 TP Stud Shear Custom Test Fixture

A specialized setup was needed to assess the strength and stiffness of the friction welded specimens fabricated for assessing effective welding parameters. Figure 84 shows the custom fixture and Figure 85 and Figure 86 show example friction welded specimens.

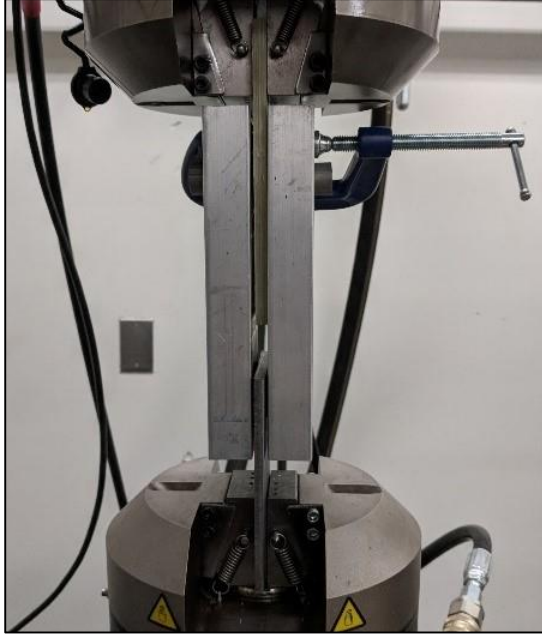


Figure 84: TP Stud Shear Testing Custom Fixture

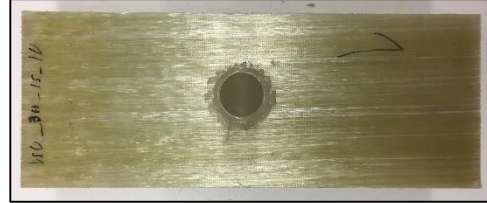


Figure 85: Double TP Stud Shear Specimen (front)

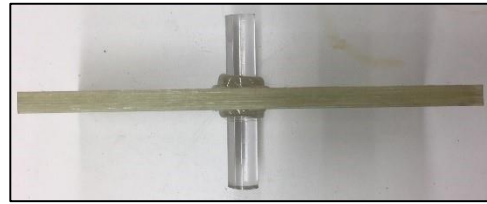


Figure 86: Double TP Stud Shear Specimen (side)

The fixture is designed to pull the specimens in tension or push them in compression in order to load the shear studs welded to the IE 5842 CFRTP to assess their strength and observe a relative stiffness. The fixture outer plates are bolted together at the bottom and gripped into the Instron test frame. The friction-welded specimen is aligned in the holes of the outer plates and the CFRTP is gripped into the Instron upper grip. In this configuration when the actuator is moved, the studs are loaded in either tension or compression. The custom fixture can be used in double-lap shear with a stud on each side or in single-lap shear with a stud only on one side. All TP stud shear tests were run in a 100-kN Instron hydraulically actuated test frame in position control with a data collection rate of 0.1 kHz.

4.4.2 Testing of Instron Welded Studs in Double TP Stud Shear Loading

The first tests done to characterize the samples defined in the Table 40 test matrix used a symmetric TP stud shear test configuration with a stud on each side of the CFRTP

reinforcement plate. This was chosen in order to have a symmetric test specimen to avoid potential asymmetric effects that could be seen in single TP stud shear test such as the effects of secondary bending.

Seventeen double TP stud shear samples we tested and the data analyzed to calculate the stud strength as shown in Equation 45, ductility of the studs (difference in stud deformation between peak load and when the load dropped to 60% of peak over the defamation at peak load) as shown in Equation 46, and whether or not both studs were failed. These results are reported in Table 41.

$$\text{Stud Strength} = \frac{\text{Peak Load}}{2 * \text{Area}} \quad \text{Equation 45}$$

$$\text{Ductility} = \frac{AP_{0.6} - AP_{Peak}}{AP_{Peak}} \quad \text{Equation 46}$$

- Peak Load is defined as the maximum load seen during the test.
- Area is defined as the cross-sectional area of the stud.
- The “2” in the denominator accounts for there being two studs.
- $AP_{0.6}$ is defined as the position of the Instron actuator when the load dropped to 60% of the peak and the data is stopped because the specimen is considered failed.

AP_{Peak} is defined as the position of the Instron actuator at the peak load in the data.

Table 41: Double TP Stud Shear Specimen Results

Sample Number	Stud Strength (MPa)	Specimen Ductility (%)	Studs Shared Load Simultaneously
Sample 1	13.5	26	
Sample 2	14.1	97	
Sample 3	27.4	4.5	X
Sample 4	12.4	66	X
Sample 5	11.7	2.1	
Sample 6	13.4	3.1	
Sample 7	10.7	9.2	X
Sample 8	15.9	19	
Sample 8-2	27.3	7.1	X
Sample 9	17.3	46	
Sample 10	26.6	99	X
Sample 11	23.9	49	X
Sample 12	14.4	11	
Sample 13-2	17.9	11	
Sample 14	21.6	5	X
Sample 15	14.4	11	
Sample 16	23.4	26.6	

Table 41 reports whether the studs shared the load simultaneously, which was established from the data based on the behavior shown. Figure 87 shows the two types of behavior that were used to establish load sharing.

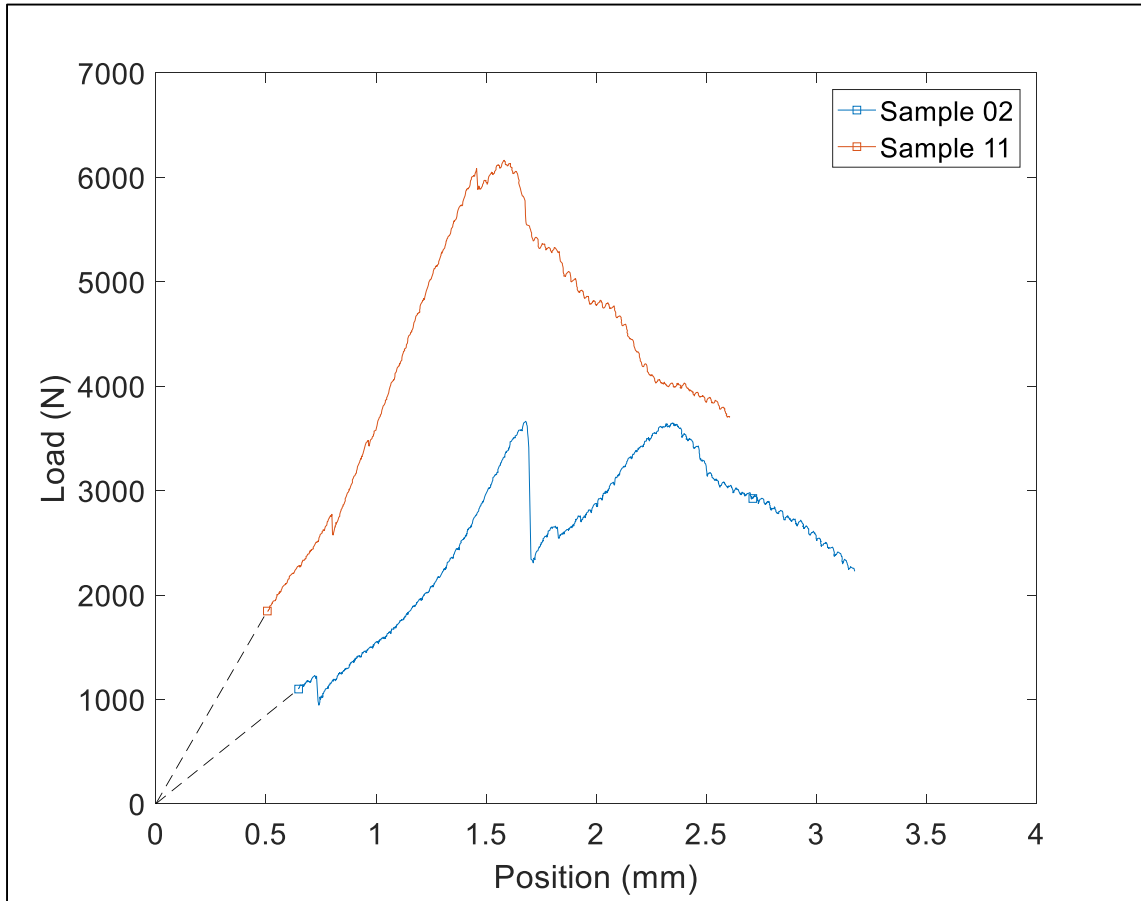


Figure 87: Load-Deformation of Studs in Double TP Stud Shear Loading

Sample 11 displays simultaneous load sharing by both of the studs. Sample 2 did not display simultaneous load sharing by the studs. In sample 2, there are clearly two independent peaks at approximately the same load showing that the studs were most likely broken one at a time. The data often showed that studs that did exhibit load sharing carried about twice the load of those without load sharing.

Based on the way strength per stud and ductility are calculated as shown in Equations 3 and 4 respectively for samples that do not have load sharing, these values may be misleading. Due to the lack of load sharing caused by the difficulty in aligning the studs well enough to consistently engage both studs simultaneously, it was decided to conduct more testing with asymmetric single TP stud shear samples.

Figure 88 and Figure 89 show side 1 and side 2 of a failed Instron welded double TP stud shear specimen respectively. There were two types of failure modes for double TP stud shear specimens. Mode 1, which occurred when the studs shared the load simultaneously or if the test was run past the first stud, resulting in both studs breaking and shearing off, as seen in Figure 89. Mode 2 occurred when the load was not shared simultaneously by both studs and the test was not run past the first stud failing.



Figure 88: Failed Instron Welded
Double TP Stud Shear Specimen
(side 1)



Figure 89: Failed Instron Welded
Double TP Stud Shear Specimen (side 2)

All the studs that sheared exhibited the same type of failure at the stud-plate interface. As can be seen in Figure 89 the studs failed at the interface between the PETg matrix and the top layer of fibers. This exposed those fibers, which can be seen where the stud was as white, and some fiber residue can be seen on the shear off stud where it was welded on.

This shows the weak point was not the weld between the PETg neat-resin stud and the PETg matrix on the composite plate, but that it was between the PETg and the fiber-reinforcement at the weld interface.

4.4.3 Testing of Instron Welded Studs in Single TP Stud Shear Loading

The second batch of testing to characterize the studs defined in the Table 40 was done using a single TP stud shear configuration. Eighteen single TP stud shear samples we tested and the data analyzed to calculate the stud strength as shown in Equation 5 and ductility as shown in Equation 4. The test results are summarized in Table 42.

$$\textit{Stud Strength} = \frac{\textit{Peak Load}}{\textit{Area}} \qquad \text{Equation 47}$$

- Peak Load is defined as the maximum load seen during the test.
- Area is defined as the cross-sectional area of the stud.

Table 42: Single TP Stud Shear Specimen Results

Specimen Name	Strength per Stud (MPa)	Ductility (%)
Specimen 1	17.3	11
Specimen 2	25.7	11
Specimen 3	25.8	220
Specimen 4	16.1	11
Specimen 5	29.4	190
Specimen 6	24.7	8.0
Specimen 7	15.6	2.1
Specimen 8	18.8	2.0
Specimen 9	17.9	42
Specimen 10	11.7	12
Specimen 11	28.4	280
Specimen 12	20.7	18
Specimen 13-3	7.62	42
Specimen 14-2	25.2	44
Specimen 14-3	24.3	24
Specimen 15	26.8	35
Specimen 15-3	23.0	2.6
Specimen 16-2	25.1	110

All single TP stud shear specimens manufactured using the Instron welder and tested at the ASCC shared the same failure mode. Figure 90 shows an example of this failure mode. It was observed that the failures all occurred at the interface between the PETg thermoplastic matrix and the fibers. The top layer of fibers, seen as white had the PETg matrix pulled off them by the stud during failure. This shows that the weakest link was the interface between the thermoplastic resin and the reinforcement fibers matching what was observed with the double TP stud shear specimens. In some specimens, the stud pulled off from the top layer of fibers but also cracked the neat-resin stud when shearing off.



Figure 90: Failed Instron Welded Single TP Stud Shear Specimen

Based on the data collected the specimens can be classified as ones with a desirable strength of above 23.4-MPa and relatively high ductility in comparison to the other specimens collected. The reported shear strength of PETg neat-resin is 62.1-MPa (9000-psi) [36], which is 2.7 times more than the shear strength of the friction welded neat-resin stud. This could be due to the E-glass reinforcement that the neat-resin stud is interacting with at the weld interface, which effectively reduces the available area for bonding the shear stud resin

to the CFRTP resin [71]. In regards to ductility the specimens can be classified as ductile and brittle, Figure 91 shows an example of each of these behaviors.

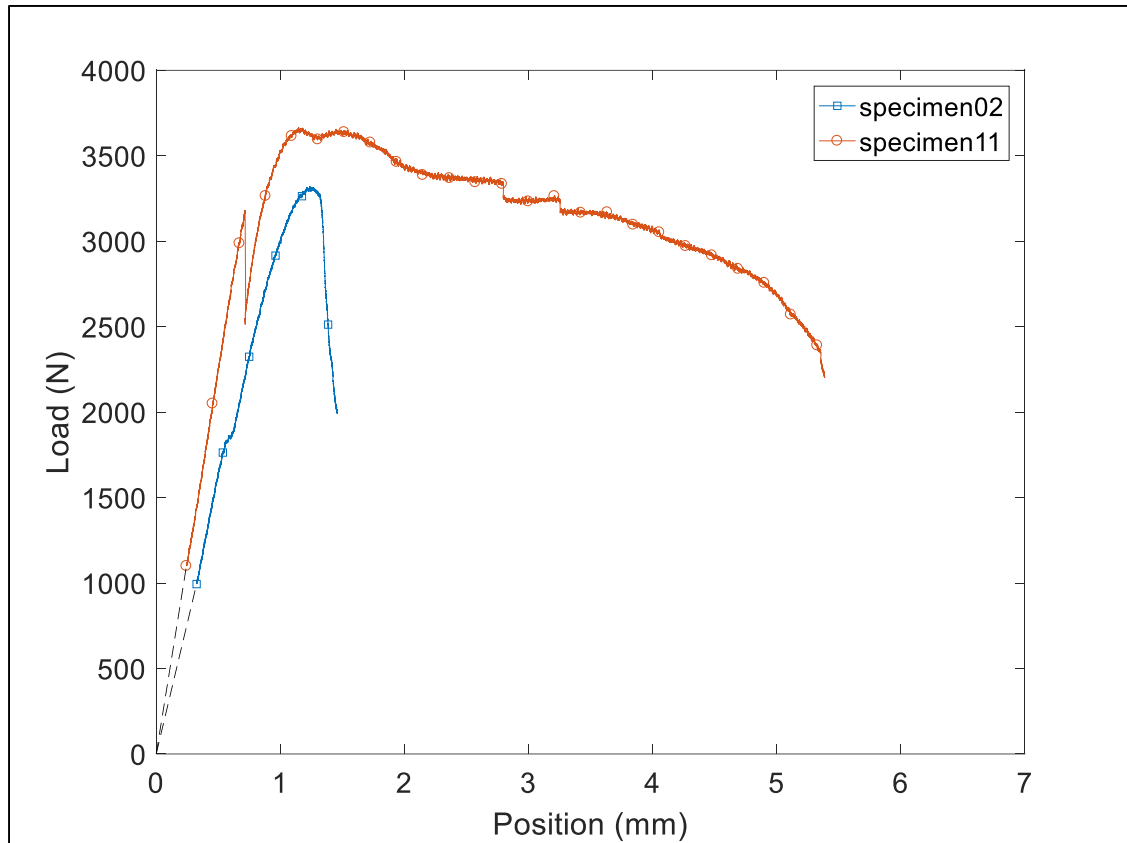


Figure 91: Single TP Stud Shear Ductility Comparison

Specimen 2 shown in blue represents a brittle behavior in regards to the calculated ductility whereas specimen 11 represents a ductile behavior. For the purposes of selecting welding parameters for construction of the assemblies, behavior that is more ductile is desirable. Ductility in the shear studs theoretically helps the assemblies share the load across all the studs, which is expected to increase beam strength and ductility.

Next, the parameter set was narrowed to two samples in order to select what set of welding parameters would be used in the assemblies. From the single TP stud shear data collected,

specimens 5 and 11 were chosen for further testing due to their high strength and ductility.

Figure 92 shows the single TP stud shear results for specimens 5 and 11.

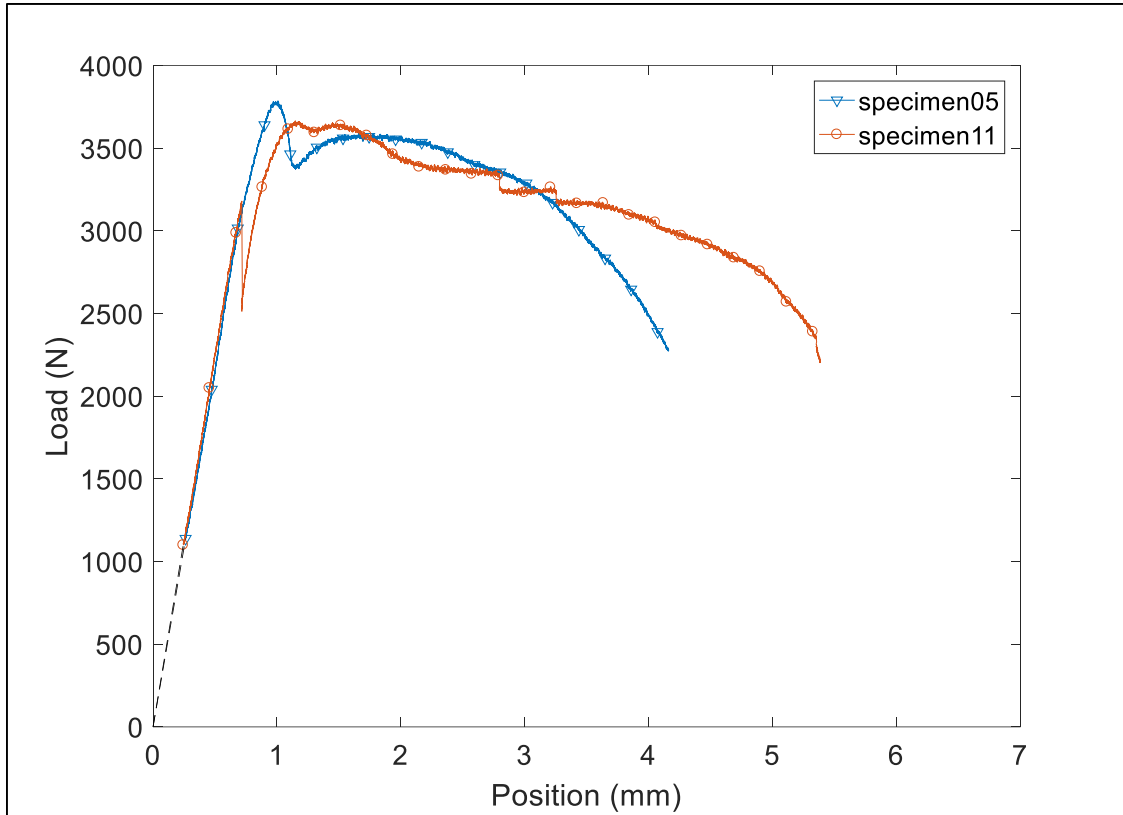


Figure 92: Load-Deformation of Studs in Single TP Stud Shear

With the specimen types narrowed down to two choices samples needed to be made on the mobile welding unit designed for welding the assemblies in order to verify suitable welds could be made using that system.

4.4.4 Testing of Mobile Welded Studs Single TP Stud Shear Loading

Initial tests were done with mobile welder before the counter-weight system was installed and based on the results of these initial tests specimen type 5 was chosen for further verification and potential use in the assemblies. Four samples were made using the mobile

welder and a counter weight system using the parameters for specimen type 5 using the beam-layup as the CFRTP. The results from these tests are shown in Table 43.

Table 43: Single TP Stud Shear Mobile Welder Specimen Type 5 Sample Results

Specimen Name	Strength per Stud (MPa)	Ductility (%)
M2 1b	25.6	210
M2 2b	25.4	160
M2 3b	25.6	51
M2 4b	24.9	47

From the four samples tested, the average strength per stud was calculated to be 25.4-MPa with a coefficient of variation of 1.3 % and the average ductility was calculated to be 117 % with a coefficient of variation of 53 %. Figure 93 shows a load versus actuator position plot for the four specimen type 5 samples made with the mobile welding unit that were tested in single TP stud shear.

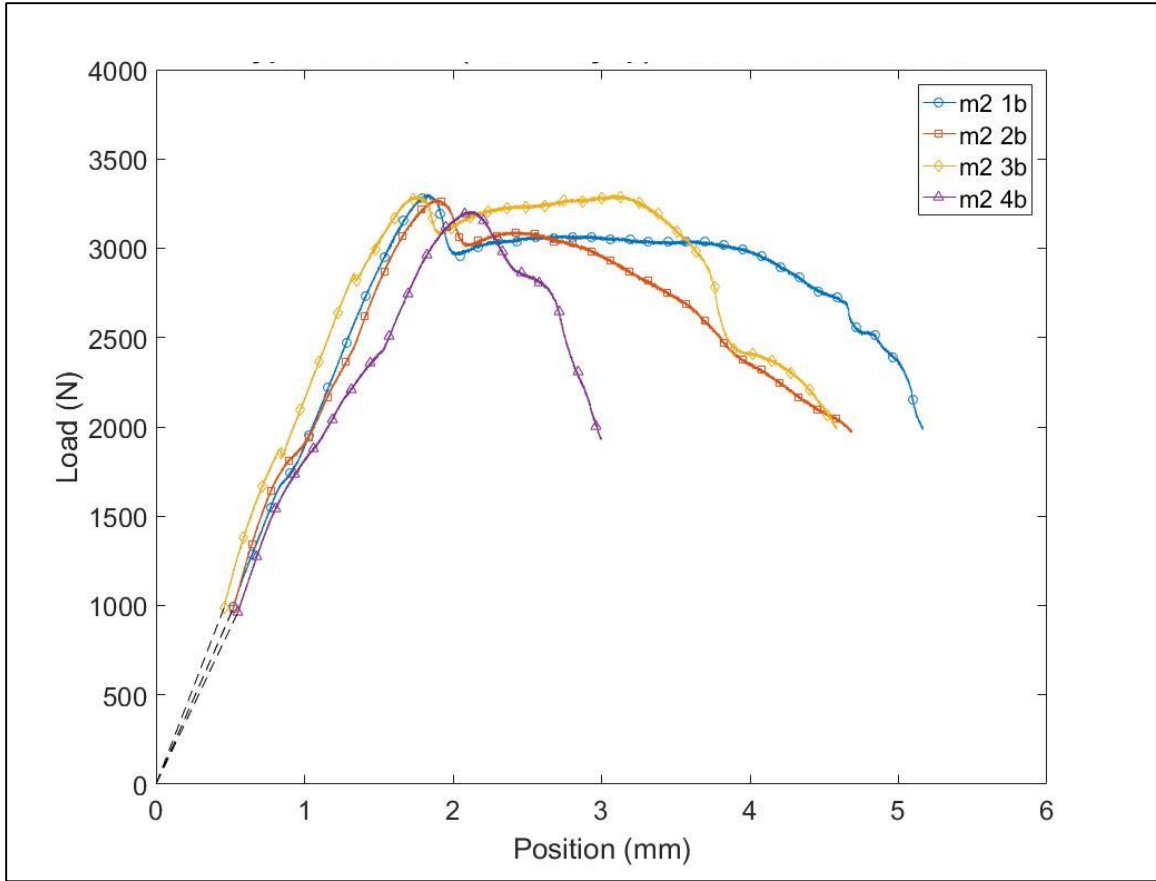


Figure 93: Type 5 Mobile Welder Single TP Stud Shear Results

These results viewed as favorable because they exceed the desired design strength per stud of 23.4-MPa and show reasonable, although highly variable, ductility. Figure 94 shows an example of the failure mode seen in the mobile welded single TP stud shear samples to the



Figure 94: Failed Mobile Welded Single TP Stud Shear Specimen

IE 5842b beam layup. The failure mode for these specimens were all the same as shown but differed from the other TP stud shear testing specimens tested. These samples were run in displacement control until the load dropped below 60% of the peak load seen during the test. It can be seen that the studs were being deformed in bearing just above the weld interface. This difference in failure modes could be due to the different fiber-architecture for the CFRTP reinforcement in these specimens. All other TP stud shear specimens were welded to unidirectional fibers oriented in the longitudinal direction whereas these specimens were being welded to a layer with the fibers off-axis by 45-degrees from the longitudinal direction.

4.4.5 Testing in Concrete-TP Stud and Concrete-CFRTP Stud Configurations

The final step in assessing the feasibility of thermoplastic composites for use in load-bearing hybrid structures as explored in this study is to assess the degree of composite action achieved by the shear transfer methods chose. This was done through the implementation of a concrete-TP and concrete-CFRTP stud test.

4.4.5.1 Specimen Design

The concrete-TP and concrete-CFRTP stud specimens were designed to load the studs in pure shear in a symmetric configuration based on what was done by Cho, et al [2]. The purpose of this test was to assess the capacity of the friction welded shear studs in a pure shear configuration embedded in concrete as would be done in a composite-concrete load bearing system. Table 44 shows the test matrix chosen for the concrete-TP and concrete-CFRTP stud samples in this study. The IE 5842b specimens have two spacings based on the proposed design of a thermoplastic composite-concrete hybrid beam discussed in

section 4.2.5. Only the larger spacing of 152.4-mm (6-inches) was chosen for the Elium concrete-CFRTP stud samples due to the time intensive nature of their fabrication.

Table 44: Concrete-TP/CFRTP Stud Test Matrix

IE 5842b (PETg)		Elium 150
76.2-mm (3-inch) stud spacing (minimum from AASHTO)	152.4-mm (6-inch) stud spacing	152.4-mm (6-inch) stud spacing

Figure 95 shows the concept design for the 76.2-mm spacing direct shear specimen. The concrete-TP and concrete-CFRTP stud specimens were designed to have the studs fully embedded in concrete to simulate pure shear in a hybrid structure. To ensure this for the 76.2-mm specimens there was 25.4-mm of concrete above the studs vertically, 76.2-mm below them and 101.6-mm from the CFRTP plate horizontally out. For the 152.4-mm specimens there is 76.2-mm of concrete above the studs vertically, 127-mm below them

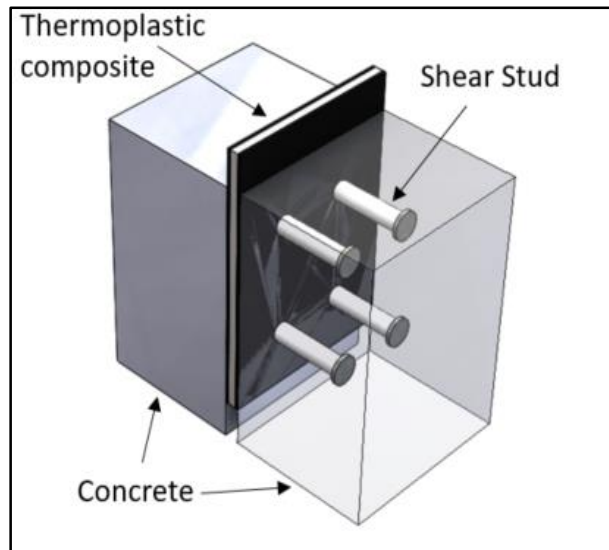


Figure 95: Concrete-CFRTP Stud 76.2-mm Concept Design

and 101.6-mm from the CFRTP horizontally out. For both specimen types, the CFRTP had 25.4-mm of clearance to travel down on the bottom of the specimen and 25.4-mm of clearance above the specimen to engage it for loading.

4.4.5.2 Specimen Manufacturing

The concrete-TP stud specimens were made with the same CFRTP reinforcement proposed as the beam specimen design and had shear studs friction welded on in the same way with self-tapping screws and washers for pullout resistance.

Figure 96 shows a 152.4-mm spacing finished concrete-CFRTP stud plate on the left and a top-down view of the plate installed in the formwork pre-concrete pour on the right to illustrate how the specimens were assembled in order for the studs to be embedded in concrete to be tested as desired in pure shear.

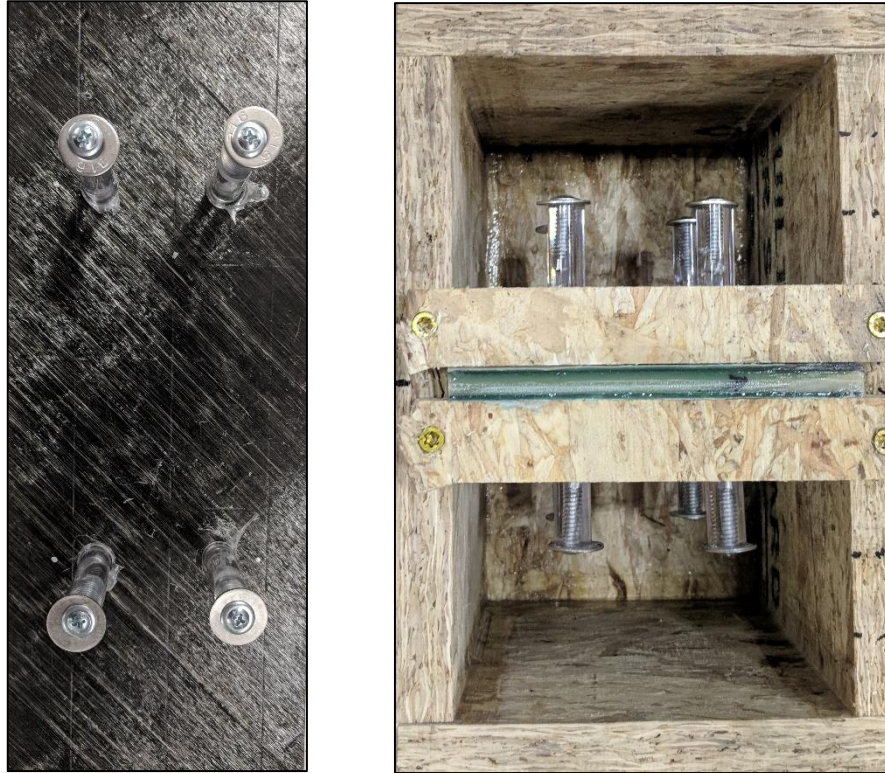


Figure 96: Concrete-TP Specimen Plate & Formwork

Each concrete-TP stud specimen was made of two CFRTP plates with four studs welded on one side at the desired spacing to mimic the beam specimen spacing. Then the plates were glued using Pliogrip adhesive to a frame of Garolite G-10 cut so that it only covered the outside 25.4-mm of the CFRTP plate and did not touch the backside of the shear stud locations. The end configuration shown in Figure 96 has the concrete-TP stud plates back to back adhered to the G-10 frame such that 101.6-mm of concrete would be cast on each side of the CFRTP effectively embedding the studs in the concrete.

Figure 97 shows the neat-resin shear studs were fabricated using 57.15-mm (2.25-inch) long rods of neat-resin PETg sourced from McMaster-Carr. Once the shear studs were friction welded onto the concrete-TP stud specimens using the mobile welder and the specimen type 5 settings a 19.05-mm (0.75-inch) diameter stainless steel washer was

placed on top and a 25.4-mm (1-inch) self-tapping screw was fastened into a pilot hole drilled into the top of the studs prior to welding. The shear stud fabricated as shown in Figure 97 follows the design outline in Figure 70.



Figure 97: Neat-Resin Shear Stud

The Elium concrete-CFRTP stud specimens were fabricated through vacuum infusion at the ASCC using the Elium 150 resin system as described in the specimen design section 4.3.2. The end result of the infusions follows the same dimensions as the 152.4-mm (6-inch) spacing IE 5842b samples and is shown in section 4.3.2 as Figure 82. The final specimens were prepared in the same manner as the concrete-TP stud specimens.

4.4.5.3 Test Setup & Instrumentation

The concrete-TP stud tests of both the 76.2-mm and 152.4-mm spaced PETg samples were conducted in a 100-kN Instron servo-hydraulic test frame with a 100-kN load cell. The setup, shown in Figure 98, was designed to load the samples in compression such that the shear studs would be engaged in pure shear embedded in the concrete. The concrete blocks

were placed on 3.175-mm thick neoprene pads and restrained at the bottom with angled metal and c-clamps to prevent the concrete from wedging out during testing. The CFRTP



Figure 98: Concrete-TP Stud Testing Setup

plate at the top of the specimen was covered with a 6.35-mm thick piece of neoprene contained in an aluminum c-channel sized to fit around the CFRTP center plate. A steel plate to distribute load across the c-channel was placed on the CFRTP and a self-leveling ball placed on top and the system closed between the two T-plates gripped in the Instron wedges. An anti-rotation post was installed on the Instron test frame to prevent the actuator from spinning during testing.

Instrumentation for the concrete-TP and concrete-CFRTP stud tests included collection of load and actuator position data from the Instron 100-kN hydraulic test frame and two LDTs

to collect the relative movement of the CFRTP to the concrete blocks. The LDTs were mounted on opposite sides of the specimen on the concrete and the probe was measuring against a wooden mount fixed to opposite sides of the CFRTP plate.

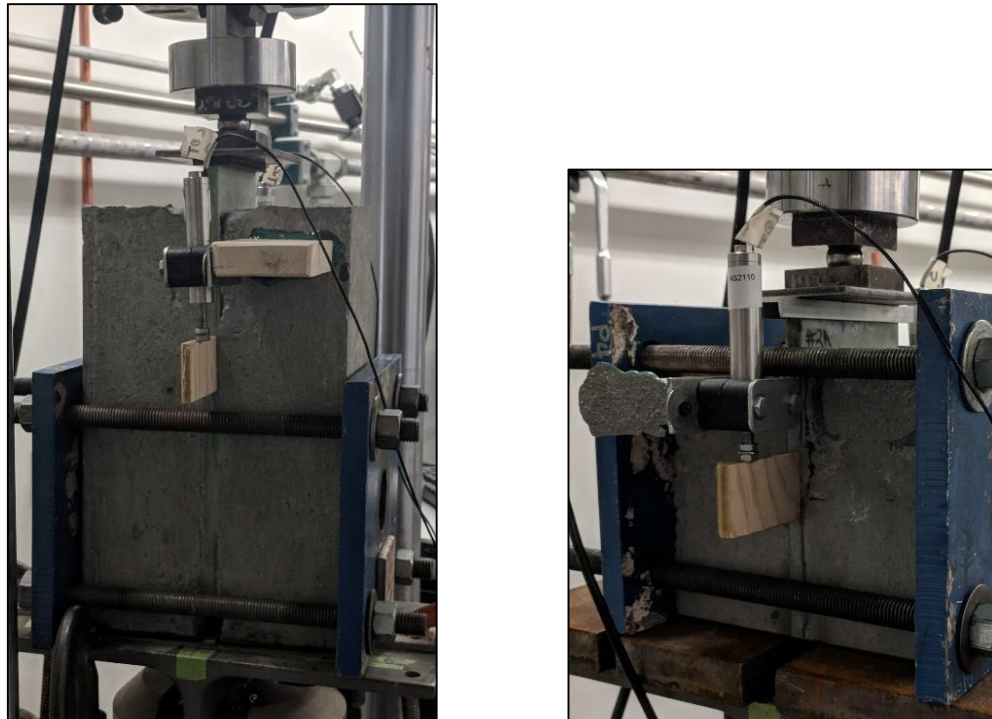


Figure 99: Elium Concrete-CFRTP Stud Configuration 1 (left) & 2 (right)

Due to complications during testing of the concrete-CFRTP stud samples, which will be elaborated on in section 4.4.3.4, specimens 2, 3, and 5 were tested in two configurations. Configuration 1 shown in Figure 99 was identical to the configuration of the 152.4-mm (6-inch) IE 5842 specimens with two exceptions. One, the tests were conducted on both a 100-kN (22.5-kip) Instron test frame and a 245-kN (55-kip) Instron test frame. Two, the original restraining mechanism for the concrete was four pieces of steel-angle clamped down to keep the concrete from wedging out during the test. This was found to be insufficient for the higher loads being seen in the concrete-CFRTP stud specimens.

Therefore, it was replaced with two metal plates held together with threaded rod and nuts, which allowed the concrete to be held tightly but did not introduce too much friction into the system since the nuts were installed finger tight. Configuration 2 shown in Figure 99 was created in order to counteract buckling that was observed in the top flange of the sample that was in compression during testing. Configuration 2 was the same as configuration 1 except that the two samples tested this way both were cut in half between the studs in the middle such that the specimen would have 4-studs instead of 8-studs. This was necessary to reducing the specimen capacity. The first sample used the top flange as originally designed, but still experienced buckling. The second sample had the top flange reduced in height by 12-mm in an effort to increase the load before buckling

4.4.5.4 Predicted Fiber-Reinforced Thermoplastic Shear Stud Results

Using the same laminate analysis code that was used to predict in-plane properties of coupon specimens in chapter 3 a simplified approximation can be made for the strength of a fiber-reinforced shear stud. The lamination theory method used combined the use of micromechanics to calculate lamina properties from the properties of the raw fiber and matrix materials and macromechanics to calculate the effective laminate properties.

The predicted in-plane shear strength of both an Elium and PETg shear stud reinforced with ± 45 -degree biaxial E-glass was calculated. The following assumptions were used for the calculations.

Assumptions:

- Shear stud failure occurs through in-plane shear of the double bias layer of composite at the shear plane where the stud meets the CFRTP reinforcement plate.

- Fiber interaction sufficient for failure in the stud in this layer occurs between the stud and CFRTP reinforcement plate
- Fibers at the failure layer in the stud are perfectly aligned at ± 45 -degrees and evenly distributed
- Failure does not occur at the matrix layer between the stud and the CFRTP reinforcement plate
- Fabrication method has no effect on the shear stud strength
- Two layers of fibers each with a thickness of 4-mm are fully engaged and contribute to the strength of the stud, both a 45 and -45-degree layer
- Fiber volume fraction (V_f) calculated to be 58.9 % from the mass of fabric used and volume of E-glass/Elium shear stud that was fabricated as a part of this study
- Fiber volume fraction (V_f) is consistent throughout the entire shear stud
- In-plane shear strength determines failure strength not inter-laminar shear between the stud and CFRTP reinforcement plate

Using E-glass reinforcement properties from literature [7] and properties for the Elium 150 resin-system [20] presented in Table 1 the prediction for shear stud strength of an E-glass/Elium shear stud was 54.3-MPa. Changing the matrix properties to ones for PETg polymer from literature [36] the prediction for shear stud strength was 42.1-MPa. These predicted values are compared to the experimental results in the discussion of results subsection of this chapter. Potential limitations of this simplified analysis to get a stud strength prediction are including in the following bullet list.

- The failure mode may be dominated by the matrix and not engage the two-layers of fibers to the effective capacity predicted by CLT
- The amount of fibers necessary to generate fiber engagement between the reinforced shear stud and CFRTP reinforcement plate is unknown
- The fibers may not be perfectly aligned at ± 45 -degrees or evenly distributed
- Fabrication method could have an effect on the strength of the stud based on how it bonds the stud to the CFRTP reinforcement and if it damages the fibers during stud installation
- The Fiber volume fraction (V_f) may not be consistent throughout the shear stud
- Inter-laminar properties may drive the stud failure as opposed to in-plane failure

4.4.5.5 Tabulated Numerical Results

Results from the concrete-TP stud test conducted to assess the capacity of the IE 5842b friction welded neat-resin shear studs embedded in concrete and loaded in pure shear are given in Table 45.

The connection stiffness values reported in Table 45 and Table 46 were calculated by finding the average of the points from LDT1 and LDT2 at 30 % and 50 % of the peak load. Then finding the slope from the averaged points.

Table 45: IE 5842b Friction Welded Concrete-TP Stud Test Results

Specimen Name	Stud Spacing	Stud Shear Stress at Peak Load (MPa)	LDT1 Peak (mm)	LDT2 Peak (mm)	Stiffness per Stud (kN/mm)
PETg 3-1	76.2-mm	21.8	0.43	0.50	8.75
PETg 3-2	76.2-mm	18.4	0.16	0.41	12.6
PETg 3-3	76.2-mm	25.8	0.80	0.43	7.19
PETg 3-5	76.2-mm	23.9	0.48	0.32	7.14
PETg 6-2	152.4-mm	17.9	0.45	0.57	5.76
PETg 6-3	152.4-mm	19.0	0.54	0.45	6.21
PETg 6-5	152.4-mm	25.0	0.35	0.54	9.43

Results from the concrete-CFRTP stud tests conducted to assess the capacity of the E-glass/Elium vacuum infused fiber-reinforced shear studs embedded in concrete and loaded in pure shear are given in Table 46. Specimen 6-2 and 6-3 each had 4-studs and specimen 6-4 and 6-5 each had 8-studs. When calculating the stud shear stress at peak load for the E-glass/Elium shear studs the peak load from the test was divided by the number of studs and the area of a stud shaft, which had a diameter of 12.7-mm (0.5-inches) the same as the PETg neat-resin studs.

Table 46: E-glass/Elium 150 Infused Concrete-CFRTP Stud Test Results

Specimen Name	Stud Spacing	Stud Shear Stress at Peak Load (MPa)	LDT1 Peak (mm)	LDT2 Peak (mm)	Stiffness per Stud (kN/mm)
E-glass/Elium 6-2	-	164	1.13	-0.03	32.0
E-glass/Elium 6-3	-	185	0.45	0.96	20.8
E-glass/Elium 6-4	152.4-mm	64.4	0.28	0.27	32.3
E-glass/Elium 6-5	152.4-mm	109	0.40	0.55	32.4

As shown in Figure 71 in section 4.2.3.4, the E-glass/Elium shear studs were infused with a radius at the bottom of the stud of 19.05-mm (0.75-inch). This was done to increase the capacity of the studs by increasing the effective shear plane area, where the stud interfaces with the CFRTP reinforcement. This provides a larger area for the transfer of forces beyond the stud shaft diameter and creates a smooth transition from the CFRTP plate up to the shaft of the shear stud; potentially reducing stress concentrations that could occur at the sharp transition between a CFRTP plate and a straight-shafted stud, like the PETg neat-resin studs. The ability to infuse the shear studs to a designed shape in a mold is an advantage of the vacuum infusion process.

4.4.5.6 Concrete-TP and Concrete-CFRTP Stud Graphical Results

Figure 100 and Figure 101 show graphics including sub-plots of load vs. LDT position and load vs. actuator position for the IE 5842b friction welded neat-resin stud PETg 76.2-mm specimen 3-1 and PETg 152.4-mm specimen 6-3 respectively.

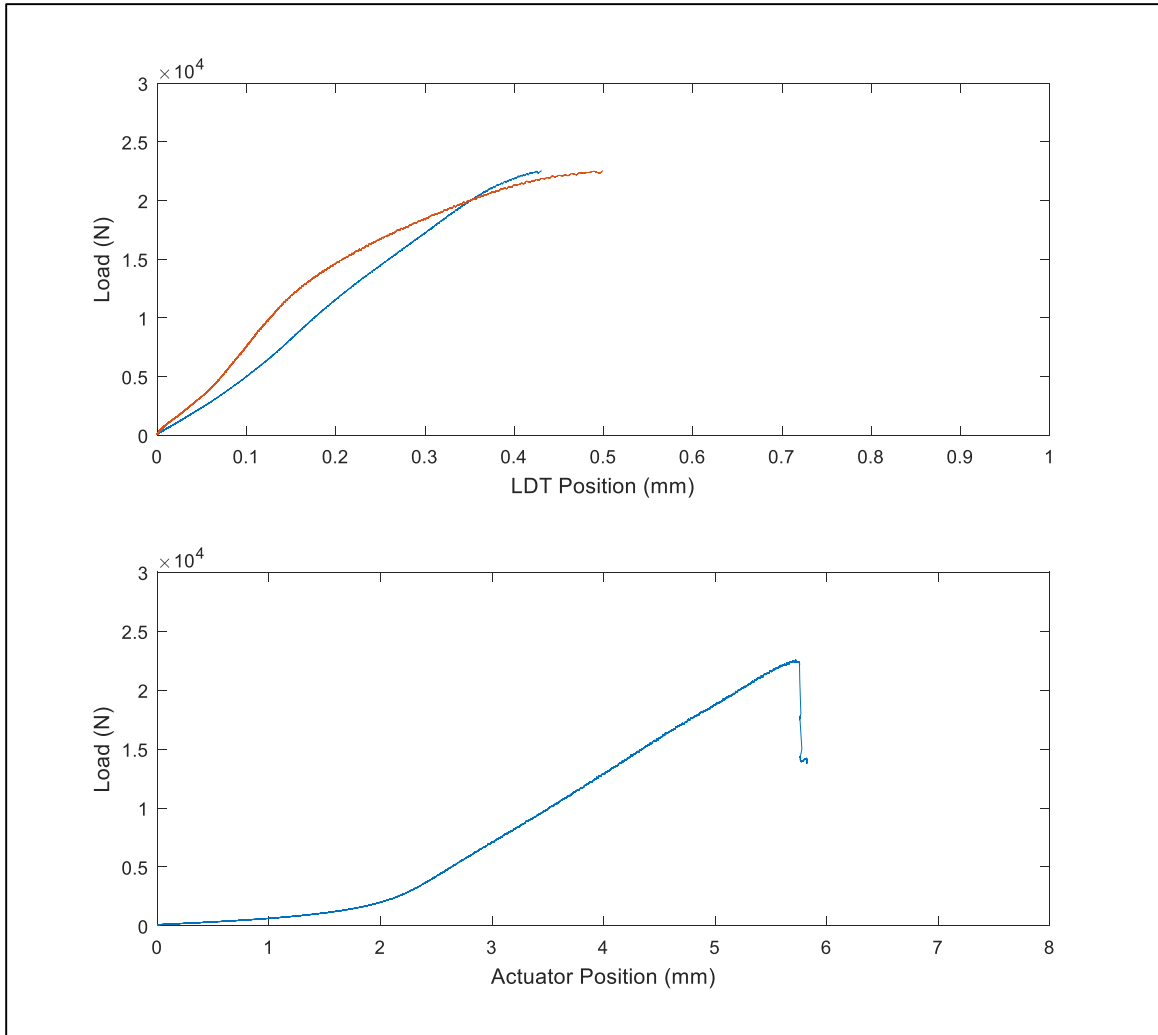


Figure 100: Concrete-TP Stud 76.2-mm Specimen 3-1 Results

All four 76.2-mm spacing samples exhibited similar behavior to what is shown in Figure 100. Results show that LDT1 & LDT2 have similar slopes and end relatively close to each other but that the shear studs do not exhibit the same ductility that was seen in the TP stud

shear testing. This could be due to the close confinement of the concrete around the studs in concrete-TP stud configuration.

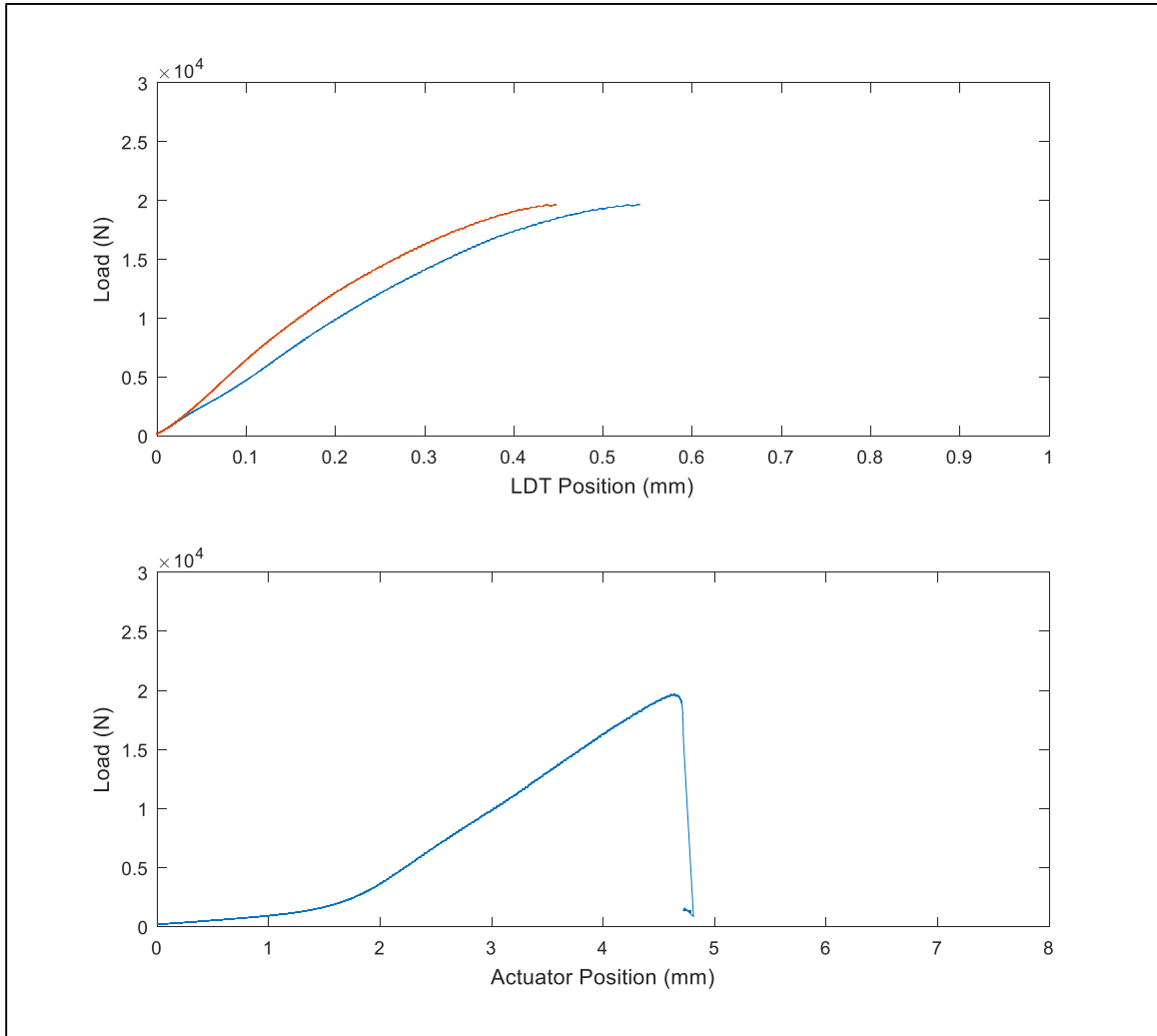


Figure 101: Concrete-TP Stud 152.4-mm Specimen 6-3 Results

All four 152.4-mm spacing samples exhibited similar behavior to what is shown in Figure 101. Results shown that LDT1 & LDT2 have similar slopes and end relatively close to each other but that the shear studs do not exhibit the same ductility that was seen in the TP stud shear testing.

Figure 102 and Figure 103 show the two halves from one side of a failed PETg concrete-TP stud specimen. All seven of the PETg concrete-TP stud specimens shared the same failure mode. One side of the specimen broke all four studs while the other side remained unbroken. In the same fashion as the IE 5842 double and single-lap shear specimens the studs failed at the interface between the top layer or two of the fibers on the CFRTP and the stud. In the concrete-TP stud samples this was more evident because there were more studs attached to the CFRTP.



Figure 102: Failed PETg Concrete-TP Stud
Specimen (CFRTP side)



Figure 103: Failed PETg Concrete-TP Stud
Specimen (Concrete side)

Four E-glass/Elium concrete-CFRTP stud samples with vacuum infused fiber-reinforced shear studs were tested, one using the original configuration, specimen 4, one using configuration 1, specimen 5 and two using configuration 2, specimens 2 and 3. Figure 104 and Figure 105 show graphics including sub-plots of load vs. LDT position and load vs. actuator position for the first samples tested 4 & 5 respectively.

Specimen 4 was tested in the original configuration used with the IE 5842b concrete-TP stud samples. It was loaded up to approximately 66-kN (14.9-kips) when the wedging forces from the concrete blocks broke the adhesive bond that holds the two sides of the sample together in the center. Based on this configuration 1 was devised in order to better confine the concrete to counteract the larger wedging forces being experienced at higher loads.

Figure 104 shows the results of testing specimen 4 until the adhesive bond in the sandwich composite was broken. The ultimate load reached by this sample does not show the ultimate strength of the studs, and the LDT data near the end of the test is not indicative of the performance of the shear studs as the LDTs were affected by the bending of the concrete and the sandwich panel breaking in the center.

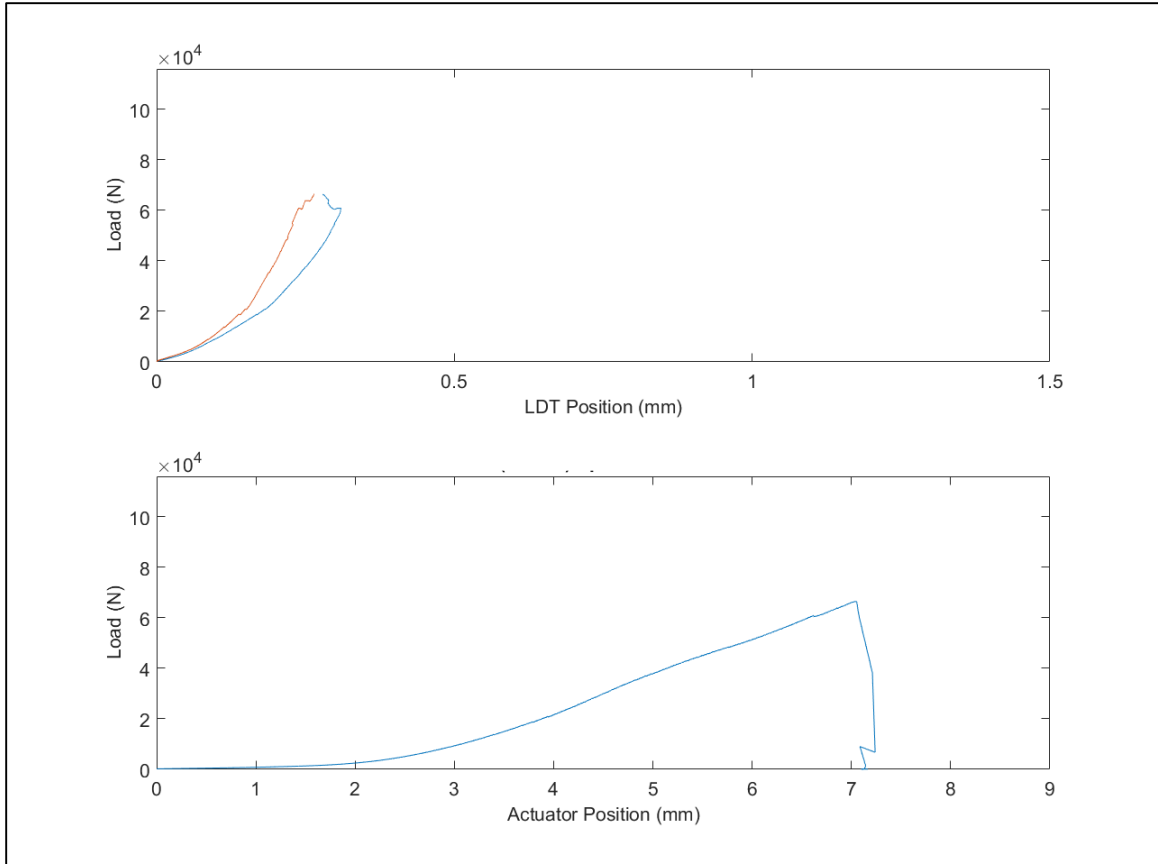


Figure 104: E-glass/Elium Concrete-CFRTP Stud Specimen 4 (8-Studs)

Specimen 5 was first tested in a 100-kN (22.5-kip) Instron test frame, however the sample reached the frame's load capacity so testing was moved to a 245-kN (55-kip) Instron test frame. Figure 105 shows the results from testing specimen 5 the second time. The failure mode seen by this specimen was buckling of the exposed top portion of the composite, shown in Figure 106. The sandwich composite used in the center of the concrete-CFRTP stud specimen that the studs were infused onto failed at the interface where it was no longer supported by the concrete. The ultimate load reached for specimen 5 does not show the ultimate strength of the studs but only represents a lower-bound since the studs were not the failure point of the specimen. The load vs. LDT position plot showed approximately linear behavior.

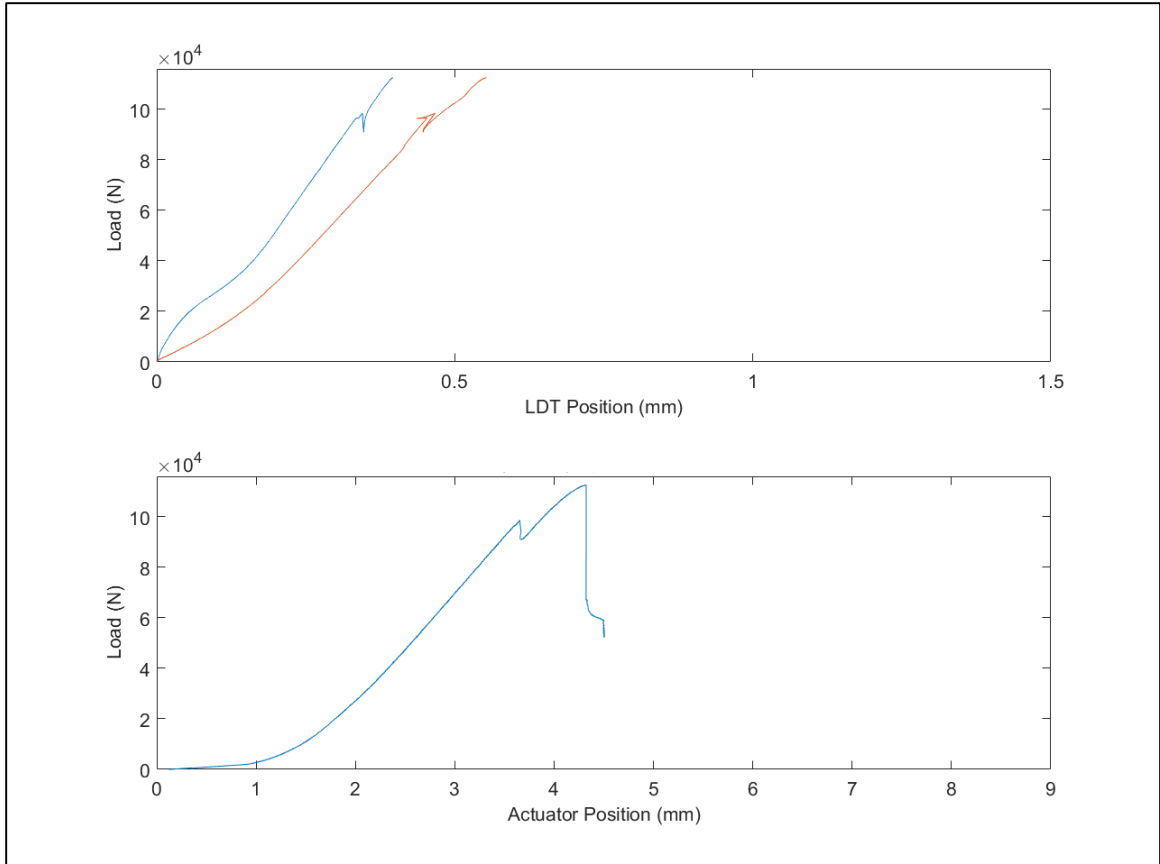


Figure 105: Elium Concrete-CFRTP Stud Specimen 5 (8-Studs)



Figure 106: Elium Concrete-CFRTP Stud Specimen 5
Failure Mode

Specimen 3 was cut in half at the center point between the two sets of studs in order to reduce the number of studs from eight to four, in an effort to make breaking the specimens more achievable. This change shown in Figure 107 made the overall dimensions of the specimen similar to the 76.3-mm (3-inch) spacing IE 5842b concrete-CFRTP stud specimens. Figure 108 and Figure 109 are plots of load vs. LDT position and load vs. actuator position for configuration 2, specimens 3 & 2 respectively.



Figure 107: Untested Configuration 2
Specimen

The failure mode of specimen 3 was the same as specimen 5, column buckling of the sandwich composite just above the concrete. Figure 108 shows the specimen 3 results for the test run on the 245-kN (55-kip) Instron test frame until the specimen failed. The same as specimen 5, specimen 3 does not represent the ultimate strength of the studs based on the failure mode seen, but the load vs. LDT data is also approximately linear.

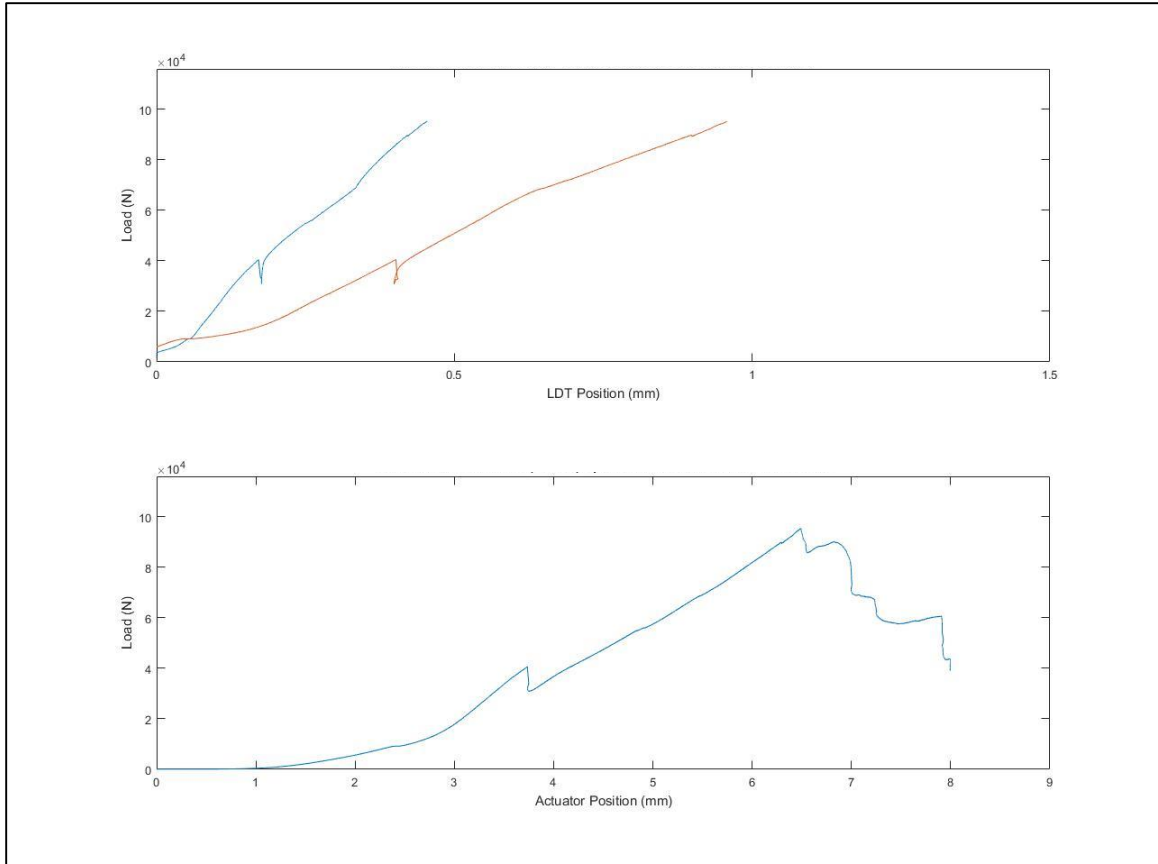


Figure 108: Elium Concrete-CFRTP Stud Specimen 3 (4-Studs)

Specimen 2 was tested using configuration 2 the same as specimen 3, but was prepared slightly differently. Like specimen 3, it was cut in half between the studs on the water-jet to separate the top four studs from the bottom to reduce the necessary load to fail the shear studs. However, the top column was also cut in an effort to increase the loads achievable before buckling occurred. The height of the top column of the sandwich composite was reduced by 12-mm (approximately 0.5-inches), which was about half of its height.

The failure mode of specimen 2 was the same as specimens 3 & 5, column buckling of the sandwich composite just above the termination of the concrete. The higher loads desired by shortening the portion of CFRTP outside the concrete in this configuration were not

achieved in testing. The ultimate load reached by specimen 2 does not represent the ultimate capacity of the shear studs due to the failure mode achieved, but the LDT data shows an approximately linear behavior for one LDT. From the load vs. LDT position data specimen 2 appears to have been loaded unevenly, it is clear that one LDT moved approximately twice as far as the LDTs in previous specimens and the other LDT showed almost no displacement.

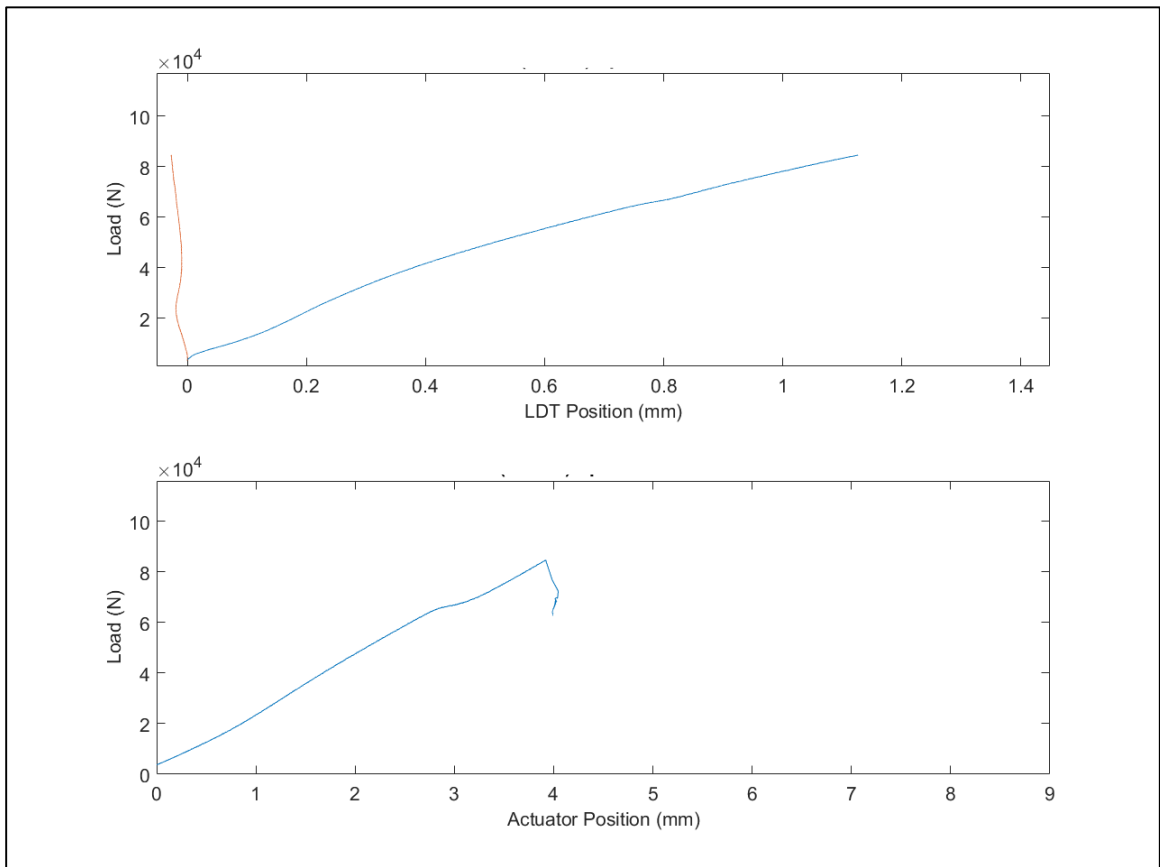


Figure 109: Elium Concrete-CFRTP Stud Specimen 2 (4-Studs)

No conclusive ultimate strength values were found from the Elium concrete-CFRTP stud specimens based on the failure modes seen in testing. The results will be discussed further in section 4.5.

4.5 Discussion of Experimental Results

The experimental results from the concrete-TP and concrete-CFRTP stud tests of both friction welded neat-resin PETg studs to IE 5842b CFRTP and the co-infused Elium shear studs and reinforcement plate are presented for comparison in Table 47.

The E-glass/Elium specimens could not be loaded to failure. However, since the load vs. LDT position plots of the samples is approximately linear during the tests an average stiffness can be calculated. The stud shear stress at peak load results reported are calculated using the peak load achieved during the test and the area of the stud shafts, therefore both the PETg neat-resin shear studs and the E-glass fiber reinforced Elium studs use their stud shaft diameter of 12.7-mm (0.5-inches) when calculating their strength. Due to the varying number of studs in the E-glass/Elium concrete-CFRTP stud tests all stiffness values from the concrete-CFRTP stud tests are reported per stud in order to make comparison of values easier.

Table 47: Concrete-TP and Concrete-CFRTP Stud Comparison

Value	PETg 76.2-mm Spacing	PETg 152.4-mm Spacing	Elium 152.4-mm Spacing
Mean Peak Load per Stud	2.90 kN	2.66 kN	16.8 kN
Mean Stud Stress at Peak Load	22.5 MPa	20.6 MPa	131 MPa*
Stud Stress at Peak Load COV	14.2 %	18.3 %	41.7 %
Mean LDT1 Peak Position	0.47 mm	0.45 mm	0.57 mm
Mean LDT2 Peak Position	0.42 mm	0.52 mm	0.44 mm
LDT1 Peak Position COV	56.3 %	21.7 %	67.8 %
LDT2 Peak Position COV	18.5 %	12.4 %	96.2 %
Mean Stiffness per Stud	8.93 N/mm	7.14 N/mm	26.5 N/mm** 32.4 N/mm***
Stiffness COV	28.9 %	28.0 %	29.8 %** 0.27 %***

**Note: This strength value is a lower-bound, not the ultimate strength of a failed stud*

***Note: Values for the configuration 2 specimens with 4-studs (specimen 2 & 3)*

****Note: Values for original and configuration 1 specimens with 8-studs (specimen 4 &*

5)

From these results, the peak values for LDTs from all three different tests show the amount of relative movement between the thermoplastic composite sandwich panel and the concrete was approximately the same. It is also notable that all the neat-resin studs showed very little ductility, achieving high loads with less than 1-mm of relative movement between the composite reinforcement and the concrete. Concrete-CFRTP specimens did not reach peak loads so an assessment of the total ductility to failure cannot be made. However, this does show that the thermoplastic shear studs used did generate composite action by demonstrating that they limited slip at the CFRTP-concrete interface under increasing load until failure of the specimen. The E-glass/Elium studs exhibited a higher ability to limit slip compared to the neat-resin PETg studs under the loads that were achieved.

Comparing the results from the two PETg spacing concrete-TP stud samples showed that the PETg 76.2-mm (3-inch) spacing was 9 % stronger and 25 % stiffer than the 152.4-mm (6-inch) spacing. The four E-glass/Elium concrete-CFRTP stud samples were separated into two groups for stiffness comparisons: group 1 was specimen 2 & 3, which had 4-studs each with a mean stiffness per stud of 26.5-N/mm, group 2 was specimen 4 & 5, which had 8-studs each with a mean stiffness per stud of 32.4-N/mm. The group 2 E-glass/Elium samples had a 22 % greater stiffness per stud than the group 1 samples.

The seven PETg concrete-TP stud samples yielded a mean peak load per stud of 2.8-kN, a mean stud stress at peak load of 21.7-MPa, and mean stiffness per stud of 8.15 N/mm. The four E-glass/Elium concrete-CFRTP stud samples yielded a mean peak load per stud of 16.6-kN, a mean stud stress at peak load of 131-MPa and a mean stiffness per stud of 29.4 N/mm. The E-glass/Elium shear studs exhibited 6 times the stress at peak load and

3.6 times the stiffness per stud of the PETg neat-resin studs. There are two major factors which could be contributing to this, one, the E-glass fiber-reinforcement present in the stud and at the interface between the stud and the CFRTP plate, and two, the increased area at the shear plane between the stud and CFRTP from the fluted shape incorporated in the E-glass/Elium stud.

The E-glass/Elium had a predicted shear strength of 54.3-MPa, which is 58 % lower than the mean stud stress at peak load of 131-MPa from the concrete-CFRTP stud test. This could be because the E-glass/Elium studs in the concrete-CFRTP stud test had a radius of 19.05-mm (0.75-inch) at the bottom extending the stud and its fiber-reinforcement beyond the stud shaft diameter that was used to calculate the experimental stud stress at peak load. The predicted stud shear strength of an E-glass/PETg stud was 42.1-MPa using the same analysis method used to predict the E-glass/Elium value. If the shear stud strength is improved by the fibers the prediction shows a 48 % increase in strength over the 21.7-MPa strength observed from the PETg concrete-TP stud tests conducted. If the fiber-reinforcement in the shear stud can engage with the fiber-reinforcement in the CFRTP plate, an improvement in stud strength like the prediction shows could occur. However, literature review conducted in this study found that for some fabrication methods such as friction welding the introduction of materials at the welding interface other than the thermoplastic polymer could decrease the bond strength by decreasing the amount of polymer available for bonding [71].

A comparison of the PETg concrete-TP stud test results to the TP stud shear testing done was also of interest. The concrete-TP stud tests yielded a mean peak load per stud and stud stress at peak load average results of 2.9-kN and 22.5-MPa for the 76.2-mm (3-inch)

spacing, and 2.66-kN and 20.6-MPa for the 152.4-mm (6-inch) spacing respectively. The single-lap shear tests of specimen type 5 fabricated using the mobile welder system yielded an mean peak load of 3.2-kN for a single stud and stud stress at peak load of 25.4-MPa. From these results, it is seen that the concrete-TP stud samples resulted in 11.4 % lower stress at peak for the 76.2-mm spacing samples and 18.9 % lower stress at peak for the 152.4-mm spacing samples when compared to the single-lap shear results prepared in the same way. The ductility results from the concrete-TP stud testing if calculated the same as for the TP stud shear testing show approximately zero ductility, which is not consistent with the TP stud shear testing. This shows that the concrete-TP stud testing has more potential for evaluating the ductility of potential thermoplastic studs in hybrid applications.

The proposed beam-layup had a tensile strength from experiments of 223-MPa, and since the concept hybrid beam design has a width of 127-mm (5-inches) and a thickness of 1.6-mm (0.06-inches) the maximum tensile load of the beam tension reinforcement would be 45.3-kN. Comparing this maximum tensile load to the mean load per stud from the concrete-TP and concrete-CFRTP stud tests, seventeen PETg studs or three E-glass/Elium studs would be necessary to transfer an equivalent load by shear. Making the same comparison with a typical steel stud with the same shaft diameter of 12.7-mm (0.5-inches), which would have a strength of 414-MPa (60-ksi), the failure load for a single stud would be 52.5-kN meaning one stud could take more load than the beam reinforcement.

Photos were taken of both the neat-resin PETg shear studs and the Elium vacuum infused shear studs after testing to show that the studs were uniformly embedded in concrete. Figure 110 shows that the small aggregate concrete used and the size of the studs and washers for pull out resistance were suitable for a hybrid composite-concrete application.



Figure 110: PETg Neat-resin PETg Shear Studs Embedded in Concrete

The vacuum infused Elium fiber-reinforced shear studs cast in concrete for concrete-CFRTP stud testing were not brought to their ultimate capacity as discussed in the graphical results due to unexpected failure in the CFRTP prior to stud failure. Figure 111 shows two different views of Elium shear studs that were tested in concrete-CFRTP stud and then had the concrete partially broken away to inspect the condition of the studs post-test. The studs clearly were fully encased in concrete, and there is no evidence of stud pull out. There is also no substantial visible damage to the shear studs from testing.

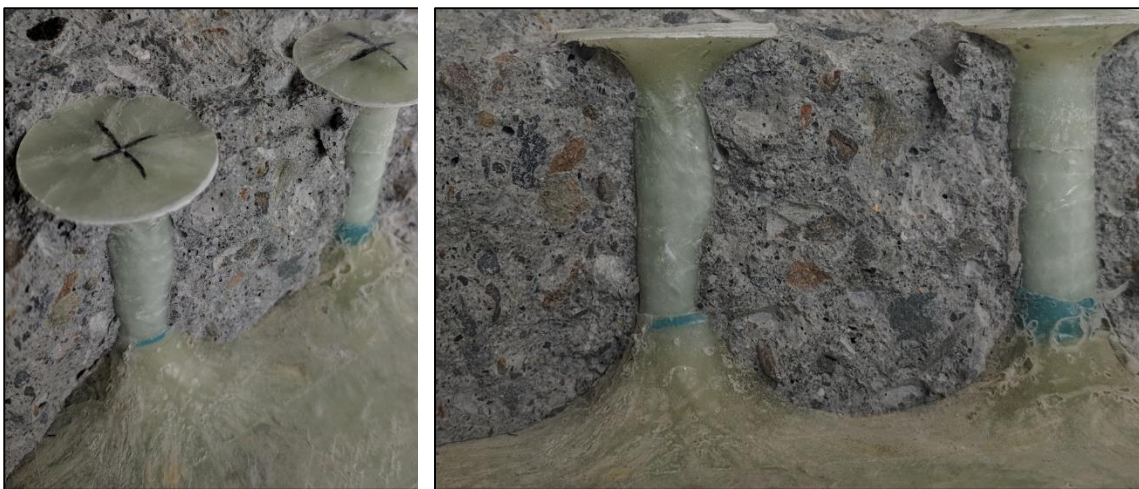


Figure 111: E-glass/Elium Shear Studs Embedded in Concrete

Figure 112 shows two different views of Elium shear studs removed from a different concrete-CFRTP stud specimen that was tested. These shear studs also show no visible damage from loading during testing when compared with the untested studs in Figure 83. This further reinforces the conclusion that the results from the concrete-CFRTP stud test represent a lower bound for the capacity of the E-glass/Elium studs.



Figure 112: Tested E-glass/Elium Shear Studs (Broken out of Concrete)

4.6 Redesigned E-glass/Elium Concrete-CFRTP Stud Specimen

Due to the failure modes of the E-glass/Elium concrete-CFRTP stud specimens that occurred in this study a new specimen design was created in order to facilitate possible future work to find the failure strength of an E-glass/Elium shear stud.

Using CLT and transformed section analysis, a sandwich composite design was iteratively developed with Euler buckling theory in order to make the CFRTP panel used in concrete-CFRTP stud test stronger to avoid the buckling/crushing failure mode seen in the specimens tested as a part of this study. For this analysis, the failure strength of the E-glass/Elium shear studs was assumed to be 30-MPa using the entire shear plane area, not

just the stud shaft area. This was done for easier comparison with the reported TP stud shear testing strength of 22-MPa for an Elium composite reported in the technical data sheet provided by Arkema [20]. The stud configuration was assumed to be the same as the 4 stud samples made in this study. Using the same shaped stud but changing the total lower radius was changed to 15.9-mm (0.625-inches), by varying the bottom flute radii from 19-mm (0.75-inch) to 9.5-mm (0.38-inch) in order to reduce the cross-sectional area to make stud failure feasible at lower loads. Then a factor of safety on the load was used to calculate the critical load for Euler buckling were done using Equation 48 [37].

$$P_{critical} = \frac{\pi^2(EI)}{(KL)^2} \quad \text{Equation 48}$$

The critical load ($P_{critical}$) necessary to prevent buckling is related to the specimen service load, which is the load necessary to fail the E-glass/Elium shear studs is based on the failure assumption of 30 MPa, 4 studs with shear plane cross-sectional area of 794 mm² per stud and a factor of safety of 2 on the load. This results in a critical load of 190.6 kN (42.92-kips) based on the specimen service load assumptions. For the direct shear configuration the end restraint coefficient, K, was assumed to be 0.7 for a pinned-clamped boundary condition. The remaining unknowns in Equation 6 are the modulus E, the moment of inertia (I), and the height (L) of the specimen in question, which is 25.4-mm (1-inch) for this specimen. The unknown EI, which was determined using transformed section analysis and CLT to design a sandwich composite made of outer skins of E-glass/Elium composite to which the studs are infused with an inner core of Garolite G10 for the situation defined, was found to be 6.11-Nm².

With the flexural modulus of G10 known to be 18.6-GPa [79], CLT was used to generate properties of defined E-glass/Elium laminates, combined with transformed section analysis in order to find the moment of inertia of the composite when transformed to have a single modulus. By iteration an E-glass/Elium laminate of fiber-architecture $[45 -45 0 0 0 0]_s$ with a flexural modulus of 49.4 GPa was found to be suitable to resist buckling and also provide enough compressive strength, 301-MPa, to prevent CFRTP crushing under the expected compressive loads.

E-glass/Elium concrete-CFRTP stud specimens with four reinforced shear studs per specimen as described above should be capable of failing the shear studs loaded in compression if the failure strength assumptions used hold true in experiments.

Another possible method for testing the E-glass/Elium studs is in single shear in a configuration similar to that used by Brena et al. [80], which pulls the FRP in tension as opposed to pushing it in compression eliminating the possibility of buckling. Figure 113 shows a diagram based on the Brena et al. setup that could be used to test the E-glass/Elium studs infused to a CFRTP plate.

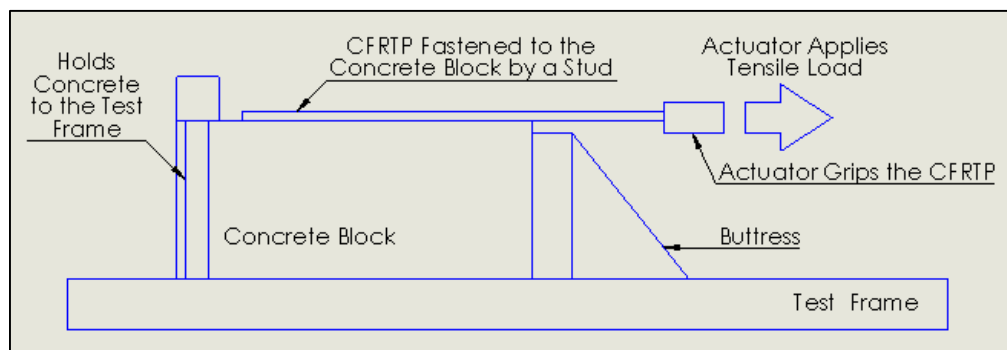


Figure 113: Stud Single Shear Test Setup (Adapted from Brena et al. [80])

This setup tests the stud in single shear with the CFRTP in tension and the concrete confined by a buttress on the actuator side and fastened down to the test frame on the backside. In this configuration, the CFRTP is in tension as it would be in the proposed beam specimen. This test configuration could pose challenges such as how to properly restrain the concrete and apply a horizontal force to put the CFRTP in tension, which would need to be overcome in order to implement it.

4.7 Conclusions and Recommendations

The exploration of shear connectors conducted in this study involved the development of two shear stud systems. The first was friction welded, neat-resin PETg shear studs to the reinforcing plate and the second was fiber-reinforced shear studs that were vacuum-infused with the reinforcement plate in a mold using the Elium 150 resin system.

Both shear stud systems were successfully manufactured and tested. Manufacturing of the two stud systems showed that the neat-resin PETg studs could be rapidly manufacturing at about 1-minute per weld, but the E-glass/Elium studs were labor and material intensive to vacuum infuse. The results and conclusions from testing of the shear stud in this study are presented in the following lists. The first summarizes the conclusions from TP stud shear testing of neat-resin PETg studs, and the second discusses the results from concrete-TP stud testing of the neat-resin PETg and concrete-CFRTP testing of fiber-reinforced Elium shear studs embedded in concrete.

From the literature review of the friction welding of thermoplastics a range of potentially suitable parameters was found and a test matrix of 16 specimen types was developed in order to assess which set of parameters was suitable for the friction welding of neat-resin

PETg studs. The studs were first fabricated using an Instron welding device to ensure a highly controllable environment for parameters and then later fabricated using a mobile welding device designed to mimic the Instron welding device but be able to weld to larger objects. All TP stud shear testing specimens were tested in TP stud shear testing in a custom fixture designed to engage the studs to assess their strength and ductility.

- Double TP stud shear testing of friction welded neat-resin PETg shear studs fabricated using the Instron welding device required further verification because the specimens did not reliably load both studs.
- Single TP stud shear testing of friction welded neat-resin PETg shear studs fabricated using the Instron welding device was conducted to eliminate issues with load sharing between studs in the double TP stud shear configuration in order to select welding parameters suitable for use with PETg neat-resin shear studs.
- Single TP stud shear testing of friction welded neat-resin PETg shear studs fabricated using the mobile welding device and specimen type 5 parameters resulted in a stud stress at peak load of 25.4-MPa, which was lower than the 29.4-MPa seen with the Instron welded samples. These results were considered reasonably close to each other.

With suitable welding parameters selected and a mold developed for the infusion of E-glass/Elium shear studs the next phase of shear stud testing implemented was concrete-TP and concrete-CFRTP stud testing of multiple studs embedded in concrete. These specimens were designed based on potential spacings chosen from AASHTO guidelines for steel shear studs [77] and were meant to assess the capacity of the studs in pure shear. Eleven direct shear samples were tested, seven PETg samples and four E-glass/Elium samples. The

results from concrete-TP and concrete-CFRTP stud testing are presented in the following list:

- Four 76.2-mm (3-inch) spacing PETg samples were successfully tested and showed a mean peak load of 2.90-kN per stud, mean stud stress at peak load of 22.5-MPa, and mean stiffness per stud of 8.93-N/mm.
- Three 152.4-mm (6-inch) spacing PETg samples were successfully testing and showed a mean peak load of 2.66-kN per stud, mean stud stress at peak load of 20.6-MPa, and mean stiffness per stud of 7.14-N/mm.
- Four E-glass/Elium concrete-CFRTP stud samples were tested but did not failed the shear studs, the failure mode of all four tests was CFRTP buckling/crushing of the plate the studs were infused to. A redesigned specimen was presented as potential option for future work.
- The results from the E-glass/Elium concrete-CFRTP stud tests conducted until plate buckling/crushing showed a mean peak load of 16.8-kN per stud, a mean stud stress at peak load of 130-MPa, and a mean stiffness per stud of 29.4-N/mm.

The stud stress at peak load, stiffness per stud, and visual study conducted showed that the E-glass/Elium shear studs provided more composite action than the PETg studs, and had residual strength at the completion of testing. The concrete-TP and concrete-CFRTP stud tests best represent the physical situation the thermoplastic shear studs would be subjected to in a hybrid composite-concrete beam. This type of testing is useful for not only assessing the strength of a shear stud but also the potential ductility that may be expected in a hybrid structure. TP stud shear testing of neat-resin PETg studs showed similar strength values for

the shear studs but indicated much higher ductility that was seen when the studs were embedded in concrete.

Based on the work done in this study the following recommendations are given:

- Other methods of thermoplastic shear transfer such as friction welded thermoplastic studs with fiber-reinforcement or additional mechanical fastening, stamp formed stock material cut on a CNC, or a thermoplastic composite rod in bearing be explored in order to expand the applications of thermoplastic reinforcement in structural design.
- Ultimate strength of a fiber-reinforced Elium shear stud fabricated through vacuum infusion be explored using the redesigned specimen as potential future work with the understanding that vacuum infused thermoplastic studs are labor intensive to fabricate.

CHAPTER 5

CONCLUSIONS AND RECOMMENDATIONS

5.1 Conclusions

This thesis focused on a preliminary assessment of the feasibility of using thermoplastic composites in hybrid composite-concrete structures. Research included characterizing the mechanical properties two CFRTP materials, an assessment of spin-welding thermoplastic shear studs, and testing thermoplastic shear studs in both tension-shear and in compression-shear when embedded in concrete.

This study has established that the assessed CFRTP composites are feasible to manufacture and have suitable mechanical properties for use in structural elements based on the standardized testing of unidirectional E-glass/Elium and E-glass/PETg thermoplastic composites. The manufacturing of thermoplastic shear studs for hybrid CFRTP-concrete members proved to be challenging, especially the infused shear studs that are time consuming to manufacture. Additional details regarding these conclusions are provided in the remainder of this chapter along with recommendations for future work.

5.1.1 CFRTP Manufacturing Feasibility & Mechanical Properties

Two thermoplastic materials were selected for exploration in this study, Elium 150 an infusible acrylic thermoplastic and PETg in the form of prepreg thermoplastic tapes. Manufacturing feasibility was proven with Elium 150 through vacuum infusion an industry accepted fabrication process commonly used with thermoset resin-systems. For PETg prepreg tapes it was proven with manual and automated stamp forming. Automated stamp

forming was chosen for its ability to produce composites with minimal fiber wash, repeatability and rapid manufacturing times. This selection of materials based on literature review and proof of manufacturing feasibility completed objective one of this study.

Standardized mechanical testing was done to acquire properties of unidirectional thermoplastic composite reinforced with E-glass in order to assess their suitability for used as structural elements in hybrid concrete-FRP systems. Tests were conducted in both the longitudinal and transverse material directions in accordance with ASTM D3039 [38] for tensile properties, ASTM D6641 [40] for compressive properties, and ASTM D7078 [41] for in-plane shear properties using composite panels manufactured in-house at the ASCC. The longitudinal and transverse data collected was presented in Table 29 and Table 30 in chapter 3.

E-glass/Elium unidirectional composites were fabricated through vacuum infusion of the Elium 150 [20] liquid-resin system and E-LR 1208 [23] unidirectional E-glass. Coupon specimens were cut from these composite panels.

- The E-glass/Elium composite had a fiber volume fraction of 43.2 % compared to 40.0 % for E-glass/vinyl ester.
- The normalized longitudinal tensile modulus and longitudinal tensile strength of E-glass/Elium are 30.7-GPa and 686-MPa respectively compared to 33.37-GPa and 835-MPa for E-glass/vinyl ester.
- The E-glass/Elium normalized longitudinal compressive strength and modulus are 587-MPa and 31.3-GPa respectively compared to 539-MPa and 30.1-GPa for E-glass/vinyl ester.

- The E-glass/Elium in-plane shear strength and modulus are 42.0-MPa and 3.21-GPa respectively compared to 42.2-MPa and 3.50-GPa for E-glass/vinyl ester.

E-glass/PETg unidirectional composites were fabricated through automated stamp forming of IE 5842b [30] prepreg fiber-reinforced thermoplastic composite tapes. Coupon specimens were cut from these composite panels manufactured at the ASCC.

- The E-glass/PETg composite had a fiber volume fraction of 36.4 % compared to 40.0 % for E-glass/vinyl ester.
- The normalized longitudinal tensile modulus and longitudinal tensile strength of E-glass/PETg are 31.0-GPa and 685-MPa respectively compared to 33.37-GPa and 835-MPa for E-glass/vinyl ester.
- The E-glass/PETg normalized longitudinal compressive strength and modulus are 341-MPa and 25.8-GPa respectively compared to 539-MPa and 30.1-GPa for E-glass/vinyl ester.
- The E-glass/PETg in-plane shear strength and modulus are 28.8-MPa and 1.48-GPa respectively compared to 42.2-MPa and 3.50-GPa for E-glass/vinyl ester.

The following conclusions were made about the thermoplastic materials selected in chapter 2 from the mechanical testing conducted as a part of this study:

- Elium thermoplastic composites perform on par with the Derakane thermoset composites in strength and stiffness, showing that it is feasible to infuse a thermoplastic composite for structural applications.

- PETg composites performed on par with the Derakane composites in tensile properties, but were weaker in compression and in-plane shear, showing it is feasible to produce a thermoplastic composite through automated stamp forming for structural applications.
- PETg composites fabricated and tested in this study did show some limitations in compression and in-plane shear but performed well in tension.

The mechanical testing conducted during this study completed objective 2 of this thesis and supported objective 3 by providing critical thermoplastic composite material information for calculations and design.

5.1.2 Thermoplastic Shear Stud Feasibility

The shear connectors explored in this study were friction welded neat-resin PETg shear studs and vacuum infused Elium fiber-reinforced shear studs. These two systems were chosen for their particular advantages. The neat-resin PETg shear studs were chosen for their novel ability to be welded and the resulting potential for a highly automated and rapid process, which could be scaled up and applied in the field if desired. The Elium shear studs were chosen for the relative ease with which they could be fiber-reinforced and their shape tailored to fit a desired design. In addition, they were most suitable for use with the infusible Elium 150 resin-system.

Initial testing was done in TP stud shear to assess the strength and stiffness of friction welded shear studs with different welding settings during fabrication. This resulted in choosing 50-kPa for a welding pressure, 300-kPa for a forging pressure, 15-seconds for welding time, and a welding velocity of 10 m/s.

A mobile welding device mimicking the function of the Instron welding device was developed in order to weld shear studs to larger structures and to demonstrate a prototype of a system that could be implemented on a larger scale in the field. Four samples were made with the final iteration of the mobile welding unit using the parameters chosen from the lap shear study, which were tested in the custom fixture to verify the results were consistent with what was seen with the samples fabricated on the Instron welding device. These samples yielded an average shear strength per stud of 25.4-MPa and showed reasonable ductility during testing. This was lower than the 29.4-MPa seen with the Instron welded sample with the sample welding parameters but was considered reasonable for this feasibility study.

The next phase of shear stud testing implemented was concrete-TP and concrete-CFRTP stud testing which created samples based off AASHTO spacing guidelines for steel shear studs with multiple studs embedded in concrete to be tested in compression. This was done to assess stud performance in a situation more like what would be seen in a hybrid structure. Four types of samples were tested in the concrete-TP and concrete-CFRTP stud configuration.

The four concrete-TP 76.2-mm (3-inch) spacing samples achieved a mean peak load per stud of 2.90-kN, a mean strength per stud of 22.5-MPa, and a mean stiffness per stud of 8.93-N/mm. The three concrete-TP 152.4-mm (6-inch) spacing samples achieved a mean peak load per stud of 2.66-kN, a mean strength per stud of 20.6-MPa, and a mean stiffness per stud of 7.14-N/mm. All four E-glass/Elium concrete-CFRTP stud samples were tested but did not achieve the desired failure mode of shearing off the studs embedded in concrete. The CFRTP reinforcement plates to which the studs were infused were not sufficiently

strong to resist buckling/crushing above the concrete where the load was applied under the higher load conditions achieved by these samples. The results from the tests conducted until plate buckling/crushing occurred showed a mean peak load per stud of 16.8-kN, a mean strength per stud of 130-MPa, and a mean stiffness per stud of 26.5-N/mm for the samples with 4 total studs and 32.4-N/mm for the samples with 8 total studs.

Comparing the PETg concrete-TP and E-glass/Elium concrete-CFRTP stud samples, it is clear that the E-glass/Elium samples are significantly stronger and stiffer. The Elium concrete-CFRTP stud samples had an 82 % higher stress at peak load and were 70 % stiffer than the 76.2-mm (3-inch) spacing PETg concrete-CFRTP stud samples, which performed better than the 152.4-mm (6-inch) spacing ones. Many factors may be contributing to this result such as the fiber-reinforcement used in the infusion of the studs and the implementation of radii at the bottom of the samples giving them a larger area in the shear plane at the plate interface than the shaft of the stud alone.

The results of this study show that the thermoplastic shear studs did generate at least partial composite action between the CFRTP and concrete. The specimen design work based on spacings and shear stud sizes from AASHTO for the two shear studs systems chosen completed objective 3 of this thesis. The TP stud shear testing and concrete-TP/CFRTP stud tests completed objective 4 by demonstrating that the studs are capable of generating at least partial composite action.

5.2 Recommendations for Future Work

Based on the findings of this study, future work on thermoplastic concrete reinforcing materials with thermoplastic shear connectors and other structural applications is recommended as detailed in the following sub-sections.

5.2.1 Thermoplastic Composite Materials

This study worked with thermoplastic polymers on the more amorphous end of the engineering polymers spectrum as described in chapter 2. Now that manufacturing feasibility has been shown for the easier to form amorphous PETg material, future work should be done with more crystalline engineering grade thermoplastic polymers such as Nylon 6, 11, and polyethylene terephthalate (PET).

TenCate performance composites offers UD prepreg composite tapes for both Nylon 6 [81] and PET [82]. These materials could be explored for use as structural reinforcement based on their higher heat deflection temperatures, increased chemical and solvent resistance, and acceptable overall strength properties. However, these thermoplastics are semi-crystalline and could be more difficult to form than an amorphous polymer.

For composite structural design, not only in-plane mechanical properties are of interest, out-of-plane properties of these materials are also of interest in the future for situations when a shear connector or other part of the system could induce out-of-plane loading on the composite. In addition, durability and fatigue of structural materials is essential for designing real world systems, which often have design lifetimes of upwards of 100 years.

The characterization of new materials, durability testing, and fatigue testing would enhance the community's knowledge of these materials, open up new opportunities for design, and further the structural applications of thermoplastic materials. In addition, exploration of the formability of semi-crystalline polymers is of interest to determine their ability to be used with certain thermoplastic manufacturing processes such as automated stamp forming.

5.2.2 Thermoplastic Composite Shear Connectors

Based on the work done in this study three new thermoplastic shear connector options are recommended for exploration.

1. Friction welded shear studs could be reinforced further by screwing a mechanical fastener down from the top or up from the bottom through the CFRTP reinforcement. This has the potential to increase the stud strength and stiffness while still being automatable. Screwing a fastener in from the bottom has the potential to engage both the welded bond on the shear stud but also the fastener in bearing with the CFRTP reinforcement plate.
2. Fiber-reinforced shear studs infused with Elixir could be created in mold to include radii at the top and bottom to provide pull out resistance and assist in shear transfer at the interface between the stud and CFRTP plate respectively then friction welded to explore the effect of fiber-reinforcement on friction welded shear studs.
3. Additional methods could be explored to decrease the fabrication time of infusible thermoplastic shear studs such as optimizing the co-infusion process, exploring infusing the studs individually, or investigating resin transfer molding (RTM).

4. Fiber-reinforced stock material in simple or off-the-shelf shapes could be stamp formed onto CFRTP plates and then cut on a CNC machine into a desired shape to lock with concrete and provide shear transfer or pull out resistance depending on the design needs. The ability for fibers to intermingle would generate higher strengths for this application.
5. A mechanical fastener could be fixed through the CFRTP to use the bearing strength of the composite to increase the capacity of the shear connection beyond a welded connection. This would also require, investigating the bearing strength of thermoplastic composite materials.

Additional work could also be conducted to explore the effect of fiber-reinforcement in thermoplastic shear studs. A finite element analysis would contribute to the understanding of stress concentrations at the interface between the stud and the reinforcement, could help size potential radii on the top and bottom, and assess shaft diameter sizes for different applications. Part of this additional work could include testing of the redesigned E-glass/Elium concrete-CFRTP stud specimen discussed in chapter 4.

5.2.3 Small-Scale Beam Testing

This study showed that the stepping stones necessary for the construction of a simple small-scale thermoplastic composite-concrete hybrid structure are feasible. Future work using the findings of this study should include the use of an IE 5842b CFRTP flat plate using the beam-layup discussed with neat-resin thermoplastic shear studs to reinforce the tension face of a prismatic concrete beam. The beam as shown in Figure 114 would be constructed with flat composite reinforcement on the bottom face of the beam to reinforce the structure

in tension, replacing normal steel tension reinforcing. The composite tension reinforcement would be mechanically attached to the concrete with the friction welded neat-resin PETg shear connectors explored in this study that mimic shear studs used in steel-concrete composite beams.

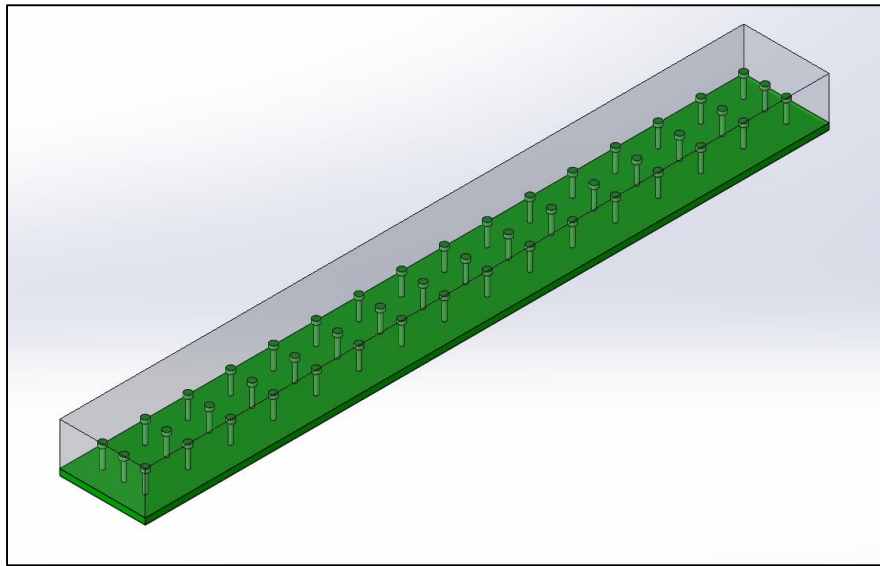


Figure 114: Proposed Beam Specimen Concept Design

Beam specimens made in this configuration could use the two spacing options of 76.2-mm (3-inches) and 152.4-mm (6-inches) center-to-center along the span discussed in chapter 4 based on the AASHTO guidelines for shear connectors.

5.2.4 Develop Optimal Cross-Sections

Flat plates do not take full advantage of thermoforming possibilities and techniques or the full potential of the thermoplastic composites being used. Three-dimensional shapes could be developed in the future, such as a double sheet pile or U-shaped cross-section, in order to take advantage of geometric shapes to carry larger loads and add the possibility of stay-in-place formwork that could carry wet concrete loads. These types of shapes could be

developed using the stamp forming process in a mold in order to explore their feasibility and capacity, then, if desired, further developed to use a pultrusion process in order to make longer continuous cross-sections which could be used for bridges, decking, columns and retaining walls.

5.2.5 Explore Other Structural Applications of Thermoplastics

Beyond CFRTP tension face reinforcement and the development of optimal cross-sections already discussed, other structural applications of thermoplastics may be of interest in the future. Structural elements such as rebar and stirrups are currently made of steel, which is effective but has many disadvantages such as susceptibility to corrosion and difficulty to form into shapes at the construction site. Fiber-reinforced thermoplastic rod could be fabricated in long straight pieces, which would be a highly automated process producing something that is space efficient to ship and store. These straight pieces could be made with surfaces designed to transfer forces between the thermoplastic and concrete like what is currently done with rebar, however thermoplastic is corrosion resistant and formable. Then in the field using heat, these could be bent into various shapes to fit the desired application such as rebar and stirrups. If feasible, this fiber-reinforced thermoplastic rod could be a versatile option for concrete reinforcing.

REFERENCES

- [1] "2017 Infrastructure Report Card: A Comprehensive Assessment of America's Infrastructure," American Society of Civil Engineers (ASCE), Reston, Virginia, 2017.
- [2] K. Warren, "Resistance Welding of Thermoplastic Composites," University of Maine, Orono, ME, 2012.
- [3] E. R. Larson, *Thermoplastic Material Selection: A Practical Guide*, Waltham, MA: Elsevier, 2015.
- [4] ACMA, "compositeslab Corrosion Resistance," ACMA, 2016. [Online]. Available: compositeslab.com/benefits-of-composites/corrosion-resistance/.
- [5] RTP Company, "Chemical and Environmental Resistance of Thermoplastics," RTP Company, 2016. [Online]. Available: www.rtpcompany.com/technical-info/chemical-resistance/.
- [6] British Plastics Federation, "Polymer Thermoplastics," *Plastipedia.co.uk*, 2018. [Online]. Available: <http://www.bpf.co.uk/plastipedia/polymers/polymer-thermoplastics.aspx>.
- [7] I. M. Daniel and O. Ishai, *Engineering Mechanics of Composite Materials* (second edition), Oxford New York: Oxford University Press, 2006.
- [8] E. Akca and A. Gursel, "A Review on the Matrix Toughness of Thermoplastic Materials," *Periodicals of Engineering and Natural Sciences*, vol. 3, no. 2, 2015.
- [9] Curbell Plastics Inc., "Material Selection Guide," Curbell Plastics Inc., 2016.
- [10] U. K. Vaidya and K. K. Chawla, "Processing of fibre reinforced thermoplastic composites," *International Materials Reviews*, vol. 53, no. 4, pp. 185-218, 2008.
- [11] Crain Communications, Inc., "Current Resin Pricing," *Plastics News*, [Online]. Available: <http://www.plasticsnews.com/resin/commodity-thermoplastics/current-pricing>.
- [12] Endura Plastics, Inc., "Material Selection Guide," Endura Plastics, Inc., 2012. [Online]. Available: <http://endura.com/material-selection-guide/>.

- [13] Tangram, "Tangram Periodic Table Issue 8," Tangram, 2010. [Online].
- [14] Globe Composite Solutions, Ltd., "What are thermoplastics?," Globe, 2018. [Online]. Available: www.globecomposite.com/thermoplastics.
- [15] RecycledPlastic.com, "Thermoplastics vs. Thermosetting Plastics," 2014. [Online]. Available: www.recycledplastic.com/index.html%3Fp=10288.html.
- [16] D. A. Steenkamer and J. L. Sullivan, "On the recyclability of cyclic thermoplastic composite material," *Elsevier Composites Par B*, pp. 745-752, 1998.
- [17] "Arkema Elium® resins for composites," Arkema, [Online]. Available: <https://www.arkema.com/en/products/product-finder/range-viewer/Elium-resins-for-composites/>.
- [18] Arkema, "Elium All grades Rev 2.5 SDS," 2016.
- [19] Arkema, "Luperox AFR40 SDS," 2015.
- [20] Arkema, "Elium 150 Tech Data Sheet GRP_20_05_2015," 2015.
- [21] J. Sloan, "Styrene: Issues and implications," *CompositesWorld*, 12 2012. [Online]. Available: <https://www.compositesworld.com/articles/styrene-issues-and-implications>.
- [22] Arkema Group, "YouTube: Elium®, the resin which makes composites recyclable," 1 June 2017. [Online]. Available: <https://www.youtube.com/watch?v=wYbBiYr1yQs>.
- [23] Vector Ply Corporation, "E-LR 1208," Phenix City.
- [24] Polystrand (PolyOne), "Polystrand Our Products," 2018. [Online]. Available: <http://www.polystrand.com/products/products.html>.
- [25] TenCate, "TenCate Advanced Composites Thermoplastic UD Tapes," 2017. [Online]. Available: <https://www.tencatecomposites.com/products/thermoplastic/ud-tapes-and-prepregs>.
- [26] SGL Group, "SGL Group Thermoplastic composite materials made from carbon and glass fibers," [Online]. Available: http://www.sglgroup.com/cms/international/products/product-groups/cm/thermoplastic-composite-materials/index.html?__locale=en.

- [27] Celanese, "Celanese Celstran CFT-TP Tapes," 2013. [Online]. Available: <http://info.celanese.com/celstran-cfr-tp-tapes-new?elq=00000000000000000000000000000000&elqCampaignId=>.
- [28] VectorSystems, "VectorSystems Flexile™ Thermoplastic Prepreg Products," 2018. [Online]. Available: <http://www.vectorams.com/thermoplastic-prepreg-products/>.
- [29] Tangram Technology Ltd. 2006, "Periodic Table of Polymers - Issue 5," 02 2008. [Online]. Available: <http://www.tangram.co.uk/TI-Polymer-Periodic%20Table.html>.
- [30] PolyOne Polystrand, "Polystrand IE 5842," 2017.
- [31] R. Lopez-Anido and M. D. Wehrle, "Opportunities to Enhance Thermoplastic Composite Material Properties," Advanced Structures and Composites Center, Orono, ME, 2017.
- [32] Simplify 3D, "Simplify 3D Filament Properties Table," 2018. [Online]. Available: <https://www.simplify3d.com/support/materials-guide/properties-table/>.
- [33] Ashland Inc, "Derakane 610 C-150 Epoxy Vinyl Ester Resin," 2016.
- [34] ASTM, "Standard Test Methods for Density and Specific Gravity (Relative Density) or Plastics by Displacement," ASTM Committee D20, 2013.
- [35] Advanced Structures and Composites Center Consortium for Manufacturing Innovation in Structural Thermoplastics, November 2017. [Online]. Available: <https://composites.umaine.edu/cmist/>.
- [36] Sheffield Plastics Inc., "VIVAK PETg Sheet Product Data," Bayer Material Science Company, Sheffield, MA, 2003.
- [37] E. J. Barbero, Introduction to Composite Materials Design 2nd Edition, Parkway: CRC Press Taylor & Francis Group, 2011.
- [38] ASTM, D3039/D3039M-14 Standard Test Method for Tensile Properties of Polymer Matrix Composite Materials, West Conshohocken, PA: ASTM International, 2016.
- [39] M. Demkowicz, "Environmental Durability of Hybrid Braided Polymer Matrix Composites for Infrastructure Applications," University of Maine, Orono, 2011.

- [40] ASTM, D6641/D6641M-14 Standard Test Method For Compressive Properties of Polymer Matrix Composite Materials Using a Combined Loading Compression (CLC) Test Fixture, West Conshohocken, PA: ASTM International, 2016.
- [41] ASTM, D7078/D7078M-12 Standard Test Method for Shear Properties of Composite Materials by V-Notched Rail Shear Method, West Conshohocken, PA: ASTM International, 2016.
- [42] ASTM, *D792-13 Standard Test Method for Density and Specific Gravity (Relative Density) of Plastics by Displacement*, West Conshohocken, PA: ASTM International, 2013.
- [43] ASTM, *D3171-15 Standard Test Methods for Constituent Content of Composite Materials*, West Conshohocken, PA: ASTM International, 2015.
- [44] E. M. Mikhail, J. S. Bethel and J. C. McGlone, "Introduction to Modern Photogrammetry," *John Wiley & Sons*, 2001.
- [45] Z. L. Kahn-Jetter and T. C. Chu, "Three-Dimensional Displacement Measurements Using Digital Image Correlation and Photogrammic Analysis," *Experimental Mechanics*, vol. 30, no. 1, pp. 10-16, 1990.
- [46] P. F. Luo, Y. J. Chao, M. A. Sutton and W. H. Peters III, "Accurate Measurement of Three-Dimensional Deformations in Deformable and Rigid Bodies Using Computer Vision," *Experimental Mechanics*, vol. 33, no. 2, 1993.
- [47] M. A. Sutton, J. J. Ortu and H. Schreier, "Image Correlation for Shape, Motion and Deformation Measurements: Basic Concepts, Theory and Application," *Springer Science & Business Media, LLC*, 2009.
- [48] A. software, "GOM Optimal Measuring Techniques," 2011.
- [49] K. Mori T. and Tanaka, "Average Stress in a matrix and average elastic energy of materials with misfitting inclusions," *Acta Metallurgica*, vol. 21, pp. 571-574, 1973.
- [50] T. Chen, G. J. Dvorak and Y. Benveniste, "Mori-Tanaka Estimates of overall elastic moduli of certain composite materials," *Journal of Applied Mechanics*, vol. 59, pp. 539-546, 1992.

- [51] S. Vel, *MEE 450 Mechanics of Composites Materials: Mori-Tanaka method for the effective properties of unidirectional fiber reinforced composites*, Orono: University of Maine MEE 450 Lecture Handout, 2016.
- [52] SteelConstruction.info, "SteelConstruction.info The Free encyclopedia for UK Steel construction information: Welding," [Online]. Available: https://www.steelconstruction.info/Welding#Drawn_arc_stud_welding.2C_process_783.
- [53] SteelConstruction.info, "SteelConstruction.info The free encyclopedia for UK steel construction information: Composite construction," [Online]. Available: https://www.steelconstruction.info/Composite_construction.
- [54] Stud Welding & Fasteners, Inc., "How Stud Welding is Used to Secure Bridges," 2018. [Online]. Available: <http://www.studweldfast.com/how-stud-welding-is-used-to-secure-bridges/>.
- [55] H. Breton, "Mechanically Fastened Fiber-Reinforced Polymer (FRP) Flexural Retrofit Systems for Reinforced Concrete Flat-Slab Bridges," University of Maine, Orono, ME, 2013.
- [56] P. Saravanakumar, N. R. Chitra and R. Murugesan, "Comparative Experimental Investigation on Behaviour and Strength of RC Frames Strengthened and Retrofitted with GFRP Composites," *KSCCE Journal of Civil Engineering*, 2014.
- [57] H. Saadatmanesh and M. R. Ehsani, "RC Beams Strengthened with GFRP Plates I: Experimental Study," *Journal of Structural Engineering*, vol. 117, no. 11, 1991.
- [58] W. An, H. Saadatmanesh and M. R. Ehsani, "RC Beams Strengthened with FRP Plates II: Analysis and Parametric Study," *Journal of Structural Engineering*, vol. 117, no. 11, 1991.
- [59] U. Meier, "Strengthening of Structures Using Carbon Fibre/Epoxy Composites," *Construction and Building Materials (Elsevier)*, vol. 9, no. 6, pp. 341-351, 1996.
- [60] M. J. Chajes, T. A. Thomson Jr, T. F. Januszka and W. W. Finch Jr, "Flexural Strengthening of Concrete Beams Using Externally Bonded Composite Materials," *Construction and Building Materials*, vol. 8, no. 3, 1994.

- [61] G.-M. Chen, "Behaviour and Strength of RC Beams Shear-Strengthened with Externally Bonded FRP Reinforcement," The Hong Kong Polytechnic University, 2010.
- [62] P. Gao, X. Gu and A. S. Mosallam, "Flexural behavior of preloaded reinforced concrete beams strengthened by prestressed CFRP laminates," *Composite Structures (Elsevier)*, vol. 157, pp. 33-50, 2016.
- [63] ACI Committee 440, "Guide for the design and construction of externally bonded FRP systems for strengthening concrete structures," Farmington Hills, MI, American Concrete Institute (ACI), 2008.
- [64] AASHTO, "Guide specifications for design of bonded FRP systems for repair and strengthening of concrete bridge elements," Washington DC, USA, American Association of State Highway and Transportation Officials, 2012.
- [65] H. B. Loring and W. G. Davids, "Mechanically Fastened Hybrid Composite Strips for Flexural Strengthening of Concrete Beams," *Construction and Building Materials (Elsevier)*, 2014.
- [66] L. C. Bank and D. Arora, "Analysis of RC Beams Strengthened with Mechanically Fastened FRP (MF-FRP) Strips," *Composite Structures (Elsevier)*, vol. 79, pp. 180-191, 2006.
- [67] J. A. Martin and A. J. Lamanna, "Performance of Mechanically Fastened FRP Strengthened Concrete Beams in Flexure," *Journal of Composites for Construction (ASCE)*, vol. 12, no. 3, pp. 257-265, 2008.
- [68] Strongwell Corporation, "Strongwell SafStrip," [Online]. Available: <http://www.strongwell.com/news/safstrip-introduced/>. [Accessed 2018].
- [69] J. H. Lee, M. M. Lopez and C. E. Bakis, "Slip Effects in Reinforced Concrete Beams with Mechanically Fastened FRP Strip," *Cement and Concrete Composites*, vol. 31, pp. 496-504, 2009.
- [70] A. Yousefpour, M. Hojjati and J.-P. Immarigeon, "Fusion bonding/welding of thermoplastic composites," *Composite Materials*, vol. 17, no. 4, pp. 303-341, 2004.
- [71] M. Troughton, Handbook of Plastics Joining, NY, USA: William Andrew Inc., 2008.

- [72] C. Ageorges and L. Ye, *Fusion Bonding of Polymer Composites: From Basic Mechanisms to Process Optimisation*, London: Springer-Verlag, 2002.
- [73] MatWeb, "Eastman Eastar GN071 Natural PETg Copolyester," Eastman, [Online]. Available:
<http://www.matweb.com/search/DataSheet.aspx?MatGUID=9aec2bc30384b5a96af1263ba5a27d7&ckck=1>.
- [74] D&M Plastics Inc. PlasticsMoulding, "All About Plastic Moulding: Polyethylene," [Online]. Available: <http://www.plasticmoulding.ca/polymers/polyethylene.htm>.
- [75] D&M Plastics Inc. PlasticsMoulding, "All About Plastic Moulding: Polypropylene," [Online]. Available:
<http://www.plasticmoulding.ca/polymers/polypropylene.htm>.
- [76] D&M Plastics Inc. PlasticsMoulding, "All About Plastic Moulding Polyvinyl Chloride (PVC)," [Online]. Available:
<http://www.plasticmoulding.ca/polymers/pvc.htm>.
- [77] AASHTO, "AASHTO LRFD Bridge Design Specifications," AASHTO, Washington, D.C., 2012.
- [78] Vector Ply, "Vector Ply E-BX 2400," Vector Ply Corporation, Phenix City, 2015.
- [79] "G-10 Fiberglass Epoxy Laminate Sheet," [Online]. Available:
<http://www.matweb.com/search/DataSheet.aspx?MatGUID=8337b2d050d44da1b8a9a5e61b0d5f85&ckck=1>.
- [80] S. F. Brena and G. N. McGuirk, "Advances on the Behavior Characterization of FRP-Anchored Carbon Fiber-Reinforced Polymer (CFRP) Sheets Used to Strengthen Concrete Elements," *International Journal of Concrete Structures and Materials*, vol. 7, no. 1, pp. 3-16, 2013.
- [81] TenCate Cetex TC910 Nylon 6 Thermoplastic Composite, "TenCate," TenCate, Camarillo.
- [82] TenCate, "TenCate Cetex TC940 PET Thermoplastic Composite," TenCate, Camarillo.

APPENDIX A: CALIBRATION INFORMATION

Equipment at the ASCC used during this study was regularly calibrated; relevant calibration information for major testing equipment used is included in Table 48. Calibration information is given for the test frames used, load cells are also calibrated with the test frame.

Table 48: Major Testing Equipment Calibration Information

Equipment ID	Description	Relevant Calibration Dates
MTL #1 (AS 107)	22.5 kip Instron Servo-Hydraulic Actuator	June 15, 2016 June 15, 2017
MTL #2 (AS 108)	22.5 kip Instron Servo-Hydraulic Actuator	June 15, 2016 June 15, 2017
MTL #3 (AS 1064)	22.5 kip Instron Servo-Hydraulic Actuator	June 14, 2016 June 15, 2017 June 30, 2018
MTL #4 (AS 511)	5-kip Instron Servo-Hydraulic Actuator	June 30, 2016 June 20, 2017
MTL 55-kip (AS 2199)	55 kipP Instron Servo-Hydraulic Actuator	December 6, 2016
MTL 55-kip LC	55 kip Instron Load Cell	December 6, 2016
2-kip Load Cell (AS 511)	2-kip Instron Load Cell	June 15, 2017

Note: Instron test frame annual calibration includes the LVDT for position control and the load cell

APPENDIX B: TECHNICAL DATA SHEETS

Appendix B contains the manufacturers materials data sheets for the materials used in this milestone. A brief outline is provided in the list below in the order they are given here.

- B1: Polystrand PETg Online Reference
- B2: Polystrand IE 5842 Technical Data Sheet
- B3: Arkema Elium 150 GRP Technical Data Sheet [20]
- B4: Vector Ply E-LR 1208 Unidirectional E-glass Technical Data Sheet [23]
- B5: Vector Ply E-BX 2400 Stitched Double Bias E-glass Technical Data Sheet [78]



Polystrand™ IE 5842

Continuous glass-reinforced thermoplastic PETG composite

Key Characteristics

Product description

Polystrand™ IE 5842 is a PETG-based thermoplastic unidirectional tape, which balances strength and toughness with excellent adhesive properties. Applications include structural components and reinforcement for wood, metal, and polymer molded or thermoformed components. The use of PETG resin imparts excellent mechanical properties, and good chemical and solvent resistance. Unidirectional tapes are available in rolls 25" wide. Custom slit widths and finished stampings are also available. Multi-ply laminates are available with plies arranged in 0 or 90 degree orientations, with maximum roll width of 125".

Technical Properties of Unidirectional Tape

Typical Properties

PROPERTY	TEST METHOD	UNITS	DATA
Glass Content	ASTM D3647	wt%	58
Areal weight	--	oz/yd ² (g/m ²)	12.0 (405)
Thickness	--	In (mm)	0.012 (0.3)
Flexural modulus	ASTM D790	MPsi (GPa)	4.18 (29)
Flexural Strength	ASTM D790	Ksi (MPa)	87 (602)
Longitudinal Tensile Modulus	ASTM D3039	MPsi (GPa)	4.14 (28.5)
Longitudinal Tensile Strength	ASTM D3039	Ksi (MPa)	82.8 (571)
In-Plane Poisson's Ratio	ASTM D3039	--	0.27
Transverse Tensile Modulus	ASTM D3039	MPsi (GPa)	0.52 (3.6)
Transverse Tensile Strength	ASTM D3039	Ksi (MPa)	1.5 (10.0)
Longitudinal Compressive Modulus	ASTM D6641	MPsi (GPa)	0.71 (4.9)
Longitudinal Compressive Strength	ASTM D6641	Ksi (MPa)	29.5 (197)
Transverse Compressive Modulus	ASTM D6641	MPsi (GPa)	0.26 (1.8)
Transverse Compressive Strength	ASTM D6641	Ksi (MPa)	5.5 (38)
In-Plane Shear Modulus	ASTM D7078	MPsi (GPa)	0.21 (1.5)
In-Plane Shear Strength	ASTM D7078	ksi (MPa)	3.0 (21)
Transverse Shear Modulus	ASTM D7078	MPsi (GPa)	0.17 (1.2)
Transverse Shear Strength	ASTM D7078	ksi (MPa)	6.7 (46)

Notes

NOTE: The data listed herein reflect typical sheet properties. They are the latest available at the time of publication and are reliable to the best knowledge of PolyOne. The properties are listed solely to give general guidance and are not to be construed as a warranty or representation for of this information or the safety and suitability of our products, either alone or in combination with other products. Users are advised to make their own test to determine the safety and suitability of each such product or product combination for their own purposes. We sell the products without

warranty. Buyers and users assume all responsibility and liability for loss or damage arising from the handling and use of our products, whether used alone or in combination with other products.

Processing

Polystrand™ IE 5842 process temperature is 420-470F (215-243C). Contact PolyOne for detailed set-up and processing guidelines.

Please contact PolyOne for data relating to a specific application or equipment.

Availability

Polystrand™ IE 5842 roll or laminated sheet is available in the US, EU and Asia Pacific regions.

CONTACT INFORMATION

For additional information, please contact PolyOne Advanced Composites at +1.866.POLYONE (+1.866.765.9663) or visit our web site at www.polyone.com.

Copyright © 2017, PolyOne Corporation. PolyOne makes no representations, guarantees, or warranties of any kind with respect to the information contained in this document about its accuracy, suitability for particular applications, or the results obtained or obtainable using the information. Some of the information arises from laboratory work with small-scale equipment which may not provide a reliable indication of performance or properties obtained or obtainable on larger-scale equipment. Values reported as "typical" or stated without a range do not state minimum or maximum properties; consult your sales representative for property ranges and min/max specifications. Processing conditions can cause material properties to shift from the values stated in the information. PolyOne makes no warranties or guarantees respecting suitability of either PolyOne's products or the information for your process or end-use application. You have the responsibility to conduct full-scale end-product performance testing to determine suitability in your application, and you assume all risk and liability arising from your use of the information and/or use or handling of any product. POLYONE MAKES NO WARRANTIES, EXPRESS OR IMPLIED, INCLUDING, BUT NOT LIMITED TO, IMPLIED WARRANTIES OF MERCHANTABILITY AND FITNESS FOR A PARTICULAR PURPOSE, either with respect to the information or products reflected by the information. This data sheet shall NOT operate as permission, recommendation, or inducement to practice any patented invention without permission of the patent owner.

ELIUM® 150

Technical Datasheet

LIQUID THERMOPLASTIC RESIN FOR GLASS-REINFORCED COMPOSITE

The **ELIUM® 150** is a low viscosity liquid, thermoplastic resin for **infusion** and **RTM** processes. Through the use of the same low pressure processes and equipments used today to produce thermoset composite parts, these formulations lead to the production of thermoplastic composites reinforced by continuous glass, carbon or natural fibers. The resulting thermoplastic composite parts show mechanical properties similar to those of parts made of epoxy resins while presenting the major advantages of being post-thermoformable and recyclable and of offering new possibilities for composite/composite or composite/metal assemblies.

APPLICATIONS AND USE	<p>ELIUM® 150 resin can be used to produce aesthetic or structural composites reinforced by glass, carbon, or other continuous fibers. This resin can be used for RTM (Resin Transfer Molding), VARI (Vacuum Assisted Resin Infusion) and other closed mold processes.</p>																
TYPICAL LIQUID RESIN PROPERTIES	<table border="1"> <tr> <th colspan="4">Property⁽¹⁾ at 25 °C</th> </tr> <tr> <td>Viscosity Brookfield LVF #2, 60 rpm</td> <td colspan="3">100 mPa.s</td> </tr> </table> <p>(1) Properties are typical values based on material tested in our laboratories. Typical values should not be construed as a guaranteed analysis of any specific lot or as specification items.</p>	Property ⁽¹⁾ at 25 °C				Viscosity Brookfield LVF #2, 60 rpm	100 mPa.s										
Property ⁽¹⁾ at 25 °C																	
Viscosity Brookfield LVF #2, 60 rpm	100 mPa.s																
TYPICAL CURING CHARACTERISTICS	<p>The ELIUM® resins are 2K based formulations that undergo radical polymerization to produce thermoplastic composite matrices. The polymerization is initiated by Peroxide compounds (Luperox®). Typical open time and peak time with 3% Luperox® EZ-FLO are:</p> <table border="1"> <thead> <tr> <th>Reactivity⁽²⁾ (200 grams)</th> <th>Infusion open time</th> <th>Injection open time</th> <th>Peak time</th> </tr> </thead> <tbody> <tr> <td>15 °C</td> <td>30 min.</td> <td>35 min.</td> <td>50 min.</td> </tr> <tr> <td>20 °C</td> <td>25 min.</td> <td>30 min.</td> <td>40 min.</td> </tr> <tr> <td>25 °C</td> <td>20 min.</td> <td>25 min.</td> <td>33 min.</td> </tr> </tbody> </table> <p>(2) If a lower reactivity infusion resin is needed, we recommend to use the Elium® 180. Please contact your Arkema representative for more information.</p> <p>The demolding can take place 5-10 minutes after reaching the peak exotherm. Open time is the amount of time during which the viscosity of the resin is low enough to inject the resin. Temperature and peroxide ratio will affect the open and peak times. The recommended peroxide ratio is from 1,5% (slow reactivity) to 3% (higher reactivity). Out of this range the resin will not polymerize properly. Room temperature polymerization leads to high conversion rate, so post-curing is generally not needed. If maximum mechanical properties are desired, post-curing at 80 °C for 4 hours is beneficial. Vinyl ester or epoxy molds with a glass transition of 100-120 °C are recommended.</p>	Reactivity ⁽²⁾ (200 grams)	Infusion open time	Injection open time	Peak time	15 °C	30 min.	35 min.	50 min.	20 °C	25 min.	30 min.	40 min.	25 °C	20 min.	25 min.	33 min.
Reactivity ⁽²⁾ (200 grams)	Infusion open time	Injection open time	Peak time														
15 °C	30 min.	35 min.	50 min.														
20 °C	25 min.	30 min.	40 min.														
25 °C	20 min.	25 min.	33 min.														

ELIUM®
BY ARKEMA

ELIUM® 150

INFUSION PROCESSING	<p>Processing by infusion can be carried out at a vacuum ranging from 100 mbar to 500 mbar, due to the good fiber impregnation behavior of the resin. Before introducing the peroxide into the resin, firmly close the container and shake vigorously. If using Luperox® AFR40, skip the shaking step. Resin and peroxide must be mixed carefully for two minutes, to reach a homogeneous color and no particles, especially at the bottom and on the sides of the mixing pot. It is recommended to position a perforated plastic film or a cap on top of the pot during infusion, to reduce the smell in the workshop and prevent curing inhibition caused by air. The low viscosity of Elium® 150 allows a quick and complete fiber wetting with infusion distance up to 500 mm. Processing by infusion can be carried out at a vacuum pressure ranging from 100 mbar to 500 mbar, due to the good fiber impregnation behavior of the resin. The flow mesh length and break length between the resin inlet(s) and vacuum tube(s) have to be dimensioned to allow a full impregnation of the laminate in 10-15 minutes at 25 °C, with an additional 5-10 cm of break material before the vacuum tube, to avoid resin entering into the vacuum tubes. Following impregnation speeds can be used to dimension flow mesh and brake lengths:</p> <ul style="list-style-type: none"> - resin impregnation speed into a laminate with flow mesh: 10 cm/min on average (15 cm for the first minute) - resin impregnation speed into a laminate without flow mesh: 1 cm/min in average <p>The remaining resin in the pot will generally foaming and change color during the peak exotherm.</p> <p>If this resin is be used in combination with a pump system (for mixing and/or infusing), the machine has to be cleaned daily with acetone for the resin circuit and with water for the peroxide circuit.</p>																																																												
INJECTION PROCESSING	<p>Light RTM processing of Elium® 150 can be done under similar conditions than standard polyester resins. Specific injection machines are required to pump the Luperox® EZ FLO, so standard machines designed for MEKP should not be used. Contact your representative to have the details on the machine type. The machine has to be cleaned daily with acetone for the resin circuit and with water for the peroxide circuit.</p>																																																												
TYPICAL MECHANICAL PROPERTIES	<table border="1" style="width: 100%; border-collapse: collapse;"> <thead> <tr style="background-color: #00AEEF; color: white;"> <th>Properties of a 4 mm unfilled resin casting</th> <th>Value</th> <th>ISO method</th> </tr> </thead> <tbody> <tr><td>Rockwell Hardness (M)</td><td>100</td><td>2039</td></tr> <tr><td>Shore D Hardness</td><td>85-90</td><td>868</td></tr> <tr><td>Tensile Strength</td><td>76 MPa</td><td>527</td></tr> <tr><td>Tensile Modulus</td><td>3.300 MPa</td><td>527</td></tr> <tr><td>Tensile Deformation</td><td>6 %</td><td>527</td></tr> <tr><td>Flexural Strength</td><td>130 MPa</td><td>178</td></tr> <tr><td>Flexural Modulus</td><td>3.250 MPa</td><td>178</td></tr> <tr><td>Compression Strength</td><td>130 MPa</td><td>684</td></tr> <tr><td>Specific Gravity</td><td>1,19</td><td>1183</td></tr> <tr><td>Heat Deflection Temperature</td><td>109 °C</td><td>75/A</td></tr> <tr><td>Maximum Continuous Temperature Service</td><td>85 °C</td><td>-</td></tr> <tr><td>Water Uptake (8 days)</td><td>0,5%</td><td>62</td></tr> <tr><td>Coefficient of Linear Expansion</td><td>0,065 mm/m/°C</td><td>2155-1</td></tr> <tr><td>Fracture Toughness Stress Intensity, K_{IC}</td><td>1,2 MPa.m^{0,5}</td><td>13586</td></tr> </tbody> </table> <table border="1" style="width: 100%; border-collapse: collapse;"> <thead> <tr style="background-color: #00AEEF; color: white;"> <th>Properties of a composite aesthetic part⁽³⁾</th> <th>Value</th> <th>ISO method</th> </tr> </thead> <tbody> <tr><td>Flexural Strength</td><td>270 MPa</td><td>14125</td></tr> <tr><td>Flexural Modulus</td><td>9.600 MPa</td><td>14125</td></tr> <tr><td>In-plane Shear Modulus</td><td>2.500 MPa</td><td>14129</td></tr> </tbody> </table> <table border="1" style="width: 100%; border-collapse: collapse;"> <thead> <tr style="background-color: #00AEEF; color: white;"> <th>Properties of a composite structural part⁽⁴⁾</th> <th>Value</th> <th>ISO method</th> </tr> </thead> </table>	Properties of a 4 mm unfilled resin casting	Value	ISO method	Rockwell Hardness (M)	100	2039	Shore D Hardness	85-90	868	Tensile Strength	76 MPa	527	Tensile Modulus	3.300 MPa	527	Tensile Deformation	6 %	527	Flexural Strength	130 MPa	178	Flexural Modulus	3.250 MPa	178	Compression Strength	130 MPa	684	Specific Gravity	1,19	1183	Heat Deflection Temperature	109 °C	75/A	Maximum Continuous Temperature Service	85 °C	-	Water Uptake (8 days)	0,5%	62	Coefficient of Linear Expansion	0,065 mm/m/°C	2155-1	Fracture Toughness Stress Intensity, K _{IC}	1,2 MPa.m ^{0,5}	13586	Properties of a composite aesthetic part ⁽³⁾	Value	ISO method	Flexural Strength	270 MPa	14125	Flexural Modulus	9.600 MPa	14125	In-plane Shear Modulus	2.500 MPa	14129	Properties of a composite structural part ⁽⁴⁾	Value	ISO method
Properties of a 4 mm unfilled resin casting	Value	ISO method																																																											
Rockwell Hardness (M)	100	2039																																																											
Shore D Hardness	85-90	868																																																											
Tensile Strength	76 MPa	527																																																											
Tensile Modulus	3.300 MPa	527																																																											
Tensile Deformation	6 %	527																																																											
Flexural Strength	130 MPa	178																																																											
Flexural Modulus	3.250 MPa	178																																																											
Compression Strength	130 MPa	684																																																											
Specific Gravity	1,19	1183																																																											
Heat Deflection Temperature	109 °C	75/A																																																											
Maximum Continuous Temperature Service	85 °C	-																																																											
Water Uptake (8 days)	0,5%	62																																																											
Coefficient of Linear Expansion	0,065 mm/m/°C	2155-1																																																											
Fracture Toughness Stress Intensity, K _{IC}	1,2 MPa.m ^{0,5}	13586																																																											
Properties of a composite aesthetic part ⁽³⁾	Value	ISO method																																																											
Flexural Strength	270 MPa	14125																																																											
Flexural Modulus	9.600 MPa	14125																																																											
In-plane Shear Modulus	2.500 MPa	14129																																																											
Properties of a composite structural part ⁽⁴⁾	Value	ISO method																																																											

Arkema
 89 boulevard National
 F-92257 La Garenne-Colombes Cedex – France
 Tel.: +33 (0)1 78 66 23 00
 Fax: +33 (0)1 78 66 23 97
 elium-composites.com

ARKEMA
 NEWARK VILMORIN

ELIUM® 150

	Tensile Strength	557 MPa	527	
	Tensile Modulus	27 GPa	527	
	Flexural Strength	700 MPa	14125	
	Flexural Modulus	27 GPa	14125	
	Compressive Strength	347 MPa	14126	
	Compressive Modulus	28 GPa	14126	
	In-plane Shear Modulus	5.600 MPa	14129	
	Charpy Impact Strength (un-notched)	206 kJ/m ²	179/2D	
	Properties of a UD composite part⁽⁵⁾		Value	ISO method
	Tensile Strength 0°	1.005 MPa	527	
	Tensile Modulus 0°	47 GPa	527	
	Tensile Strength 90°	53 MPa	527	
	Tensile Modulus 90°	12 GPa	527	
	Flexural Strength	1.230 MPa	14125	
	Flexural Modulus	45 GPa	14125	
	Compression Strength	900 MPa	14126	
	Lap shear Strength	22 MPa	4587	
Interlaminar Fracture Toughness Energy, G _{IC}	1.370 J/m ²	15024		
(3) Molded by RTM with Rovcore™ 450/85/450(16) from Chomarat, fiber volume content: 11% (4) Molded by RTM with a plain weave fabric from Chomarat, fiber volume content: 53% (5) Molded by infusion, with UD from Chomarat, fiber volume content: 58%				
THERMOFORMING	Fiber-reinforced Elium® parts can be thermoformed with heat and pressure. The use of a water-free peroxide for the Elium® polymerization is recommended when composite parts need to be thermoformed. This process requires the heating of the consolidated part at 180-200 °C for a few minutes, and the compression at a pressure between 5 and 20 bars depending on the reinforcement type and the thickness of the part.			
ADHESIVE ASSEMBLY	Fiber-reinforced composites made with ELIUM® resins can be assembled with adhesives. The SAF® 30 adhesive, from AEC Polymers, is recommended for structural bonding. A cohesive rupture is obtained with tensile lap shear strength at 17,5 MPa, according to the EN-1465. This adhesive is also recommended to bond metals, with lap-shear strength ranging from 18 to 21 MPa (aluminum 1050A, 6060 and 6061, stainless steel, steel).			
CERTIFICATES and APPROVALS	The manufacturing, quality control and distribution of products, by Altuglas International, comply with one or more of the following programs or standard: Responsible care, ISO9001, ISO14001, ISO/TS16949, OSHAS18001.			
STANDARD PACKAGES	These resins are supplied in non-returnable drums with net weight of 200 kg.			
STORAGE	The shelf life of the resin in original sealed container is 6 months at a temperature not higher than 25 °C. For further information we advise you to read carefully the current Safety Data Sheet.			

The statements, technical information and recommendations contained herein are believed to be accurate as of the date hereof. Since the conditions and methods of use of the product and of the information referred to herein are beyond our control, ARKEMA expressly disclaims any and all liability as to any results obtained or arising from any use of the product or reliance on such information; NO WARRANTY OF FITNESS FOR ANY PARTICULAR PURPOSE, WARRANTY OF MERCHANTABILITY OR ANY OTHER WARRANTY, EXPRESS OR IMPLIED, IS MADE CONCERNING THE GOODS DESCRIBED OR THE INFORMATION PROVIDED HEREIN. The information provided herein relates only to the specific product designated and may not be applicable when such product is used in combination with other materials or in any process. The user should thoroughly test any application before commercialization. Nothing

Arkema, Société anonyme au capital de 1 000 000 000 € - Siège social : 100 rue de la République - 42000 Saint-Etienne - France
 - Chomarat 01/02/2013 - Droim - Cédex photo: Arkema, N.C.

Arkema
 89 boulevard National
 F-92257 La Garenne-Colombes Cedex - France
 Tel.: +33 (0)1 78 66 23 00
 Fax: +33 (0)1 78 66 23 97
elium-composites.com

ARKEMA
 NEW MATERIALS FOR THE FUTURE

ELIUM® 150

contained herein constitutes a license to practice under any patent and it should not be construed as an inducement to infringe any patent and the user is advised to take appropriate steps to be sure that any proposed use of the product will not result in patent infringement.

See MSDS for Health & Safety Considerations

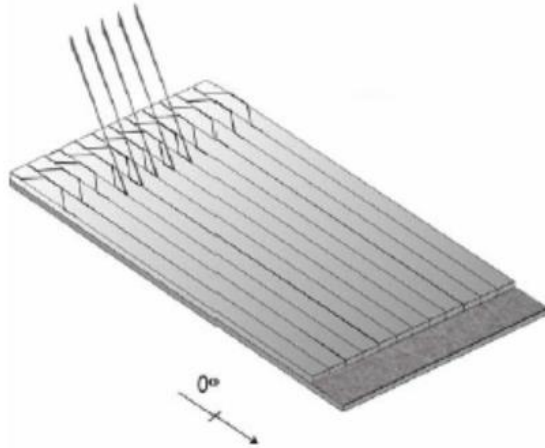
Date: May 2015

ARKEMA Société anonyme au capital de 630 296 000 euros - 445 004 086 RCS Nanterre
- Créée le 03/02/2013 - Drouin - Cédex phosor - Arkema, NRC C

Arkema
89 boulevard National
F-92257 La Garenne-Colombes Cedex - France
Tel.: +33 (0)1 78 66 23 00
Fax: +33 (0)1 78 66 23 97
elium-composites.com

ARKEMA
RESEARCH & INNOVATION

B4: Vector Ply E-LR 1208 Unidirectional E-glass [23]



E-LR 1208

Fiber Type: E-Glass
 Architecture: 0° Unidirectional
 Dry Thickness: 0.019 in. / 0.48 mm
 Total Weight: 12.85 oz/sq.yd / 436 g/sq.m

VECTORSPORTS™



Roll Specifications			Fiber Architecture Data	
Roll Width:	Roll Weight:	Roll Length:	0 ° :	11.95 oz/sq.yd / 405 g/sq.m
50 in / 1270 mm	152 lb / 69 kg	131 yd / 120 m	45 ° :	n/a
			90 ° :	n/a
			- 45 ° :	n/a
			Polyester Veil:	0.90 oz/sq.yd / 31 g/sq.m

1: Packaging: box or bag.
 2: Weights do not include polyester stitching.

Laminated Properties

0 °

0 °

Laminated Properties		
Laminate Weight (lb/sq.ft)	E-LR 1208 Resin Infused	E-LR 1208 Open Mold
Fiber	0.09	0.09
Resin	0.04	0.08
Total	0.13	0.17

Physical Properties		
	E-LR 1208 Resin Infused	E-LR 1208 Open Mold
Density (g/cc)	1.84	1.62
Fiber Content (% by Wt.)	69%	52%
Thickness (in)	0.013	0.020

Laminate Modulus		
(MSI)	E-LR 1208 Resin Infused	E-LR 1208 Open Mold
Ex	5.13	3.58
Ey	1.65	1.12
Gxy	0.49	0.31
Ex,flex.	4.78	3.33
Ey,flex.	1.53	1.04

Ultimate Stress		
(KSI)	E-LR 1208 Resin Infused	E-LR 1208 Open Mold
Long. Ten.	97	68
Long. Comp.	97	68
Trans. Ten.	33	22
Trans. Comp.	33	22
In-Plane Shear	15	9
Long. Flex.	103	72
Trans. Flex.	33	22

In-Plane Stiffness, "EA"		
10 ³ lb/in	E-LR 1208 Resin Infused	E-LR 1208 Open Mold
(EA)x	69	73
(EA)y	22	23
(GA)xy	7	6

Ultimate In-Plane Load		
lb/in	E-LR 1208 Resin Infused	E-LR 1208 Open Mold
Long. Ten.	1,305	1,386
Long. Comp.	1,305	1,386
Trans. Ten.	443	457
Trans. Comp.	443	457
In-Plane Shear	196	188

Notes:

- 1: Resin infused laminate made with vinyl ester resin 200 cps viscosity @ 77° F.
- 2: Open mold laminate made with polyester resin.
- 3: All standard reinforcements should be infused with a flow aid or Vectorfusion® reinforcements.



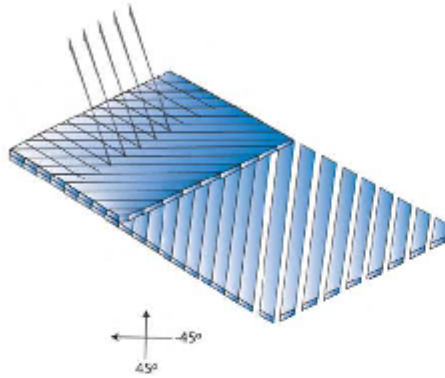
3500 Lakewood Dr. Phenix City, AL 36867 tel. 334 291 7704 fax. 334 291

Disclaimer:

As a service to customers, Vectorply Corporation ("VP") may provide computer-generated predictions of the physical performance of a product using a reinforcement fabric produced by VP in combination with other materials or systems.

VP makes no warranty whatsoever as to the accuracy of any such predicted physical performance, and customer acknowledges that customer is solely responsible for determining the performance and fitness for a particular use of any product produced by customer utilizing a fabric or material produced or manufactured by VP. Specifications of reinforcements may change without notice.

B5: Vector Ply B-BX 2400 Double Bias E-glass Technical Data Sheet [78]



E-BX 2400

Fiber Type: E-Glass
 Architecture: 45/-45 Double Bias
 Dry Thickness: 0.029 in. / 0.74 mm
 Total Weight: 24.20 oz/sq.yd / 821 g/sq.m

Roll Specifications			Fiber Architecture Data	
Roll Width:	Roll Weight:	Roll Length:	0 ° :	n/a
50 in / 1270 mm	228 lb / 104 kg	105 yd / 96 m	45 ° :	12.10 oz/sq.yd / 410 g/sq.m
			90 ° :	n/a
			-45 ° :	12.10 oz/sq.yd / 410 g/sq.m
			Chopped Mat :	n/a

1: Packaging: box or bag.
 2: Weights do not include polyester stitching.

Laminated Properties

45 °

45 °

Laminate Weight				
	E-BX 2400 Resin Infused		E-BX 2400 Open Mold	
Fiber	0.17 lb/sq.ft	0.82 kg/sq.m	0.17 lb/sq.ft	0.82 kg/sq.m
Resin	0.07 lb/sq.ft	0.35 kg/sq.m	0.14 lb/sq.ft	0.67 kg/sq.m
Total	0.24 lb/sq.ft	1.17 kg/sq.m	0.31 lb/sq.ft	1.49 kg/sq.m

Physical Properties				
	E-BX 2400 Resin Infused		E-BX 2400 Open Mold	
Density	1.10 oz/cu.in	1.90 g/cc	0.98 oz/cu.in	1.69 g/cc
Fiber Content	70% by Wt.	52% by Vol.	55% by Wt.	37% by Vol.
Thickness	0.024 in	0.6 mm	0.035 in	0.9 mm

Laminate Moduli				
	E-BX 2400 Resin Infused		E-BX 2400 Open Mold	
	Ex	3.48 MSI	23.98 GPa	2.57 MSI
Ey	3.48 MSI	23.98 GPa	2.57 MSI	17.73 GPa
Gxy	0.47 MSI	3.25 GPa	0.36 MSI	2.51 GPa
Ex,flex.	3.30 MSI	22.78 GPa	2.44 MSI	16.84 GPa
Ey,flex.	3.30 MSI	22.78 GPa	2.44 MSI	16.84 GPa

Ultimate Stress				
	E-BX 2400 Resin Infused		E-BX 2400 Open Mold	
	Long. Ten.	65.9 KSI	454.1 MPa	48.7 KSI
Long. Comp.	65.9 KSI	454.1 MPa	48.7 KSI	335.6 MPa
Trans. Ten.	65.9 KSI	454.1 MPa	48.7 KSI	335.6 MPa
Trans. Comp.	65.9 KSI	454.1 MPa	48.7 KSI	335.6 MPa
In-Plane Shear	9.4 KSI	65.0 MPa	7.3 KSI	50.2 MPa
Long. Flex.	78.6 KSI	542.0 MPa	58.1 KSI	400.6 MPa
Trans. Flex.	78.6 KSI	542.0 MPa	58.1 KSI	400.6 MPa

In-Plane Stiffness, "EA"				
	E-BX 2400 Resin Infused		E-BX 2400 Open Mold	
	(EA)x	84,399 lb/in	14,780 N/mm	89,352 lb/in
(EA)y	84,399 lb/in	14,780 N/mm	89,352 lb/in	15,647 N/mm
(GA)xy	11,441 lb/in	2,004 N/mm	12,654 lb/in	2,216 N/mm

Ultimate In-Plane Load				
	E-BX 2400 Resin Infused		E-BX 2400 Open Mold	
	Long. Ten.	1,598 lb/in	280 N/mm	1,692 lb/in
Long. Comp.	1,598 lb/in	280 N/mm	1,692 lb/in	296 N/mm
Trans. Ten.	1,598 lb/in	280 N/mm	1,692 lb/in	296 N/mm
Trans. Comp.	1,598 lb/in	280 N/mm	1,692 lb/in	296 N/mm
In-Plane Shear	229 lb/in	40 N/mm	253 lb/in	44 N/mm

Notes:

- 1: Resin infused laminate made with a poly / vinyl ester resin blend.
- 2: Open mold laminate made with poly / vinyl ester resin blend.
- 3: All standard reinforcements should be infused with a flow aid or Vectorfusion® reinforcements.
- 4: All properties are given assuming a symmetric or quasi-symmetric laminate schedule.



3500 Lakewood Dr. Phenix City, AL 36867 tel. 334 291 7704 fax. 334 291 7743

REV: 6/16/2015

Disclaimer:

As a service to customers, Vectorply Corporation ("VP") may provide computer-generated predictions of the physical performance of a product using a reinforcement fabric produced by VP in combination with other materials or systems.

VP makes no warranty whatsoever as to the accuracy of any such predicted physical performance, and customer acknowledges that customer is solely responsible for determining the performance and fitness for a particular use of any product produced by customer utilizing a fabric or material produced or manufactured by VP. Specifications of reinforcements may change without notice.

APPENDIX C: CLASSICAL LAMINATION THEORY (CLT) MATLAB CODE

For the purposes of this study classical lamination theory (CLT) code written in the Matlab coding environment that utilizes both micro and macro mechanics written by Camerin Seigars utilizing resources from classroom lecture, colleagues, journal papers and textbooks [7] [37] [49] [50] were used. The code used is given:

```
%*****%
%*
%*          LAMINATE ANALYSIS CODE V3.1          *%
%*
%*          Author: Camerin Seigars              *%
%*          Date:      July 19th, 2016 V1        *%
%*          Revisions: June 9th, 2018 V2        *%
%*                      June 22nd, 2018 V3      *%
%*
%*****%
function CLT_V3
%*****%
%***          User Instructions          ***%
%*****%
%This code implements both CLT for micromechanics and macromechanics
%User must define method for inputs, either method 1, which uses
%micromechanics to calculate the lamina properties or method 2, which
%uses user input properties for the lamina.
%If method 1 is used the user must define either Halpin-Tsai or
%Mori-Tanaka methods for overall technique, other methods may be
selected
%if using the Halpin-Tsai method section, if micro method 1 is chosen
the
%code defaults to the Halpin-Tsai method, though inside this section of
%code other choices can be selected.
%%
disp('***** ')
disp('***** LAMINATE ANALYSIS CODE V3.1 ***** ')
disp('***** ')
%*****%
%***          INPUTS          ***%
%*****%
%%%%%%%%%%%%%%
%%% Two Methods of CLT: User Must Choose %%%
%%%%%%%%%%%%%%
%Method 1: User dictates constitutive properties:
%Set method equal to 1
%Method 2: User dictates effective/lamina properties:
%Use specify effective properties section
%Set method equal to 0
```

```

method = 1;
%%%%%%%%%%%%%%%%%%%%%%%%%%%%%%%%%%%%%%%%%%%%%%%%%%%%%%%%%%%%%%%%%%%%%%%%
%%% Two Methods of Micromechanics: User Must Choose %%%
%%%%%%%%%%%%%%%%%%%%%%%%%%%%%%%%%%%%%%%%%%%%%%%%%%%%%%%%%%%%%%%%%%%%%%%%
%Method Micro 1: Micromechanics performed using Halpin-Tsai method and
%rule of mixtures to find lamina properties.
%Set method equal to 1
%Method Micro 2: Micromechanics uses Mori-Tanaka method to find lamina
%properties.
%Set method equal to 0
micro = 1;
%%
if method
    %%%%%%%%%%%%%%%%%%%%%%%%%%%%%%%%%%%%%%%%%%%%%%%%%%%%%%%%%%%%%%%%%%%%%%%%%
    %%% Specify Constitutive Properties of the Base Materials %%%
    %%%%%%%%%%%%%%%%%%%%%%%%%%%%%%%%%%%%%%%%%%%%%%%%%%%%%%%%%%%%%%%%%%%%%%%%%
    %***** Method 1 *****%
    % Solution strategy showed to me by Ben Smith from Barbero textbook
    % FRP Input (Don't forget to update h for the thickness %)
    %*****%
    %*** Input Parameters for Method 1 ***%
    %*****%
    % Fiber Volume Fraction, Vf - % Fibers by Volume in the Composite %
    %Vf = 0.3891; %E-glass/PETg IE 5842 Trial 3 (natural)
    %Vf = 0.364; %E-glass/PETg IE 5842b Trial - (black)
    Vf = 0.400; %E-glass/Derakane 610-C Vacuum infused
    %Vf = 0.432; %E-glass/Elium 150 Vacuum infused
    % Solve for percent matrix by volume %
    Vm = 1 - Vf;
    %Assumes no voids in the composite.
    %*****%
    % Fiber-reinforcement Base Material Inputs %
    %*****%
    %All inputs should be in Pascals, (Pa)
    %Note: This code assumes the fiber material to be isotropic
    Fft = 3450*10^6;
    %Set for E-glass Strength (Daniel 2nd Edition)
    Ef = 73*10^9;
    %Set for E-glass Modulus (Daniel 2nd Edition)
    nuf = 0.23;
    %Set for E-glass Poisson's Ratio (Daniel 2nd Edition)
    %E-glass properties from Daniel 2nd Edition, Table A.2, which
contains
    %the mechanical and thermal properties of representative fibers
    %*****%
    % Matrix Base Material Inputs %
    %*****%
    %All inputs should be in Pascals, (Pa)
    %*** Elium 150 Thermoplastic Resin-System ***%
    Fmt = 76*10^6;
    %Set for Elium Longitudinal Tensile Matrix Strength
    Fmc = 130*10^6;
    %Set for Elium Longitudinal Compressive Matrix Strength
    Em = 3300*10^6;
    %Set for Elium Longitudinal Matrix Elastic Modulus
    %Used the Elium 150 GFRP Technical Data Sheet from Arkema
    %*** PETg Thermoplastic Polymer - Vivak Data Sheet ***%

```

```

%      Fmt = 53*10^6;
%      %Set for PETg Longitudinal Tensile Matrix Strength
%      Fmc = 55*10^6;
%      %Set for PETg Longitudinal Compressive Matrix Strength
%      Em  = 2206*10^6;
%      %Set for PETg Longitudinal Matrix Elastic Modulus
%      % Poisson's Ratio of PEI Thermoplastic Matrix %
num = 0.37;      %Set for PEI from Barbero
%Used because no value was known for Elium or PETg
%*** Derakane 610-C Thermosetting Resin-System ***%
%      Fmt = 71*10^6;
%      %Set for Derakane Longitudinal Tensile Matrix Strength
%      Fmc = 127*10^6;
%      %Set for Derakane Longitudinal Comp. Matrix Strength
%      Em  = 3500*10^6;
%      %Set for Derakane Longitudinal Matrix Elastic Modulus
%      num = 0.35;
%      %Set for Derakane from Daniel 2nd Edition
%Used Derakane 610-C Technical Data Sheet from Ashland & Daniel
book
%*****%
%*** Method 1 Specific Calculations ***%
%*****%
% Calculate Shear Moduli for Fibers and Matrix %
%Assumes the fiber and matrix materials are isotropic
% Shear Modulus of Fibers, (Pa) %
Gf = Ef/2/(1 + nuf); % (Gere and Goodno Equation 1-22)
% Shear Modulus of Matrix, (Pa) %
Gm = Em/2/(1+num); % (Gere and Goodno Equation 1-22)
%*****%
%* Lamina Modulus Calculations *%
%*****%
if micro
%*****%
%* Method Micro 1 *%
%*****%
%*****%
%*** Rule of Mixtures Calculations ***%
%*****%
% Longitudinal Modulus of the lamina, E1, (Pa) %
E1  = Ef*Vf+Em*Vm;
%(Daniel Equation 3.23 and Barbero Equation 4.24)
% Longitudinal In-plane Poisson's Ratio, nu12, (-) %
nu12 = nuf*Vf+num*Vm;
%(Daniel Equation 3.24, uses same assumptions as for E1)
%*****%
%*** Halpin-Tsai Calculations ***%
%*****%
%Curve-fitting parameter, usually between 1 and 2, (Daniel)
%Can be obtained from experiments, (Daniel)
%Assume zeta equals 1 for hexagonal arrays (glass and carbon
%composites with high fiber volume ratios, (Daniel).
%zeta = 1;
%Assume zeta equals 2 for square arrays (boron
composite), (Daniel)
%Assume zeta equals 2 for circular or square fibers, (Barbero)
zeta = 2;

```

```

%Assume zeta as follows for rectangular fibers, (Barbero)
%Dimensions of the fiber cross-section:
%a = 1;
%b = 1;
%zeta = (2*a)/b;
% Calculate EtaE, for the Halpin-Tsai Method %
%Uses the zeta parameter defined above
etaE = (Ef/Em-1)/(Ef/Em+zeta);
%(Daniel Equation 3.35 and Barbero Equation 4.31)
%The two books show different forms of the same equation.
%Transverse modulus of the lamina, E2, (Pa) %
E2 = Em*(1+zeta*etaE*Vf)/(1-etaE*Vf);
%(Daniel Equation 3.35 and Barbero Equation 4.31)
% In-plane shear modulus, G12, (Pa) %
%Select In-Plane Shear Method 1
%Method 1: User selects the default method, Halpin-Tsai
%shear = 1;
%Method 2/3: Moves to next if/else to select other method
%shear = 0;
shear = 1;
if shear
    %Assumes isotropic fibers, (Daniel 3.49)
    % Halpin-Tsai %
    %Calculate EtaG, for the Halpin-Tsai Method
    %Uses zeta parameter defined above
    etaG = (Gf-Gm)/(Gf+(zeta*Gm)); % (Daniel 3.50)
    G12 = Gm*(1+(etaG*zeta*Vf))/(1-(etaG*Vf)); % (Daniel 3.50)
else
    %Select 2/3 In-Plane Shear Method %
    %Method 2: User has selected the cylindrical assemblage
model
    %shear2 = 1;
    %Method 3: User has selected the rule of mixtures method
    %shear2 = 0;
    shear2 = 1;
    if shear2
        %Cylindrical Assemblage Model (or)
        %Self-Consistent Field Model:
        G12 = Gm*((1+Vf)+(1-Vf)*Gm/Gf)/((1-Vf)+(1+Vf)*Gm/Gf);
        %(Barbero Equation 4.37 (or) Daniel 3.52)
        %Two books show different forms of the same equation if
        %isotropic fibers are assumed, i.e, G12f = Gf.
    else
        % Rule of Mixtures %
        G12 = (Gf*Gm)/((Vf*Gm)+(Vm*Gf));
    end
end
% Intralaminar (Transverse) Shear Modulus Calculation %
%Semi-empirical stress partitioning parameter technique
%Parameter eta4
eta4 = (3-((4*num)+(Gm/Gf)))/(4*(1-num)); % (Barbero
4.45)
% Intralaminar Shear Modulus, G23, (Pa) %
G23 = Gm*(Vf + eta4*(Vm))/(eta4*Vm+(Vf*Gm/Gf)); % (Barbero
4.45)
% Intralaminar Poisson's Ratio, nu23, (-) %

```

```

3.42) nu23 = (E2/(2*G23))-1; % Adapted from (Daniel
defined %Derived from the transversely isotropic equation for G23
%in Daniel 2nd edition for composite materials.
else
%*****%
%* Method Micro 2 *%
%*****%
%*****%
%*** Mori-Tanaka Calculations ***%
%*****%
%Adapted from MEE 450 taught by Senthil Vel (2016)
%Assuming isotropic fiber material %
%Longitudinal and transverse properties are the same.
% Elastic Moduli of Isotropic Fibers %
E1f = Ef;
E2f = Ef;
G12f = Gf;
G23f = Gf;
% Poisson's Ratio of Isotropic Fibers %
nu12f = nu_f;
%* Determine Hill's Elastic Moduli for the Fiber *%
kf = 1/(4/E2f-1/G23f-4*nu12f^2/E1f);
lf = 2*nu12f*kf;
mf = G23f;
nf = E1f+lf^2/kf;
pf = G12f;
%* Determine Hill's Elastic Moduli for the Matrix *%
km = Em/(2-2*num - 4*num^2);
lm = 2*num*km;
mm = Em/(2*(1+num));
nm = Em+lm^2/km;
pm = Em/(2*(1+num));
%* Calculate Effective Hill's Elastic Moduli for the Composite
*%
k = (Vf*kf*(km + mm) + Vm*km*(kf + mm))/...
(Vf*(km + mm) + Vm*(kf + mm));
l = (Vf*lf*(km + mm) + Vm*lm*(kf + mm))/...
(Vf*(km + mm) + Vm*(kf + mm));
m = (mm*mf*(km+2*mm) + km*mm*(Vf*mf+Vm*mm))/...
(km*mm + (km + 2*mm)*(Vf*mm+Vm*mf));
n = Vm*nm + Vf*nf +(1 - Vf*lf - Vm*lm)*((lf-lm)/(kf-km));
p = (2*Vf*pm*pf+Vm*(pm*pf+pm^2))/(2*Vf*pm + Vm*(pf+pm));
%* Calculate Effective Engineering Properties for the Composite
*%
% Longitudinal Elastic Modulus, E1, (Pa) %
E1 = n - l^2/k;
% Transverse Elastic Modulus, E2, (Pa) %
E2 = 4*m*(k*n-l^2)/((k+m)*n-l^2);
% In-Plane Poisson's Ration, nu12, (-) %
nu12 = l/(2*k);
% In-Plane Shear Modulus, G12, (Pa) %
G12 = p;
% Intralaminar Shear Modulus, G23, (Pa) %
G23 = m;
% Intralaminar Poisson's Ratio, nu23, (-) %

```

```

        nu23 = E2/(2*G23)-1;
end
%*****%
%* Lamina Strength Calculations *%
%*****%
% Lamina Tensile Strengths %
%fiber dominated failure mode, Fltf
%matrix dominated failure mode, Fltm
Fltf = Fft*(Vf+Em/Ef*Vm); %(Daniel Equation 5.7)
%Longitudinal tensile strength (fiber dominated)
Fltm = Fmt*(Ef/Em*Vf+Vm); %(Daniel Equation 5.8)
%Longitudinal tensile strength (matrix dominated)
%Check for Fiber or Matric Dominated Failure
%Based on discussion with Ben Smith and Phil Bean, June 2018
Flt = min(Fltf,Fltm); %Daniel Textbook Section 5.2, pp. 98-100
% Fracture Toughness Mode I %
G1c = 334; % Set to E-glass/Polyester value, (Barbero Table 1.3)
%E-glass/Polyester value of 334 J/m^2 is the default value used
from
%Barbero Table 1.3 if the value is not known for the material
system
%being analyzed.
lambda022 = 2*(1/E2-nu12^2*E2^2/E1^3); %(Barbero Equation 4.100)
% Transition Thickness %
ttran = 0.0006; %Set to E-glass/Epoxy, (Barbero Section 4.4.8)
% Transverse Tensile Strength %
F2t = sqrt(G1c/1.12^2/pi()/ (ttran/4)/lambda022);
%(Barbero Equation 4.99)
% Fracture Toughness Mode II %
GIIc = 456; % Set to E-glass/Polyester, (Barbero Table 1.3)
%E-glass/Polyester value of 456 J/m^2 is the default value used
from
%Barbero Table 1.3 if the value is not known for the material
system
%being analyzed.
lambda044 = 1/G12; % (Barbero Equation 4.114)
% In-Plane Shear Strength %
F6 = sqrt(GIIc/pi()/ (ttran/4)/lambda044); %(Barbero Equation 4.113)
% Fiber Misalignment, see Barbero Table 1.3 %
alphasigma = 2.97*pi()/180; %Set to E-glass/Epoxy
chi = G12*alphasigma/F6; %(Barbero Equation 4.86)
% Longitudinal Compressive Strength %
Flc = G12*(1+4.76*chi)^-0.69; %(Barbero Equation 4.85)
%Adjustment Factor for Voids
Cv = 1;
%Set to 1 if no voids is assumed, else see Barbero Equation 4.102
% Transverse Compressive Strength %
F2c = Fmc*Cv*(1+(Vf-sqrt(Vf))*(1-Em/Ef)); %(Barbero Equation 4.105)
%%
else
%%%%%%%%%%%%%%%%%%%%%%%%%%%%%%%%%%%%%%%%%%%%%%%%%%%%%%%%%%%%%%%%%%%%%%%%%%
%% Specify Effective Properties of the Composite Material %%
%%%%%%%%%%%%%%%%%%%%%%%%%%%%%%%%%%%%%%%%%%%%%%%%%%%%%%%%%%%%%%%%%%%%%%%%%%
%***** Method 2 *****%
% Solution strategy presented in Senthil Vel's Composites Class
%All inputs should be in Pascals, (Pa)
% Young's (Tensile) Modulus in the 1 Direction %

```

```

E1=e9;
% Poisson's Ration in the 12 Direction %
nu12=0.23;
% Young's (Tensile) Modulus in the 2 Direction %
E2=6.313e9;
% Shear Modulus in the 12 Direction %
G12=5.949e9;
%* Specify Material Strength Data (Pa) *%
%* Strength Properties *%
% Tensile Strength in the 1 Direction %
F1t = 2200 * (10^6);
% Compressive Strength in the 1 Direction %
F1c = 1700 * (10^6);
% Tensile Strength in the 2 Direction %
F2t = 55 * (10^6);
% Compressive Strength in the 2 Direction %
F2c = 220 * (10^6);
%Tensile Strength in the 3 Direction %
F3t = 0 * (10^6);
%Compressive Strength in the 3 Direction %
F3c = 0*(10^6);
% Shear Strength %
F4 = 0 * (10^6);
F5 = 0 * (10^6);
% Shear Strength %
F6 = 70 * (10^6);
end
%%
%%%%%%%%%%%%%%%%%%%%%%%%%%%%%%%%%%%%%%%%%%%%%%%%%%%%%%%%%%%%%%%%%%%%%%%%%%
%***                               Lamina Properties                               ***%
%%%%%%%%%%%%%%%%%%%%%%%%%%%%%%%%%%%%%%%%%%%%%%%%%%%%%%%%%%%%%%%%%%%%%%%%%%
% Lamina Thickness (h) in meters %
% Lamina thickness refers to the thickness of a single lamina, or layer
in
% the composite layup. Classical lamination theory assumes all layers
in
% the composite have the same thickness defined as h.
h = 0.00044;
%E-glass/Elium layer thickness from test samples, meters, (m)
%Vacuum infused Elium 150 resin and E-LR 1208 UD E-glass w/ veil
%h = 0.00043;
%E-glass/Derakane layer thickness from test samples, meters, (m)
%Vacuum infused Derakane 610-C resin and E-LR 1208 UD E-glass w/ veil
%h = 0.00024
%E-glass/PETg layer thickness from test samples, meters, (m)
%Automated stamp formed from Polystrand IE 5842b prepreg tapes
%%
%%%%%%%%%%%%%%%%%%%%%%%%%%%%%%%%%%%%%%%%%%%%%%%%%%%%%%%%%%%%%%%%%%%%%%%%%%
%***       Specify the Laminate Fiber-Architecture       ***%
%%%%%%%%%%%%%%%%%%%%%%%%%%%%%%%%%%%%%%%%%%%%%%%%%%%%%%%%%%%%%%%%%%%%%%%%%%
%* Fiber Orientation of the kth Layer *%
%Defines the orientations of the fibers in the composite laminate, each
%lamina has a orientation theta in degrees defined by the ThetaArray.
ThetaArray = [0];
disp(strcat('Fiber-Architecture, Theta Array for Lamina (degrees): '));
disp(strcat([' ', num2str(ThetaArray), '']));
%%

```

```

%*****%
%*** Tsu-Wu Method Applied Loads for a Laminate ***%
%*****%
%These units loads are for the Tsai-Wu based calculations.
%The Fxt, Fxc, and Fxy calculations use the failure strains and
%independently defined unit loads to calculate these values.
%Units of N given in N/m %
Nx = 1;
Ny = 0;
Nxy = 0;
%Units of M given in Nm/m %
Mx = 0;
My = 0;
Mxy = 0;
%%
%*****%
%*** Calculate the Failure Strains ***%
%*****%
%Calculates the failure strains based on lamina strengths and
%stiffnesses as dictated in one of the two methods.
e1t = F1t/E1;
e2t = F2t/E2;
e1c = F1c/E1;
e2c = F2c/E2;
g6u = F6/G12;
%%
%*****%
%*** Print Effective Properties ***%
%*****%
disp('*****')
disp('*** Lamina Properties: ***')
disp('*****')
if method
    disp('*** Micromechanics Used: ***')
    if micro
        disp('*** Halpin-Tsai Method ***')
        disp('*****')
    else
        disp('*** Mori-Tanaka Method ***')
        disp('*****')
    end
else
    disp('*****')
    disp('*** Lamina Properties Defined by User ***')
    disp('*****')
end
end
disp(strcat(['F1t (MPa): ', num2str(round(F1t/1e6,0)) ]));
disp(strcat(['F1c (MPa): ', num2str(round(F1c/1e6,0)) ]));
disp(strcat(['F2t (MPa): ', num2str(round(F2t/1e6,1)) ]));
disp(strcat(['F2c (MPa): ', num2str(round(F2c/1e6,1)) ]));
disp(strcat(['F6 (MPa): ', num2str(round(F6/1e6,1)) ]));
disp(strcat(['E1 (GPa): ', num2str(round(E1/1e9,1)) ]));
disp(strcat(['E2 (GPa): ', num2str(round(E2/1e9,2)) ]));
disp(strcat(['G12 (GPa): ', num2str(round(G12/1e9,2)) ]));
disp(strcat(['G23 (GPa): ', num2str(round(G23/1e9,2)) ]));
disp(strcat(['nu12 (-): ', num2str(round(nu12,3)) ]));
disp(strcat(['nu23 (-): ', num2str(round(nu23,3)) ]));

```

```

%%
%*****
%***      CALCULATIONS      ***%
%*****
% Determine the number of layers %
N = length(ThetaArray);
% Laminate height in meters, (m) %
H = N * h;
%* Evaluate laminate interface locations Z_k *%
for k = 1:N+1
    ZCoord(k)=-H/2+(k-1)*h;
end
%disp('Z (mm) =');disp(strcat(' ',num2str(ZCoord/1e-3),' '));disp(' ')
%*** Compute the reduced stiffness matrix ***%
Q = ReducedStiffness(E1,nul2,E2,G12);
%disp('Q (GPa) =')
%disp([Q]/1e9)
%*** Compute the reduced compliance matrix ***%
S = ReducedCompliance(E1,nul2,E2,G12);
%disp('S (TPa^-1)=')
%disp([S]*1e12)
%*** Compute the off-axis reduced stiffness matrices ***%
for k = 1:N
    QBar{k}=OffAxisStiffness(ThetaArray(k),Q);
    % % % disp(strcat('QBar{ ',num2str(k),' } (GPa) ='));
    % % % disp(QBar{k}/1e9)
end
%*** Compute the off-axis reduced compliance matrix ***%
for k = 1:N
    SBar{k} = OffAxisCompliance(ThetaArray(k),S);
    % % % disp(strcat('SBar{ ',num2str(k),' } (TPa^-1)='))
    % % % disp(SBar{k}*1e12)
end
%*** Compute the Transformation Matrix T ***%
for k = 1:N
    T{k} = TMatrix(ThetaArray(k));
    % % % disp(strcat('Transformation Matrix{ ',num2str(k),' }'));
    % % % disp(T{k})
end
%*** Compute laminate ABD stiffness matrix ***%
[A,B,D,ABD,a,b,d,abd]=ComputeABD(QBar,ZCoord);
%*** Compute the midsurface strains and curvatures ***%
[Epsilon0,Kappa0] =
MidsurfaceStrainsCurvatures(abd,Nx,Ny,Nxy,Mx,My,Mxy);
%disp('Midsurface strains Epsilon0 (micro m/m):')
%disp(Epsilon0/1e-6)
%disp('Midsurface curvatures Kappa0 (1/m):')
%disp(Kappa0)
% z locations of points where strains and stresses will be evaluated %
zpoints=linspace(-H/2,H/2,5000);
%* Evaluated strains, stresses and factor of safety at the various *%
%*** z locations ***%
for n = 1:length(zpoints)
    %Determine the layer that the z location belongs to
    z = zpoints(n); %z coordinate
    k = WhichLayer(ZCoord,z); % layer number
    %Strains in the x-y coordinate system

```

```

    StrainsXY= ComputeStrainsXY(Epsilon0,Kappa0,z);
    EpsilonX(n)=StrainsXY(1);
    EpsilonY(n)=StrainsXY(2);
    GammaXY(n)=StrainsXY(3);
    %Stresses in the x-y coordinate system
    StressesXY = ComputeStressesXY(StrainsXY,QBar{k});
    SigmaX(n)=StressesXY(1);
    SigmaY(n)=StressesXY(2);
    TauXY(n)=StressesXY(3);
    %Stresses in the 1-2 coordinate system
    Stresses12 = ComputeStresses12(StressesXY, ThetaArray(k));
    Sigma1(n)=Stresses12(1);
    Sigma2(n)=Stresses12(2);
    Tau12(n)=Stresses12(3);
    %Calculate factor of safety using the Tsai-Wu failure criterion
    [Sfa(n), Sfr(n)] = TsaiWu(F1t,F1c,F2t,F2c,F6,Stresses12);
end
%*****%
%*** Tsai-Wu Failure Theory Output ***%
%*****%
%disp('Tsai-Wu Failure Theory Safety Factors:')
%disp('Minimum factor of safety S_{fa} (actual state of stress):')
%disp(min(Sfa))
%disp('Minimum factor of safety |S_{fr}| (reversed state of stress):')
%disp(min(abs(Sfr)))
%%
%*****%
%
%***                               Plotting
%***%
%*****%
%
% Plot the through-thickness variation of strains %
% figure(1)
% plot(EpsilonX/1e-6,zpoints/H);
% xlabel('\epsilon_{x} ({\mu}m/m) ');
% ylabel('z/H');
% figure(2)
% plot(EpsilonY/1e-6,zpoints/H);
% xlabel('\epsilon_{y} ({\mu}m/m) ');
% ylabel('z/H');
% figure(3)
% plot(GammaXY/1e-6,zpoints/H);
% xlabel('\gamma_{xy} ({\mu}rad) ');
% ylabel('z/H');
% % Plot the through-thickness variation of stresses %
% figure(4)
% plot(SigmaX/1e6,zpoints/H);
% xlabel('\sigma_{x} (MPa) ');
% ylabel('z/H');
% figure(5)
% plot(SigmaY/1e6,zpoints/H);
% xlabel('\sigma_{y} (MPa) ');
% ylabel('z/H');
% figure(6)
% plot(TauXY/1e6,zpoints/H);
% xlabel('\tau_{xy} (MPa) ');

```

```

% ylabel('z/H');
% figure(7)
% plot(Sigma1/1e6,zpoints/H);
% xlabel('\sigma_{1} (MPa)');
% ylabel('z/H');
% figure(8)
% plot(Sigma2/1e6,zpoints/H);
% xlabel('\sigma_{2} (MPa)');
% ylabel('z/H');
% figure(9)
% plot(Tau12/1e6,zpoints/H);
% xlabel('\tau_{12} (MPa)');
% ylabel('z/H');
% % Plot the through-thickness variation of factor of safety Sfa %
% figure(10)
% plot(Sfa,zpoints/H);
% xlabel('S_{fa}');
% ylabel('z/H');
% % Plot the through-thickness variation of factor of safety Sfr %
% figure(11)
% plot(abs(Sfr),zpoints/H);
% xlabel('|S_{fr}|');
% ylabel('z/H');
%%
% Calculate the Effective Strengths %
disp('*****')
disp('*** Effective Laminate Properties: ***')
disp('*****')
%Output number of layers in the laminate
disp(strcat(['Number of layers: ', 'N = ', num2str(N)]));
%*****
%***          Strain Failure Criteria          ***%
%*** Determine factor of safety to get Fxt          ***%
%*****%
%*** Compute the midsurface strains and curvatures ***%
[Epsilon0,Kappa0] = MidsurfaceStrainsCurvatures(abd,1,0,0,0,0,0);
% z locations of points where strains and stresses will be evaluated %
zpoints=linspace(-H/2,H/2,5000);
% Define initial Factor of Safety (FS) values as zero %
FS1 = 0; FS2 = 0; FS3 = 0;
%* Evaluate Strains, Stresses, and FS at zpoints to Find Failure *%
for n = 1:length(zpoints)
    %Determine the layer that the z location belongs to
    z = zpoints(n); %z coordinate
    k = WhichLayer(ZCoord,z); % layer number
    %Strains in the x-y coordinate system
    StrainsXY= ComputeStrainsXY(Epsilon0,Kappa0,z);
    %Stresses in the x-y coordinate system
    StressesXY = ComputeStressesXY(StrainsXY,QBar{k});
    %Stresses in the 1-2 coordinate system
    Stresses12 = ComputeStresses12(StressesXY, ThetaArray(k));
    %Strains in the 1-2 coordinate system
    Strain12 = S*Stresses12;
    if Strain12(1)<0
        FS1(n)=elc/-Strain12(1);
    elseif Strain12(1)>0
        FS1(n)=elt/Strain12(1);
    end
end

```

```

end
if Strain12(2)<0
    FS2(n)=e2c/-Strain12(2);
elseif Strain12(2)>0
    FS2(n)=e2t/Strain12(2);
end
if Strain12(3)==0
    FS3(n) = 0;
else
    FS3(n)=g6u/abs(Strain12(3));
end
end
FS_tension = min([min(FS1(FS1>0)),min(FS2(FS2>0)),min(FS3(FS3>0))])/H;
% Display strength based on minimum factor of safety %
disp(strcat(['Fxt (MPa): ',num2str(round(min(FS_tension)/1e6,0))]);
%*****%
%***          Strain Failure Criteria          ***%
%*** Determine factor of safety to get Fxc      ***%
%*****%
%*** Compute the midsurface strains and curvatures ***%
[Epsilon0,Kappa0] = MidsurfaceStrainsCurvatures(abd,-1,0,0,0,0,0);
% z locations of points where strains and stresses will be evaluated %
zpoints=linspace(-H/2,H/2,5000);
% Define initial Factor of Safety (FS) values as zero %
FS1 = 0; FS2 = 0; FS3 = 0;
%* Evaluate Strains, Stresses, and FS at zpoints to Find Failure *%
for n = 1:length(zpoints)
    %Determine the layer that the z location belongs to
    z = zpoints(n); %z coordinate
    k = WhichLayer(ZCoord,z); % layer number
    %Strains in the x-y coordinate system
    StrainsXY= ComputeStrainsXY(Epsilon0,Kappa0,z);
    %Stresses in the x-y coordinate system
    StressesXY = ComputeStressesXY(StrainsXY,QBar{k});
    %Stresses in the 1-2 coordinate system
    Stresses12 = ComputeStresses12(StressesXY, ThetaArray(k));
    %Strains in the 1-2 coordinate system
    Strain12 = S*Stresses12;
    if Strain12(1)<0
        FS1(n)=e1c/-Strain12(1);
    elseif Strain12(1)>0
        FS1(n)=e1t/Strain12(1);
    end
    if Strain12(2)<0
        FS2(n)=e2c/-Strain12(2);
    elseif Strain12(2)>0
        FS2(n)=e2t/Strain12(2);
    end
    if Strain12(3)==0
        FS3 = 0;
    else
        FS3(n)=g6u/abs(Strain12(3));
    end
end
end
FS_compression =
min([min(FS1(FS1>0)),min(FS2(FS2>0)),min(FS3(FS3>0))])/H;
% Display strength based on minimum factor of safety %

```

```

disp(strcat(['Fxc (MPa):
',num2str(round(min(FS_compression)/1e6,0))]));
%*****%
%***          Strain Failure Criteria          ***%
%***  Determine factor of safety to get Fxy  ***%
%*****%
%*** Compute the midsurface strains and curvatures ***%
[Epsilon0,Kappa0] = MidsurfaceStrainsCurvatures(abd,0,0,1,0,0,0);
% z locations of points where strains and stresses will be evaluated %
zpoints=linspace(-H/2,H/2,5000);
% Define initial Factor of Safety (FS) values as zero %
FS1 = 0; FS2 = 0; FS3 = 0;
%* Evaluate Strains, Stresses, and FS at zpoints to Find Failure *%
for n = 1:length(zpoints)
    %Determine the layer that the z location belongs to
    z = zpoints(n); %z coordinate
    k = WhichLayer(ZCoord,z); % layer number
    %Strains in the x-y coordinate system
    StrainsXY= ComputeStrainsXY(Epsilon0,Kappa0,z);
    %Stresses in the x-y coordinate system
    StressesXY = ComputeStressesXY(StrainsXY,QBar{k});
    %Stresses in the 1-2 coordinate system
    Stresses12 = ComputeStresses12(StressesXY, ThetaArray(k));
    %Strains in the 1-2 coordinate system
    Strain12 = S*Stresses12;
    if Strain12(1)<0
        FS1(n)=e1c/-Strain12(1);
    elseif Strain12(1)>0
        FS1(n)=elt/Strain12(1);
    end
    if Strain12(2)<0
        FS2(n)=e2c/-Strain12(2);
    elseif Strain12(2)>0
        FS2(n)=e2t/Strain12(2);
    end
    if Strain12(3)==0
        FS3 = 0;
    else
        FS3(n)=g6u/abs(Strain12(3));
    end
end
FS_shear = min([min(FS1(FS1>0)),min(FS2(FS2>0)),min(FS3(FS3>0))])/H;
% Display strength based on minimum factor of safety %
disp(strcat(['Fxy (MPa): ',num2str(round(min(FS_shear)/1e6,1))]));
%*****%
%***  Laminate Effective Property Calculations  ***%
%***          Determine Ex, Ey, Gxy, nuxy          ***%
%*****%
%* Finds the effective moduli and Poisson's ratio for the laminate *%
% Calculate Longitudinal Modulus, Ex, (Pa) %
Ex = (1/H)/abd(1,1);
disp(strcat(['Ex (GPa): ',num2str(round(Ex/1e9,2))]));
% Calculate the Transverse Modulus, Ey, (Pa) %
Ey = (1/H)/abd(2,2);
disp(strcat(['Ey (GPa): ',num2str(round(Ey/1e9,2))]));
% Calculate the In-Plane Shear Modulus, Gxy, (Pa) %
Gxy = ABD(3,3)/H;

```

```

disp(strcat(['Gxy (GPa): ',num2str(round(Gxy/1e9,2))]);
% Calculate the in plane Poisson's Ratio, nuxy, (-) %
nuxy = ABD(1,2)/ABD(2,2);
disp(strcat(['nuxy (-): ',num2str(round(nuxy,3))]);
end
%%
%*****%
%***          Reduced Compliance Matrix          ***%
%*****%
function S = ReducedCompliance(E1,nu12,E2,G12)
S11 = 1 / E1;
S12 = -nu12 / E1;
S22 = 1 / E2;
S66 = 1 / G12;
S = [S11 S12 0;S12 S22 0; 0 0 S66];
end
%%
%*****%
%***          Reduced Stiffness Matrix          ***%
%*****%
function Q = ReducedStiffness(E1,nu12,E2,G12)
nu21 = (E2 / E1) * nu12;
Q11 = E1 / (1 - (nu12 * nu21));
Q12 = (nu12 * E2) / (1 - (nu12 * nu21));
Q22 = E2 / (1 - (nu12 * nu21));
Q66 = G12;
Q = [Q11 Q12 0;Q12 Q22 0; 0 0 Q66];
end
%%
%*****%
%***          Off-axis Stiffness Matrix          ***%
%*****%
function QBar = OffAxisStiffness(theta,Q)
m=cosd(theta);
n=sind(theta);
Q11=Q(1,1); Q12=Q(1,2); Q22=Q(2,2); Q66=Q(3,3);
QBar11 = (Q11 * m^4) + (2 * (Q12 + (2 * Q66)) * m^2 * n^2) + (Q22 *
n^4);
QBar12 = ((Q11 + Q22 - (4 * Q66)) * n^2 * m^2) + (Q12 * (n^4 + m^4));
QBar16 = ((Q11 - Q12 - (2 * Q66)) * n * m^3) + ((Q12 - Q22 +...
(2 * Q66)) * n^3 * m);
QBar22 = (Q11 * n^4) + (2 * (Q12 + (2 * Q66)) * n^2 * m^2) +...
(Q22 * m^4);
QBar26 = ((Q11 - Q12 - (2 * Q66)) * n^3 * m) + ((Q12 - Q22 +...
(2 * Q66)) * n * m^3);
QBar66 = ((Q11 + Q22 - (2 * Q12) - (2 * Q66)) * n^2 * m^2) +...
(Q66 * (n^4 + m^4));
QBar =[QBar11 QBar12 QBar16; QBar12 QBar22 QBar26; QBar16 QBar26
QBar66];
end
%%
%*****%
%***          Off-axis Compliance Matrix          ***%
%*****%
function SBar = OffAxisCompliance(theta,S)
m = cosd(theta);
n = sind(theta);

```

```

S11 = S(1,1); S12 = S(1,2); S22 = S(2,2); S66 = S(3,3);
SBar11 = (S11 * m^4) + (((2 * S12) + S66) * n^2 * m^2) + (S22 * n^4);
SBar12 = ((S11 + S22 - S66) * n^2 * m^2) + (S12 * (n^4 + m^4));
SBar16 = (((2 * S11) - (2 * S12) - S66) * n * m^3) +...
        (((2 * S12) - (2 * S22) + S66) * n^3 * m);
SBar22 = (S11 * n^4) + (((2 * S12) + S66) * n^2 * m^2) + (S22 * m^4);
SBar26 = (((2 * S11) - (2 * S12) - S66) * n^3 * m) +...
        (((2 * S12) - (2 * S22) + S66) * n * m^3);
SBar66 = (2 * ((2 * S11) + (2 * S22) - (4 * S12) - S66) * n^2 * m^2)...
        + (S66 * (n^4 + m^4));
SBar = [SBar11 SBar12 SBar16; SBar12 SBar22 SBar26; SBar16 SBar26
        SBar66];
end
%%
%*****%
%***      Transformation Matrix      ***%
%*****%
function T = TMatrix(theta)
m = cosd(theta);
n = sind(theta);
T = [m^2 n^2 2*m*n; n^2 m^2 -2*m*n; -m*n m*n (m^2)-(n^2)];
end
%%
%*****%
%***      Compute ABD Matrices      ***%
%*****%
function [A,B,D,ABD,a,b,d,abd]=ComputeABD(QBar,ZCoord)
% First calculate A, B and D matrices by summing over
% all the layers
N = length(ZCoord) - 1;
A = zeros(3,3);
B = zeros(3,3);
D = zeros(3,3);
for k = 1:N
    A = A + QBar{k} * ( ZCoord(k+1) - ZCoord(k) );
    B = B + QBar{k} * ( ZCoord(k+1)^2 - ZCoord(k)^2 ) * 0.5;
    D = D + QBar{k} * ( ZCoord(k+1)^3 - ZCoord(k)^3 ) / 3;
end
% Next, arrange the A, B and D into a 6x6 ABD stiffness matrix
ABD = [A B; B D];
% Find the laminate [abd] compliance matrix
abd = inv(ABD);
% Extract the a, b and d matrices from the [abd] matrix
a = abd(1:3,1:3);
b = abd(1:3,4:6);
d = abd(4:6,4:6);
end
%%
%*****%
%***      Compute Midsurface Strains and Curvatures      ***%
%*****%
function [Epsilon0,Kappa0] = MidsurfaceStrainsCurvatures...
        (abd,Nx,Ny,Nxy,Mx,My,Mxy)
% Calculate midsurface strains and curvatures column array
EpsilonKappaArray = abd * [Nx; Ny; Nxy; Mx; My; Mxy];
% Extract the midsurface strains and curvatures
Epsilon0 = EpsilonKappaArray(1:3,1);

```

```

Kappa0 = EpsilonKappaArray(4:6,1);
end
%%
%*****
%*** Determine the layer number given the z coordinate ***%
%*****
function LayerNum = WhichLayer(ZCoord,z)
%Inputs:
% ZCoord is an array of interface locations
% z is the z-coordinate of a point
%Outputs:
% LayerNum is the layer to which point z belongs to
% Total number of layers in laminate
N = length(ZCoord)-1;
% Check layer by layer to see if ZCoord(k) <= z <= ZCoord(k+1)
for k = 1:N
    if (z>= ZCoord(k)) && (z<=ZCoord(k+1))
        LayerNum = k; % assign layer number if ZCoord(k) <= z <=
ZCoord(k+1)
    end
end
end
end
%%
%*****
%*** Compute the strains in the global coordinate ***%
%*** system given the midsurface strains and curvatures ***%
%*****
function StrainsXY= ComputeStrainsXY(Epsilon0,Kappa0,z)
%Inputs:
% Epsilon0 is a 3x1 array of mid-surface strains
% Kappa0 is a 3x1 array of mid-surface curvatures
% z is the z-coordinate of the location for calculating the strains
%Outputs:
% StrainsXY is a 3x1 array of strains in the x-y coordinate system
% Array of strains in the x-y coordinate system
StrainsXY = Epsilon0 + (z * Kappa0);
end
end
%%
%*****
%*** Compute the stresses in the global coordinate ***%
%*** system given the midsurface strains and curvatures ***%
%*****
function StressesXY = ComputeStressesXY(StrainsXY,QBar)
%Inputs:
% StrainsXY is a 3x1 array of strains in the x-y coordinate system
% QBar is a 3x3 of off-axis stiffnesses of layer k
%Outputs:
% StressesXY is a 3x1 array of stresses in the x-y coordinate system
% Array of stresses in the x-y coordinate system
StressesXY = QBar * StrainsXY;
end
end
%%
%*****
%*** Compute the stresses in the principal material coordinate ***%
%*** system given the midsurface strains and curvatures ***%
%*****
function Stresses12 = ComputeStresses12(StressesXY, theta)

```

```

%Inputs:
% StressesXY is a 3x1 array of stresses in the x-y coordinate system
% theta is orientation of the fibers in layer k
%Outputs:
% Stresses12 is a 3x1 array of stresses in the 1-2 coordinate system
T = TMatrix(theta);
%Transform the stresses from the x-y to the 1-2 coordinate system
Stresses12 = T * StressesXY;
end
%%
%*****%
%***          Tsai-Wu failure criteria          ***%
%***    Determine factors of safety Sfa and Sfr    ***%
%*****%
function [Sfa, Sfr]=TsaiWu(F1t,F1c,F2t,F2c,F6,Stresses12)
%Inputs:
% F1t,..., F6 are the lamina strengths
% Stresses12 is a 3x1 array of stresses in the 1-2 coordinate system
%Outputs:
% Sfa and Sfr are the factos of safety (actual and reversed-in-sign)
%Calculate Tsai-Wu Parameters
f1 = (1 / F1t) - (1 / F1c);
f11 = 1 / (F1c * F1t);
f2 = (1 / F2t) - (1 / F2c);
f22 = 1 / (F2c * F2t);
f66 = 1 / (F6 * F6);
%Determine the Coefficients a & b
a =
(f11*Stresses12(1)*Stresses12(1))+(f22*Stresses12(2)*Stresses12(2))...
+(f66 * Stresses12(3)*Stresses12(3))-
(sqrt(f11*f22)*Stresses12(1)...
*Stresses12(2));
b = (f1*Stresses12(1))+(f2 * Stresses12(2));
%Determine the Factor of Safety
%*****%
%***          Factor of Safety, Sfa          ***%
%*****%
Sfa = (-b + sqrt((b * b) + (4 * a))) / (2 * a);
%*****%
%***          Reversed Factor of Safety, Sfr          ***%
%*****%
Sfr = (-b - sqrt((b * b) + (4 * a))) / (2 * a);
end
%%
%*****%
%***          Vesion 1 Revision Log          ***%
%*****%
% Original V1: Created Code, MEE 450 taught by Prof. Vel, July 19th,
2016:
% Original code used lamina input values to conduct macromechanics
% based analysis for composite materials
%*****%
%***          Vesion 2 Revision Log          ***%
%*****%
% Original V2: Micromechanics method addition, June 9th, 2018:
% Added micromechanics methods to the code based on colaberation with
% Ben Smith and material from Barbero.

```

```

% Added necessity for user to define if micromechanics is necessary
% Added original material section for constituent materials
%*****%
%***                               Vesion 3 Revision Log                               ***%
%*****%
% Original V3: June 22nd, 2018
% Formatting updates and clarification of comments, prep work for V3.1
% V3.1: Material Property and Micromechanics update, June 25th, 2018:
% Added Derakane 610-C to the resin-property section
% Updated and expanded the Halpin-Tsai calculation sub-section
% Added Mori-Tanaka method as method choice for micromechanics
% Added necessity for user to define either Mori-Tanaka or Halpin-Tsai
% References section added at the end of the code
% Expansion of G12 analytical methods, three methods under Halpin-Tsai
% A brief user instructions section was added.
% Updated labels on output fields to command window.
% Updated overall code formatting and indentation.
%%
%%*****%
%%***                               References                               ***%
%%*****%
% I. M. Daniel and O. Ishai, Engineering Mechanics of Composite
Materials,
% 2nd Edition. New York: Oxford University Press, Inc., 2006.
% E. J. Barbero, Introduction to Composite Materials Design, 2nd
Edition
% New York: CRC Press, 2011.
% Mori, T., and Tanaka, K., 1973, Average stress in a matrix and
average
% elastic energy of materials with misfitting inclusions, Acta
% Metallurgica, Vol. 21, pp. 571-574.
% Chen T., Dvorak G. J., and Benveniste, Y., 1992, Mori-Tanaka
estimates
% of overall elastic moduli of certain composite materials, Journal of
% Applied Mechanics, Vol. 59, pp. 539-546.
%%

```

BIOGRAPHY OF THE AUTHOR

Camerin Michael Seigars was born in Augusta, Maine on September 16, 1993. He was raised in Gardiner, Maine and graduated from Gardiner Area High School. He attended the University of Maine in Orono (UMaine) and graduated with a Bachelor's of Science in Mechanical Engineering with High Honors in 2016. He entered the graduate program in Mechanical Engineering at UMaine upon graduating from undergrad and pursued his masters at the Advanced Structures and Composites Center (ASCC).

Camerin is an avid road cyclist who participates in the Dempsey Challenge annually, and is an avid reader, and movie connoisseur. He passionately watches Fraiser and British mystery film.

Camerin is a candidate for the Master of Science degree in Mechanical Engineering from the University of Maine in August 2018.